



A QUANTITATIVE FEEDBACK THEORY FCS DESIGN  
FOR THE SUBSONIC ENVELOPE OF THE VISTA F-16  
INCLUDING CONFIGURATION VARIATION AND  
AERODYNAMIC CONTROL EFFECTOR FAILURES

THESIS

Vincent J. Cacciatore  
2nd Lieutenant, USAF

AFIT/GE/ENG/95D-04

**DISTRIBUTION STATEMENT A**

Approved for public release  
Distribution Unlimited

DEPARTMENT OF THE AIR FORCE  
AIR UNIVERSITY  
**AIR FORCE INSTITUTE OF TECHNOLOGY**

Wright-Patterson Air Force Base, Ohio

AFIT/GE/ENG/95D-04

A QUANTITATIVE FEEDBACK THEORY FCS DESIGN  
FOR THE SUBSONIC ENVELOPE OF THE VISTA F-16  
INCLUDING CONFIGURATION VARIATION AND  
AERODYNAMIC CONTROL EFFECTOR FAILURES

THESIS

Vincent J. Cacciatore  
2nd Lieutenant, USAF

AFIT/GE/ENG/95D-04

19960617 013

Approved for public release; Distribution unlimited

# DISCLAIMER NOTICE



**THIS DOCUMENT IS BEST QUALITY AVAILABLE. THE COPY FURNISHED TO DTIC CONTAINED A SIGNIFICANT NUMBER OF PAGES WHICH DO NOT REPRODUCE LEGIBLY.**

AFIT/GE/ENG/95D-04

A QUANTITATIVE FEEDBACK THEORY FCS DESIGN  
FOR THE SUBSONIC ENVELOPE OF THE VISTA F-16  
INCLUDING CONFIGURATION VARIATION AND  
AERODYNAMIC CONTROL EFFECTOR FAILURES

THESIS

Presented to the Faculty of the School of Engineering  
of the Air Force Institute of Technology

Air University

In Partial Fulfillment of the  
Requirements for the Degree of  
Master of Science

Vincent J. Cacciatore, B.S. Electrical Engineering  
2nd Lieutenant, USAF

December, 1995

Approved for public release; Distribution unlimited

### *Acknowledgements*

First, I would like to take this opportunity and express my appreciation to Dr. Constantine Houpis and Dr. Meir Pachter for sharing their vast wealth of knowledge and for diligently editing this manuscript.

Next, I want to thank my family and friends for their unwavering support throughout this entire 18 month ordeal. To my parents, a.k.a Joseph and Carol Cacciatore, for their indefatigable motivation and boundless love. To Michael Russo and Matthew Deans, for their tolerance of my incessant complaints, and to my classmates for their witty, and sometimes not so witty, humor.

Finally, I dedicate this thesis, consisting of some 225 pages and well over 1400 hours of blinding work, to Kimberley Michelle Wall for her patience, understanding, and love that enabled me to see through the delirium and remain focused on my priorities. I leave you with this excerpt from a poem that Kimberley gave me and that epitomizes my AFIT experience:

*If you want a thing bad enough  
To go out and fight for it  
Work day and night for it  
Give up you time and your peace  
and your sleep for it  
... Then you'll get it!*  
(Success-Berton Bailey)

Vincent J. Cacciatore

*Table of Contents*

	Page
Acknowledgements . . . . .	ii
List of Figures . . . . .	viii
List of Tables . . . . .	xv
List of Symbols . . . . .	xvi
Abstract . . . . .	xviii
I. Introduction . . . . .	1-1
1.1 Problem . . . . .	1-2
1.2 Summary of Current Literature . . . . .	1-3
1.2.1 Quantitative Feedback Theory Research . . . . .	1-3
1.2.2 Failure Modeling . . . . .	1-4
1.3 Assumptions . . . . .	1-5
1.4 Scope . . . . .	1-6
1.5 Standards . . . . .	1-6
1.6 Approach/Methodology . . . . .	1-6
1.7 Organization . . . . .	1-8
1.8 Materials, Data and Equipment . . . . .	1-8
1.9 Other Support . . . . .	1-8
II. Design Methodology . . . . .	2-1
2.1 MISO QFT Design . . . . .	2-1
2.1.1 Structure . . . . .	2-1
2.1.2 Plant Uncertainty . . . . .	2-2
2.1.3 Frequency Templates . . . . .	2-3

	Page
2.1.4 Specifications . . . . .	2-4
2.1.5 Nominal Plant Selection . . . . .	2-5
2.1.6 Nichols Chart QFT Boundaries . . . . .	2-7
2.1.7 Loop Shaping - Synthesis of the QFT Compensator	2-7
2.1.8 Prefilter Design . . . . .	2-9
2.1.9 MISO Design Summary . . . . .	2-10
2.2 MIMO QFT Design . . . . .	2-11
2.2.1 Structure . . . . .	2-11
2.2.2 Weighting Matrix . . . . .	2-12
2.2.3 Diagonal Dominance . . . . .	2-12
2.2.4 MIMO Equivalence . . . . .	2-12
2.3 Time simulations . . . . .	2-14
2.4 Design Guidelines . . . . .	2-15
III. VISTA F-16 Aircraft Model . . . . .	3-1
3.1 VISTA F-16 . . . . .	3-1
3.2 Flight Scenarios . . . . .	3-1
3.3 LTI Aircraft Model Generation . . . . .	3-3
3.4 Longitudinal Aircraft Model . . . . .	3-5
3.5 Lateral/Directional Aircraft Model . . . . .	3-6
3.6 Transfer Function Generation . . . . .	3-7
3.7 Actuator Model . . . . .	3-8
IV. Control Surface Failure Modeling . . . . .	4-1
4.1 Longitudinal Stability and Control Derivatives . . . . .	4-1
4.1.1 <i>M</i> Equation Analysis . . . . .	4-2
4.1.2 <i>Z</i> Equation Analysis . . . . .	4-6
4.2 Lateral Stability and Control Derivatives . . . . .	4-9

	Page	
4.2.1	Y Equation . . . . .	4-9
4.2.2	L Equation . . . . .	4-10
4.2.3	N Equation . . . . .	4-12
4.3	Disturbance Modeling . . . . .	4-12
4.3.1	Longitudinal Model . . . . .	4-13
4.3.2	Lateral Model . . . . .	4-13
4.4	Failure Model Generation . . . . .	4-13
4.5	Failure Modeling Summary . . . . .	4-14
V.	Longitudinal FCS Design . . . . .	5-1
5.1	Longitudinal Design . . . . .	5-1
5.1.1	Longitudinal QFT Structure . . . . .	5-1
5.1.2	Longitudinal Specifications . . . . .	5-3
5.1.3	Loaded and Effective Plants . . . . .	5-7
5.1.4	Frequency Templates . . . . .	5-8
5.1.5	QFT Generated Bounds . . . . .	5-16
5.1.6	Compensator Design . . . . .	5-18
5.1.7	Prefilter Design . . . . .	5-19
5.2	Time Simulations . . . . .	5-20
5.2.1	$C^*$ Tracking Responses . . . . .	5-21
5.2.2	Maximum Command Gradient . . . . .	5-22
5.3	Design Validation . . . . .	5-27
5.3.1	Stability Validation . . . . .	5-27
5.3.2	Tracking Validation . . . . .	5-27
5.3.3	External Disturbance Rejection Validation . . . . .	5-28
5.3.4	Time Domain Validation . . . . .	5-29
5.4	Longitudinal Design Summary . . . . .	5-33

	Page
VI. Lateral/Directional FCS Design . . . . .	6-1
6.1 Lateral/Directional Design . . . . .	6-1
6.1.1 Lateral/Directional QFT Structure . . . . .	6-1
6.1.2 Lateral Specifications . . . . .	6-6
6.1.3 Loaded and Effective Plants . . . . .	6-11
6.1.4 Frequency templates . . . . .	6-14
6.1.5 QFT Generated Bounds . . . . .	6-23
6.1.6 Compensator Design . . . . .	6-25
6.1.7 Prefilter Design . . . . .	6-29
6.2 Time Simulations . . . . .	6-30
6.2.1 Tracking . . . . .	6-31
6.2.2 Maximum Command Gradients . . . . .	6-37
6.3 Design Validation . . . . .	6-39
6.3.1 Stability Validation . . . . .	6-39
6.3.2 Tracking Validation . . . . .	6-41
6.3.3 External Disturbance Rejection Validation . . . . .	6-41
6.3.4 Time Domain Validation . . . . .	6-44
6.4 Lateral/Directional Design Summary . . . . .	6-53
VII. Conclusions and Recommendations . . . . .	7-1
7.1 Conclusions . . . . .	7-1
7.2 Recommendations . . . . .	7-3
Appendix A. Failure Model Generation Macro . . . . .	A-1
Appendix B. Parameter Space Data Points . . . . .	B-1

	Page
Appendix C. Longitudinal Channel Time Response . . . . .	C-1
C.1 Longitudinal Unit $C*_{cmd}$ Step Input Time Response (Healthy)	C-2
C.2 Longitudinal Unit $C*_{cmd}$ Step Input Time Response (25% Sta- bilator Failure) . . . . .	C-7
C.3 Longitudinal Maximum $C*_{cmd}$ Step Input Time Response (Healthy)	C-12
C.4 Longitudinal Maximum $C*_{cmd}$ Step Input Time Response (25% Stabilator Failure) . . . . .	C-17
C.5 Longitudinal Channel Disturbance Time Response . . . . .	C-22
 Appendix D. Lateral Channel Time Response . . . . .	 D-1
D.1 Lateral Unit $P_{cmd}$ Step Input Time Response (Healthy) . . .	D-2
D.2 Lateral Unit $P_{cmd}$ Step Input Time Response (45% Triple Fail- ure) . . . . .	D-7
D.3 Lateral Maximum $P_{cmd}$ Step Input Time Response (Healthy)	D-13
D.4 Lateral Maximum $P_{cmd}$ Step Input Time Response (45% Triple Failure) . . . . .	D-18
D.5 Lateral Channel Disturbance Time Response . . . . .	D-23
 Appendix E. Matlab's "Linmod" Function . . . . .	 E-1
 Bibliography . . . . .	 BIB-1
 Vita . . . . .	 VITA-1

*List of Figures*

Figure	Page
2.1. MISO QFT Design Structure . . . . .	2-1
2.2. Typical Flight Envelope . . . . .	2-3
2.3. QFT Frequency Template $TP_e(j\omega_i)$ for some $\omega = \omega_i$ . . . . .	2-4
2.4. QFT Tracking Specifications . . . . .	2-5
2.5. Disturbance Specification . . . . .	2-6
2.6. Gain Margin/Frequency and Phase Margin/Frequency Definitions . . . . .	2-6
2.7. QFT Stability $B_S(j\omega)$ and Composite $B_o(j\omega)$ Bounds . . . . .	2-8
2.8. QFT Loop Shaping . . . . .	2-9
2.9. Compensated Closed-Loop Frequency Response without Prefilter . . . . .	2-10
2.10. Compensated Closed-Loop Frequency Response with Prefilter . . . . .	2-11
2.11. A 2X2 MIMO QFT Design Structure Including An External Disturbance . . . . .	2-12
2.12. Equivalent MISO Loops for MIMO QFT Structure, with Diagonal $F$ Matrix . . . . .	2-14
3.1. VISTA F-16 . . . . .	3-2
3.2. Block Diagram of Plant and External Disturbance Input . . . . .	3-8
4.1. $\frac{\Delta M_\alpha}{M_\alpha}$ vs. $\zeta_e$ . . . . .	4-6
4.2. $\frac{\Delta Z_\alpha}{Z_\alpha}$ vs $\zeta_e$ . . . . .	4-8
4.3. Failure Modeling Automation Flow Diagram . . . . .	4-14
5.1. Longitudinal QFT Feedback Structure . . . . .	5-1
5.2. Allocation of $q$ and $g_{pil}$ in $C^*$ Parameter versus $\bar{q}$ . . . . .	5-3
5.3. MIMO QFT Design Structure . . . . .	5-3
5.4. Step Response Used to Define Longitudinal Response Specifications . . . . .	5-5
5.5. Step Input Time Response of QFT Upper and Lower Longitudinal Tracking Bound Models . . . . .	5-6

Figure	Page
5.6. Frequency Response of Effective Plants $P_e$ . . . . .	5-9
5.7. Frequency Response of Disturbance Plants $P_D$ . . . . .	5-9
5.8. Healthy Aircraft Frequency Templates . . . . .	5-11
5.9. Healthy Aircraft Frequency Template for $\omega = 1rps$ . . . . .	5-11
5.10. 15% Horizontal Stabilator Failure Frequency Template for $\omega = 1rps$ . .	5-12
5.11. 25% Horizontal Stabilator Failure Frequency Template for $\omega = 1rps$ . .	5-12
5.12. Healthy Aircraft Frequency Template for $\omega = 30rps$ . . . . .	5-14
5.13. 15% Horizontal Stabilator Failure Frequency Template for $\omega = 30rps$ .	5-14
5.14. 25% Horizontal Stabilator Failure Frequency Template for $\omega = 30rps$ .	5-15
5.15. Illustration of High Frequency Failure Effects on QFT Frequency Tem- plates . . . . .	5-15
5.16. Plant Templates for VISTA Experiencing 25% Horizontal Stabilator Fail- ure . . . . .	5-16
5.17. QFTCAD Tracking Bounds . . . . .	5-17
5.18. QFTCAD External Disturbance Bounds . . . . .	5-19
5.19. QFTCAD Nominal Loop Shaping . . . . .	5-20
5.20. QFTCAD Prefilter Design . . . . .	5-21
5.21. Unit $C^*$ Step Response of Compensated System, Healthy Aircraft and 25% Stabilator Failure Plants ( $\bar{q} < 200 \text{ lbs}/ft^2$ ) [1 of 2] . . . . .	5-22
5.22. Unit $C^*$ Step Response of Compensated System, Healthy Aircraft and 25% Stabilator Failure Plants ( $\bar{q} < 200 \text{ lbs}/ft^2$ ) [2 of 2] . . . . .	5-23
5.23. Unit $C^*$ Step Response of Compensated System, Healthy Aircraft and 25% Stabilator Failure Plants ( $\bar{q} > 200 \text{ lbs}/ft^2$ ) [1 of 2] . . . . .	5-23
5.24. Unit $C^*$ Step Response of Compensated System, Healthy Aircraft and 25% Stabilator Failure Plants ( $\bar{q} > 200 \text{ lbs}/ft^2$ ) [2 of 2] . . . . .	5-24
5.25. Maximum $C^*$ Command Profile . . . . .	5-25
5.26. Nichols Chart of low $\bar{q}$ Plants . . . . .	5-26
5.27. QFTCAD Stability Validation . . . . .	5-27
5.28. QFTCAD Tracking Validation . . . . .	5-28

Figure	Page
5.29. QFTCAD Disturbance Rejection Validation . . . . .	5-29
5.30. Maximum $C^*$ Step Response of Compensated System, Healthy Aircraft and 25% Stabilator Failure Plants ( $\bar{q} < 200 \text{ lbs/ft}^2$ ) [1 of 2] . . . . .	5-30
5.31. Maximum $C^*$ Step Response of Compensated System, Healthy Aircraft and 25% Stabilator Failure Plants ( $\bar{q} < 200 \text{ lbs/ft}^2$ ) [2 of 2] . . . . .	5-30
5.32. Maximum $C^*$ Step Response of Compensated System, Healthy Aircraft and 25% Stabilator Failure Plants ( $\bar{q} > 200 \text{ lbs/ft}^2$ ) [1 of 2] . . . . .	5-31
5.33. Maximum $C^*$ Step Response of Compensated System, Healthy Aircraft and 25% Stabilator Failure Plants ( $\bar{q} > 200 \text{ lbs/ft}^2$ ) [2 of 2] . . . . .	5-32
5.34. Disturbance Unit Step Response of Compensated System, 25% Stabilator Failure Plants ( $\bar{q} < 200 \text{ lbs/ft}^2$ ) [1 of 2] . . . . .	5-34
5.35. Disturbance Unit Step Response of Compensated System, 25% Stabilator Failure Plants ( $\bar{q} < 200 \text{ lbs/ft}^2$ ) [2 of 2] . . . . .	5-34
5.36. Disturbance Unit Step Response of Compensated System, 25% Stabilator Failure Plants ( $\bar{q} > 200 \text{ lbs/ft}^2$ ) [1 of 2] . . . . .	5-35
5.37. Disturbance Unit Step Response of Compensated System, 25% Stabilator Failure Plants ( $\bar{q} > 200 \text{ lbs/ft}^2$ ) [2 of 2] . . . . .	5-35
5.38. Final QFT Longitudinal FCS . . . . .	5-36
6.1. General MIMO QFT System with an External Disturbance Included . . . . .	6-2
6.2. Lateral/Directional 2 X 2 MIMO System with an External Disturbance and Dutch Roll Damper . . . . .	6-2
6.3. Dutch Roll Damper Structure . . . . .	6-3
6.4. Root Locus Plots and Closed Loop Poles for Healthy Aircraft with Dutch Roll Damping Loop . . . . .	6-4
6.5. Root Locus Plots and Closed Loop Poles for 45% Rudder Failure with Dutch Roll Damping Loop . . . . .	6-4
6.6. Root Locus Plots and Closed Loop Poles for 45% Stabilator, 45% Aileron, and 45% Rudder Failures with Dutch Roll Damping Loop . . . . .	6-5
6.7. Roll Channel Level 1, 2 and 3 Tracking Specifications . . . . .	6-8

Figure	Page
6.8. Lateral Channel Tracking and Cross-coupling Specifications . . . . .	6-9
6.9. Lateral Channel Disturbance Rejection Specifications . . . . .	6-10
6.10. Frequency Response of Loaded Plant Models ( $P_L$ ) . . . . .	6-13
6.11. Frequency Response of External Disturbance Plant Models ( $P_D$ ) . . . . .	6-13
6.12. Frequency Response of Effective Plant Models ( $P_e$ ) . . . . .	6-14
6.13. Diagonal Dominance Validation . . . . .	6-15
6.14. Healthy Aircraft, Beta Templates . . . . .	6-16
6.15. Healthy Aircraft, Roll Templates . . . . .	6-16
6.16. 45% Aileron Failure, Beta ( $\beta$ ) Templates . . . . .	6-18
6.17. 45% Aileron Failure, Roll ( $p$ ) Templates . . . . .	6-18
6.18. 45% Aileron Failure, Roll ( $p$ ) Template for $\omega = 1$ rps . . . . .	6-19
6.19. 45% Rudder Failure, Beta ( $\beta$ ) Template for $\omega = 30$ rps . . . . .	6-19
6.20. 45% Rudder Failure, Beta ( $\beta$ ) Templates . . . . .	6-20
6.21. 45% Rudder Failure, Roll ( $p$ ) Templates . . . . .	6-20
6.22. 45% Differential Stabilator Failure, Beta ( $\beta$ ) Templates . . . . .	6-21
6.23. 45% Differential Stabilator Failure, Roll ( $p$ ) Templates . . . . .	6-21
6.24. 45% Triple Failure, Beta ( $\beta$ ) Templates . . . . .	6-22
6.25. 45% Triple Failure, Roll ( $p$ ) Templates . . . . .	6-22
6.26. QFTCAD Stability and Tracking Bounds for the Roll Channel of the Healthy VISTA F-16 . . . . .	6-24
6.27. QFTCAD Stability and Tracking Bounds for the Roll Channel of VISTA F-16 Experiencing a 45% Triple Failure . . . . .	6-24
6.28. QFTCAD Stability and Tracking Bounds for the Beta Channel of the Healthy VISTA F-16 . . . . .	6-25
6.29. QFTCAD Stability and Tracking Bounds for the Beta Channel of the VISTA F-16 Experiencing a 45% Triple Failure . . . . .	6-26
6.30. QFT External Disturbance Bounds for Roll Channel . . . . .	6-26
6.31. QFT External Disturbances Bounds for Beta Channel . . . . .	6-27

Figure	Page
6.32. QFTCAD Tracking Bounds and Nominal Loop for Roll Channel with 45% Triple Failure . . . . .	6-28
6.33. QFTCAD Tracking Bounds and Nominal Loop for Beta Channel with 45% Triple Failure . . . . .	6-29
6.34. Roll Unit Step Response of Compensated System Healthy Aircraft and 45% Triple Failure Plants ( $\bar{q} < 150 \text{ lbs/ft}^2$ ) [1 of 3] . . . . .	6-32
6.35. Unit Roll Step Response of Compensated System Healthy Aircraft and 45% Triple Failure Plants ( $\bar{q} < 150 \text{ lbs/ft}^2$ ) [2 of 3] . . . . .	6-32
6.36. Unit Roll Step Response of Compensated System Healthy Aircraft and 45% Triple Failure Plants ( $\bar{q} < 150 \text{ lbs/ft}^2$ ) [3 of 3] . . . . .	6-33
6.37. Unit Roll Step Response of Compensated System Healthy Aircraft and 45% Triple Failure Plants ( $\bar{q} > 150 \text{ lbs/ft}^2$ ) [1 of 3] . . . . .	6-33
6.38. Unit Roll Step Response of Compensated System Healthy Aircraft and 45% Triple Failure Plants ( $\bar{q} > 150 \text{ lbs/ft}^2$ ) [2 of 3] . . . . .	6-34
6.39. Unit Roll Step Response of Compensated System Healthy Aircraft and 45% Triple Failure Plants ( $\bar{q} > 150 \text{ lbs/ft}^2$ ) [3 of 3] . . . . .	6-34
6.40. Unit Beta Step Response of Compensated System Healthy Aircraft and 45% Triple Failure Plants [1 of 3] . . . . .	6-35
6.41. Unit Beta Step Response of Compensated System Healthy Aircraft and 45% Triple Failure Plants [2 of 3] . . . . .	6-36
6.42. Unit Beta Step Response of Compensated System Healthy Aircraft and 45% Triple Failure Plants [3 of 3] . . . . .	6-36
6.43. Maximum Roll Command Gradient . . . . .	6-38
6.44. Maximum Sideslip Command Gradient . . . . .	6-39
6.45. QFT Stability Validation for the Sideslip ( $\beta$ ) Channel . . . . .	6-40
6.46. QFT Stability Validation for the Roll ( $p$ ) Channel . . . . .	6-40
6.47. QFT Tracking Validation for the Lateral/Directional Channel ( $\bar{q} < 150 \text{ lbs/ft}^2$ ) . . . . .	6-42
6.48. QFT Tracking Validation for the Lateral/Directional Channel ( $\bar{q} > 150 \text{ lbs/ft}^2$ ) . . . . .	6-42

Figure	Page
6.49. QFT External Disturbance Validation . . . . .	6-43
6.50. Maximum Roll Gradient Step Response of Compensated System, Healthy Aircraft and 45% Triple Failure Plants ( $\bar{q} < 150 \text{ lbs/ft}^2$ ) [1 of 3] . . . .	6-45
6.51. Maximum Roll Gradient Step Response of Compensated System, Healthy Aircraft and 45% Triple Failure Plants ( $\bar{q} < 150 \text{ lbs/ft}^2$ ) [2 of 3] . . . .	6-45
6.52. Maximum Roll Gradient Step Response of Compensated System, Healthy Aircraft and 45% Triple Failure Plants ( $\bar{q} < 150 \text{ lbs/ft}^2$ ) [3 of 3] . . . .	6-46
6.53. Maximum Roll Gradient Step Response of Compensated System, Healthy Aircraft and 45% Triple Failure Plants ( $\bar{q} > 150 \text{ lbs/ft}^2$ ) [1 of 3] . . . .	6-46
6.54. Maximum Roll Gradient Step Response of Compensated System, Healthy Aircraft and 45% Triple Failure Plants ( $\bar{q} > 150 \text{ lbs/ft}^2$ ) [2 of 3] . . . .	6-47
6.55. Maximum Roll Gradient Step Response of Compensated System, Healthy Aircraft and 45% Triple Failure Plants ( $\bar{q} > 150 \text{ lbs/ft}^2$ ) [3 of 3] . . . .	6-47
6.56. Maximum Sideslip Gradient Step Response of Compensated System, Healthy Aircraft and 45% Triple Failure Plants [1 of 3] . . . . .	6-48
6.57. Maximum Sideslip Gradient Step Response of Compensated System, Healthy Aircraft and 45% Triple Failure Plants [2 of 3] . . . . .	6-49
6.58. Maximum Sideslip Gradient Step Response of Compensated System, Healthy Aircraft and 45% Triple Failure Plants [3 of 3] . . . . .	6-49
6.59. Disturbance Step Response of Compensated System, 45% Triple Failure Plants ( $\bar{q} < 150 \text{ lbs/ft}^2$ ) [1 of 3] . . . . .	6-50
6.60. Disturbance Step Response of Compensated System, 45% Triple Failure Plants ( $\bar{q} < 150 \text{ lbs/ft}^2$ ) [2 of 3] . . . . .	6-51
6.61. Disturbance Step Response of Compensated System, 45% Triple Failure Plants ( $\bar{q} < 150 \text{ lbs/ft}^2$ ) [3 of 3] . . . . .	6-51
6.62. Disturbance Step Response of Compensated System, 45% Triple Failure Plants ( $\bar{q} > 150 \text{ lbs/ft}^2$ ) [1 of 3] . . . . .	6-52
6.63. Disturbance Step Response of Compensated System, 45% Triple Failure Plants ( $\bar{q} > 150 \text{ lbs/ft}^2$ ) [2 of 3] . . . . .	6-52
6.64. Disturbance Step Response of Compensated System, 45% Triple Failure Plants ( $\bar{q} > 150 \text{ lbs/ft}^2$ ) [3 of 3] . . . . .	6-53

Figure	Page
6.65. Final QFT Lateral FCS . . . . .	6-54
E.1. Phillips' Compensated system Stability Validation . . . . .	E-2

*List of Tables*

Table	Page
1.1. Test Matrix . . . . .	1-7
2.1. Control Surface Rate and Deflection Limits for the VISTA F-16 . . . . .	2-15
3.1. Basic Aircraft Data . . . . .	3-1
3.2. Units of Aircraft Model States . . . . .	3-4
5.1. MILSTD Longitudinal Time Domain Tracking Specifications (Level 1,2,3)	5-4
5.2. QFT Upper and Lower Tracking Bound Model Step Response Characteristics . . . . .	5-7
6.1. MILSTD 1797A Recommended Roll Mode Time Constants(seconds) .	6-6
6.2. Model settling times(seconds) . . . . .	6-7
6.3. Roll Performance Specifications for MIL STD 1797A Class IV Aircraft	6-10
6.4. Speed Range for MIL STD 1797A Class IV Aircraft . . . . .	6-11
6.5. MIMO Plant Transfer Function Description . . . . .	6-12

*List of Symbols*

Symbol	Page
F QFT Prefilter . . . . .	2-1
G QFT Compensator . . . . .	2-1
$T_R$ Tracking Control Ratio . . . . .	2-1
$T_D$ Disturbance Rejection Control Ratio . . . . .	2-1
$P(s)$ Plant . . . . .	2-2
$P_j$ An Individual Plant . . . . .	2-3
$\mathcal{P}$ Design Set of Plants . . . . .	2-3
$T_{RU}$ Upper Tracking Bound . . . . .	2-4
$T_{RL}$ Lower Tracking Bound . . . . .	2-4
$\delta_R$ Magnitude Difference Between Upper and Lower Tracking Models . . . . .	2-5
$\omega_h$ Bandwidth Frequency . . . . .	2-5
$P_o$ Nominal Plant . . . . .	2-5
$B_R(j\omega)$ QFT Tracking Bounds . . . . .	2-7
$B_D(j\omega)$ QFT Disturbance Bounds . . . . .	2-7
$B_S(j\omega)$ QFT Stability Bounds . . . . .	2-7
$B_o(j\omega)$ QFT Composite Bounds . . . . .	2-7
$M_L$ Composite Stability Bound . . . . .	2-7
$T_{RU}$ Lower Tracking Model . . . . .	2-9
$T_{RL}$ Upper Tracking Model . . . . .	2-9
<b>R</b> Reference Signal . . . . .	2-11
<b>D</b> Disturbance Input . . . . .	2-11
<b>Y</b> System Output . . . . .	2-11
<b>W</b> Weighting Matrix . . . . .	2-12
$d_{ij}$ External and Cross-coupling Disturbance . . . . .	2-13
$q_{ij}$ Reciprocal of Effective Plant Elements . . . . .	2-13

Symbol	Page
rps radians per second . . . . .	2-15
$\omega_\phi$ Phase Margin Frequency . . . . .	2-15
<b>A</b> Stability Derivative Matrix . . . . .	3-3
<b>B</b> Control Derivative Matrix . . . . .	3-3
$\delta_{flap}$ Flaperon Deflection . . . . .	3-5
$\delta_{elev}$ Elevator Deflection . . . . .	3-5
$\delta_{dtail}$ Differential Tail Deflection . . . . .	3-6
$\delta_{ail}$ Aileron Deflection . . . . .	3-6
$\delta_{rud}$ Rudder Deflection . . . . .	3-6
$p$ Roll Rate . . . . .	3-7
$r$ Yaw Rate . . . . .	3-7
$\beta$ Sideslip Angle . . . . .	3-7
<b>P<sub>D</sub></b> Disturbance Model . . . . .	3-8
$\zeta'_e$ Elevator Damage Level . . . . .	4-4
$\zeta_a$ Aileron Damage Level . . . . .	4-9
$\zeta_r$ Rudder Damage Level . . . . .	4-9
$\zeta_{dt}$ Differential Tail Damage Level . . . . .	4-9
$C_{l_{pF}}$ Failed Roll Damping Stability Derivative . . . . .	4-11
<b><math>\Gamma_{lat}</math></b> Lateral Disturbance Model . . . . .	4-12
<b><math>\Gamma_{long}</math></b> Longitudinal Disturbance Model . . . . .	4-12

*Abstract*

Fault tolerant flight control systems for combat aircraft are an alternative to excessively redundant aircraft designs or reconfigurable control laws. However, due to the range of flight conditions within a combat aircraft's operational flight envelope, the variety of its configurations, and the unavailability of an aerodynamic data base for damaged aircraft, designing fault tolerant systems is a complicated endeavor. Quantitative Feedback Theory is a robust control design technique especially well suited to manage the structured parametric uncertainty inherent in this problem, and consequently is applied as the primary design tool for this research. Furthermore, realistic failure models are developed for the VISTA F-16 and physical saturation constraints are applied to the control effectors. The ensuing fault tolerant design is subjected to realistic control inputs and validated with the applicable MILSTD specifications.

A QUANTITATIVE FEEDBACK THEORY FCS DESIGN  
FOR THE SUBSONIC ENVELOPE OF THE VISTA F-16  
INCLUDING CONFIGURATION VARIATION AND  
AERODYNAMIC CONTROL EFFECTOR FAILURES

*I. Introduction*

With twenty percent of aircraft losses in combat and a significant percentage of aircraft losses in peacetime attributed to flight control system failures, the justification for designing fault tolerant control systems becomes apparent [18]. However until recent innovations in Self-Repairing Flight Control concepts, redundancy was the only design technique employed to manage such failures [18]. This brute force dependence on redundancy increased the weight, complexity and expense of combat aircraft while consequently reducing their payload, range, and operational effectiveness [13]. Self-Repairing Flight Control (SRFC) concepts, such as integrated components, drop in modules, autonomous maintenance diagnostics, and ultimately, fault tolerant flight control laws, significantly increased combat aircraft availability while also reducing the cost of acquiring and maintaining the aircraft [18], viz, life cycle cost.

Fault Tolerant Flight Control Laws have certain advantages over their conventional counterparts. Fault tolerant control systems do not require excessive redundancy and control effector overdesign, while affording enhanced stability margins. In essence, the fault tolerant flight control system transfers dependence on any particular control surface to the entire aircraft system. If an actuator and primary control surface fail, control authority may be maintained by utilizing the aircrafts healthy control surfaces or thrust vectoring capabilities, if applicable. Thus, the additional weight of possibly quadruplex replication of essential flight control elements is mitigated. Also, designers often increase the size of a control surface to account for battle damage losses [4]. Since this loss of control authority is an anticipated flight scenario in a fault tolerant design, airframe designers

can confidently reduce control surface overdesign without compromising the pilot's safety. Finally as an additional enhancement, fault tolerant flight control systems are designed to provide adequate stability in a variety of failure conditions so that the pilot can either continue the mission or in the worst case, safely bail out. The benefits to the Air Force in designing such a control law are evident. By employing fault tolerant flight control systems, there will be a reduction in casualties, weight and maintenance while providing increased performance, survivability, and affordability.

Just as there are a variety of approaches to effectively develop a self-repairing aircraft, there are an equal number of strategies proposed to design a fault tolerant flight control law. However there are several factors that make Quantitative Feedback Theory (QFT) the chosen method of design. First, QFT is a robust control technique that, unlike other design approaches, accounts for wide variations in structured plant parameter uncertainty.[9][10] Second, from the frequency template graphics generated in QFT, an engineer is able to discern whether the design can be accomplished by a single controller or whether gain scheduling will be necessary. Third, one of QFT's most salient features is that it enables the designer to input performance specifications at the beginning of the design process. By adding these specifications early in the process, intelligent decisions can be made to reduce the number of design iterations necessary to achieve an acceptable design. Finally, though fault detection and isolation schemes have been found to successfully manage failure cases, these approaches require a significantly robust system to provide reliable information.[8]. The compensators generated via the QFT technique insure this robustness. Therefore, due to Quantitative Feedback Theory's ability to handle wide variations in plant uncertainty, the graphical tools employed in the technique, and the introduction of performance specifications at the onset of the design, QFT is selected as the primary design tool.

### *1.1 Problem*

The main objective of this research is to design a robust Flight Control System (FCS) using QFT which is tolerant to flight control effector damage from the outset. Specifically, this FCS is designed to be robust enough to provide nominal flight control

for the healthy aircraft, while providing stabilization for the aircraft with damaged control effectors. In addition to the primary objective, it is also the purpose of this research to systematically determine the maximum control effector damage that the proposed QFT design can accommodate.

## 1.2 Summary of Current Literature

*1.2.1 Quantitative Feedback Theory Research.* The United States Air Force through the Wright Laboratory Flight Dynamics Directorate Control Techniques Branch (WL/FIGS) and in affiliation with the graduate program at the Air Force Institute of Technology, has been a proponent of QFT since the early 1980's.[7] In that time, and due largely to the collaboration of Dr. Constantine Houpis and Dr. Issac Horowitz, the "father" of QFT, WL/FIGS has sponsored over 25 QFT driven flight control masters theses. The most current research in the area of full envelope flight control employing QFT was conducted by Lieutenant Odel Reynolds in 1993 [16] and Major Scott Phillips in 1994 [15].

Reynolds presented the first full subsonic envelope flight control system using QFT in his 1993 masters thesis. Previously, Quantitative Feedback Theory's mathematically rigorous nature limited its applicability as a control design technique. Without a computer design program to manage the numerous calculations involved in applying the theory, only designs with appropriately limited scopes were undertaken. However, in 1992 Richard Sating developed the first Quantitative Feedback Theory CAD package using *Mathematica* [19], and future generations of QFT designers were empowered to tackle more involved flight control problems. Lieutenant Reynolds used this increased capability to successfully design a flight control system for the VISTA F-16, incorporating the entire subsonic envelope in his design. This successful design enhanced the prominence of QFT as a robust control theory, and cleared the way for future full envelope FCS designs.

Phillips further demonstrated the capabilities of QFT by expanding Reynold's operational flight envelope through increased plant parameter variation, i.e., adding different external fuel tank configurations to the aircraft. Adding these variations enlarged the total number of plants by a factor of 4, resulting in a QFT design that would have been im-

possible before Sating's QFTCAD program. Not only was Phillips able to show that QFT could handle such a wide variation in parametric uncertainty, but as an experienced F-16 pilot, he was able to combine pilot preference and engineering expertise in the selection and blending of feedback variables. His selection of feedback variables and the inclusion of additional actuator rate and deflection saturation nonlinearities, allowed Phillips to construct a flight control system that was capable of meeting Level 1 flying qualities as dictated by the MILSTD 1797A [1] while simultaneously satisfying real world constraints. Finally, Phillips' analog design was transformed into the discrete domain and loaded into the Simulation Rapid Prototyping Facility [3] for further testing and evaluation. The next step, which Captain Pete Eide is currently developing at WL/FIGS, is to load Phillips' QFT based controller aboard the VISTA F-16 for man-in-the-loop flight tests. The first phase of these simulations evaluate the stability of Phillips' design, and the initial results have been very positive.

*1.2.2 Failure Modeling.* The quality and reliability of a QFT based design is heavily dependent on the accuracy of the plant models employed in its design. However, as a general rule, control engineers are not supplied with all the data necessary to model control surface failures exactly.[18] Aerodynamic data obtained from wind tunnel tests usually do not include a "rubber aircraft,"[14] where failures can be simulated by removal of aerodynamic surfaces. If engineers were given this data, the difficulty of modeling realistic failures would be greatly reduced. Due primarily to this limitation, and the inability of computer programs to employ this failure data in their simulation algorithms, previous fault tolerant flight control designs have modeled aerodynamic control surface failures as mere actuator failures. By handling failures in this way, designers are able to avoid modeling the effects of failures on the aircraft's dynamics. In other words, by modeling battle damage as actuator failures, engineers willfully disregard the warranted changes in the aircraft's stability derivatives. From a state-space viewpoint, this approach results in either "zeroing out" [12] or scaling the B matrix. Though modeling damage as actuator failures proves to be sufficient for other types of control problems [12], for a realistic evaluation of the effects of battle damage on an aircraft's control system this type of modeling is inadequate.

A more realistic approach was presented by Captain Mark S. Keating in his 1993 QFT MS thesis. Captain Keating was able to formulate the equations necessary to model control effector failures on the dynamics of an aircraft assuming asymmetric control surface damage. Though Keating's effort focussed on an unmanned research vehicle, his equations can be adapted to accommodate any airframe. In addition to modeling the change in dynamics caused by control effector failures, Keating also applied an external disturbance to account for the inherent cross-coupling of the lateral/directional and longitudinal aircraft channels. By modeling this coupling simply as an equivalent disturbance input into the system, Keating was able to maintain separation of the lateral/directional and longitudinal channels. This was a dramatic improvement on past failure designs because it realistically modeled battle damage and enabled the designer to reduce the complexity of the design.

### *1.3 Assumptions*

It is assumed that the linear time invariant models (LTI) generated by Phillips accurately represent the VISTA F-16 through the entire subsonic flight envelope. In generation of these models the following assumptions are made:

1. Time spans of interest are short, ranging from 3 to 5 seconds in duration.
2. The aircraft is assumed a rigid body (assuming bending modes are not excited).
3. The reference coordinate system is fixed to the body of the aircraft and centered at the aircraft center of mass.
4. The earth is an inertial reference, and the atmosphere is fixed with respect to the earth, which is valid because the gyros and accelerometers used for control systems are incapable of sensing the angular velocity and acceleration of the earth.
5. The mass of the aircraft is constant.
6. Quasisteady flow is assumed, thus all derivatives with respect to velocity rates of change and unsteady aerodynamics are neglected.
7. The aircraft is symmetric about the XZ plane.

8. High amplitude command inputs and aircraft responses do not invalidate the assumed linear model.

Additional assumptions are:

1. Phillips' models represent the maximum uncertainty inherent in the healthy aircraft with configuration variation.
2. Aircraft orientation and velocity measurements are available.

#### *1.4 Scope*

The scope of this thesis includes compensator and prefilter designs for both the longitudinal and lateral/directional aircraft channels. The longitudinal design is strictly a MISO structure with single control surface failures, while the lateral/directional FCS is a 2X2 MIMO control system involving single, double, and triple control surface failures. In addition to the failure conditions imposed on the flight control design, rate and actuator saturation nonlinearities are included to simulate real world physical constraints. Success of the design is determined by meeting the MIL STD 1797A Level 1 flying qualities for the healthy aircraft and Level 2 or 3 for the failed aircraft.

#### *1.5 Standards*

The primary source of flying qualities specifications is the MILSTD 1797A.

#### *1.6 Approach/Methodology*

1. Employ the Simulation/Rapid-Prototyping Facility (SRF) [3] to generate the healthy aircraft models for the entire subsonic envelope of the VISTA F-16 including configuration variation. These models have been developed previously in Phillip's thesis [15] and need only to be validated for use in this design.
2. Simulate various levels of control effector damage by individually altering the healthy plant model stability and control derivatives. A similar failure modeling process was developed in Keating's thesis [11] and is adapted to fit the VISTA airframe.

3. Include single failures for the longitudinal channel and multiple failure cases in the lateral/directional channel where multiple control effectors are present. The entire test matrix can be found on Table 1.1.

Types of Failures	Longitudinal	Lat/Directional		
	Elevator	Diff Tail	Rudder	Ailerons
No Failures	Healthy	Healthy	Healthy	Healthy
Single Failures	Fail 15%	Fail 25%	H <sup>1</sup>	H
	Fail 25%	Fail 45%	H	H
	H	H	Fail 25%	H
	H	H	Fail 45%	H
	H	H	H	Fail 25%
	H	H	H	Fail 45%
Multiple Failures	H	Fail 25%	Fail 25%	H
	H	Fail 25%	H	Fail 25%
	H	H	Fail 25%	Fail 25%
	H	Fail 25%	Fail 25%	Fail 25%
	H	Fail 45%	Fail 45%	H
	H	Fail 45%	H	Fail 45%
	H	H	Fail 45%	Fail 45%
	H	Fail 45%	Fail 45%	Fail 45%

Table 1.1 Test Matrix

4. Accommodating all of the plants listed in the test matrix, and utilizing the QFT design technique, construct a compensator (or digital controller) able to meet Level 1, 2 or 3 flying qualities depending on the condition of the aircraft.
5. Simulate the design in *Matlab*, driving the basic aircraft system with a maximum command gradient, and including realistic control effector saturation limitations. These simulations involve subjecting the compensated closed loop system to a step command input and evaluating the aircraft response. If the step response satisfies the MILSTD 1797A flying qualities specifications then the design is complete; if the system does not meet these specifications then it may be necessary to repeat step 4. Unfortunately, unless a routine, that incorporates changes in the aircraft dynamics

---

<sup>1</sup>Represents Healthy Aircraft

due to control effector failures can be added to the existing SRF simulator, full non linear simulations will be unavailable to validate this design.

### *1.7 Organization*

Chapter *II* overviews the Quantitative Feedback Theory MISO and MIMO design procedures and the specific design guidelines. The VISTA F-16 model is examined in Chapter *III*, and the failure modeling process is detailed in Chapter *IV*. The first four chapters cover the problem definition and setup, while Chapters *V* and *VI* explain the actual longitudinal and lateral/directional designs. The final designs as well as conclusions and recommendations provide closure in Chapter *VII*.

### *1.8 Materials, Data and Equipment*

Phillips' linear time invariant (LTI) models are essential to the satisfactory completion of this thesis. No special equipment is required in this design other than a SPARC station 2 or greater and accompanying *Matlab*, MIMO QFTCAD,  $\LaTeX$ , and SunOS software.

### *1.9 Other Support*

Dr. Meir Pachter, Dr. Constantine H. Houpis, and Major Dean Schneider serve on the thesis committee and Captain Peter Eide serves as the Air Force sponsor for this project. Dr. Pachter and Dr. Houpis are the committee co-chairman.

## II. Design Methodology

This chapter outlines the basics of Quantitative Feedback Theory[9], the time simulations and specific guidelines used in the design.

Quantitative Feedback Theory (QFT) is a two degree of freedom frequency domain robust control design technique that emphasizes the use of feedback to achieve particular system tolerances despite plant uncertainty and cross-coupling effects.[5] The essence of a QFT design is to insure that a system's tracking and cross-coupling responses are members of a set of desired responses through the development of a single set of minimal-order compensators, the prefilter ( $F$ ) and compensator ( $G$ ). The details of a MISO (Multiple-Input Single-Output) QFT design are presented followed by an overview of the MIMO (Multiple-Input Multiple-Output) case. Finally, to adequately focus this discussion, it is anticipated that the reader has a basic understanding of the fundamentals of conventional control theory.

### 2.1 MISO QFT Design

*2.1.1 Structure.* The basic QFT structure shown in Fig. 2.1 is a unity feedback system with the plant ( $P$ ) and the compensator ( $G$ ) in cascade and the prefilter ( $F$ ) in series with the closed loop. Given this structure, the control ratios for tracking  $T_R$  and disturbance rejection  $T_D$  are developed in Eqs. (2.1) and (2.2).

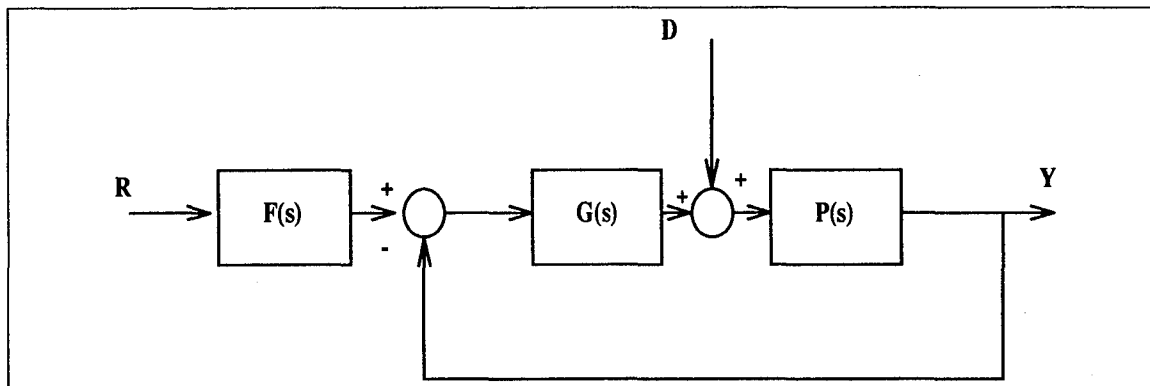


Figure 2.1 MISO QFT Design Structure

$$T_R(s) = \frac{Y(s)}{R(s)} = \frac{F(s)G(s)P(s)}{1 + G(s)P(s)} = \frac{F(s)L(s)}{1 + L(s)} \quad (2.1)$$

$$T_D(s) = \frac{Y(s)}{D(s)} = \frac{P(s)}{1 + G(s)P(s)} = \frac{P(s)}{1 + L(s)} \quad (2.2)$$

Where  $L(s) = G(s)P(s)$  is the loop transmission function.

*2.1.2 Plant Uncertainty.* In this specific flight control design, the longitudinal channel is a 1x1 system, and the plant  $P(s)$  from Fig. 2.1 represents the Laplace transform of the aircraft's longitudinal differential equations of motion. In general, the inputs to an aircraft plant are the control effectors (the stabilator, rudder and aileron deflections), and the outputs of the system are the aircraft states (position, velocity and acceleration). The coefficients of the aircraft differential equations are the stability and control derivatives. These derivatives are dependent on numerous factors. The most prominent of these factors are altitude, airspeed, aircraft center of gravity, and of particular interest in this design, aerodynamic control effector failures.

An aircraft, in normal operation, transitions through a range of altitudes, and airspeeds within its flight envelope represented by the X's in Fig. 2.2. In addition to the changes in altitude and airspeed the aircraft can also experience possible aerodynamic control effector failures, and different CG locations due to external stores or fuel consumption. These varying CG positions and failures add two additional dimensions to the flight envelope such that an aircraft flying at 10,000 feet, Mach .4 ,with 2 external fuel tanks, and 45% rudder failure is represented by a unique set of stability and control derivatives in this design. Each of these factors which influences an aircraft's control response, can only be anticipated by the designer a priori. Therefore, the parametric uncertainty, or more particularly, structured plant parameter uncertainty confronts the aircraft controls designer. In a robust control design, such as QFT, this structured uncertainty must be defined or at least bounded in order to proceed with the design process. In a QFT design this quantification of parameter uncertainty is accomplished via frequency templates.

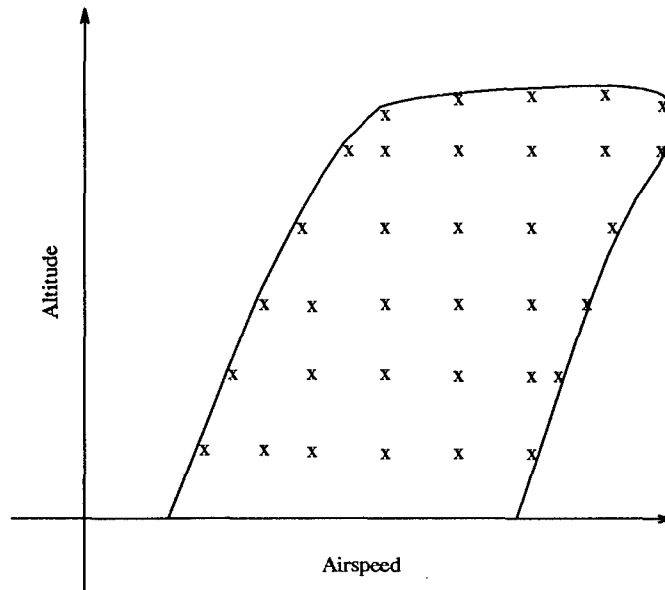


Figure 2.2 Typical Flight Envelope

*2.1.3 Frequency Templates.* QFT frequency templates are the graphical interpretation of the quantified design uncertainty. They are formed in two distinct steps. First, transfer function matrices ( $P_j$ ) are generated over the entire range of possible plant configurations discussed in the previous section, where each transfer function comprises one plant in the design set  $\mathcal{P}$ . The exact number of plants needed to define the parameter space is highly dependent on the specific design problem, however the goal in any design is to accurately define the space with the minimum number of plants. The greater the number of plants the more exactly the uncertainty is quantified, but with an increasing number of plants the computation burden becomes inhibiting. Finally, the frequency response of each  $J$  plant is generated, and then mapped onto a two dimensional graph representing the relative magnitude and phase at a particular frequency. The resulting graph, or frequency template, displays the uncertainty inherent in the design.

Figure 2.3 illustrates an example of a QFT frequency template, where the X's represent specific plants. Frequency templates enable the designer to see patterns otherwise obscured in the transfer function data. If the plants are widely dispersed on the frequency templates, then some additional configurations must be evaluated to further resolve the uncertainty. If there is a tight group of points within one region and only a few cases an

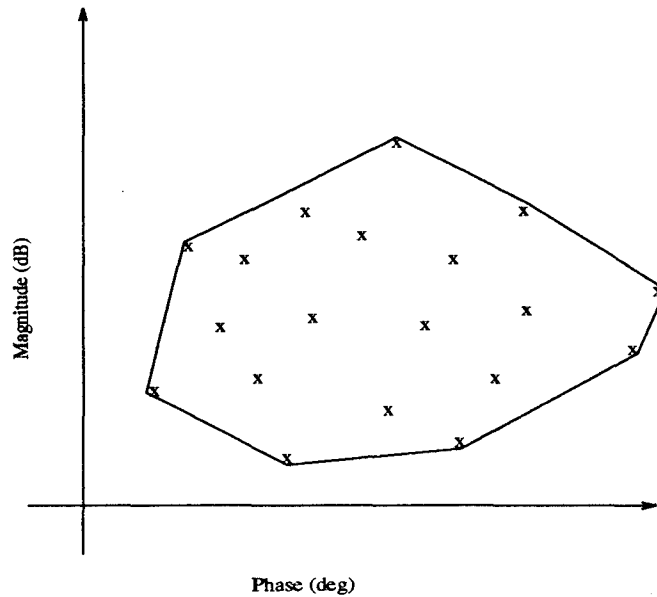


Figure 2.3 QFT Frequency Template  $TP_e(j\omega_i)$  for some  $\omega = \omega_i$

extended distance apart, then those “rebel” plant cases must be investigated. It is possible that those plant cases represent some unfeasible physical configuration, or are simply too problematic to include in the design set. The information content of the frequency templates is extensive, and the feedback to the designer is immediate and dramatic. Important decisions, such as whether to keep those rebel plants, divide the design into two “compensator scheduled” systems, or add plant cases to the design set, can be made intelligently at this point in the design. This ability to graphically examine the uncertainty early in the design process is one of the ways in which the transparency of QFT is experienced by the designer.

*2.1.4 Specifications.* In addition to the frequency templates, the control system designer witnesses the transparency of QFT through the incorporation of closed-loop control system performance specifications at the beginning of the design process. After quantifying the uncertainty and constructing the frequency templates, the next step in the design procedure is to generate frequency domain tracking and disturbance models. An example of typical tracking models,  $T_{RU}$  (upper bound) and  $T_{RL}$  (lower bound), are shown in Fig. 2.4. These models form the boundaries of the desired tracking responses, also known as the thumbprint specifications, and are developed based on satisfying two

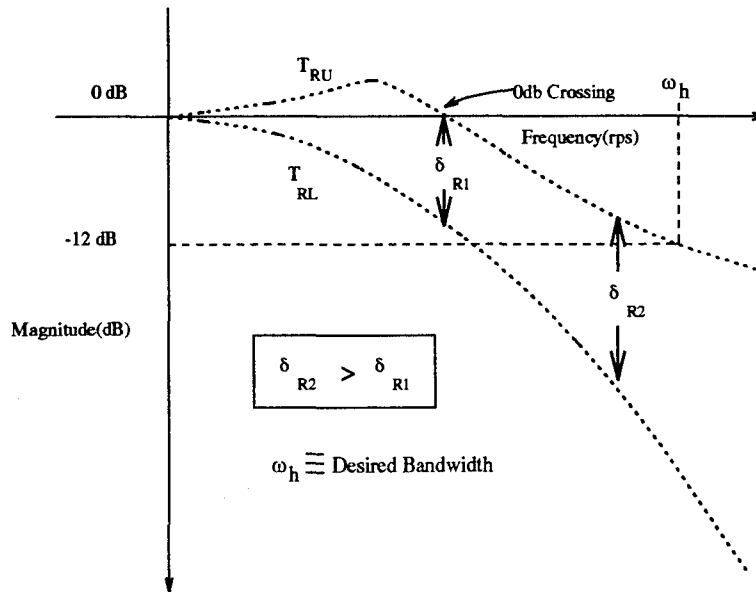


Figure 2.4 QFT Tracking Specifications

criteria. The boundaries must meet the desired second order step forcing function figures of merit for underdamped and overdamped responses, as well as the QFT requirement on the  $\delta_R$  spread. Quantitative Feedback Theory requires that  $\delta_R$ , or the magnitude difference between the upper and lower tracking models at a particular frequency, is monotonically increasing for frequencies above the 0 dB crossing frequency of  $T_{RU}$ . Finally, to satisfy the performance specifications the actual responses must lie within these boundaries at least for frequencies less than  $\omega_h$ .

The external disturbance rejection specifications for a FCS design are typically modelled by a constant magnitude for all frequencies as shown in Fig. 2.5, and the stability specifications are expressed in terms of open loop phase and/or gain margins indicated on Fig. 2.6.

*2.1.5 Nominal Plant Selection.* Before QFT boundaries can be generated, a nominal plant must be selected. Selection of a nominal plant is highly dependent on a particular design but some guidelines are presented in the references.[5][7][9] Once selected the nominal plant ( $P_o$ ) is the only plant employed for the remainder of the design. All of the boundaries and compensators are synthesized based on this nominal plant.

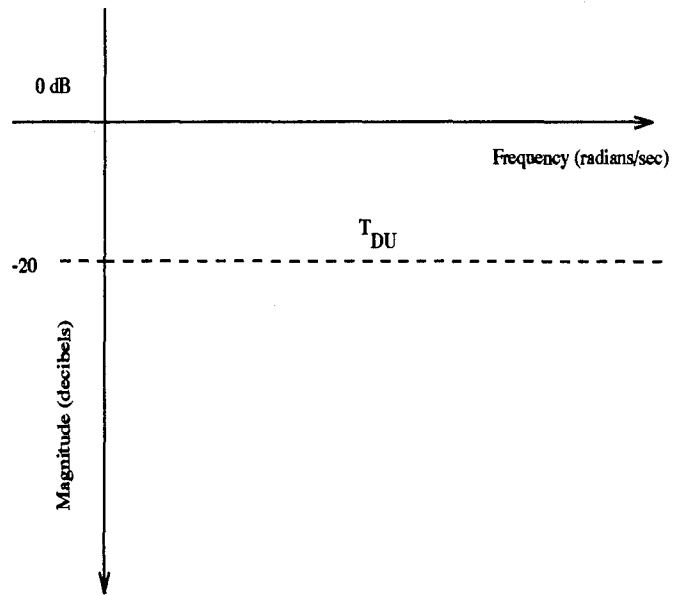


Figure 2.5 Disturbance Specification

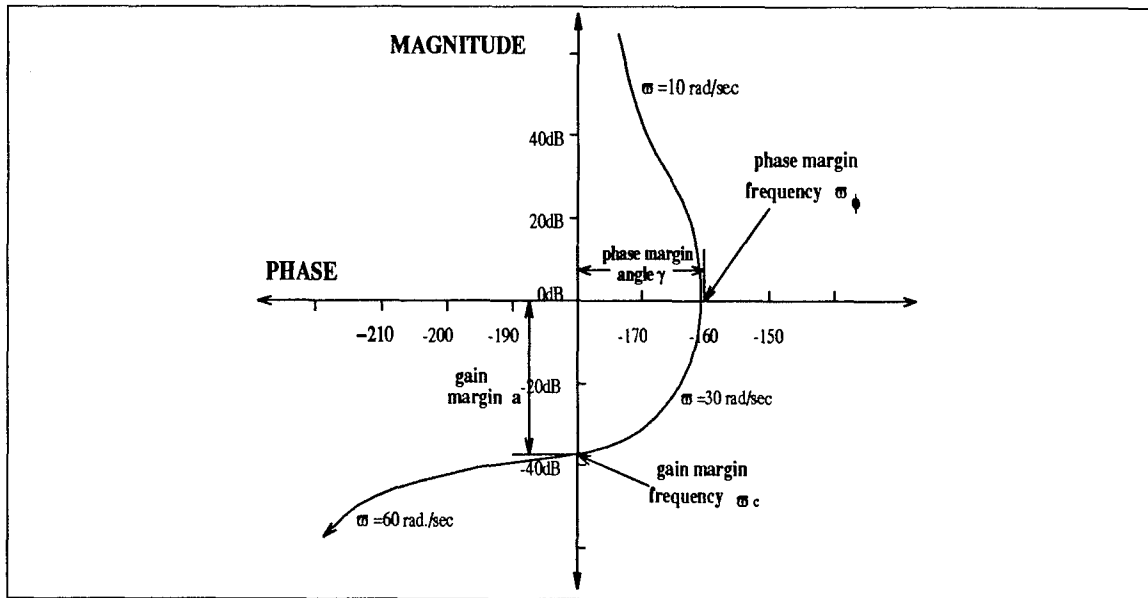


Figure 2.6 Gain Margin/Frequency and Phase Margin/Frequency Definitions

*2.1.6 Nichols Chart QFT Boundaries.* With the frequency templates, design specifications, and nominal plant selection developed in previous sections, the next step of a MISO QFT design is to generate the QFT stability, tracking, disturbance, and composite boundaries. The synthesis of QFT boundaries is a fairly involved process that is left for the references to explain in detail. Fortunately, the designer does not have to be overly concerned with the boundary generation, since the QFT CAD package completely automates this process. Once the frequency templates, and design specifications are loaded, the 'Bounds' option is selected and all of the Nichols chart frequency bounds are established. The tracking and disturbance boundaries ( $B_R(j\omega)$  and  $B_D(j\omega)$ ) are limits associated with particular frequencies plotted on the Nichols chart, and the stability boundaries ( $B_S(j\omega)$ ) are contours encircling the 0 dB -180° point on the Nichols chart. Via QFT CAD, each of these boundaries can be viewed independently or combined in a composite boundary. The composite boundary ( $B_o(j\omega)$ ) represents the most restrictive boundary at each frequency, where the most restrictive boundary requires the most gain to satisfy. Fig. 2.7 shows a sample set of QFT Nichols chart design boundaries. Notice that there is only one boundary for each frequency since this figure represents the composite QFT boundary. With all the boundaries synthesized the designer is now able to intelligently construct the QFT robust compensator  $G$ .

*2.1.7 Loop Shaping - Synthesis of the QFT Compensator.* The compensator  $G$  is synthesized by first mapping the nominal open-loop ( $GP_o(s)$ ) frequency response onto the QFT Nichols chart with its associated stability, tracking, and disturbance boundaries. Poles, and zeros are added and modified along with the gain until the nominal loop meets the QFT composite boundaries. This process of modifying the compensator until the nominal open-loop satisfies the QFT boundaries is known as loop shaping. An example of QFT loop shaping is shown in Fig. 2.8, where the nominal loop wraps around the composite stability bound, or  $M_L$  contour, while maintaining a gain sufficient to clear, or be tangent to, each composite bound shown on the Nichols chart. If the nominal loop intersects the stability contour then a zero must be included to provide the necessary increase in phase to circumvent the contour. If the loop wraps around the  $M_L$  contour exactly but some of the composite boundaries are not satisfied then additional gain must be added and

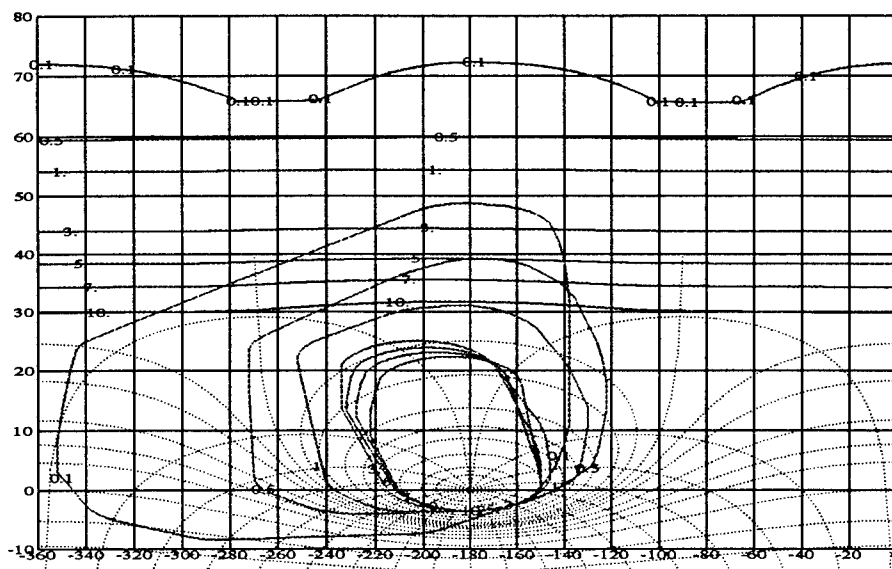


Figure 2.7 QFT Stability  $B_S(j\omega)$  and Composite  $B_o(j\omega)$  Bounds

the poles and zeros readjusted. This “trial and error” approach is performed with ease given the QFT CAD software. This software enables the designer to visualize the tradeoffs between increasing the gain and order of the compensator and meeting the required bounds. Since these tradeoffs are entirely graphical, the engineer can instantaneously determine whether the system meets specifications or whether further modifications are necessary. This instantaneous feedback to the designer dramatically reduces the number of design iterations required to successfully construct the robust compensator.

There are two additional concerns the designer faces while loop shaping. First, the system must be at least Type 1 to achieve zero steady-state error for a step input. Therefore, the compensator must include a pole at the origin if the chosen nominal plant is Type 0. Second, saturation may occur if the system gain is increased without reservation. Though it may be possible to satisfy the composite boundaries for all frequencies by consistently increasing this gain, the resulting compensator may not be implementable due to control surface rate or deflection saturation.

Meeting all the required QFT composite boundaries with the nominal loop transmission function insures that the system has the necessary robustness to guarantee that the closed-loop frequency response of all the plants lies between the upper and lower tracking

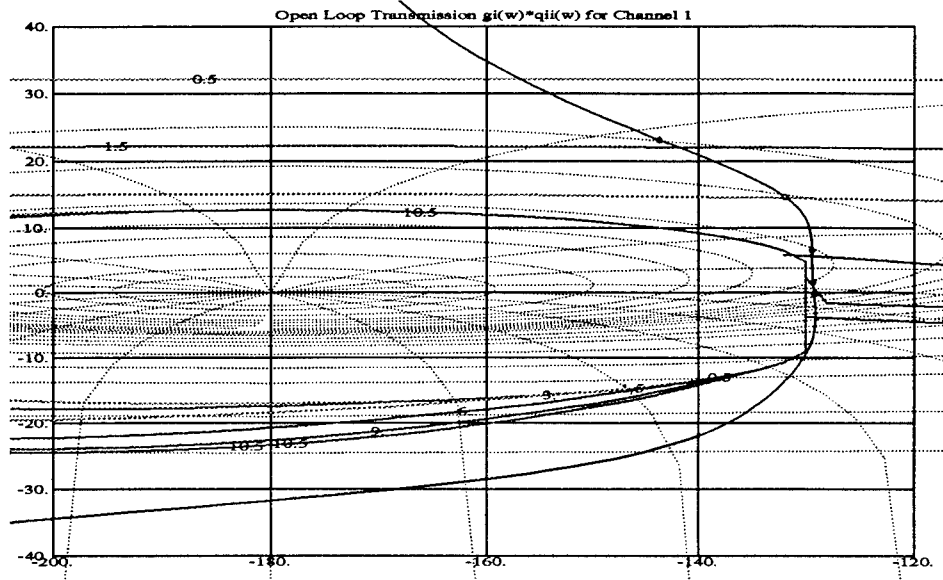


Figure 2.8 QFT Loop Shaping

models in Fig. 2.4, that the system can maintain the required stability margin, and that the system can reject a particular level of external disturbance. It is important to stress that if the nominal loop design satisfies the required QFT bounds then every plant used to synthesize the frequency templates also meets the established specifications. Use of the nominal plant is merely a way of reducing the complexity of the design.

*2.1.8 Prefilter Design.* As Fig. 2.9 illustrates, the compensator ( $G$ ) has provided the system with the required robustness to fit between the tracking models. This robustness, however, does not necessarily insure the system has the desired frequency response characteristics. It is the purpose of the prefilter ( $F$ ) to position the robust tracking response between the upper and lower tracking models as shown in Fig. 2.10. The resulting control ratio with the prefilter included is found in Eq. (2.3).

$$T_R = \frac{FGP}{1 + GP} \quad (2.3)$$

By positioning the closed-loop frequency response between  $T_{R_U}$  and  $T_{R_L}$  a successful MISO QFT design has been completed.

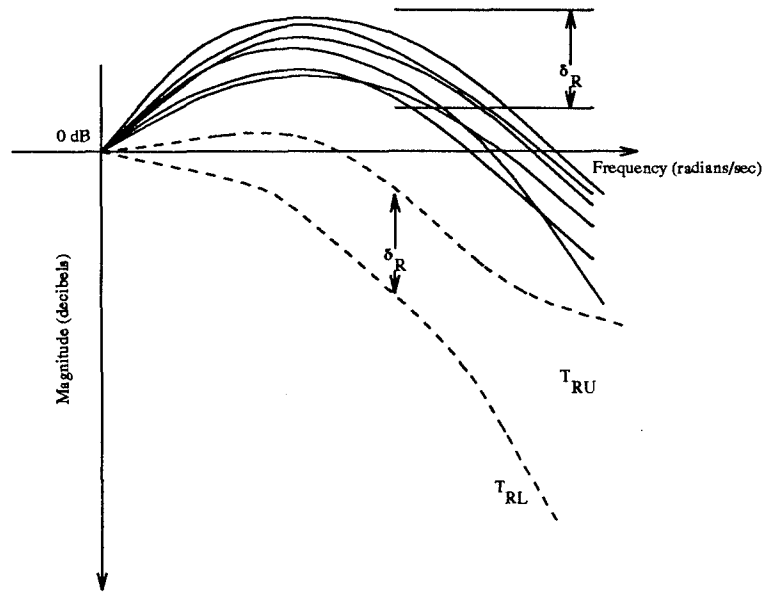


Figure 2.9 Compensated Closed-Loop Frequency Response without Prefilter

*2.1.9 MISO Design Summary.* Before examining the MIMO QFT case, it is helpful to briefly summarize the key features of the MISO development. The setup of the MISO design involves defining the unity gain feedback structure, identifying the region of structured plant parametric uncertainty, establishing the stability, tracking, and disturbance models, and generating the frequency templates. The templates allow the designer to visualize the uncertainty in the design and make some intelligent decisions including selection of the nominal plant. With this plant the QFT composite bounds are formed and the nominal loop is mapped onto the QFT Nichols chart. A compensator is then synthesized in the loop shaping process to clear the associated bounds on the Nichols chart. The last step in the MISO QFT design is to position the tracking responses within the upper and lower tracking models via the prefilter. Thus, a single compensator ( $\mathbf{G}$ ) and prefilter ( $\mathbf{F}$ ) is obtained, and a robust design over a specific region of parametric plant uncertainty is established. This technique contrasts to “point design” methods requiring a set of compensators to guarantee similar robustness.

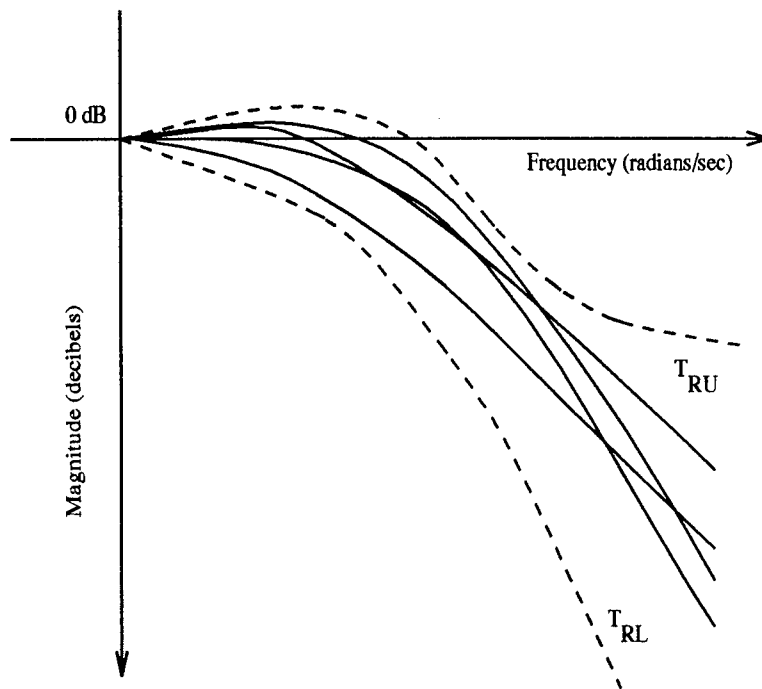


Figure 2.10 Compensated Closed-Loop Frequency Response with Prefilter

## 2.2 MIMO QFT Design

2.2.1 *Structure.* Figure 2.11 represents the general 2X2 QFT MIMO system including an external disturbance. The purpose of this system is to track a desired reference signal  $\mathbf{R}$  while rejecting the effects of the external disturbance  $\mathbf{D}$  on the output  $\mathbf{Y}$ . The corresponding matrices identified in this figure are:

$$\mathbf{F} = \begin{bmatrix} f_1 & 0 \\ 0 & f_2 \end{bmatrix} \mathbf{G} = \begin{bmatrix} g_1 & 0 \\ 0 & g_2 \end{bmatrix} \mathbf{P}_e = \begin{bmatrix} p_{e11} & p_{e12} \\ p_{e21} & p_{e22} \end{bmatrix} \mathbf{P}_D = \begin{bmatrix} p_{d11} \\ p_{d21} \end{bmatrix} \quad (2.4)$$

where

$$\mathbf{P}_e = \mathbf{P}\mathbf{W} \quad (2.5)$$

Unlike the MISO case, solving the MIMO design problem found in Fig. 2.11 yields a complex closed form expression. By treating the MIMO case as  $m^2$  equivalent MISO cases [9] the designer is able to circumvent this complex MIMO expression and focus on the more tractable mathematics associated with the MISO cases.



assumes a diagonal compensator ( $\mathbf{G}$ ) and prefilter ( $\mathbf{F}$ ) found in Eq. 2.4. The control ratio for each diagonal MISO loop is given by

$$t_{ii} = \frac{f_{ii}g_iq_{ii} + d_{ii}q_{ii}}{1 + g_iq_{ii}} = t_{r_{ii}} + t_{d_{ii}} \quad (2.7)$$

$$t_{r_{ii}} = \frac{f_{ii}g_iq_{ii}}{1 + g_iq_{ii}} \quad t_{d_{ii}} = \frac{d_{ii}q_{ii}}{1 + g_iq_{ii}} \quad (2.8)$$

and the off-diagonal control ratios are:

$$t_{ij} = t_{d_{ij}} = \frac{d_{ij}q_{ii}}{1 + g_iq_{ii}} \quad i \neq j \quad (2.9)$$

The  $d_{ij}$  terms in Eqs. (2.8) and (2.9) represent both the external disturbance and cross-coupling disturbance inputs into the system. The relationship established in Eq. (2.10) was developed by Captain Dennis Trosen in his 1993 thesis to incorporate the external disturbance input into the MIMO equivalent MISO systems. [21]

$$d_{ij} = (d_{ext})_{ij} + c_{ij} \quad (2.10)$$

where

$$(d_{ext})_{ij} = \sum_{k=1}^x \left[ \frac{p_{d_{kj}}}{q_{ik}} \right] \quad (2.11)$$

$$c_{ij} = - \sum_{k \neq i}^m \left[ \frac{t_{kj}}{q_{ik}} \right] \quad (2.12)$$

Substituting Eqs. (2.11) and (2.12) into Eq. (2.10):

$$d_{ij} = \sum_{k=1}^x \left[ \frac{p_{d_{kj}}}{q_{ik}} \right] - \sum_{k \neq i}^m \left[ \frac{t_{kj}}{q_{ik}} \right] \quad (2.13)$$

Where  $x$  represents the number of disturbance inputs and  $m$  represents the dimension of the plant matrix ( $\mathbf{P}$ ). These disturbance inputs make the MISO cases truly equivalent to the MIMO system. As for the  $q_{ij}$  terms, they represent the reciprocals of the effective

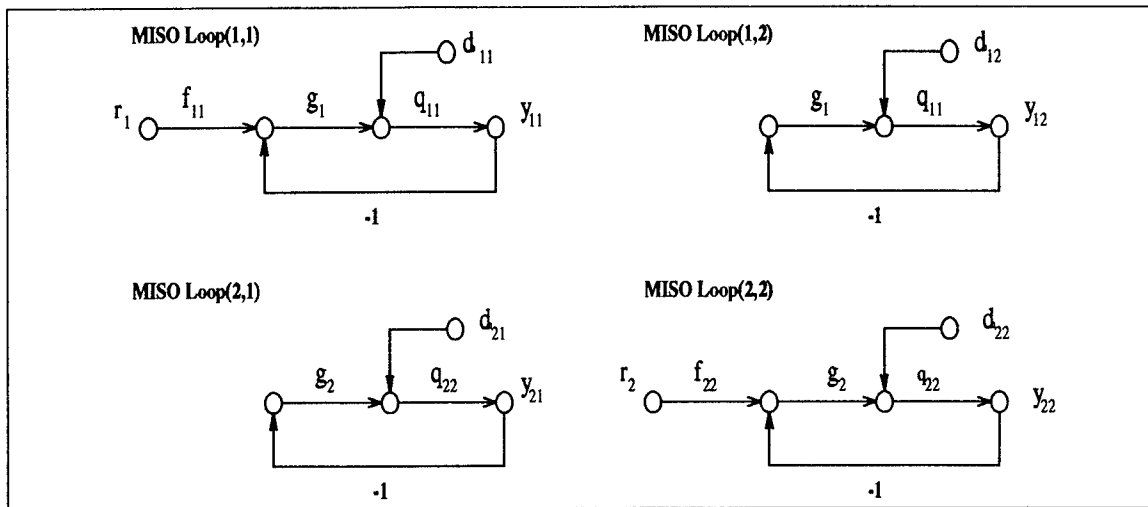


Figure 2.12 Equivalent MISO Loops for MIMO QFT Structure, with Diagonal  $F$  Matrix plant elements. The origin of the  $q_{ij}$  terms is shown in Eqs. (2.14) and (2.15).

$$\mathbf{P}_e^{-1} = \begin{bmatrix} p_{e11}^* & p_{e12}^* \\ p_{e21}^* & p_{e22}^* \end{bmatrix} \quad (2.14)$$

$$\mathbf{Q} = \begin{bmatrix} q_{11} & q_{12} \\ q_{21} & q_{22} \end{bmatrix} = \begin{bmatrix} \frac{1}{p_{e11}^*} & \frac{1}{p_{e12}^*} \\ \frac{1}{p_{e21}^*} & \frac{1}{p_{e22}^*} \end{bmatrix} \quad (2.15)$$

For complete treatment of this equivalence between the MIMO and the  $m^2$  cases the reader is directed to the references. [5] [8] [21]

Before examining the plant models in Chap. III some details concerning the time simulations and design guidelines need to be addressed.

### 2.3 Time simulations

The time simulations are achieved via the *Matlab* Runge Kutta 45 numerical integration routine and *Simulink*. [2][20] The step size is limited to  $10^{-4}$  seconds, and the integrators are set with zero initial conditions. For the maximum command responses, rate and deflection saturation limits are incorporated in the design. These limits are imposed via *Simulink's* *Saturation* and *Rate Limiter* functions.

Control Surface	Deflection Limit	Rate Limit
Horizontal Tail	±20 degrees	60 degrees/sec
Differential Tail	±7 degrees	60 degrees/sec
Flaperons	±20 degrees	60 degrees/sec
Rudder	±30 degrees	60 degrees/sec

Table 2.1 Control Surface Rate and Deflection Limits for the VISTA F-16

#### 2.4 Design Guidelines

Some additional guidelines are:

1. The bandwidth of concern is 0.5 to 3.5 rps in agreement with previous research and the MILSTD 1797A that has established this frequency range as the pilot's bandwidth.
2. The bending modes for the VISTA are isolated to frequencies above 30 rps. Therefore it is essential that the phase margin frequency  $\omega_\phi$  is below 30 rps. In a QFT design this can be accomplished by locating the nominal plant at the highest (largest relative magnitude) point on the 30 rps frequency templates to insure a 30° phase margin for the rest of the design plants.
3. To facilitate transformation of this analog design to an actual digital Flight Control Computer (FCC) the poles and zeros of the controllers can not exceed 60 rps. This figure is calculated based on a 50 Hz sampling rate which is typical of a modern FCC.
4. Following Phillips' design, the compensator gain is limited by real world constraints such as rate and deflection saturation limits. The actual control surface saturation and rate limits for the VISTA F-16 can be found in Table 2.1.
5. To achieve the primary goal of this design, compensators are to be constructed for the longitudinal and lateral/directional channels that provide nominal flight control for the healthy aircraft and stabilization and debilitated performance for the failed cases. Satisfying these demands may require that the performance of the healthy aircraft is sacrificed to provide adequate robustness for the more severe failures. Ultimately the aircraft must be able to meet Level 1, 2 or 3 flying quality specifications for the failed aircraft and Level 1 or 2 for the healthy aircraft.

### III. VISTA F-16 Aircraft Model

This chapter examines the modelling of the healthy VISTA (Variable In-flight Stability Test Aircraft) F-16, including the longitudinal, lateral/directional, and actuator models. Further information concerning control effector failure modeling follow in Chap. IV.

To quantify the parameter uncertainty involved in the subsonic flight envelope of the VISTA F-16 FCS design, which includes changes in the aircraft CG, linear time-invariant (LTI) aircraft models are generated that span the airspeed-altitude-CG parameter space. These aircraft models are used as the plants in the ensuing QFT design.

#### 3.1 VISTA F-16

The two seat VISTA F-16 is a modification of the F-16D model, adding additional flight control components such as the variable stability flight control system (VSS), and the additional weight that can be attributed to these components. The VSS provides the evaluation pilot with the real flight motions, accelerations, and handling qualities he would feel if seated in the cockpit of a simulated aircraft [22]. The schematic of the VISTA and accompanying basic aircraft data can be found on Fig. 3.1 and on Table 3.1.

#### 3.2 Flight Scenarios

As an extension of Phillips' work, this research includes the full subsonic envelope of the VISTA F-16 from 1,000 to 50,000 feet and from 0.2 to 0.8 Mach with the following configuration variations:

1. Clean(no external fuel tanks)

Basic Data for VISTA F-16	
Wing Area	323.20 SQ FT
V Tail Area	54.80 SQ FT
Rudder Area	11.65 SQ FT
Aileron Area	26.56 SQ FT
Stabilator Area	63.70 SQ FT

Table 3.1 Basic Aircraft Data

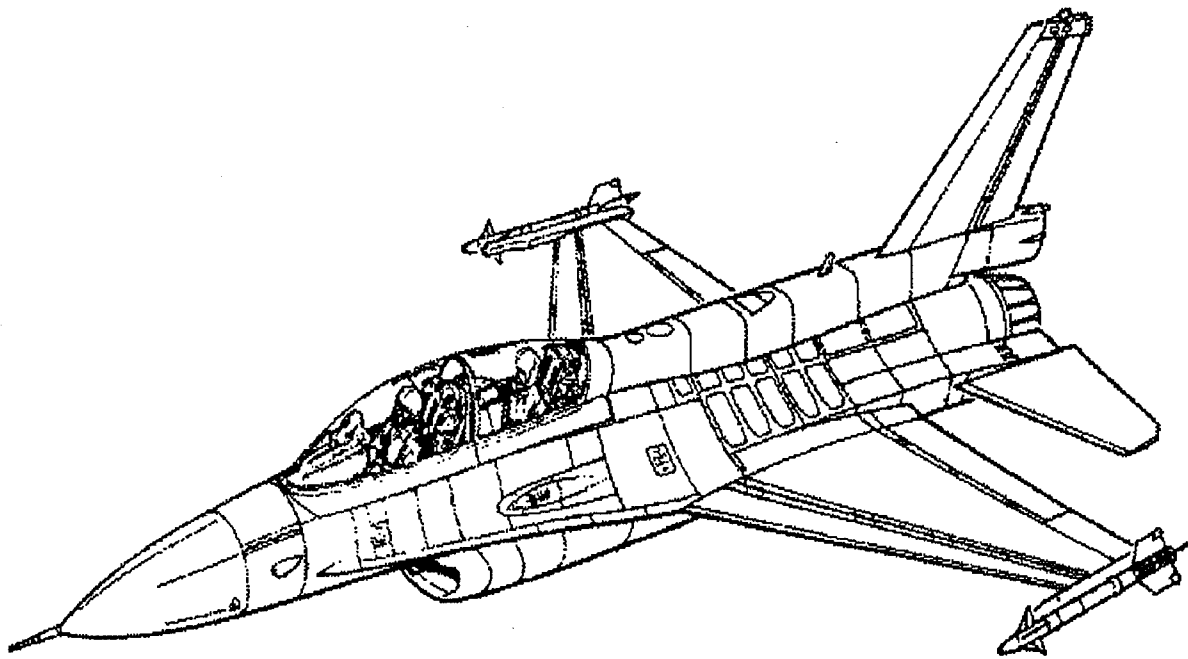


Figure 3.1 VISTA F-16

2. Centerline fuel tank

3. Two wing tanks

Phillips also included a three tank configuration at the beginning of his research but later abandoned this set up in lieu of generating a higher-order compensator to satisfy the increase in plant parameter uncertainty. Therefore, in this research the 3 tank configuration is also not included.

It is important to note that the LTI models originated from the Simulated Rapid Prototyping Facility(SRF) at WL/FIGS and that this program did not initialize at low airspeeds when loaded with certain tank configurations. This failure to initialize manifested as “strange behavior at the left edge of the flight envelope”[6] when Phillips’ design was loaded into the *Aviator* nonlinear simulator. Therefore the current design may also exhibit the similar behavior since the failure models are based on Phillips’ original 282 plants. More detailed information including procedures used by Reynolds and Phillips in determining SRF plants for the left side of the flight envelope can be found in the literature [16]. As an addition to the configuration variation introduced by Phillips, this research examines the effects of control effector failures. These failure cases are explained in Chap. IV.

### *3.3 LTI Aircraft Model Generation*

The LTI aircraft models were generated by Major Phillips in his 1994 Thesis [15]. The SRF trims the aircraft at a selected altitude, airspeed and CG within its flight envelope, then linearizes the aircraft’s equations of motion about this selected operating point. In this process of linearizing the nonlinear aircraft equations of motion, the SRF utilizes a database of VISTA wind tunnel data to determine the stability derivatives in the form of state-space **A** and **B** matrices. The arrangement of the stability derivatives in the

State	Units
$\theta$	deg
$u$	ft/sec
$\alpha$	deg
$q$	deg/sec
$\phi$	deg
$\beta$	deg
$p$	deg/sec
$r$	deg/sec

Table 3.2 Units of Aircraft Model States

state-space equation  $\dot{\mathbf{x}} = \mathbf{Ax} + \mathbf{Bu}$  is shown in Eq. 3.1.

$$\begin{bmatrix} \dot{\theta} \\ \dot{u} \\ \dot{\alpha} \\ \dot{q} \\ \dot{\phi} \\ \dot{\beta} \\ \dot{p} \\ \dot{r} \end{bmatrix} = \begin{bmatrix} 0 & 0 & 0 & 1 & 0 & 0 & 0 & 0 \\ X_{\theta} & X_u & X_{\alpha} & X_q & 0 & 0 & 0 & 0 \\ Z_{\theta} & Z_u & Z_{\alpha} & Z_q & 0 & 0 & 0 & 0 \\ M_{\theta} & M_u & M_{\alpha} & M_q & 0 & 0 & 0 & 0 \\ 0 & 0 & 0 & 0 & 0 & 0 & 1 & \phi_r \\ 0 & 0 & 0 & 0 & Y_{\phi} & Y_{\beta} & Y_p & Y_r \\ 0 & 0 & 0 & 0 & 0 & L_{\beta} & L_p & L_r \\ 0 & 0 & 0 & 0 & 0 & N_{\beta} & N_p & N_r \end{bmatrix} \begin{bmatrix} \theta \\ u \\ \alpha \\ q \\ \phi \\ \beta \\ p \\ r \end{bmatrix} \tag{3.1}$$

$$+ \begin{bmatrix} 0 & 0 & 0 & 0 & 0 \\ X_{\delta_{elev}} & 0 & X_{\delta_{flap}} & 0 & 0 \\ Z_{\delta_{elev}} & 0 & Z_{\delta_{flap}} & 0 & 0 \\ M_{\delta_{elev}} & 0 & M_{\delta_{flap}} & 0 & 0 \\ 0 & 0 & 0 & 0 & 0 \\ 0 & Y_{\delta_{aftail}} & 0 & Y_{\delta_{ail}} & Y_{\delta_{rud}} \\ 0 & L_{\delta_{aftail}} & 0 & L_{\delta_{ail}} & L_{\delta_{rud}} \\ 0 & N_{\delta_{aftail}} & 0 & N_{\delta_{ail}} & N_{\delta_{rud}} \end{bmatrix} \begin{bmatrix} \delta_{elev} \\ \delta_{aftail} \\ \delta_{flap} \\ \delta_{ail} \\ \delta_{rud} \end{bmatrix}$$

The units of each of the states listed in Eq. (3.1) are listed in Table 3.2. It is evident from this state-space representation that the longitudinal and lateral channels are considered

completely decoupled. This is consistent with the steady level trim conditions at which the plants are generated.

### 3.4 Longitudinal Aircraft Model

The state space longitudinal aircraft model extracted from Eq. (3.1) is

$$\begin{bmatrix} \dot{\theta} \\ \dot{u} \\ \dot{\alpha} \\ \dot{q} \end{bmatrix} = \begin{bmatrix} 0 & 0 & 0 & 1 \\ X_{\theta} & X_u & X_{\alpha} & X_q \\ Z_{\theta} & Z_u & Z_{\alpha} & Z_q \\ M_{\theta} & M_u & M_{\alpha} & M_q \end{bmatrix} \begin{bmatrix} \theta \\ u \\ \alpha \\ q \end{bmatrix} + \begin{bmatrix} 0 \\ X_{\delta_{elev}} \\ Z_{\delta_{elev}} \\ M_{\delta_{elev}} \end{bmatrix} \begin{bmatrix} \delta_{elev} \end{bmatrix}. \quad (3.2)$$

The flap function of the F-16 flaperons is selected only during the takeoff and landing phases of flight. Since this design is only concerned with the MILSTD Category A nonterminal phase of flight, the  $\delta_{flap}$  control input is eliminated.

Pilot control inputs are typically spaced no further apart than five seconds, so five seconds is accepted as an appropriate time period of interest in manual flight control system design. Due to the dominance of the short period mode in this time scale following a control input, the short period approximation is used in the longitudinal channel design process. The resulting short period approximation state-space model is shown in Eq. (3.3).

$$\begin{bmatrix} \dot{\alpha} \\ \dot{q} \end{bmatrix} = \begin{bmatrix} Z_{\alpha} & Z_q \\ M_{\alpha} & M_q \end{bmatrix} \begin{bmatrix} \alpha \\ q \end{bmatrix} + \begin{bmatrix} Z_{\delta_{elev}} \\ M_{\delta_{elev}} \end{bmatrix} \begin{bmatrix} \delta_{elev} \end{bmatrix} \quad (3.3)$$

In Eq. (3.3), the control input  $\delta_{elev}$  refers to the symmetric deflection of the VISTA's horizontal stabilator.

The corresponding state-space output equation  $y = \mathbf{C}\mathbf{x} + \mathbf{D}u$  for this short period longitudinal system is,

$$y = \begin{bmatrix} 1 & 0 \\ 0 & 1 \end{bmatrix} \begin{bmatrix} \alpha \\ q \end{bmatrix} + \begin{bmatrix} 0 \\ 0 \end{bmatrix} \begin{bmatrix} \delta_{elev} \end{bmatrix}. \quad (3.4)$$

Finally to establish the convention that positive elevator deflection results in positive changes in  $q$  and  $\alpha$ , the sign of the SRF generated  $\mathbf{B}$  matrix of Eq. (3.3) is negated.

Since the SRF linearization scheme completely decouples the longitudinal and lateral/direction channels (Eq. (3.1)), the  $\delta_{flap}$  is eliminated as a control input, and the short period approximation is applied, the resulting longitudinal system appears to be a 2nd-order single-input single-output (SISO) system. However as Chap. IV explains, control effector failure induces an additional input into the system, yielding a multiple-input single-output (MISO) system.

### 3.5 Lateral/Directional Aircraft Model

Unlike the longitudinal channel where the short period approximation is made, the full lateral state-space model including the roll, dutch roll, and spiral modes is used in the lateral channel design. The lateral state-space model extracted from Eq. (3.1) is listed in Eq. (3.5).

$$\begin{aligned} \begin{bmatrix} \dot{\phi} \\ \dot{\beta} \\ \dot{p} \\ \dot{r} \end{bmatrix} &= \begin{bmatrix} 0 & 0 & 1 & \phi_r \\ Y_\phi & Y_\beta & Y_p & Y_r \\ 0 & L_\beta & L_p & L_r \\ 0 & N_\beta & N_p & L_r \end{bmatrix} \begin{bmatrix} \phi \\ \beta \\ p \\ r \end{bmatrix} \\ &+ \begin{bmatrix} 0 & 0 & 0 \\ Y_{\delta_{ftail}} & Y_{\delta_{ail}} & Y_{\delta_{rud}} \\ L_{\delta_{ftail}} & L_{\delta_{ail}} & L_{\delta_{rud}} \\ N_{\delta_{ftail}} & N_{\delta_{ail}} & N_{\delta_{rud}} \end{bmatrix} \begin{bmatrix} \delta_{ftail} \\ \delta_{ail} \\ \delta_{rud} \end{bmatrix} \end{aligned} \quad (3.5)$$

In Eq. (3.5) the three control inputs  $\delta_{ftail}$ ,  $\delta_{ail}$ , and  $\delta_{rud}$  correspond to differential deflection of the horizontal stabilator, aileron deflection, and rudder deflection, respectively.

The corresponding state-space output equation  $y = \mathbf{C}\mathbf{x} + \mathbf{D}u$  for the lateral system is,

$$y = \begin{bmatrix} 1 & 0 & 0 & 0 \\ 0 & 1 & 0 & 0 \\ 0 & 0 & 1 & 0 \\ 0 & 0 & 0 & 1 \end{bmatrix} \begin{bmatrix} \phi \\ \beta \\ p \\ r \end{bmatrix} + \begin{bmatrix} 0 & 0 & 0 \\ 0 & 0 & 0 \\ 0 & 0 & 0 \\ 0 & 0 & 0 \end{bmatrix} \begin{bmatrix} \delta_{aftail} \\ \delta_{ail} \\ \delta_{rud} \end{bmatrix} \quad (3.6)$$

Similar to the action taken in the longitudinal channel, the sign of the SRF generated  $\mathbf{B}$  matrix of Eq. (3.5) is negated. This action establishes the convention that positive aileron and differential tail deflection results in a positive change in  $p$  and the convention that a positive rudder deflection results in a positive change in  $r$  and a negative change in  $\beta$ .

Ultimately the lateral plant model represents a 3 X 2 aircraft system with an additional disturbance input added to model coupling of the lateral/directional and longitudinal aircraft channels as explained in Chap. IV.

### 3.6 Transfer Function Generation

The LTI aircraft models developed in previous sections must be manipulated into the transfer function format for input into the QFT CAD. The development of these transfer function matrices follows from the state-space representation identified in Eqs. (3.7) and (3.8), where the the disturbance  $\mathbf{\Gamma}$  matrix is discussed in Chap. III.

$$\dot{\mathbf{x}}(t) = \mathbf{A}\mathbf{x}(t) + \mathbf{B}\mathbf{u}(t) + \mathbf{\Gamma}d(t) \quad (3.7)$$

$$\mathbf{y}(t) = \mathbf{C}\mathbf{x}(t) \quad (3.8)$$

Transforming Eqs. (3.7) and (3.8) into the Laplace domain and manipulating the state space representation into transfer function format:

$$\mathbf{y}(s) = \mathbf{P}(s)\mathbf{u}(s) + \mathbf{P}_D(s)\mathbf{d}(s) \quad (3.9)$$

where:

$$\mathbf{P}(s) = \mathbf{C}[s\mathbf{I} - \mathbf{A}]^{-1}\mathbf{B} \quad (3.10)$$

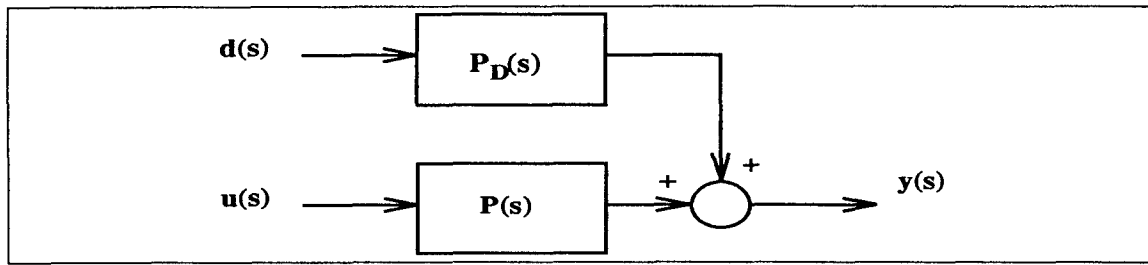


Figure 3.2 Block Diagram of Plant and External Disturbance Input

$$\mathbf{P}_D(s) = \mathbf{C}[s\mathbf{I} - \mathbf{A}]^{-1}\mathbf{\Gamma} \quad (3.11)$$

Equation 3.9 is symbolically represented in Fig. 3.2.

Substituting Eqs. (3.10) and (3.11) into Eq. (3.9):

$$\mathbf{y}(s) = \mathbf{C}[s\mathbf{I} - \mathbf{A}]^{-1}\mathbf{B}\mathbf{u} + \mathbf{C}[s\mathbf{I} - \mathbf{A}]^{-1}\mathbf{\Gamma}\mathbf{d}(s) \quad (3.12)$$

Finally, Eq. (3.9) is automated via the 'ss2tf' *Matlab* function and the appropriate transfer function matrices ( $\mathbf{P}$  and  $\mathbf{P}_D$ ) are generated.

### 3.7 Actuator Model

The fourth-order actuator model used in Reynold's thesis is also chosen for this design and has the transfer function given in Eq. (3.13).

$$\frac{\delta_{control}(s)}{\delta_{control(cmd)}(s)} = \frac{(20.2)(71.4)^2(144.8)}{(s + 20.2)(s + 144.8)[s^2 + 2(0.736)(71.4)s + (71.4)^2]} \quad (3.13)$$

The "control" subscript in Eq. (3.13) refers to any of the control surfaces of the aircraft. As discussed in Reynold's thesis, a fourth-order model is chosen to replace the simpler first-order model because the higher-order model adds approximately 50 degrees of phase lag to the system at 30 rps and even more at higher frequencies. This additional phase lag has a significant impact on the designer's ability to stabilize the system, and, as Reynolds suggests, "should always be used in robust control design"[16].

#### IV. Control Surface Failure Modeling

Aerodynamic control effector failures have two significant effects on an airframe. The first, and most direct, effect is the attenuation of the forces and moments the control surfaces can generate. The second, and less obvious effect of aerodynamic control surface damage, is the alteration of an aircraft's dynamics as represented by its stability derivatives. In 1993 Captain Mark Keating derived the equations to model the effect of control surface failures on an aircraft's control and stability derivatives. Though these equations were developed for the Lambda Unmanned Research Vehicle (URV), they can be adapted to accommodate any airframe. This chapter overviews Keating's pioneering work and develops the modifications needed to adapt his failure model to the VISTA F-16.

##### 4.1 Longitudinal Stability and Control Derivatives

The effect of control surface failure can be determined by analyzing the three non-dimensionalized longitudinal equations of motion found, e.g., in Blakelock [2].

$$\left(\frac{mU}{S\bar{q}}\dot{u} - C_{x_u}u\right) + \left(-\frac{c}{2U}C_{x_\alpha}\dot{\alpha} - C_{x_\alpha}\alpha\right) + \left(-\frac{c}{2U}C_{x_q}\dot{\theta} - C_w(\cos\Theta)\theta\right) = C_{x_{\delta_e}}\delta_e \quad (4.1)$$

$$-C_{z_u}u + \left(\frac{mU}{S\bar{q}} - \frac{c}{2U}C_{z_\alpha}\right)\dot{\alpha} - C_{z_\alpha}\alpha + \left(-\frac{mU}{S\bar{q}} - \frac{c}{2U}C_{z_q}\right)\dot{\theta} - C_w(\sin\Theta)\theta = C_{z_{\delta_e}}\delta_e \quad (4.2)$$

$$-C_{m_u}u + \left(\frac{c}{2U}C_{m_\alpha}\dot{\alpha} - C_{m_\alpha}\alpha\right) + \left(\frac{I_y}{S\bar{q}c}\ddot{\theta} - \frac{c}{2U}C_{m_q}\dot{\theta}\right) = C_{m_{\delta_e}}\delta_e \quad (4.3)$$

Keating made the following assumptions:

1. Fuselage effects are negligible.
2. Control surface failure has a negligible impact on the stability derivatives in the longitudinal Eq. (4.1), consequently this equation can be removed from consideration.
3. The (battle) damage does not change the aircraft's mass significantly, thus  $C_w$  can be neglected.

Eliminating Eq. (4.1) leaves only the  $Z$  equation (Eq. (4.2)) and the  $M$  equation (Eq. (4.3)) to be analyzed, which are utilized in the current research since only the short period dynamics are of interest.

4.1.1 *M Equation Analysis.* Some further simplifications to Eq. (4.3) can be made by neglecting  $C_{m_u}$  and  $C_{m_{\dot{\alpha}}}$ .  $C_{m_u}$  is due primarily to the lift generated on the wing, thus elevator damage has little effect on this stability derivative, and  $C_{m_{\dot{\alpha}}}$  accounts for downwash effects which are assumed to be negligible (see Chap. I). Eliminating the aforementioned stability derivatives leaves only the changes in  $C_{m_\alpha}$ ,  $C_{m_q}$  and  $C_{m_{\dot{\epsilon}_e}}$  to be considered.

First, the  $C_{m_\alpha}$  stability derivative is discussed. The purpose of this derivation is to isolate the moment generated by the wing-body structure from the moment generated by the tail section. By isolating moments the effects of tail surface removal can be determined explicitly. From Roskam Eq.(4.21)[17] the total aerodynamic moment  $M_A$  is expressed as

$$M_A = \bar{q} S_w \bar{c} C_{M_{total}} \quad (4.4)$$

where  $\bar{q}$  is the dynamic pressure,  $S_w$  is the aerodynamic area of the wing,  $\bar{c}$  is the mean aerodynamic chord (MAC), and  $C_{M_{total}}$  is the total aerodynamic moment defined in Eq. (4.7).

$$C_{M_{total}} = C_{M_{total_1}} + C_{M_{total_2}} \quad (4.5)$$

where

$$C_{M_{total_1}} = (C_{L_{\sigma_{wb}}} + C_{L_{\alpha_{wb}}} \alpha) (\bar{X}_{CG} - \bar{X}_{AC_{wb}}) \quad (4.6)$$

$$C_{M_{total_2}} = C_{m_{AC_{wb}}} - C_{L_{\alpha_t}} \eta_t \frac{S_t}{S_w} (\bar{X}_{AC_t} - \bar{X}_{CG}) \left[ \alpha + (\epsilon_o + \frac{d\epsilon}{dt} \alpha) + i_t \right] \quad (4.7)$$

The substitutions in Eqs. (4.8) through (4.13) are made to further simplify Eqs. (4.6) and (4.7).

$$a_t \equiv C_{L_{\alpha_t}} \quad (4.8)$$

$$a_w \equiv C_{L_{\alpha_{wb}}} \quad (4.9)$$

$$l_t \equiv (\bar{X}_{AC_t} - \bar{X}_{CG}) \quad (4.10)$$

$$\Delta X_{CG} \equiv (\bar{X}_{CG} - \bar{X}_{AC_{wb}}) \quad (4.11)$$

$$\eta_t \equiv \frac{\bar{q}_t}{\bar{q}} \quad (4.12)$$

$$k \equiv \frac{d\epsilon}{dt} \quad (4.13)$$

Where  $a_t$  and  $a_w$  represent the slopes of the tail and wing lift vs.  $\alpha$  curve respectively,  $\Delta X_{CG}$  is the distance between the aircraft center of gravity and the aerodynamic center of the wing-body ( $wb$ ),  $l_t$  is the effective distance between the aerodynamic center of the horizontal stabilator and the aircraft's center of gravity,  $\eta_t$  is the dynamic pressure attenuation ratio at the tail, and  $k$  is the downwash angle gradient. For the VISTA F-16  $a_t$  and  $a_w$  are assumed to be nearly identical and are determined along with  $\Delta X_{CG}$  from the SRF data for each plant case. The effective tail arm length  $l_t$  is extrapolated from the VISTA F-16 schematic as the distance between the tail and the nominal center of gravity at FS320.654, approximately 15.86 feet. A dynamic pressure ratio  $\eta_t$  of 0.90, and a downwash gradient  $k$  of 0.33 are used in this design. The interested reader is directed to the literature [17] for a more detailed explanation of these last two constants.

Making the appropriate substitutions into Eq. (4.5):

$$C_{M_{total}} = (C_{L_{o_{wb}}} + a_w \alpha) \Delta X_{CG} + C_{m_{AC_{wb}}} - a_t \eta_t \frac{S_t}{S_w} l_t (1 - k) \alpha \quad (4.14)$$

Eq. (4.14) is then substituted into Eq. (4.4) and rewritten as:

$$M_{total} = \bar{q} S_w \bar{c} \left[ (C_{L_{o_{wb}}} + a_w \alpha) \Delta X_{CG} + C_{m_{AC_{wb}}} - a_t \eta_t \frac{S_t}{S_w} l_t (1 - k) \alpha \right] \quad (4.15)$$

The total aerodynamic moment in Eq. (4.15) can be subdivided into a moment due to the wing and a moment due to the tail as shown in Eq. (4.16).

$$M_{total} = M_{wing} + M_{tail} \quad (4.16)$$

By regrouping terms in Eq. (4.15) corresponding to Eq. (4.16) the following two equations emerge.

$$M_{wing} = \bar{q} S_w \bar{c} \left[ (C_{L_{o_{wb}}} + a_w \alpha) \Delta X_{CG} + C_{m_{AC_{wb}}} \right] \quad (4.17)$$

$$M_{tail} = -\bar{q} \bar{c} a_t \eta_t S_t l_t (1 - k) \alpha \quad (4.18)$$

Assuming that the lift coefficient at  $\alpha = 0$  ( $C_{L_{o_w b}}$ ) and the moment coefficient due to the difference between the wing aerodynamic center and the center of gravity ( $C_{m_{AC_{w_b}}}$ ) terms do not change with removal of tail surface area, Keating's Eqs. (3.4) and (3.5), respectively, are:

$$M_{wing} = \bar{q}\bar{c}S_w a_w \Delta X_{CG} \alpha \quad (4.19)$$

$$M_{tail} = -\bar{q}\bar{c}\eta_t S_t a_t l_t (1 - k) \alpha \quad (4.20)$$

Unlike the URV, the  $\Delta X_{CG}$  for the VISTA is negative since the aircraft is statically unstable. Therefore both  $M_{wing}$  and  $M_{tail}$  are negative and hence develop a negative  $M_{total}$  shown in Eq. (4.21).

$$-M_{total} = \bar{q}\bar{c} [S_w a_w \Delta X_{CG} + \eta_t S_t a_w l_t (1 - k)] \alpha \quad (4.21)$$

Now  $M_{total}$  is defined as  $-(M_{\alpha UF})\alpha$  or in other words the dimensional stability derivative for the undamaged aircraft (UF) multiplied by  $\alpha$ .

$$M_{\alpha UF} = \bar{q}\bar{c} [S_w a_w \Delta X_{CG} + \eta_t S_t a_w l_t (1 - k)] \quad (4.22)$$

The VISTA F-16 does not have trailing edge elevators as on the URV, therefore the damaged area of the horizontal stabilator corresponds to the damaged area of the elevator. This difference in the design of the elevator between Lambda and VISTA simplifies some of Keating's equations in application to the VISTA F-16 failure problem; for example, Keating defined an additional damage variable  $\zeta'_e$  found in Eq. (4.23)

$$\zeta'_e = \frac{(\zeta_e - 1)S_e + S_t}{S_t} \quad (4.23)$$

to isolate the damage to the control effector rather than effecting the entire horizontal stabilator. However in the VISTA F-16 (see Table 3.1), the aerodynamic area of the elevator ( $S_e$ ) and the aerodynamic area of the tail ( $S_t$ ) are identical hence  $\zeta'_e = \zeta_e$ . This  $\zeta_e$  replacement is made throughout the longitudinal channel failure analysis to modify Keating's equations to the VISTA F-16.

With a damaged elevator, the dimensional stability derivative ( $M_{\alpha F}$ ) becomes:

$$M_{\alpha F} = \bar{q}\bar{c} [S_w a_w \Delta X_{CG} + \zeta_e \eta_t S_t a_w l_t (1 - k)] \quad (4.24)$$

where  $\zeta_e$  is added to Eq. (4.22) representing the proportion of tail area remaining after damage. If  $\zeta_e = 1$  then the aircraft remains undamaged and if  $\zeta_e = .75$  then the aircraft has experienced a 25% reduction in horizontal stabilator area.

The effect on  $C_{m_\alpha}$  can be expressed in terms of the change in dimensional stability derivatives ( $\Delta M_\alpha$ ) where

$$\Delta M_\alpha = M_{\alpha UF} - M_{\alpha F} \quad (4.25)$$

Substituting Eqs. (4.22) and (4.24) into Eq. (4.25) yields

$$\Delta M_\alpha = \bar{q}\bar{c} [(1 - \zeta_e) \eta_t S_t a_w l_t (1 - k)] \quad (4.26)$$

To non-dimensionalized this change, Eq. (4.26) is divided by Eq. (4.24).

$$\frac{\Delta M_\alpha}{M_\alpha} = \frac{(1 - \zeta_e) \eta_t S_t a_w l_t (1 - k)}{[S_w a_w \Delta X_{CG} + \zeta_e \eta_t S_t a_w l_t (1 - k)]} \quad (4.27)$$

This ratio represents the fraction of  $C_{m_{\alpha UF}}$  which has been lost due to damage. Therefore, the first damaged dimensionless stability derivative is

$$C_{m_{\alpha F}} = C_{m_{\alpha UF}} \left[ 1 - \left( \frac{\Delta M_\alpha}{M_\alpha} \right) \right] \quad (4.28)$$

Figure 4.1 shows the relationship between the damage level ( $1 - \zeta_e$ ) and the change in the nondimensional stability derivative  $C_{m_{\alpha F}}$ . From this figure it can be seen that as  $\zeta_e$  decreases, or, as the damage level increases,  $C_{m_{\alpha F}}$  decreases. This is the anticipated result, because it indicates that the system becomes increasingly unstable without the stabilizing effect of the healthy horizontal stabilator.

The remaining derivatives,  $C_{m_q}$  and  $C_{m_{\dot{\delta}_e}}$ , show a simple proportional relationship between the effective area of the tail and the respective value of the stability derivative.

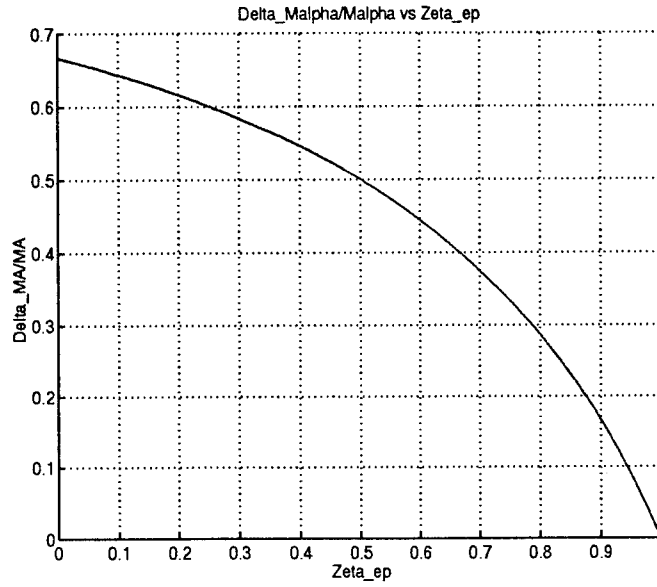


Figure 4.1  $\frac{\Delta M_\alpha}{M_\alpha}$  vs.  $\zeta_e$

These relationships are shown in Eqs. (4.29) and (4.30).

$$C_{m_{qF}} = \zeta_e C_{m_{qUF}} \quad (4.29)$$

$$C_{m_{\delta_e F}} = \zeta_e C_{m_{\delta_e UF}} \quad (4.30)$$

**4.1.2 Z Equation Analysis.** Eq. (4.2) (repeated below) describes the forces in the z-axis direction.

$$-C_{z_u} u + \left( \frac{mU}{S\bar{q}} - \frac{c}{2U} C_{z_{\dot{\alpha}}} \right) \dot{\alpha} - C_{z_\alpha} \alpha + \left( -\frac{mU}{S\bar{q}} - \frac{c}{2U} C_{z_q} \right) \dot{\theta} - C_w (\sin \Theta) \theta = C_{z_{\delta_e}} \delta_e \quad (4.31)$$

Following a similar line of reasoning employed for the  $M$  equation analysis, the  $u$  and  $\dot{\alpha}$  stability derivatives as well as  $C_w$  are neglected. The analysis for  $C_{z_\alpha}$  is nearly identical to  $C_{m_\alpha}$ , with the goal of the ensuing derivation to once again isolate the effects of the wing-body and tail airframe components on the aircraft's dynamics. In this situation, however, the forces in the z direction are examined and not the moments they generate.

Once again, isolating the effects of the wing and body Eq. (4.32) emerges.

$$Z_{total} = Z_{wing} + Z_{tail} \quad (4.32)$$

where Eqs. (4.33) and (4.34) are developed by removing the moment arm from Eqs. (4.19) and (4.20) and conforming to the convention that the lift acts in the negative z direction.

$$Z_{wing} = -\bar{q}S_w a_w \alpha \quad (4.33)$$

$$Z_{tail} = -\bar{q}\eta S_t a_t (1 - k) \alpha \quad (4.34)$$

Substituting Eqs. (4.33) and (4.34) into (4.32) yields:

$$Z_{total} = -\bar{q}\alpha [S_w a_w + \eta S_t a_t (1 - k)] \quad (4.35)$$

Now  $Z_{total}$  is defined as  $Z_{\alpha UF} \alpha$  or in other words the dimensional stability derivative for the undamaged aircraft ( $UF$ ) multiplied by  $\alpha$ .

$$Z_{\alpha UF} = -\bar{q}[S_w a_w + \eta S_t a_t (1 - k)] \quad (4.36)$$

Following the damage level convention established for the  $M$  equation, Eq. (4.37) is developed by removing a portion of the tail surface area  $S_t$  with the addition of the scaling term  $\zeta_e$  and the ( $F$ ) notation.

$$Z_{\alpha F} = -\bar{q}[S_w a_w + \zeta_e \eta S_t a_t (1 - k)] \quad (4.37)$$

The damage level effects on  $Z_\alpha$  can then be quantified by taking the difference between the failed and unfailed  $Z_\alpha$  terms. The results are found in Eq. (4.38).

$$\Delta Z_\alpha = Z_{\alpha UF} - Z_{\alpha F} \quad (4.38)$$

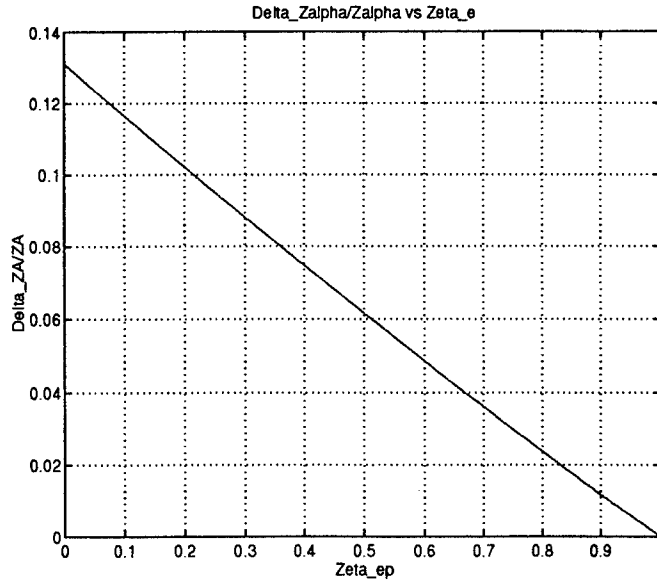


Figure 4.2  $\frac{\Delta Z_\alpha}{Z_\alpha}$  vs  $\zeta_e$

Substituting Eqs. (4.35) and (4.37) into Eq. (4.38) yields:

$$\Delta Z_\alpha = -\bar{q}(1 - \zeta_e)\eta S_t a_t (1 - k) \quad (4.39)$$

In order to nondimensionalize the change in  $Z_\alpha$ , Eq. (4.39) is divided by Eq. (4.35) producing:

$$\frac{\Delta Z_\alpha}{Z_\alpha} = \frac{(1 - \zeta_e)\eta S_t a_t (1 - k)}{S_w a_w + \eta S_t a_t (1 - k)} \quad (4.40)$$

Finally a general equation is derived that can transform a healthy dimensional or nondimensional stability derivative into a stability derivative reflecting the effects of control surface effector removal.

$$C_{z_{\alpha F}} = C_{z_{\alpha UF}} \left[ 1 - \frac{\Delta Z_\alpha}{Z_\alpha} \right] \quad (4.41)$$

Figure 4.2 shows the effect of increased damage level on the change in  $Z_\alpha$

Referring back to Eq. (4.2) the only coefficients that are left for discussion are  $C_{z_q}$  and  $C_{z_{\delta_e}}$ . Since the lift generated during a pitching motion ( $C_{z_q}$ ), and the lift generated by deflection of the horizontal stabilator are both directly related to the tail surface area

the failure analysis for the  $Z$  equation is completed with Eqs. (4.42) and (4.43).

$$C_{z_{qF}} = \zeta_e C_{z_{qUF}} \quad (4.42)$$

$$C_{z_{\delta_e F}} = \zeta_e C_{z_{\delta_e UF}} \quad (4.43)$$

#### 4.2 Lateral Stability and Control Derivatives

In addition to the control effectors found on the Lambda URV, the VISTA also includes the use of the differential tail to be used in roll control. This additional control effector is similar to the aileron. Hence in the failure analysis that follows the differential tail is treated as an additional aileron input into the system.

Maintaining consistency with the longitudinal failure analysis, the respective damage levels  $\zeta_a$ ,  $\zeta_r$ , and  $\zeta_{dt}$  represent the percentage of aileron, rudder, and differential tail surface area removed after control effector failure.

Unlike the longitudinal channel, no approximations are employed to reduce the dynamics of interest and consequently the failure analysis of the full lateral aircraft dynamics is developed. The equations of motion for the lateral channel are found in Blakelock [2] and are listed below.

$$-\frac{b}{2U} C_{y_p} \dot{\phi} - C_{y_{\phi}} \phi + \left( \frac{mU}{S\bar{q}} - \frac{b}{2U} C_{y_r} \right) \dot{\psi} - C_{y_v} \psi + \frac{mU}{S\bar{q}} \dot{\beta} - C_{y\beta} \beta = C_{y_{\delta_a}} \delta_a + C_{y_{\delta_r}} \delta_r + C_{y_{\delta_{dt}}} \delta_{dt} \quad (4.44)$$

$$\frac{I_x}{S\bar{q}b} \ddot{\phi} - \frac{b}{2U} C_{l_p} \dot{\phi} - \frac{J_{xz}}{S\bar{q}b} \ddot{\psi} - \frac{b}{2U} C_{l_r} \dot{\psi} - C_{l_\beta} \beta = C_{l_{\delta_a}} \delta_a + C_{l_{\delta_r}} \delta_r + C_{l_{\delta_{dt}}} \delta_{dt} \quad (4.45)$$

$$-\frac{J_{xz}}{S\bar{q}b} \ddot{\phi} - \frac{b}{2U} C_{n_p} \dot{\phi} + \frac{I_z}{S\bar{q}b} \ddot{\psi} - \frac{b}{2U} C_{n_r} \dot{\psi} - C_{n\beta} \beta = C_{n_{\delta_a}} \delta_a + C_{n_{\delta_r}} \delta_r + C_{n_{\delta_{dt}}} \delta_{dt} \quad (4.46)$$

4.2.1 *Y Equation.* The  $Y$  equation is repeated below:

$$-\frac{b}{2U} C_{y_p} \dot{\phi} - C_{y_{\phi}} \phi + \left( \frac{mU}{S\bar{q}} - \frac{b}{2U} C_{y_r} \right) \dot{\psi} - C_{y_v} \psi + \frac{mU}{S\bar{q}} \dot{\beta} - C_{y\beta} \beta = C_{y_{\delta_a}} \delta_a + C_{y_{\delta_r}} \delta_r + C_{y_{\delta_{dt}}} \delta_{dt} \quad (4.47)$$

$C_{y_p}$ ,  $C_{y_r}$ , and  $C_{y_\beta}$  represent the magnitude of the side force created by each of the lateral states of the aircraft, and each of these stability derivatives is directly proportional

to aerodynamic control effector area. Consequently, the vertical stabilator is the only control effector that develops a  $y$  directional force, hence Eqs. (4.48), (4.49), and (4.50) are established.

$$C_{y_{\beta F}} = \zeta_r' C_{y_{\beta UF}} \quad (4.48)$$

$$C_{y_{rF}} = \zeta_r' C_{y_{rUF}} \quad (4.49)$$

$$C_{y_{\beta F}} = \zeta_r' C_{y_{\beta UF}} \quad (4.50)$$

Where the effective area of the vertical stabilator or  $\zeta_r'$  is determined by removing the damaged rudder area  $(\zeta_r - 1)S_r$  from the vertical stabilator area  $S_f$  as shown in Eq. (4.51).

$$\zeta_r' = \frac{(\zeta_r - 1)S_r + S_f}{S_f} \quad (4.51)$$

Each of the control derivatives are directly proportional to the effective area of their respective control effector area. Eqs. (4.52) through (4.54) reflect this proportional relationship.

$$C_{y_{\delta_r F}} = \zeta_r C_{y_{\delta_r UF}} \quad (4.52)$$

$$C_{y_{\delta_a F}} = \zeta_a C_{y_{\delta_a UF}} \quad (4.53)$$

$$C_{y_{\delta_{dt} F}} = \zeta_{dt} C_{y_{\delta_{dt} UF}} \quad (4.54)$$

Since the aileron deflection on the VISTA F-16 creates a negligible force in the  $y$  direction,  $C_{y_{\delta_a UF}} = 0$ .

*4.2.2 L Equation.* The  $L$  equation is repeated below:

$$\frac{I_x}{S\bar{q}b} \ddot{\phi} - \frac{b}{2U} C_{l_p} \dot{\phi} - \frac{J_{xz}}{S\bar{q}b} \ddot{\psi} - \frac{b}{2U} C_{l_r} \dot{\psi} - C_{l_\beta} = C_{l_{\delta_a}} \delta_a + C_{l_{\delta_r}} \delta_r + C_{l_{\delta_{dt}}} \delta_{dt} \quad (4.55)$$

The  $C_{l_p}$  derivative represents the damping of the aircraft's rolling moment. Keating reasoned that only the wings and horizontal tail surface area significantly contributes to the magnitude of  $C_{l_p}$ . Therefore, Keating removed the vertical stabilator from consideration in the failure analysis. However, Roskam's Eq. (4.159) repeated below as Eq. (4.56) shows

that the vertical stabilator does contribute to  $C_{l_p}$ .

$$C_{l_p} = C_{l_{pwb}} + C_{l_{pH}} + C_{l_{pV}} \quad (4.56)$$

where  $wb$ ,  $H$ , and  $V$  represent the wingbody, horizontal and vertical tail aircraft components respectively.

Based on Eq. (4.56) and VISTA's substantially greater vertical stabilator area than the Lambda URV, the inclusion of the vertical stabilator in the failure analysis is warranted. The end result of this derivation is Eq. (4.57) which establishes the relationship between the failed  $C_{l_{pF}}$  derivative and the effective area of the wings, and both stabilators remaining after control effector failure.

$$C_{l_{pF}} = \zeta_{ar} C_{l_{pUF}} \quad (4.57)$$

where

$$\zeta_{ar} = \frac{(\delta_{dt} - 1)S_t + (\delta_a - 1)S_a + (\delta_r - 1)S_r + S_w + S_f + S_t}{S_w + S_f + S_t} \quad (4.58)$$

Only the vertical stabilator provides  $r$  and  $\beta$  damping thus  $C_{l_r}$  and  $C_{l_\beta}$  are both proportional to the effective area of the vertical stabilator.

$$C_{l_{rF}} = \zeta_r C_{l_{rUF}} \quad (4.59)$$

$$C_{l_{\beta F}} = \zeta_r C_{l_{\beta UF}} \quad (4.60)$$

The control derivatives are once again proportional to the control surface area and Eqs. (4.61) through (4.63) reflect this relationship.

$$C_{l_{\delta_a F}} = \zeta_a C_{l_{\delta_a UF}} \quad (4.61)$$

$$C_{l_{\delta_r F}} = \zeta_r C_{l_{\delta_r UF}} \quad (4.62)$$

$$C_{l_{\delta_{dt} F}} = \zeta_{dt} C_{l_{\delta_{dt} UF}} \quad (4.63)$$

4.2.3 *N Equation.* The  $N$  equation is repeated below:

$$-\frac{J_{xz}}{S\bar{q}b}\ddot{\phi} - \frac{b}{2U}C_{n_p}\dot{\phi} + \frac{I_z}{S\bar{q}b}\ddot{\psi} - \frac{b}{2U}C_{n_r}\dot{\psi} - C_{n\beta}\beta = C_{n\delta_a}\delta_a + C_{n\delta_r}\delta_r + C_{n\delta_{dt}}\delta_{dt} \quad (4.64)$$

All of the  $N$  stability derivatives are directly proportional to the effective area of the vertical stabilator and these relationships are quantified in the following equations:

$$C_{n_{pF}} = \zeta_r' C_{n_{pUF}} \quad (4.65)$$

$$C_{n_{rF}} = \zeta_r' C_{n_{rUF}} \quad (4.66)$$

$$C_{n_{\beta F}} = \zeta_r' C_{n_{\beta UF}} \quad (4.67)$$

The control derivatives are also directly proportional to their respective aerodynamic surfaces as found in the following equations:

$$C_{n_{\delta_a F}} = \zeta_a C_{n_{\delta_a UF}} \quad (4.68)$$

$$C_{n_{\delta_r F}} = \zeta_r C_{n_{\delta_r UF}} \quad (4.69)$$

$$C_{n_{\delta_{dt} F}} = \zeta_{dt} C_{n_{\delta_{dt} UF}} \quad (4.70)$$

### 4.3 *Disturbance Modeling*

Keating introduced an external disturbance into both the longitudinal and lateral channels to model the inherent cross-coupling created by asymmetric control effector failure. In the longitudinal channel this external disturbance represents the effect of losing a portion of the horizontal stabilator on the trim of the aircraft, and in the lateral channel this external disturbance represents the additional rolling moment and sideslip angle introduced by a damaged horizontal stabilator. Both of these VISTA models referred to in Keating's work as  $\Gamma_{lat}$  and  $\Gamma_{long}$ , are identical to the Lambda research vehicle and are completely explained in Keating's Thesis. The general models are given in Eqs. (4.71) through (4.74).

#### 4.3.1 Longitudinal Model.

$$\dot{\mathbf{x}}_d = \mathbf{A}\mathbf{x}_d + \mathbf{\Gamma}_{\text{long}}\delta_{trim} \quad (4.71)$$

$$\begin{bmatrix} \dot{u}_d \\ \dot{\alpha}_d \\ \dot{q}_d \\ \dot{\theta}_d \end{bmatrix} = \mathbf{A} \begin{bmatrix} u_d \\ \alpha_d \\ q_d \\ \theta_d \end{bmatrix} + \frac{1 - \zeta_e}{\zeta_e} \begin{bmatrix} 0 \\ \frac{Z_{\delta_e}}{U - Z_{\dot{\alpha}}} \\ M_{\delta_e} + \frac{M_{\dot{\alpha}} Z_{\delta_e}}{U - Z_{\dot{\alpha}}} \\ 0 \end{bmatrix} \delta_{trim} \quad (4.72)$$

#### 4.3.2 Lateral Model.

$$\dot{\mathbf{x}}_d = \mathbf{A}\mathbf{x}_d + \mathbf{\Gamma}_{\text{lat}}\delta_e \quad (4.73)$$

$$\begin{bmatrix} \dot{\beta}_d \\ \dot{p}_d \\ \dot{\phi}_d \\ \dot{r}_d \end{bmatrix} = \mathbf{A} \begin{bmatrix} \beta_d \\ p_d \\ \phi_d \\ r_d \end{bmatrix} + \frac{1 - \zeta_e}{\zeta_e} \begin{bmatrix} 0 \\ \frac{L_{\delta_{\alpha UF}}}{6\Lambda} \\ 0 \\ \frac{\kappa_{\nu} L_{\delta_{\alpha UF}}}{6\Lambda} \end{bmatrix} \delta_{trim} \quad (4.74)$$

where  $\delta_{trim} \approx 5$  degrees,  $\Lambda = 1 - \frac{J_{xz}^2}{I_x I_z}$ , and  $\kappa_{\nu} = J_{xz}/I_z$

#### 4.4 Failure Model Generation

From the failure analysis, the relationships are established to model failures as changes in the dimensional or nondimensional stability and control derivatives. These derivatives are acquired from Phillips' 1994 design.[15] The plants are edited for input into *Matlab*, and loaded into a *Matlab* script file (Appendix A) where the failure analysis is performed according to the equations developed previously. The failed plants in the form of **A** and **B** matrices are then loaded into another script file that forms the appropriate transfer functions including the disturbance functions, and are then formatted for input into QFTCAD. This procedure is used in both longitudinal and lateral/directional designs to generate the failure models for this design, and is outlined in Fig. 4.3.

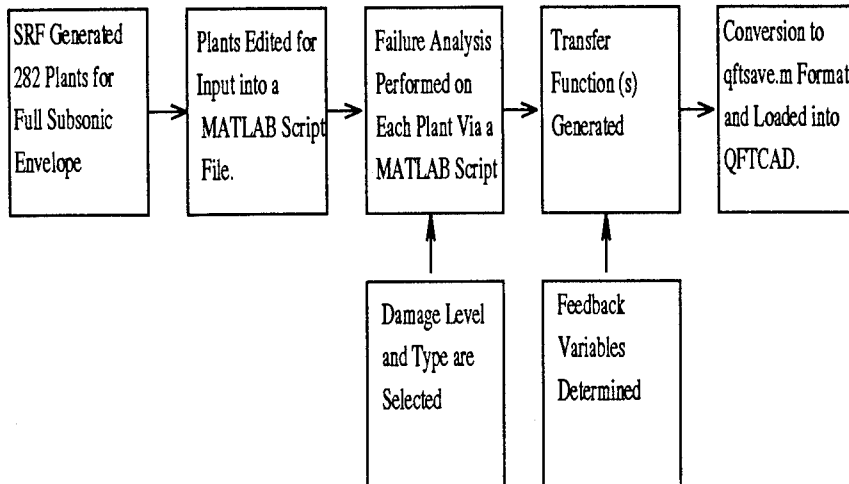


Figure 4.3 Failure Modeling Automation Flow Diagram

#### 4.5 Failure Modeling Summary

In this chapter, Keating's failure modeling scheme is examined and the necessary changes are made to accommodate the VISTA F-16. The most prominent adaptations made to Keating's equations involves the obvious differences between the URV and VISTA airframes. Some of these differences are: the URV has two small rudders working in tandem versus the VISTA which has a single, large rudder, the URV has trailing edge elevators while the VISTA has a stabilator, and the URV uses only ailerons while the VISTA incorporates both the ailerons and differential tail for roll control. Given these adaptations Keating's analysis is extended to the VISTA F-16, and the focus is shifted towards developing the external disturbance failure models. Ultimately, the actual failure model generation is discussed, and an overview of the entire sequence of events in the failure modeling process is given in Fig. 4.3.

## V. Longitudinal FCS Design

The purpose of this chapter is to examine the entire longitudinal design process from the generation of the feedback variables to compensator design and specification validation.

### 5.1 Longitudinal Design

**5.1.1 Longitudinal QFT Structure.** The first step in any QFT design is to define the feedback structure. To simulate the failure effects discussed in Chap. IV, an external disturbance plant in Fig. 5.1 is added to the general MISO QFT structure found in Fig. 2.1. Furthermore, in this research the longitudinal channel structure is of particular interest because, unlike traditional methods, an innovation is employed as the feedback variable. This variable  $C^*$  is actually a blending of the pitch rate  $q$  and the normal acceleration at the pilot's station  $N_z$ . This blending was the result of Phillips' research. As an experienced F-16 pilot, he reasoned that at low dynamic pressure  $\bar{q}$  the pilot is focused on tracking the pitch rate since the g loading is unavailable. However when the energy state of the aircraft is increased, the pilot shifts his attention towards tracking normal acceleration. This shift in focus is simulated through the use of the  $C^*$  variable, which represents a weighted combination of the  $q$  and  $N_z$  aircraft states (See Eqs. (5.1) and (5.2)).

$$C^* = K_1 q + K_2 N_z \quad (5.1)$$

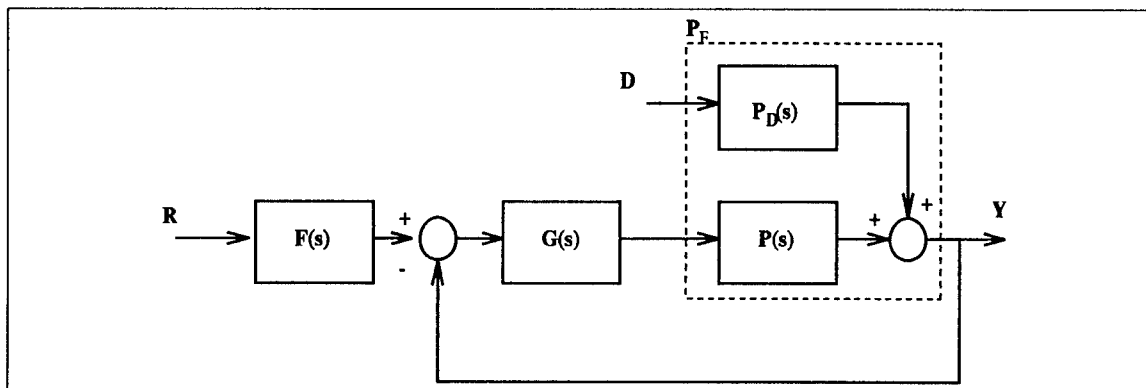


Figure 5.1 Longitudinal QFT Feedback Structure

$$N_z = \left(\frac{\pi}{5796}\right)[U(\dot{\alpha} - q) - l_x \dot{q}] \quad (5.2)$$

Note that  $l_x$  is the distance from the pilot station to nominal aircraft center of gravity, approximately 13.95 feet, and  $U$  is the trim velocity in the  $x$  body axis direction. Further explanation of the  $N_z$  equation derivation is provided in Reynold's thesis [16].

The  $C^*$  weighting is  $\bar{q}$  dependent and the gradient adopted in this research is shown in Fig. 5.2. The two lines on this gradient represent the relative gains  $K_1$  and  $K_2$  in Eq. (5.1). At low  $\bar{q}$ ,  $q$  is the dominant feedback variable, and at high  $\bar{q}$ ,  $N_z$  dominates. This gradient is designed such that the crossing point, represented by the equal weighting of the two feedback variables, occurs at approximately 200 lbs/ft<sup>2</sup>, and the gains,  $K_1$  and  $K_2$  settle to 0.8 and 0.2 above 600 lbs/ft<sup>2</sup>. It is also worth mentioning that the asymptotic gradient in Fig. 5.2 is not the same  $C^*$  gradient found in Fig. 4.3 of Phillips' thesis. Phillips spent a considerable portion of his research refining the  $C^*$  variable, and in that time, attempted various blending schemes. From this work, he determined that the asymptotic scheme most accurately represented the pilot's tracking tendencies, and hence included it in the formulation of  $C^*$ . As a simple oversight, however, the linear gradient was printed in his thesis instead of the asymptotic gradient. As a consequence of this oversight, the linear weighting in Fig. 4.3 is attempted in the current design, and an interesting finding emerges in the process. The gradient with the linear weighting generates greater parametric plant uncertainty within the pilots bandwidth than the asymptotic weighting. This increase in uncertainty within the pilots bandwidth suggests that the incorporation of the physical world actually improves the design, and ultimately motivates the application of the asymptotic scheme in this research.

Due to the static instability of the VISTA F-16 in the subsonic envelope, it is traditional to incorporate an inner loop for stability purposes. However, Phillips found for the VISTA that an inner loop needlessly complicated the feedback structure while shifting the plant uncertainty from the pilot's bandwidth towards the higher frequency ranges. This shift limits the pilot's ability to control the aircraft and is deemed unacceptable. Hence, an inner loop design is not included in this research.

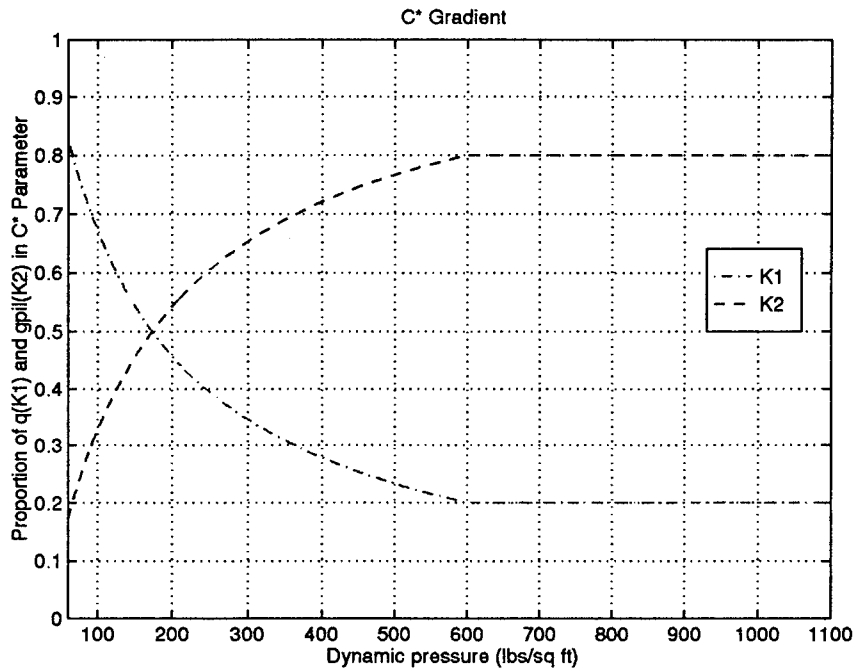


Figure 5.2 Allocation of  $q$  and  $g_{pil}$  in  $C^*$  Parameter versus  $\bar{q}$

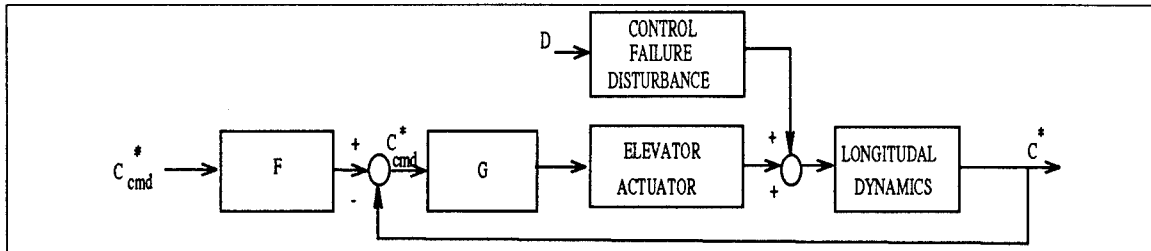


Figure 5.3 MIMO QFT Design Structure

With the inner loop question resolved, the  $C^*$  variable defined, and external disturbances added, the longitudinal QFT feedback structure with its associated 1X1 prefilter ( $F$ ) and compensator ( $G$ ) appears as shown in Fig. 5.3.

*5.1.2 Longitudinal Specifications.* There are four sets of specifications for the longitudinal channel that must be defined to continue with the QFT design procedure. The performance specifications for tracking, stability, and external disturbance rejection are developed in the following sections.

5.1.2.1 *Tracking Specifications.* The MILSTD 1797A defines time domain specifications for Level 1, 2, and 3 handling qualities in terms of pitch rate response to a step stick force input. The exact specifications for the onset delay ( $t_1$ ), the onset rate ( $\Delta t$ ), and the minimum damping ratio ( $\frac{\Delta q_2}{\Delta q_1}$ ) can be found on Table 5.1 corresponding to Fig. 5.4. However, as Phillips determined, there are some difficulties in applying these time specifications to a full envelope flight control design involving an innovation as the feedback variable. These difficulties arise due to a couple factors. First, in this design the  $C^*$ , not pitch rate, variable is tracked. Second, the time domain specifications for  $\Delta t$  have a dependence on velocity  $V$  and thus change for each flight scenario. Finally, the time domain specifications must be transformed into the frequency domain for use in the QFT design.

Parameter	Level 1	Level 2	Level 3
$t_1$	$t_{1,max} \leq 0.12 \text{ s}$	$t_{1,max} \leq 0.17 \text{ s}$	$t_{1,max} \leq 0.21 \text{ s}$
$\Delta t$	$\frac{9}{V} \leq \Delta t \leq \frac{500}{V}$	$\frac{3.2}{V} \leq \Delta t \leq \frac{1600}{V}$	No specification
$\frac{\Delta q_2}{\Delta q_1}$	$\frac{\Delta q_2}{\Delta q_1} \leq 0.30$	$\frac{\Delta q_2}{\Delta q_1} \leq 0.60$	$\frac{\Delta q_2}{\Delta q_1} \leq 0.85$

Table 5.1 MILSTD Longitudinal Time Domain Tracking Specifications (Level 1,2,3)

Phillips circumvented the first of these difficulties by identifying that at low dynamic pressure,  $C^*$  is primarily composed of pitch rate (Fig. 5.2) and that the onset delay and rate are the dominating requirements at this pressure. Given this understanding, the MILSTD specifications for pitch rate response can be applied as an approximation to  $C^*$  specifications. Next, the floating specification issue is settled by properly selecting upper and lower limits on  $\Delta t$ . Finally, the last obstacle in the way of synthesizing QFT tracking bound models is overcome when reasonable approximations are made to translate the time domain specifications into the frequency domain.

Phillips' Level 1 tracking bound models (See Eqs. (5.3) and (5.4)) provide the foundation for the Level 2 and 3 models. Though a detailed explanation of these models can be found in the literature [15], some specifics are important to introduce. Phillips began with a natural frequency  $\omega_n$  of 0.7. This  $\omega_n$  was selected because most of the plant uncertainty for the healthy as well as the failed aircraft occurs at frequencies less than or equal to 1 rps, and this selection insures that the responses with the greatest overshoot and slowest

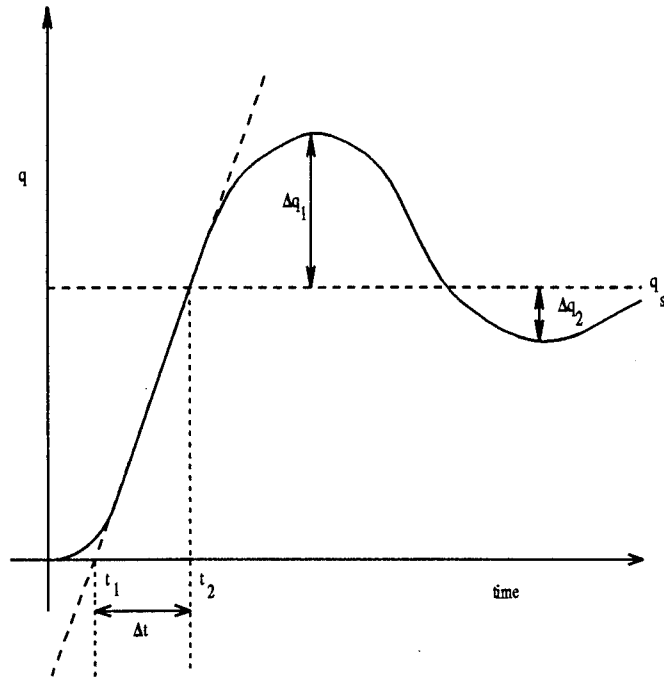


Figure 5.4 Step Response Used to Define Longitudinal Response Specifications

settling time are placed in the pilot's bandwidth. To satisfy the Level 1  $t_1$  requirement a pole is positioned at 2 rps, and then to insure a monotonically increasing separation between upper and lower tracking bounds  $\delta_r$ , another pole is added at 3 rps.

$$T_{R_U} = \frac{5(s + 0.7)^2}{(s^2 + 0.56s + 0.49)(s + 5)} \quad (5.3)$$

$$T_{R_{L1}} = \frac{6}{(s + 2)(s + 3)} \quad (5.4)$$

As Table 5.1 illustrates, the primary specification for the Level 2 and Level 3 models is the onset delay  $t_1$ . Though the MILSTD develops specifications for Level 2 and Level 3 minimum damping ratios, only variations in the lower tracking bounds are considered in this research. It is assumed that if a healthy aircraft can not exceed the upper tracking bound, i.e. faster settling time, then a damaged aircraft with reduced control surface area can not either. Therefore the upper tracking bound serves as the model for all three levels of handling qualities. The lower tracking specifications, however, varies with each Level of handling qualities. The Level 2 (Eq. (5.5)) and Level 3 (Eq. (5.6)) models are

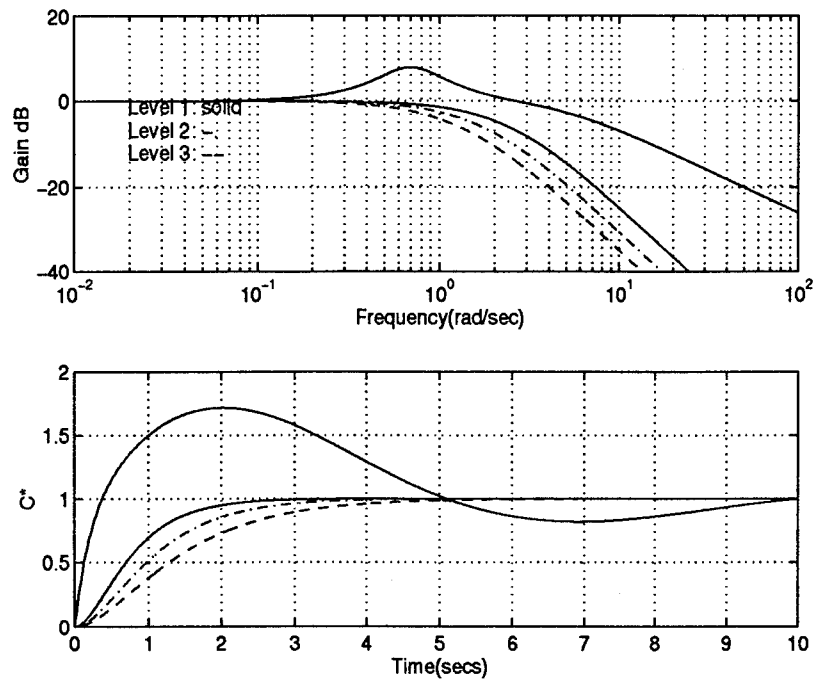


Figure 5.5 Step Input Time Response of QFT Upper and Lower Longitudinal Tracking Bound Models

synthesized by increasing the onset delay time for  $T_{RL1}$  until these models approach the degraded specifications listed in Table 5.1. Manipulating  $T_{RL1}$  to generate the other lower bounds guarantees satisfaction of the QFT requirement for a monotonically increasing  $\delta_r$  as well. The time response for Level 1, 2 and 3 specifications can be found on Fig. 5.5 and in tabular form on Table 5.2.

$$T_{RL2} = \frac{3}{(s + 1.5)(s + 2)} \quad (5.5)$$

$$T_{RL3} = \frac{1.8}{(s + 1)(s + 1.8)} \quad (5.6)$$

**5.1.2.2 Stability Specifications.** The open loop frequency response of all plants, healthy as well as failed, must have a phase margin angle of at least 30 degrees and a gain margin of at least 6 dB as dictated by MILSTD 1797A stability specifications. These specifications are entered directly into QFTCAD to generate the stability bounds, and the 6 dB gain margin is verified visually using the stability validation function of QFTCAD.

Model	$t_1$	$\Delta t$	$\frac{\Delta q_2}{\Delta q_1}$
$T_{RU}$	0	0.215	0.255
$T_{RL1}$	0.113	1.132	overdamped
$T_{RL2}$	0.162	1.158	overdamped
$T_{RL3}$	0.206	2.085	overdamped

Table 5.2 QFT Upper and Lower Tracking Bound Model Step Response Characteristics

5.1.2.3 *External Disturbance Rejection Specifications.* There is no specific external disturbance rejection specifications established in the MILSTD. Consequently, an arbitrary value of -20 dB is imposed on the design as discussed in Chap. II. This level of disturbance rejection is accepted with the understanding that further analysis of this specification is required later in the design.

5.1.2.4 *Performance Benchmarks.* The following longitudinal performance criteria must be satisfied to meet current F-16 flight control system performance.

1. Attain  $25^\circ \alpha$ , but do not exceed  $30^\circ$
2. Achieve 9 g's but do not exceed 9.45 g's

Limiters prevent the aircraft from exceeding the  $30^\circ$  angle-of-attack and the 9.45 g load factor restrictions. Unfortunately, a limiter scheme is not implemented due to time restrictions experienced in this research. These limitations are necessary to maintain the integrity of the airframe and safety of the pilot, therefore before flight testing this design a limiting scheme should be developed.

5.1.3 *Loaded and Effective Plants.* The healthy plants are obtained from Phillips' research in the form of state-space **A** and **B** matrices. These 282 plants, representing three dimensions of plant parameter variation (altitude, airspeed, and center of gravity location), are subjected to the failure modeling process described in Chap. IV. The end result of this failure modeling routine is a failed aircraft plant for each healthy plant. Therefore the original 282 plants are consequently doubled for each failure level selected, where a failure level is defined in Chap. IV as a percentage loss in elevator area. Initially two plant sets are generated, one for the 15% damage level and another for the 25% damage level. These

two damage levels are selected based on Keating's work with the URV. [11] Keating found that a successful QFT design was achievable for an aircraft experiencing a 25% reduction in elevator surface area, thus 25% is chosen as a preliminary upper limit failure case. The 15% damage level is selected as a comparison to the 25% level, and as a backup plant set if a successful QFT design can not be implemented for the 25% failure case.

Given the  $C^*$  structure developed earlier in this chapter, as well as the aircraft and disturbance models, a *Matlab* macro is used to develop the associated QFT tracking and external disturbance transfer functions found in Eqs. (3.10) and (3.11). Since the longitudinal design represents a MISO case, the plant and external disturbance transfer function matrices are both 1x1 in dimension. These transfer functions are loaded into QFTCAD and the pole/zero cancellation routine is performed. This routine eliminates any pole/zero pairs within a 0.001 tolerance, and removes any dynamics greater than  $10^{\pm 5}$  rps. After performing this cancellation process, the loaded plant models are placed in series with the fourth-order actuator model described in Chap. III to form the effective plants. The frequency response of these plants found in Fig. 5.6 confirms that the majority of plant uncertainty is constrained to frequencies less than 1 rps. The external disturbance plants demonstrate a similar property and are illustrated in Fig. 5.7.

*5.1.4 Frequency Templates.* After loading the plant cases into the QFTCAD program and generating the plant matrices  $\mathbf{P}$ ,  $\mathbf{P}_e$ , and  $\mathbf{P}_D$ , the CAD 'Temp' option is selected and the frequency templates are automatically formed. The templates are identified over the frequencies given in Eq. (5.7).

$$\omega = 0.05, 0.075, 0.1, 0.25, 0.5, 0.75, 1, 3, 5, 7, 10, 13, 20, 25, 30, 50 \quad (5.7)$$

*5.1.4.1 Healthy Aircraft Templates.* One of the assumptions made in this research is that Phillips' LTI models incorporate all of the uncertainty inherent in the configuration variations he introduced. In his thesis there is a detailed explanation of how the number of boundary plants was increased to accommodate possible uncertainty found in plants that were not on the "edge of the envelope." This discussion is left to be reviewed by the interested reader. [15]

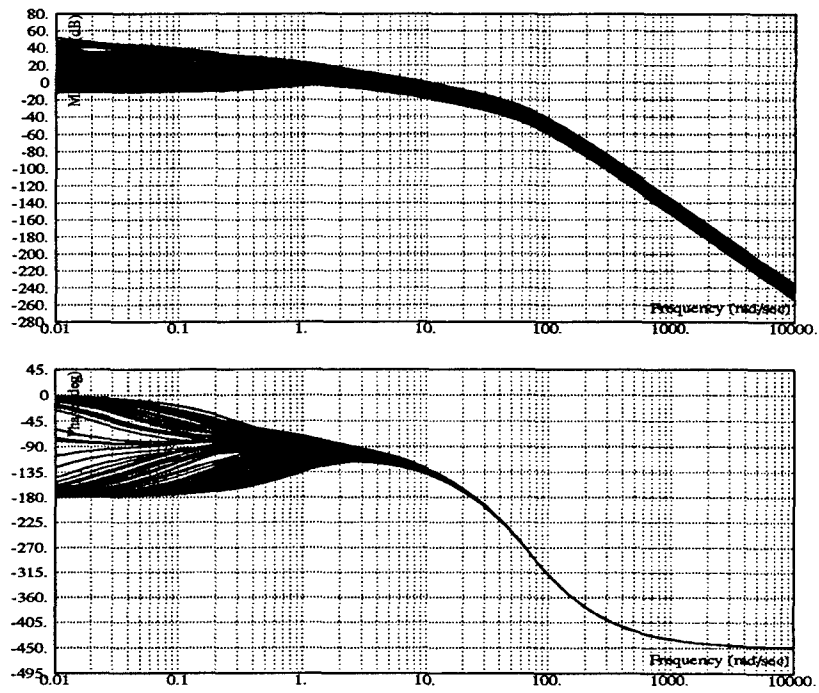


Figure 5.6 Frequency Response of Effective Plants  $P_e$

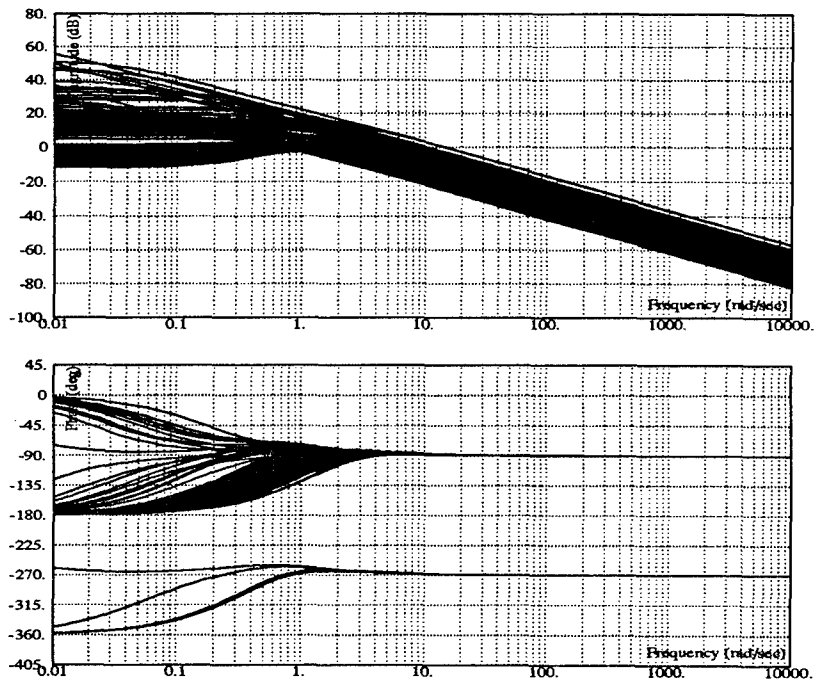


Figure 5.7 Frequency Response of Disturbance Plants  $P_D$

Before proceeding with the analysis of the failure frequency templates, Phillips' healthy plant templates are employed as a benchmark to insure that there are no errors in the *Matlab* and *Mathematica* macros or in the plant files. The frequency templates afford an excellent opportunity to compare the two plant sets which should be identical at this point in the design. Unfortunately, upon comparing the healthy templates from Phillips' design with those generated in this design, several differences surfaced. After a thorough investigation of the transfer function formulation routines, a few discrepancies between the two designs are unearthed. The first, and most obvious, discrepancy involved the number of models employed to form the frequency templates. Following Phillips' inability to stabilize the 3 tank configuration over the entire subsonic flight envelope, he removed 83 plants from the original 282 in the healthy design set  $\mathcal{P}$ . This reduction in the number of plants caused Phillips' templates to become significantly smaller than the templates formed in this research. Also, a faulty *Matlab* linearization function known as 'linmod' was used in Phillips' research. This function is to blame for the second discrepancy in healthy frequency templates, and is explained further in Appendix E. After generating the  $C^*$  variable without this *Matlab* function the two plant sets were indistinguishable. Finally, it is decided to proceed with the plant templates (Figs. 5.8 and 5.9) developed in this research as the accurate healthy aircraft templates without the 3 tank configuration. A complete list of the flight condition/configuration data points used in the design is contained in Appendix B.

*5.1.4.2 Failed Aircraft Templates.* The frequency templates provide the first opportunity to determine the extent of control effector failures on the aircraft system. Figures 5.10 and 5.11 illustrate the failure effects at low frequencies ( $\omega = 1$  rps). Holding frequency constant, the overall trend is for the templates to expand in a downward direction as the damage level increases. The 15% failure templates grew approximately 3 dB in magnitude and 2 degrees in phase, while the 25% templates increased approximately 5 dB in magnitude and 3 degrees in phase. Overall, the log magnitude and phase of template expansion appears to be proportional to control effector damage level.

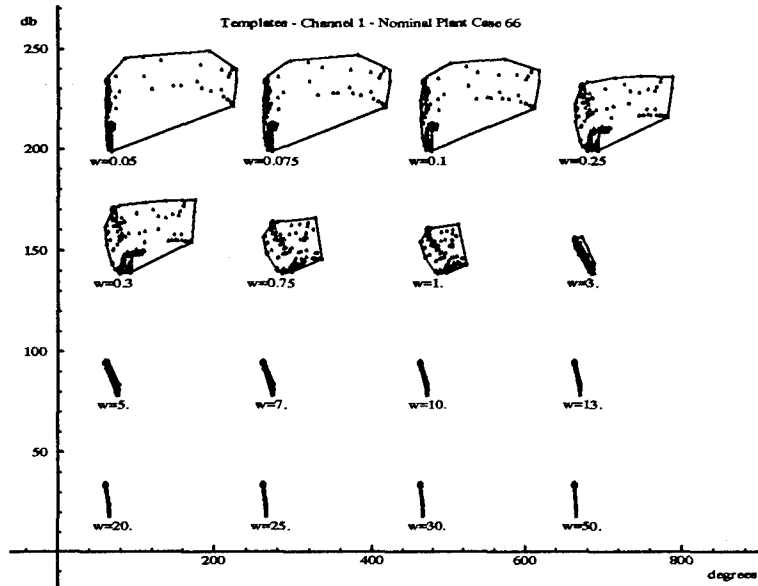


Figure 5.8 Healthy Aircraft Frequency Templates

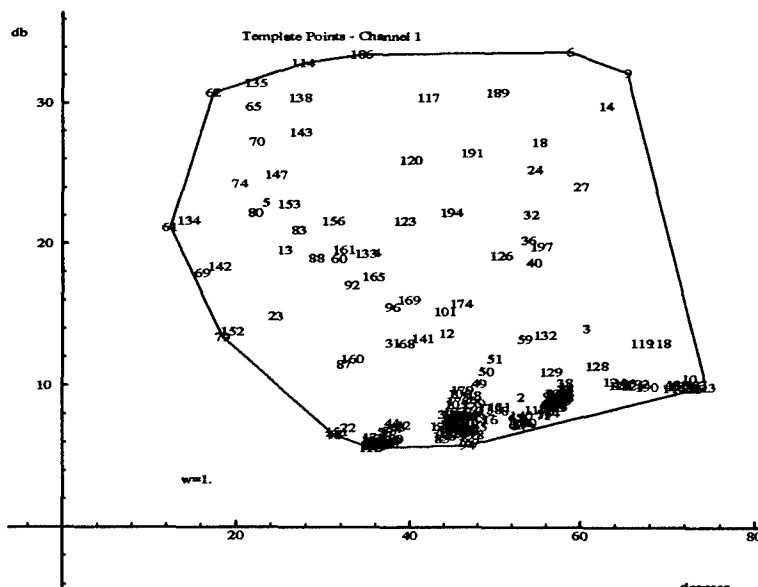


Figure 5.9 Healthy Aircraft Frequency Template for  $\omega = 1 rps$

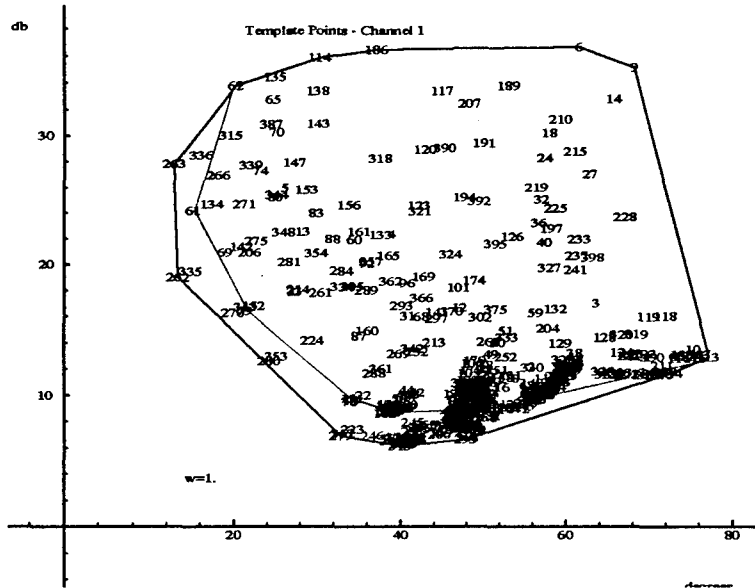


Figure 5.10 15% Horizontal Stabilator Failure Frequency Template for  $\omega = 1 rps$

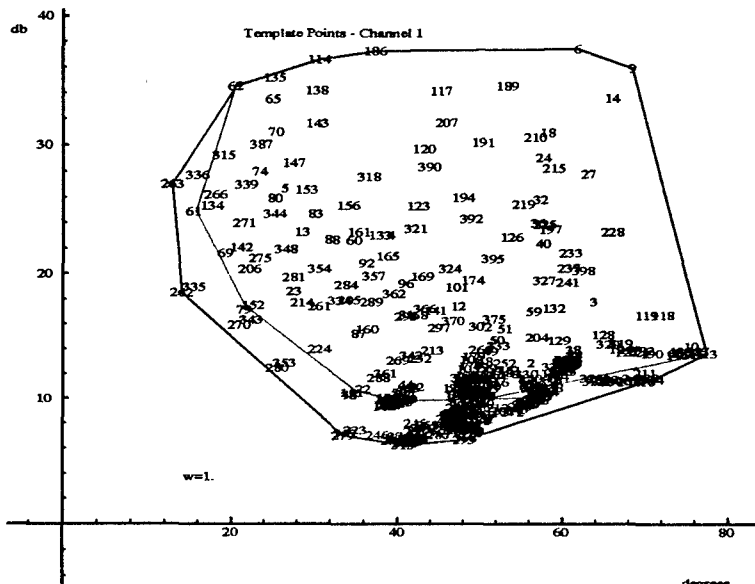


Figure 5.11 25% Horizontal Stabilator Failure Frequency Template for  $\omega = 1 rps$

At higher frequencies,  $\omega \geq 30\text{rps}$ , the templates in Figs. 5.13 and 5.14 exhibit a dramatic increase in area when compared with the healthy aircraft template in Fig. 5.12. The low dynamic pressure plants, located on the bottom of the failure frequency templates, maintain a pattern similar to the low frequency plants in Fig. 5.10, while the high dynamic pressure plants, located on top of the frequency template, decrease in magnitude but increase in phase. It is very difficult to distinguish a pattern in these high frequency failure templates due to the large number of variables influencing their behavior. However, after closely examining the template data and plant generation process, some strong relationships become apparent. From a comparison of Figs. 5.12, 5.13 and 5.14 the failure templates exhibit a dependence on the damage level, as well as the  $C^*$  gradient. Because the high  $\bar{q}$  plants are primarily composed of normal acceleration, the high dynamic pressure plants increase in phase, and both the normal acceleration and pitch rate transfer functions only differ in their numerators, it appears that the zeroes of the normal acceleration plants are less effected by failures than the zeroes of the pitch rate transfer functions. Increasing the frequencies from the 1 to 30 rps, the failed plants tend to rotate clockwise on the Nichols chart while decreasing in magnitude as the frequency increases. This swirl effect is illustrated in Fig. 5.15. To further support this relationship the 200 lbs/ft<sup>2</sup> plants which represent nearly an equal blend of pitch rate and normal acceleration feedback are located in the center of the failed templates and exhibit only a change in magnitude corresponding to the damage level. The swirl effect extends Phillips' innovation to the failure environment, and further emphasizes the importance of properly selecting the feedback variable in a robust aircraft design.

Overall, there is not a substantial difference in magnitude and phase between the 25% failure and 15% failure templates, therefore the 25% failure plant set is applied for the remainder of the longitudinal design. If a successful QFT design can not be implemented with this plant set, or if the time simulations involving the saturation nonlinearities create insurmountable stability problems, then the 15% failure plants will replace the 25% cases. The 25% failure plants combined with the healthy plants are identified in Fig. 5.16.





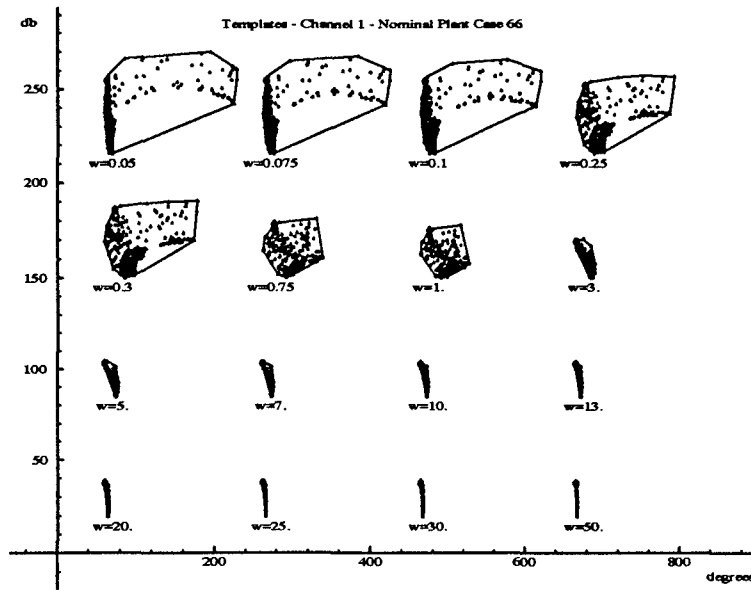


Figure 5.16 Plant Templates for VISTA Experiencing 25% Horizontal Stabilator Failure

5.1.5 *QFT Generated Bounds.* To continue with the generation of the QFT tracking and external boundaries, the nominal plant must be selected in accordance with the specifications outlined in Chap. II. The #66 plant (SRF plant model #70) is chosen as the nominal plant due to its location on top of the 30 rps frequency template.

5.1.5.1 *Tracking Bounds.* Figure 5.17 displays the tracking bounds for the 25% failure case. There are some important features of these tracking bounds that should be highlighted. The first, and probably most significant, feature effecting the design is that the tracking bounds reflect the increase in template size due to failures. Comparing the healthy tracking bounds and those generated for the failure cases, an increase in gain of approximately 5 dB is noticeable within the pilot's bandwidth. Second, though the tracking bounds form a valley permitting a reduced compensator gain, it is doubtful that this valley can be exploited in the design. Phillips' stability validation indicates that the healthy models require a significant increase in phase just to maintain stability at the lower frequency range of interest. Finally, the lower frequency range bounds roughly between 0.05 and 0.1 rps are particularly difficult to achieve, a finding not isolated to the failure cases.

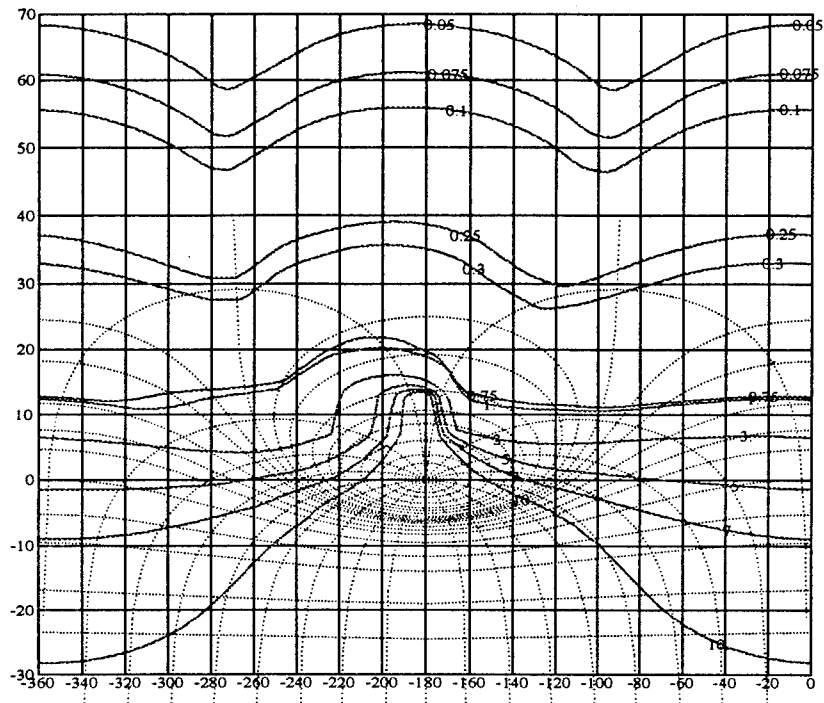


Figure 5.17 QFTCAD Tracking Bounds

*5.1.5.2 External Disturbance Bounds.* The external disturbance bounds are illustrated in Fig. 5.18. From this figure it is obvious that the external disturbance rejection bounds are virtually unachievable. As an example, to satisfy the external disturbance rejection bound at  $\omega = 1$  an increase in gain of approximately 25 dB is required. Such a drastic increase in gain would certainly cause rate and deflection saturation problems later in the design, especially since Phillips design, which was concerned with only the healthy cases, experienced mild saturation under a significantly reduced system gain. Therefore, as a first attempt to solve this gain problem, a degraded specification of -11 dB is introduced and the bounds are regenerated. Unfortunately, this new specification does not substantially reduce the system gain necessary to clear the bounds. Next, the addition of an external disturbance input is reexamined, and an engineering compromise is made. By stating that the aircraft can not reject -20 dB of the disturbance input, this is equivalent to saying that the pilot may experience some effects of a 25% reduction in elevator surface area. Since the goal of this design is to construct a flight control system not an autopilot system, it is accepted that the pilot may have to apply some command inputs after a

failure occurs in order to maintain control of the aircraft. Finally, the compensator gain required to achieve tracking will also help minimize the effect of the external disturbance. This can be seen from analyzing Eq. (5.8) obtained from Eq. (2.2).

$$T_D(j\omega) = \frac{Y(j\omega)}{D(j\omega)} = \frac{P_D(j\omega)}{1 + G(j\omega)P(j\omega)} \quad (5.8)$$

If  $|G(j\omega)P(j\omega)| \gg 1$  in the bandwidth of concern, then

$$T_D(j\omega) = \frac{Y(j\omega)}{D(j\omega)} \approx \frac{1}{G(j\omega)} = \frac{1}{K_G G'(j\omega)} \quad (5.9)$$

Thus, as seen on Eq. (5.9) any increase in  $K_G$  to achieve tracking reduces the effect of the external disturbance on the output. However, this explanation does not give the designer license to simply ignore the external disturbance problem, for an external disturbance can excite the bending modes of the aircraft or possibly cause the system to become unstable. Therefore, the refined external disturbance goal is to remove the disturbance bounds from consideration, and proceed with the development of the compensator  $G$ . Once the design is complete, an external disturbance rejection validation is examined and time simulations are run to determine the extent of the disturbance effects on the system.

*5.1.6 Compensator Design.* The three constraints, discussed in Chap. II, that are imposed on the compensator, combined with the deleterious effects of the fourth-order actuator model and the statically unstable F-16 model, represent a serious challenge in the QFT loop shaping process. Several design iterations are necessary to satisfy the required QFT bounds and develop the final compensator design in Eq. (5.10). A brief description of the design process follows.

Since the nominal plant  $P_o$  is Type 0, the compensator must contain a pole at the origin for  $L_o = P_o G$  to be Type 1. Thus, the loop shaping process is initialized with  $L_{o1} = \frac{1}{s} P_o = G_1 P_o$ . Two zeros and an additional pole are added to  $G_1$  yielding the final compensator design in Fig. 5.19. It is important to note that the most restrictive aspect of this process is circumventing the stability contour with a minimal order compensator. The two zeros are positioned to achieve the maximum possible increase in phase. Though

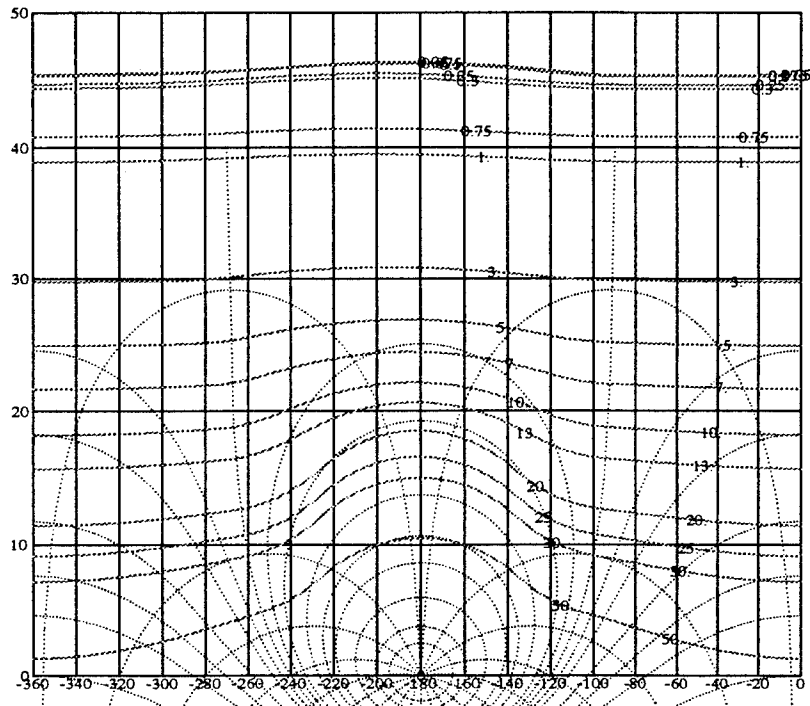


Figure 5.18 QFTCAD External Disturbance Bounds

it appeared during the loop shaping that the zero at 2.3 rps can be shifted to a lower frequency allowing the system a sufficient increase in phase to clear the top of the  $M_L$  contour, the step response of the system became increasingly more intolerable as the zero was reduced in frequency. This is significant because it demonstrates a possible upper limit on the level of uncertainty this design can incur and still achieve the required the stability and tracking specifications.

The final longitudinal compensator  $G$  is:

$$G = \frac{4.45(s + 2.3)(s + 12.5)}{s(s + 43)} \quad (5.10)$$

**5.1.7 Prefilter Design.** The goal of the prefilter design is to position the compensated system between the upper and lower tracking bounds now that the system has the necessary robustness. Initially, a simple pole is placed at 3.5 rps to insure that the system provides the adequate response over the pilot's bandwidth. The final prefilter design incorporates a zero to shift some higher frequency plants within the tracking boundaries. The

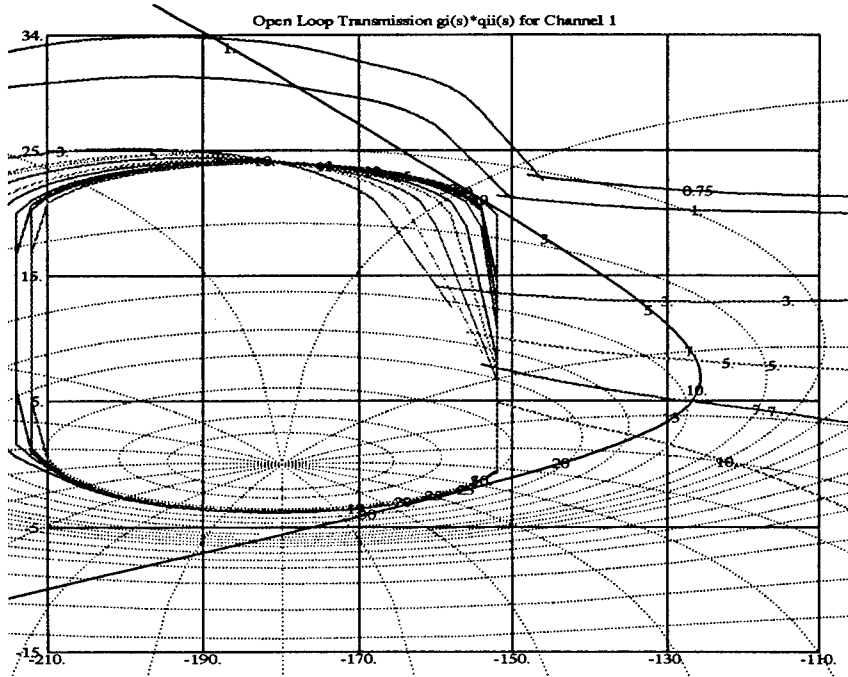


Figure 5.19 QFTCAD Nominal Loop Shaping

QFTCAD prefilter Nichols chart shown in Fig. 5.20 illustrates that the system satisfies the tracking boundaries within the bandwidth of interest.

$$F = \frac{0.25(s + 6)}{s + 1.5} \quad (5.11)$$

## 5.2 Time Simulations

The purpose of the time simulations is to demonstrate that the compensated system satisfies the various longitudinal time domain specifications. For these simulations a sample of 20 time responses is displayed over the specific  $\bar{q}$  range identified on each figure. This sampling is based on analyzing the data in Appendix C for all 398 LTI plant cases and discerning those cases that comprise the limits of the overall time responses. An alternative method of validating this selection of plant cases is to analyze the plants that lie on a boundary of frequency templates. The 20 plant cases selected via the time response data should correspond exactly to these boundary plants. To further discriminate the impaired and unimpaired plant cases, the failed plants are denoted by dashed lines on the figures,

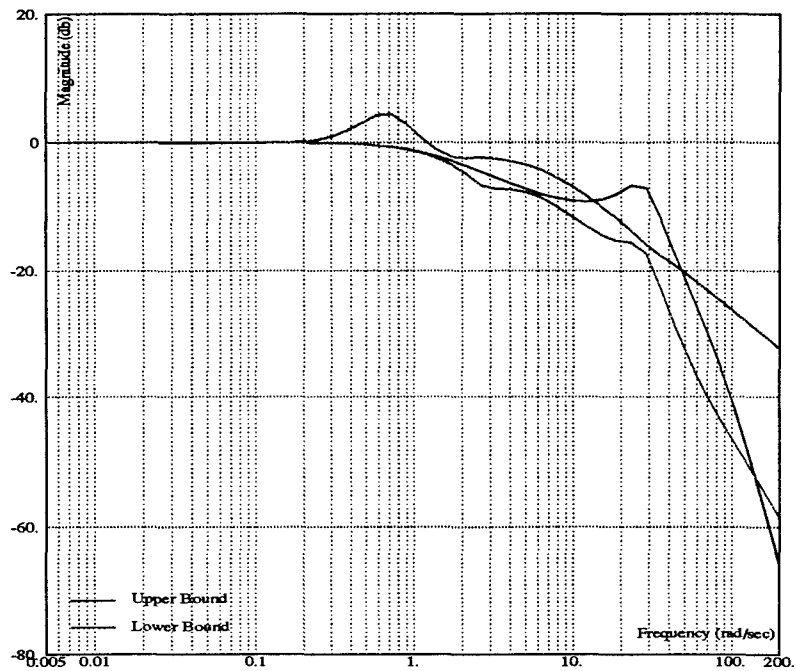


Figure 5.20 QFTCAD Prefilter Design

and the healthy plants are denoted by the solid lines. This line convention is maintained throughout this report.

**5.2.1  $C^*$  Tracking Responses.** Proceeding with a worst case design scenario, Figs. 5.21 and 5.22 represent the unit step tracking responses of the low  $\bar{q}$  compensated system. Also, the MILSTD flying quality levels are superimposed on the  $C^*$  tracking responses to simplify performance evaluation. As expected, the failed plants exhibit less damping and increased onset delay than the healthy plants. It is apparent from these figures that the healthy aircraft plants satisfy Level 1 flying qualities specifications while the failed aircraft meet at least Level 2 specifications. In addition, the angle of attack ( $\alpha$ ) response displays the effect of the elevator failure since most of the failed plants do not attain half of the maximum healthy aircraft's  $\alpha$ . The  $C^*$  blending is easily identifiable within the  $q$  and  $g_{pil}$  time responses as well. It is important to remember that the  $C^*$  is the feedback variable and not pitch rate  $q$ . This explains why neither the pitch rate or the normal acceleration at the pilot's station  $g_{pil}$  responses settle to the same steady state value. Finally, the failure plants dominate the elevator deflection authority but do not

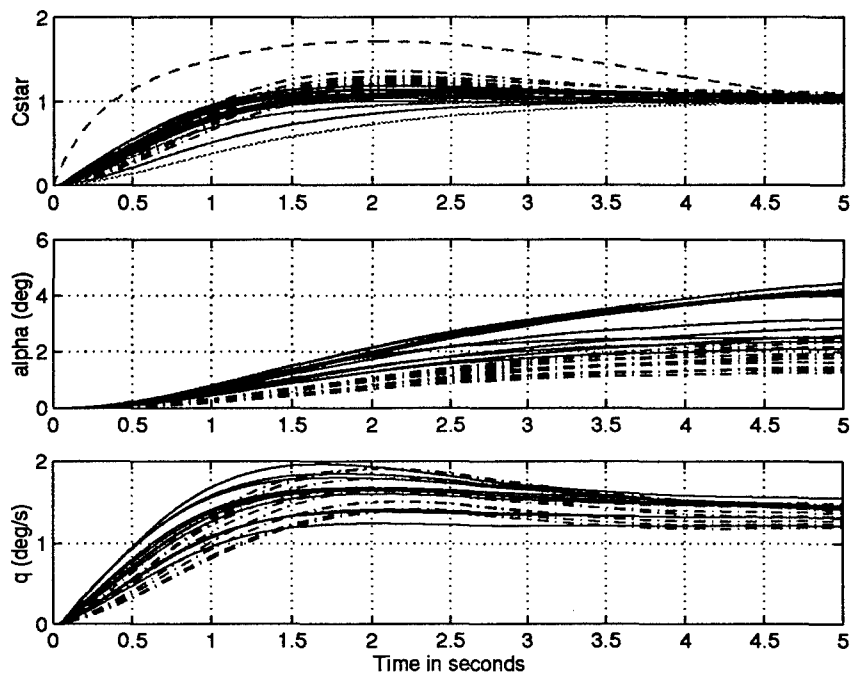


Figure 5.21 Unit  $C^*$  Step Response of Compensated System, Healthy Aircraft and 25% Stabilator Failure Plants ( $\bar{q} < 200 \text{ lbs}/ft^2$ ) [1 of 2]

have a significant impact on the elevator rate. All of these plots are further supported by the tabular data found in Appendix C.

Figures 5.23 and 5.24 illustrate the longitudinal design dependency on  $\bar{q}$ . The ballooning witnessed for the low  $\bar{q}$  failed plants in Fig. 5.21 is non-existent for the higher energy plants. All of the high  $\bar{q}$  responses, healthy as well as failed, meet Level 1 specifications. The pitch rate response is noticeably faster, the  $g$  loading is nearly doubled and the demand placed on the elevator authority is reduced by approximately 3 degrees in comparison to the low  $\bar{q}$  plants.

**5.2.2 Maximum Command Gradient.** The unit step simulations generate the data necessary to determine whether the system satisfies the time domain Level 1 or 2 specifications. These simulations also provide an opportunity to calculate the maximum command input that can be applied to the system without causing rate and deflection saturation. Phillips employed the following relations to construct such a maximum  $C^*$

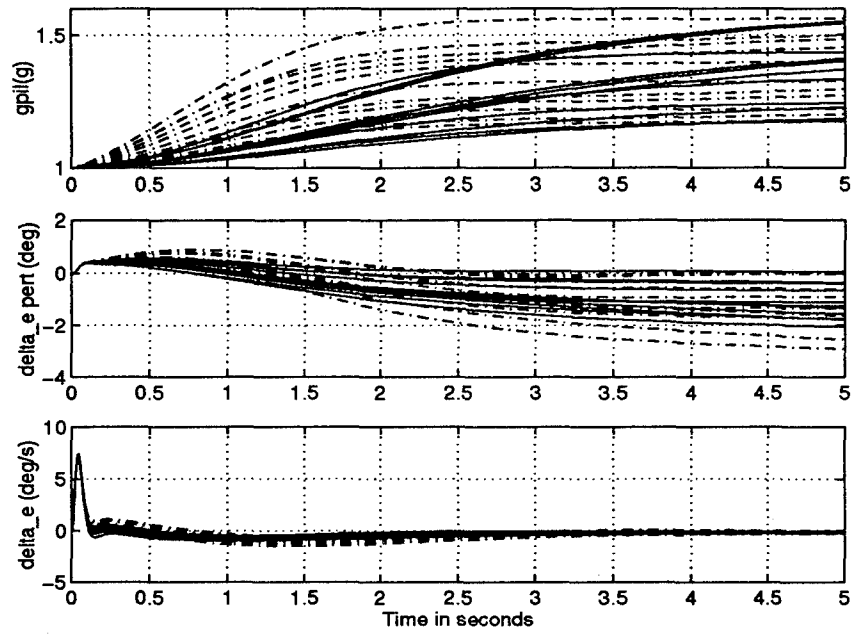


Figure 5.22 Unit  $C^*$  Step Response of Compensated System, Healthy Aircraft and 25% Stabilator Failure Plants ( $\bar{q} < 200 \text{ lbs/ft}^2$ ) [2 of 2]

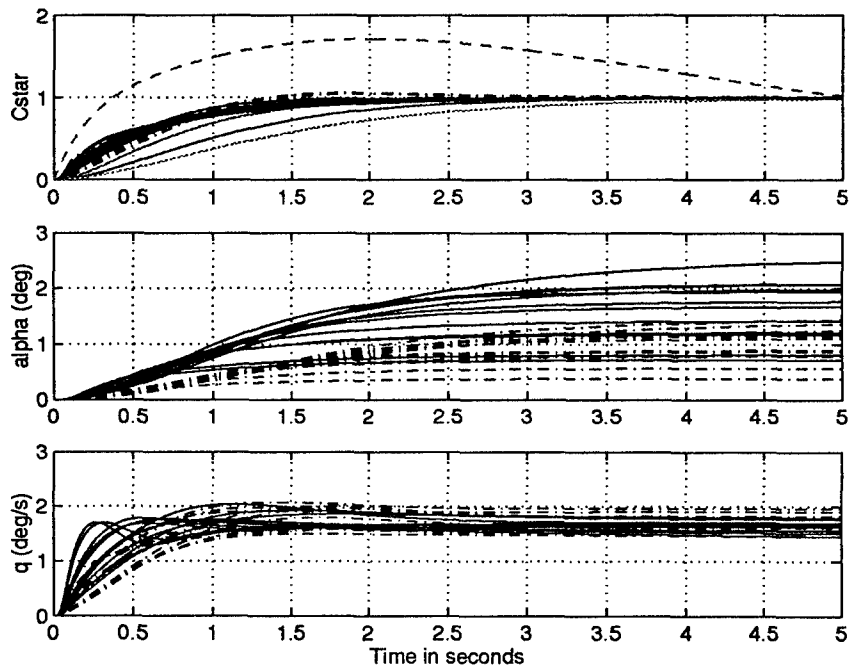


Figure 5.23 Unit  $C^*$  Step Response of Compensated System, Healthy Aircraft and 25% Stabilator Failure Plants ( $\bar{q} > 200 \text{ lbs/ft}^2$ ) [1 of 2]

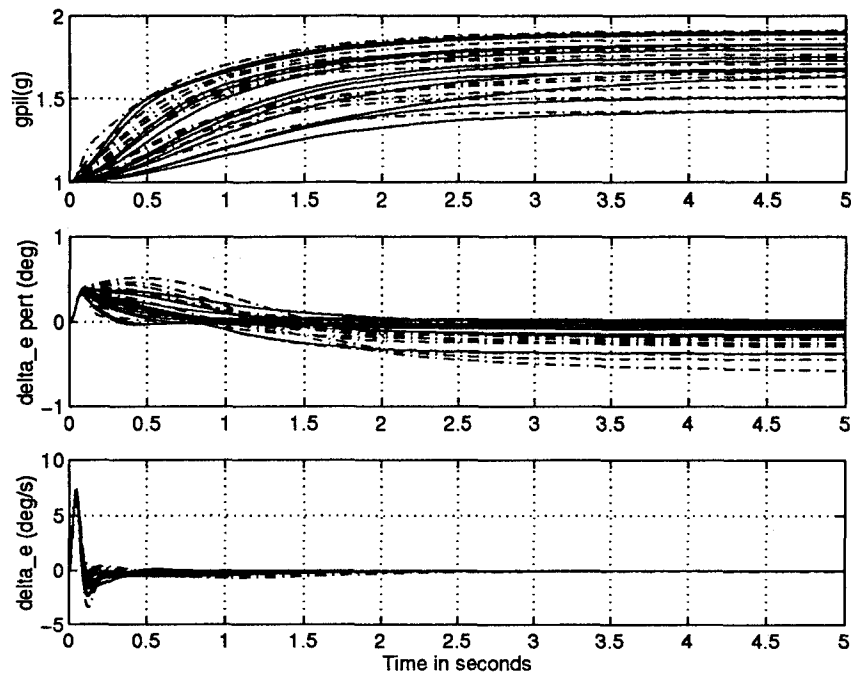


Figure 5.24 Unit  $C^*$  Step Response of Compensated System, Healthy Aircraft and 25% Stabilator Failure Plants ( $\bar{q} > 200 \text{ lbs/ft}^2$ ) [2 of 2]

command profile given the unit step responses:

$$\left[ \begin{array}{l} \frac{20 - \text{trim}_{elev}}{\max\{\delta_{elev(pert)}\}}, \text{ for } \delta_{elev(pert)} > 0, \\ \text{and} \\ -\frac{20 + \text{trim}_{elev}}{\min\{\delta_{elev(pert)}\}}, \text{ for } \delta_{elev(pert)} < 0 \end{array} \right] \quad (5.12)$$

$$\frac{60}{\delta_{elev(max)}} \quad (5.13)$$

$$\frac{25 - \alpha_{trim}}{\alpha_{pert(++)}} \quad (5.14)$$

$$\frac{8}{g_{pil(++)}} \quad (5.15)$$

As an additional constraint there is one healthy plant and one failed plant for each  $\bar{q}$  point. Therefore, the minimum of Eqs. (5.12) and (5.13) and the maximum of Eqs. (5.14) through (5.15) for each  $\bar{q}$  case is employed in the development of the boundaries. This procedure generates the worst case restrictions on the aircraft. The maximum command

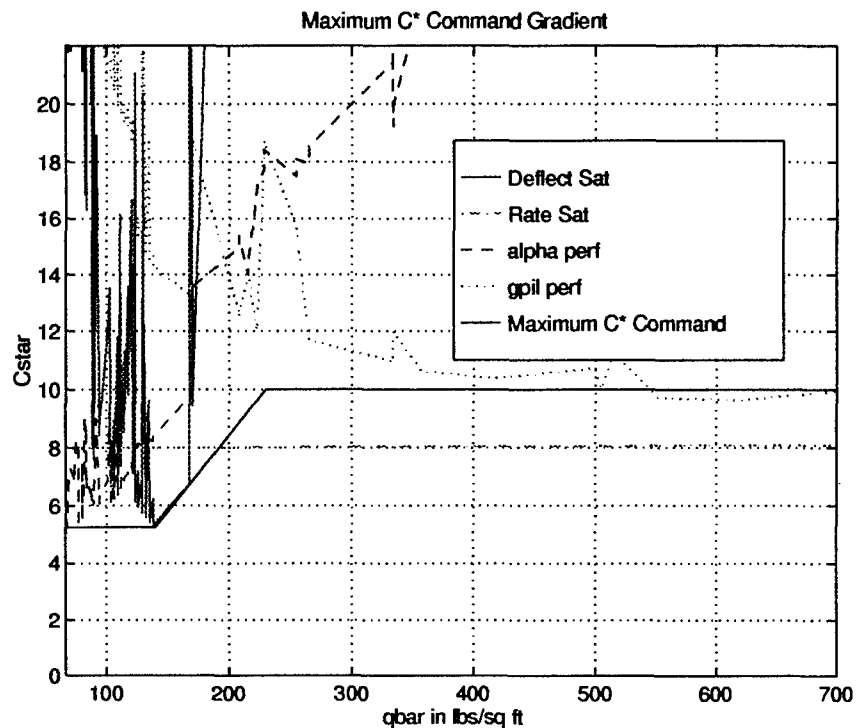


Figure 5.25 Maximum  $C^*$  Command Profile

gradient must fit under the saturation boundaries given by Eqs. ( 5.12) and ( 5.13) while simultaneously maintaining a level greater than the performance boundaries represented by Eqs.( 5.14) and (5.15). The command profile is found in Fig. 5.25. It is apparent from this figure that the performance boundaries can not be achieved without rate saturating the actuators. It is also apparent that the  $g_{pil}$  performance specifications are meaningless and unachievable for the low  $\bar{q}$  range, while the alpha performance specifications become unachievable for the high  $\bar{q}$  plants. Furthermore, after flight testing his control system on the SRF nonlinear simulator, Phillips admitted that his command profile, which avoids both rate and saturation limits over the entire  $\bar{q}$  range, was probably 'too conservative.' [6] Ultimately, some compromises are required to balance control effector saturation and performance specifications. Since the rate saturation boundaries prove to be the limiting factor, they are effectively ignored, while the alpha performance specifications are deemed valid for the plants under  $200 \text{ lbs/ft}^2$  and the  $g_{pil}$  specifications are valid for plants in excess of  $200 \text{ lbs/ft}^2$ .

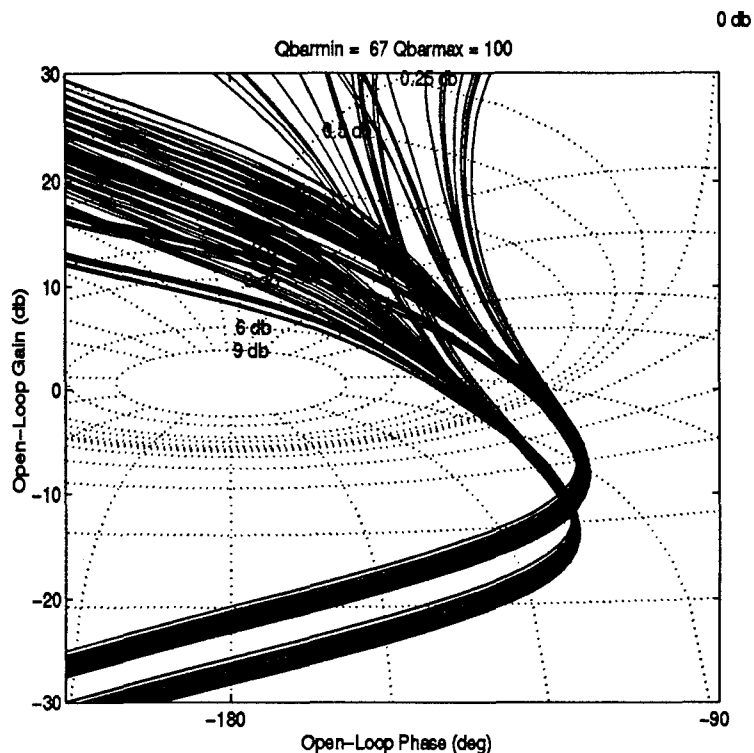


Figure 5.26 Nichols Chart of low  $\bar{q}$  Plants

When the rate and deflection saturation nonlinearities are added to the design, the system becomes unstable for several plants within the  $\bar{q}$  range of 100 to 150  $lbs/ft^2$ . To stabilize the system two courses of action are presented. Either gain scheduling can be introduced into the longitudinal system to adjust the demand on the elevator over the range of dynamic pressure, or the maximum command gradient can be reduced over this low  $\bar{q}$  range. The first course of action is found to be unacceptable since the plants causing the most difficulty are the low  $\bar{q}$  plants and they already define the top of the stability contour(see Fig. 5.26). The only plants that can be reduced in gain are the high  $\bar{q}$  plants and they are already acceptable. The second course of action proves to be more fruitful. After some trial and error, the rate saturation limits could be exceeded while the deflection saturation limits, especially in the low  $\bar{q}$  could not. If the deflection saturation limits are exceeded the VISTA becomes unstable. The final maximum command profile is reduced slightly in the low  $\bar{q}$  range, and the stability problems dissipate.

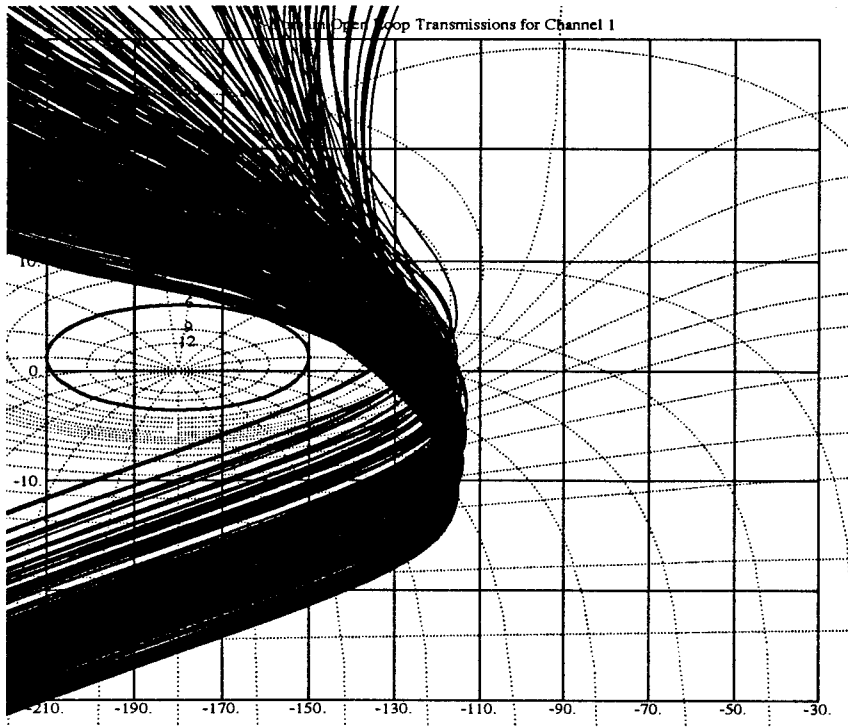


Figure 5.27 QFTCAD Stability Validation

### 5.3 Design Validation

As the final step in the design process, QFTCAD is utilized to verify that the system satisfies the frequency and time domain stability, tracking, and external disturbance specifications.

**5.3.1 Stability Validation.** Since the QFT design process is based on the manipulation of one nominal plant, it is necessary to guarantee that all 398 plants (199 healthy + 199 failed) meet the 30 degree phase margin and 6 dB gain margin stability requirements before concluding the design. As indicated on Fig. 5.27 all of the plants both healthy and failed meet the stability bounds, hence one of the major design goals is accomplished.

**5.3.2 Tracking Validation.** Though the lower frequency bounds can not be achieved during the loop shaping process, the tracking responses within the pilot's bandwidth met Level 1 and 2 specifications as seen in Fig. 5.28.

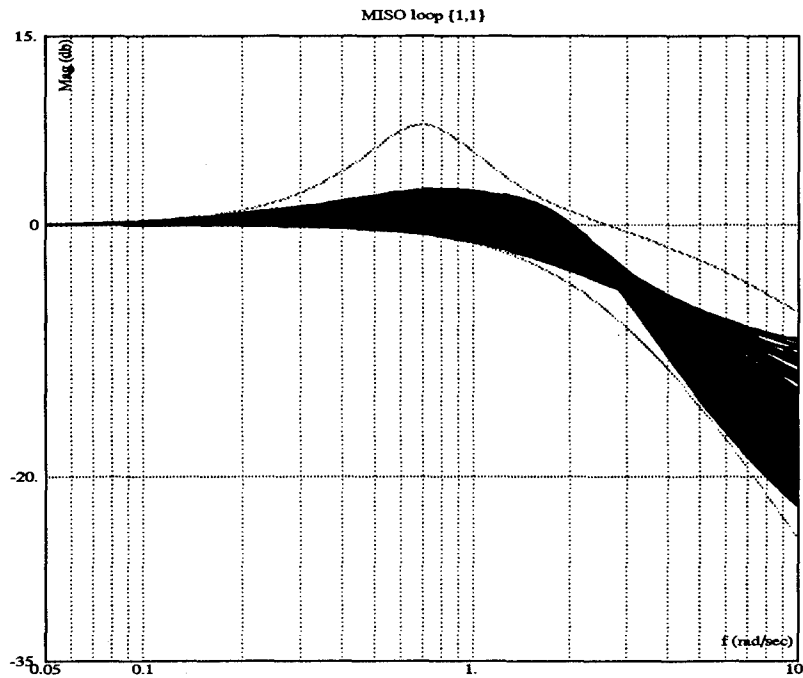


Figure 5.28 QFTCAD Tracking Validation

*5.3.3 External Disturbance Rejection Validation.* Unfortunately, the system shown in Fig. 5.29 does not exhibit the overall level of external disturbance rejection initially mandated. The problem plants represented by those exceeding the 0 dB limit at 2 rps and those exceeding the -11 dB limit at 30 rps, are identified as the low dynamic pressure failure plants. The external disturbance simulations are necessary to determine if these trouble plants can be controlled by a human pilot.

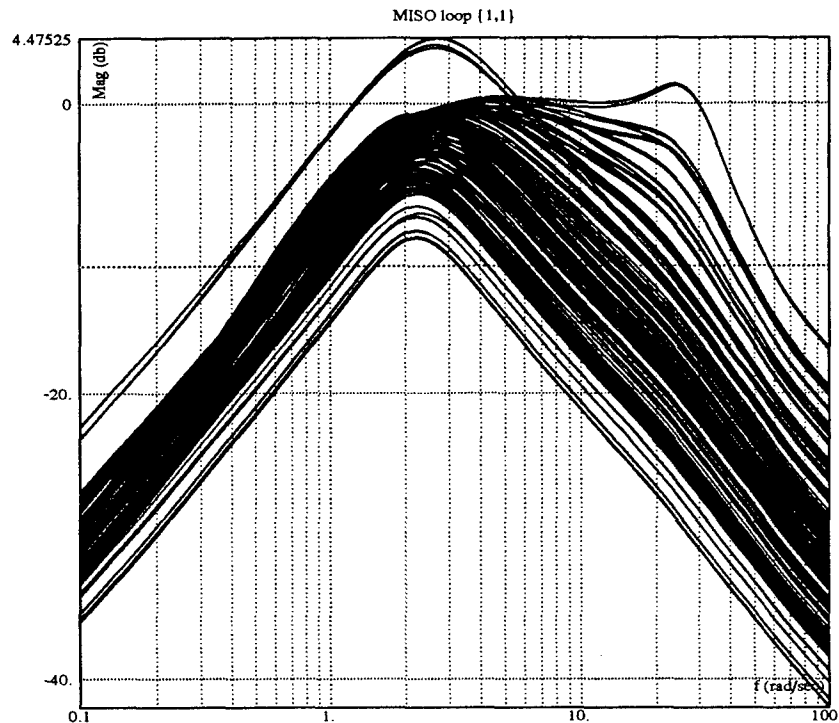


Figure 5.29 QFTCAD Disturbance Rejection Validation

#### 5.3.4 Time Domain Validation.

5.3.4.1 *C\* Tracking Responses.* The compromise between performance for the healthy aircraft and stability for the failed aircraft is clearly seen in the low  $\bar{q}$  simulations found in Figs. 5.30 and 5.31. The healthy aircraft can only achieve  $25^\circ$  of  $\alpha$  for approximately half of the plant cases, while the elevator ( $\delta_e$ ) is driven to its maximum deflection by the failure cases. The healthy plants also display significantly less onset delay and overshoot than the failed plants, yet the failed plants are still within the Level 2 flying qualities specifications supported by the tabular data in Appendix C. These effects demonstrate that the compensator allows the failed plants to saturate the elevator deflection, while simultaneously achieving nearly nominal performance by a majority of the healthy plants. Hence another major thesis goal is satisfied.

The dynamic pressure ( $\bar{q}$ ) has the most substantial effect on the system responses of any of the plant parameters introduced in this design, and this fact is clearly illustrated in the comparison of Figs. 5.30 and 5.31 with Figs. 5.32 and 5.33. The performance criteria

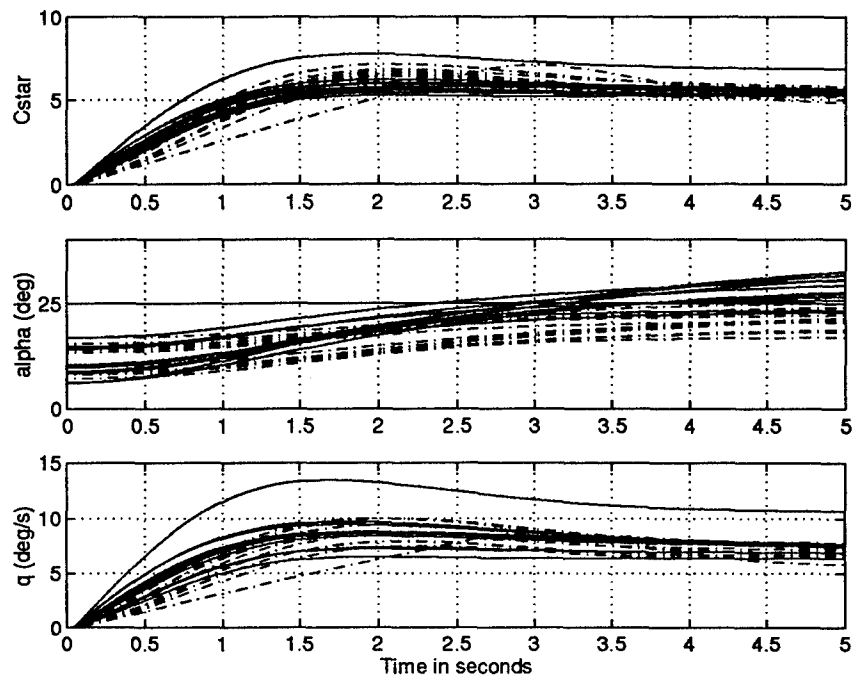


Figure 5.30 Maximum  $C^*$  Step Response of Compensated System, Healthy Aircraft and 25% Stabilator Failure Plants ( $\bar{q} < 200 \text{ lbs/ft}^2$ ) [1 of 2]

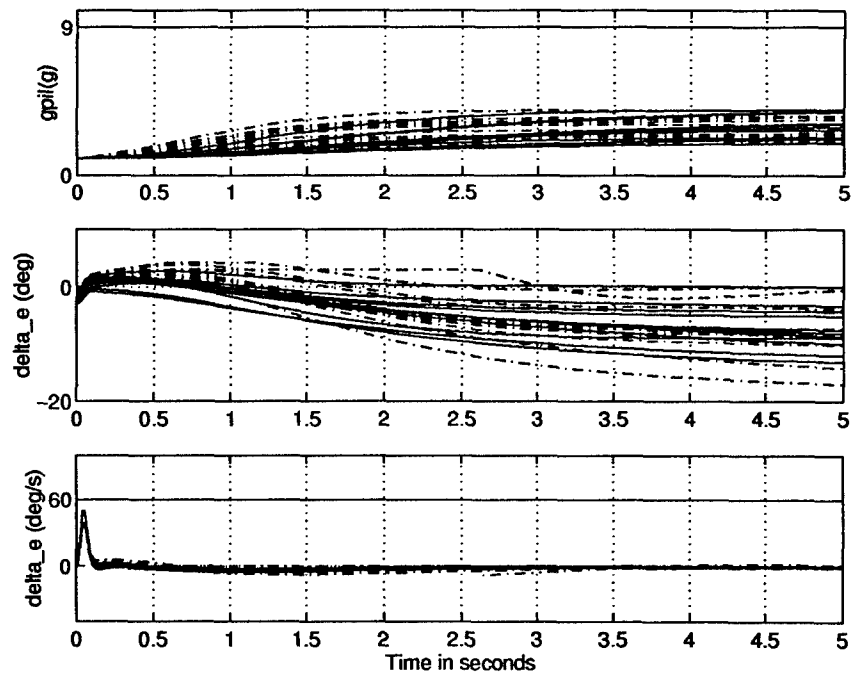


Figure 5.31 Maximum  $C^*$  Step Response of Compensated System, Healthy Aircraft and 25% Stabilator Failure Plants ( $\bar{q} < 200 \text{ lbs/ft}^2$ ) [2 of 2]

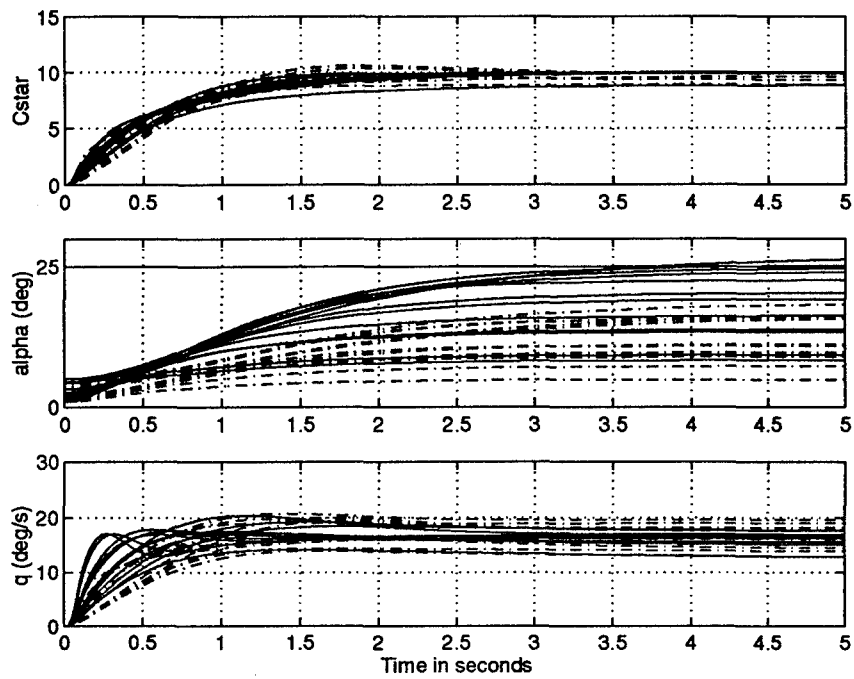


Figure 5.32 Maximum  $C^*$  Step Response of Compensated System, Healthy Aircraft and 25% Stabilator Failure Plants ( $\bar{q} > 200 \text{ lbs/ft}^2$ ) [1 of 2]

focus shifts away from meeting  $25^\circ$  of  $\alpha$  for the low  $\bar{q}$  plants and towards meeting the 9 g's at the pilot station for the high  $\bar{q}$  plants. The majority of healthy plants either meet or exceed the g loading benchmark, while the majority of failed plants are slightly lower than the 9 g benchmark. Furthermore, there is significant dynamic pressure to generate the pitching moment with much less deflection of the elevator both for the failed and healthy plant cases. Moreover, saturating the elevator rate does not cause the same stability problems experienced when deflecting the elevator to saturation. Thus, the more aggressive maximum command profile proves to be beneficial in satisfying the required benchmarks.

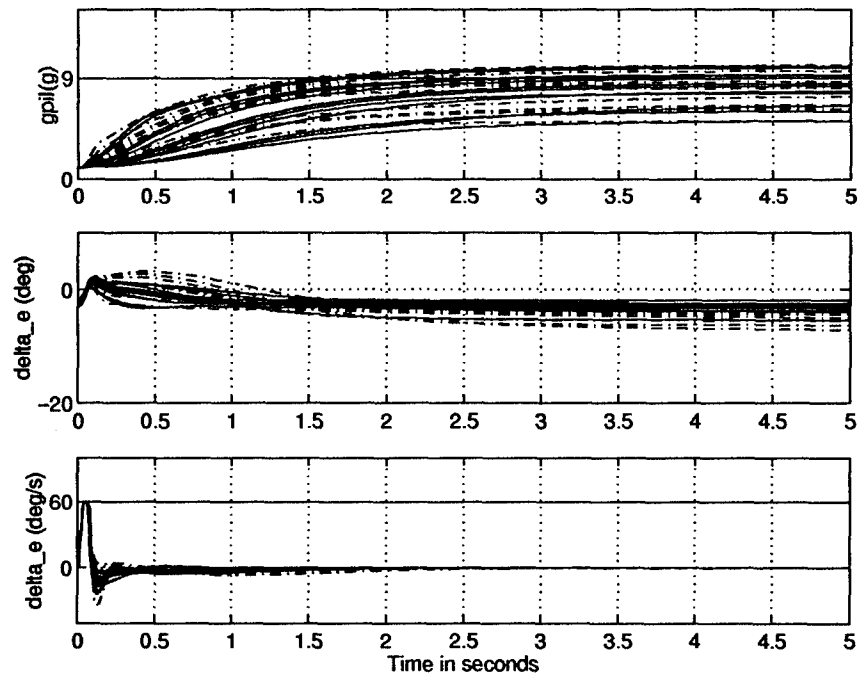


Figure 5.33 Maximum  $C^*$  Step Response of Compensated System, Healthy Aircraft and 25% Stabilator Failure Plants ( $\bar{q} > 200 \text{ lbs/ft}^2$ ) [2 of 2]

*5.3.4.2 Disturbance.* On the list of design criteria that are of vital importance to the system, the disturbance responses ranked the lowest. Keating modeled the longitudinal disturbance to reflect the change in trim due to a reduction in the elevator area. There are two goals in this disturbance analysis. First, the system must maintain stability, and, second,  $C^*$  must settle within the 5 second time period of interest. As the data found in Appendix C.5 and the disturbance responses for both low and high dynamic pressure found in Figs. 5.34 through 5.37 can attest both of these design criteria are achieved. In addition the maximum disturbance input caused a 0.80 g load and 10 deg/sec pitch rate change in the aircraft state. Both worst case scenarios can be countered by a human pilot and do not represent significant threats to the stability of the aircraft. Finally though the actuator rate limits are exceeded for the higher  $\bar{q}$  plants found in Fig. 5.37, the crucial deflection limits are not exceeded by either high or low  $\bar{q}$  plant cases, hence this degraded level of external disturbance is accepted as a consequence of designing a fault tolerant flight control system.

#### *5.4 Longitudinal Design Summary*

This chapter examines the complete longitudinal QFT design process including the development of the QFT structure, tracking model generation, frequency template failure analysis, compensator design and simulation evaluation. The first step in the design procedure is to fabricate the QFT feedback structure. In this design an innovation is applied as the feedback variable. The purpose of this innovation, known as  $C^*$ , is to combine pilot preference and engineering expertise in the formulation of a realistic FCS for the VISTA F-16. Though  $C^*$  more accurately reflects the pilot's tracking tendencies, the MILSTD only provides specifications for traditional pitch rate tracking. Approximations are necessary to translate the pitch rate tracking specifications to  $C^*$  and the onset rate  $t_i$  emerged as the dominant specification. With the tracking requirements set, the other stability and performance criteria are taken directly from the applicable requirements. The longitudinal design plant set  $\mathcal{P}$  is generated by *Matlab* macros to represent plant parameter variations over a range of altitude, airspeed, center of gravity, and of course control effector failure cases. Through the QFTCAD program the frequency templates are then formed, affording the

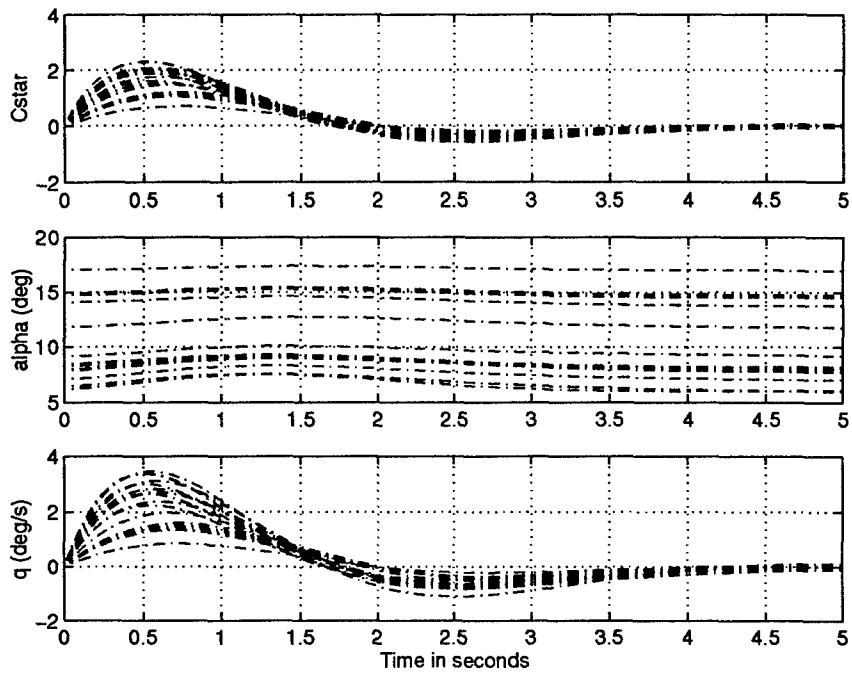


Figure 5.34 Disturbance Unit Step Response of Compensated System, 25% Stabilator Failure Plants ( $\bar{q} < 200 \text{ lbs/ft}^2$ ) [1 of 2]

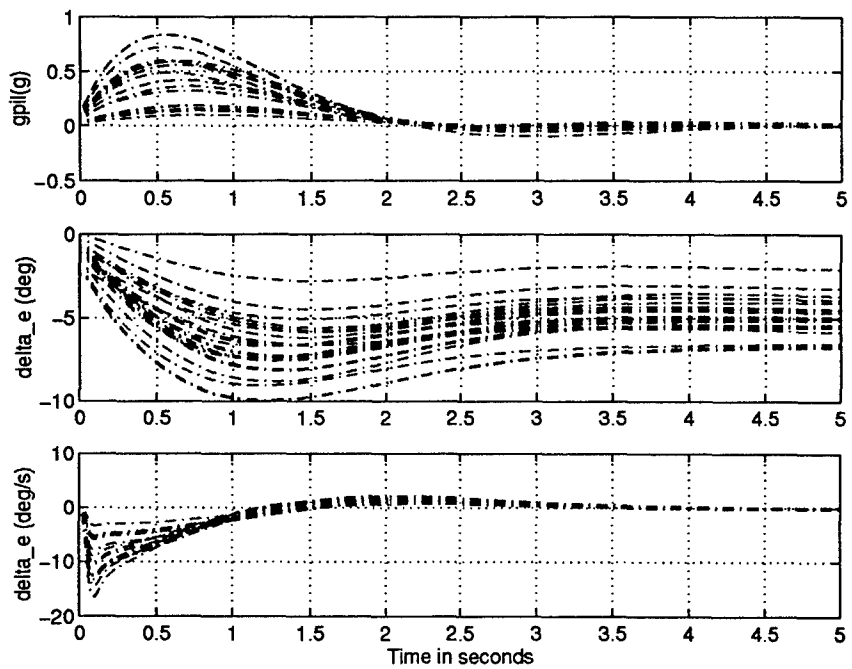


Figure 5.35 Disturbance Unit Step Response of Compensated System, 25% Stabilator Failure Plants ( $\bar{q} < 200 \text{ lbs/ft}^2$ ) [2 of 2]

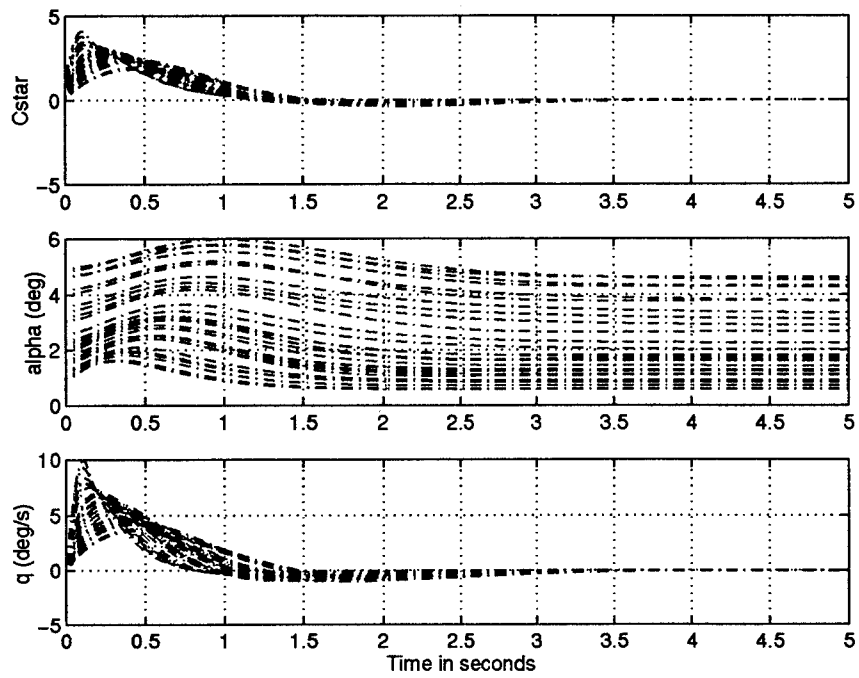


Figure 5.36 Disturbance Unit Step Response of Compensated System, 25% Stabilator Failure Plants ( $\bar{q} > 200 \text{ lbs/ft}^2$ ) [1 of 2]

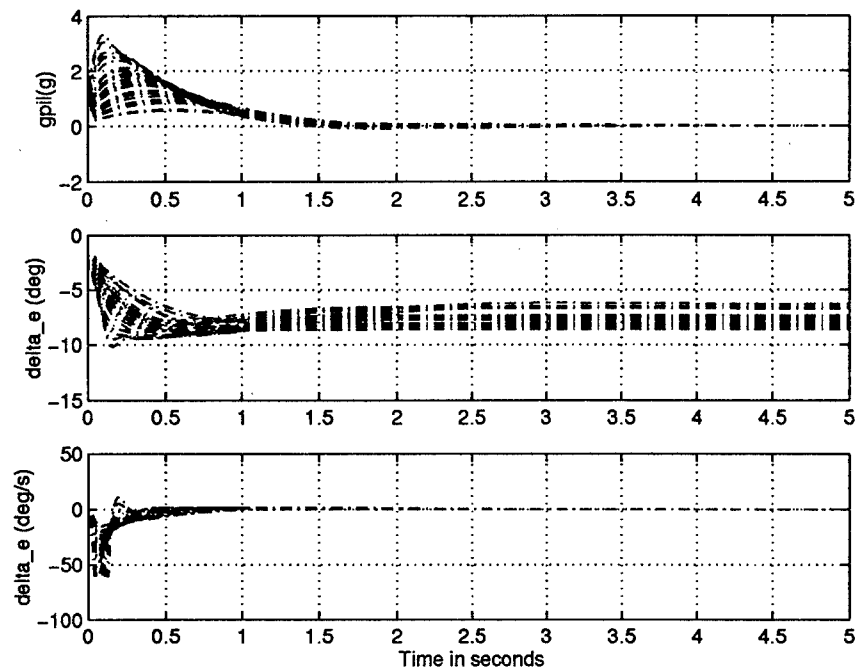


Figure 5.37 Disturbance Unit Step Response of Compensated System, 25% Stabilator Failure Plants ( $\bar{q} > 200 \text{ lbs/ft}^2$ ) [2 of 2]

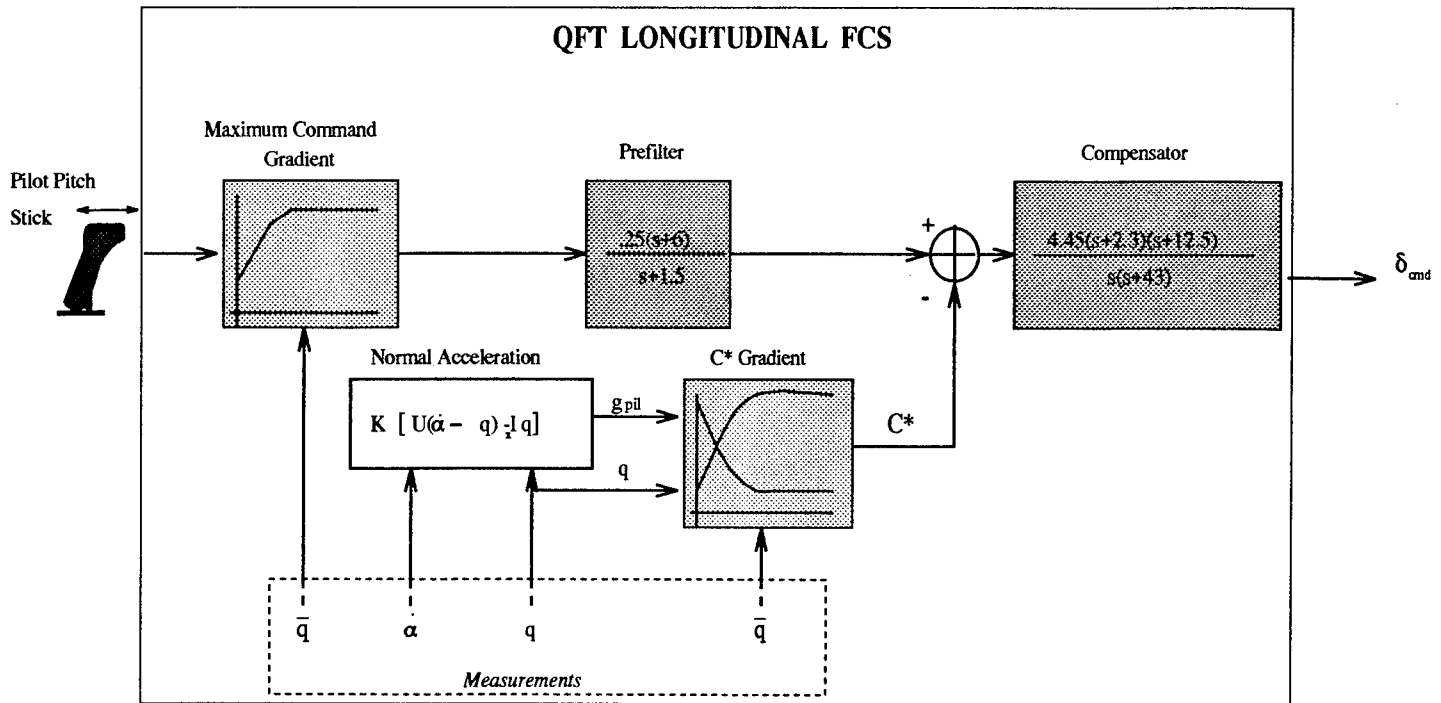


Figure 5.38 Final QFT Longitudinal FCS

first opportunity to determine the extent of control effector failures on the aircraft system. Though the templates expand both in magnitude and phase with increasing damage levels, the magnitude is most significantly impacted overall. From this analysis, the 25% failure level case is selected and the QFT bounds are generated. The tracking bounds reflect the template failure effects, expanding primarily in magnitude with respect to the healthy plants, while the external disturbance bounds present a unique problem and require some additional attention. With the composite bounds generated, the design advances to the loop shaping process. Though exceptionally restricted, a successful QFT compensator is formed and the design focus shifts towards performance evaluation. The initial unit step simulations and frequency domain validation with the exception of the external disturbance rejection prove to be quite encouraging. Finally, a maximum command gradient, as well as the rate and deflection saturation limitations are applied to the design and the results are evaluated. The final design appears as displayed in Fig. 5.38. A more complete evaluation of the design objectives and failure analysis follows in Chap. VII.

## VI. Lateral/Directional FCS Design

This chapter covers the complete lateral/directional channel design process from the QFT feedback structure to the design of the compensators and specification validation.

### 6.1 Lateral/Directional Design

**6.1.1 Lateral/Directional QFT Structure.** Once again the first step in any QFT design is the formulation of the feedback structure. The general MIMO plant structure in Fig. 6.1 is repeated from Chap. III. Including a diagonal prefilter (**F**) and compensator (**G**), a dutch roll damper circuit and actuator dynamics the specific lateral/directional MIMO QFT structure can be found in Fig. 6.2. It is important to note that only the aileron and differential tail actuator dynamics are represented on Fig. 6.2. The rudder actuator, missing from this figure, is actually incorporated into the plant model through a dutch roll circuit. Furthermore, there are three inputs to the lateral/directional aircraft plant, yet there are only two feedback variables, roll rate  $p$  and sideslip  $\beta$ . Therefore, a  $3 \times 2$  weighting matrix **W** is necessary to square the plant.

The incorporation of a dutch roll damper circuit (See Fig. 6.3) in the lateral/directional channel is a traditional method of eliminating the transient yaw rate resulting from an aileron deflection.[2] This circuit consists of feeding yaw rate  $r$  through a washout filter to command a counter rudder deflection. Yaw rate is selected as the control variable since it reflects an aircraft's dutch roll response, while the rudder is commanded because it primarily excites an aircraft's dutch roll mode. The purpose of the washout filter is to allow the pilot to command a steady-state yaw rate without causing an uncoordinated maneuver. The washout filter is simply a high-pass filter which, due to its position in the feedback path, enables the dutch roll damping circuit to remove (washout) a high frequency yaw rate response. The washout filter used in this design is found in Eq. (6.1).

$$H_{wash} = \frac{K\tau s}{1 + \tau s} \quad (6.1)$$

Selection of the feedback gain  $K$  and the washout filter time constant  $\tau$  is highly dependent on the aircraft, its flight condition, and other plant parameters. For the VISTA F-16, both

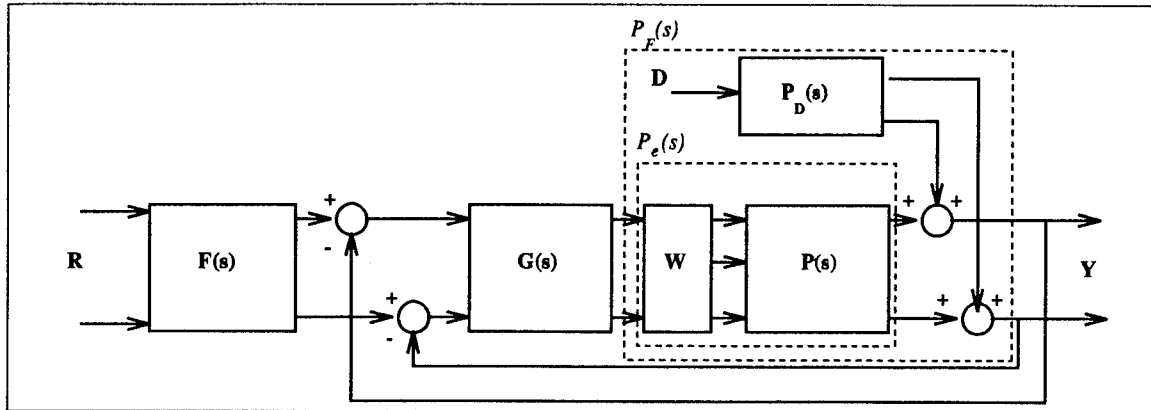


Figure 6.1 General MIMO QFT System with an External Disturbance Included

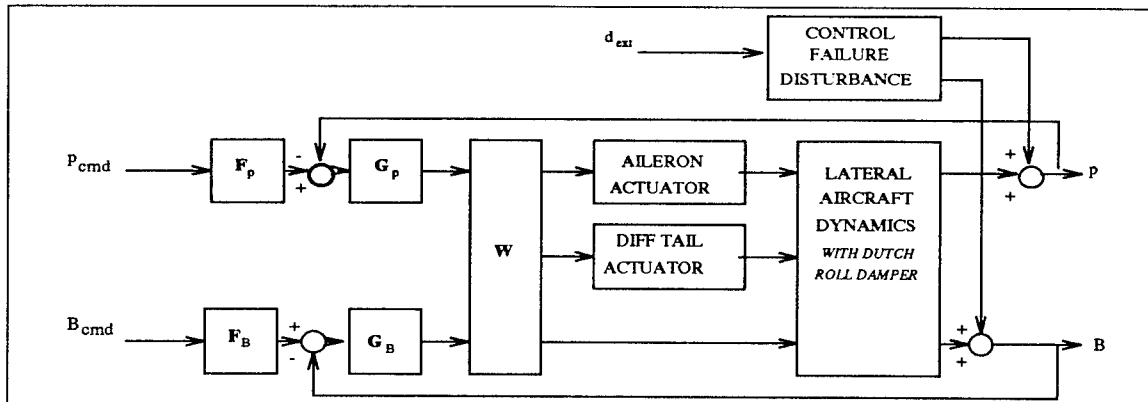


Figure 6.2 Lateral/Directional 2 X 2 MIMO System with an External Disturbance and Dutch Roll Damper

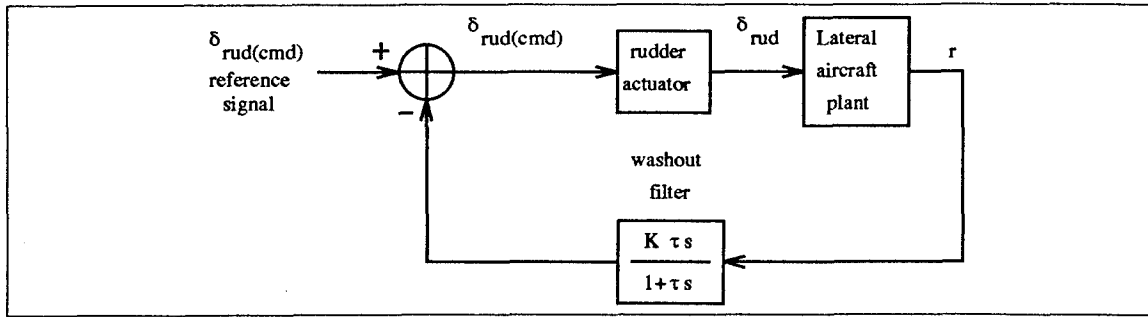


Figure 6.3 Dutch Roll Damper Structure

Reynolds [16] and Phillips [15] found that a  $\tau = 3.33$  seconds maximizes dutch roll damping for the low  $\bar{q}$  flight condition, hence this value is selected in the current design. Choosing  $\tau = 3.33$  seconds and  $K = 1$ , a root locus analysis is conducted on a range of plant cases to determine some robust gain for  $K$  that can be applied for the entire design set  $\mathcal{P}$ .

The first step in the root locus analysis is to select a subset of  $\mathcal{P}$  representative of the entire lateral/directional parameter space. Phillips found that the aircraft system differed most dramatically from one dynamic pressure extreme to the other, so a low and high  $\bar{q}$  flight condition was selected in his research. Since failure effects were not considered in previous VISTA research, the failures must be represented in the subset as well. Thus, yaw rate/rudder ( $r/\delta_r$ ) transfer functions are developed according to the procedure outlined in Chap. III for a low and high  $\bar{q}$  flight condition from each failure case in the design set. Given these transfer functions, a root locus is generated for each plant case. The root locus plots in Figs. 6.4, 6.5, and 6.6 are representative of the entire range of healthy and failed plants. It is evident from Figs. 6.5 and 6.6 that only the rudder failures effect the dutch roll mode, and the natural frequency of the dutch roll mode poles is reduced with rudder failure. The next step is to select a gain  $K$  to provide the maximum damping ratio for both the high and low  $\bar{q}$  plant cases. The '+' on the root locus plots represents the position of the closed loop poles for a gain = 1.4. Notice this gain only maximizes the high and low  $\bar{q}$  healthy aircraft damping (See Fig 6.4). As a compromise among the various plant sets, a unity gain is selected for the remainder of the design.

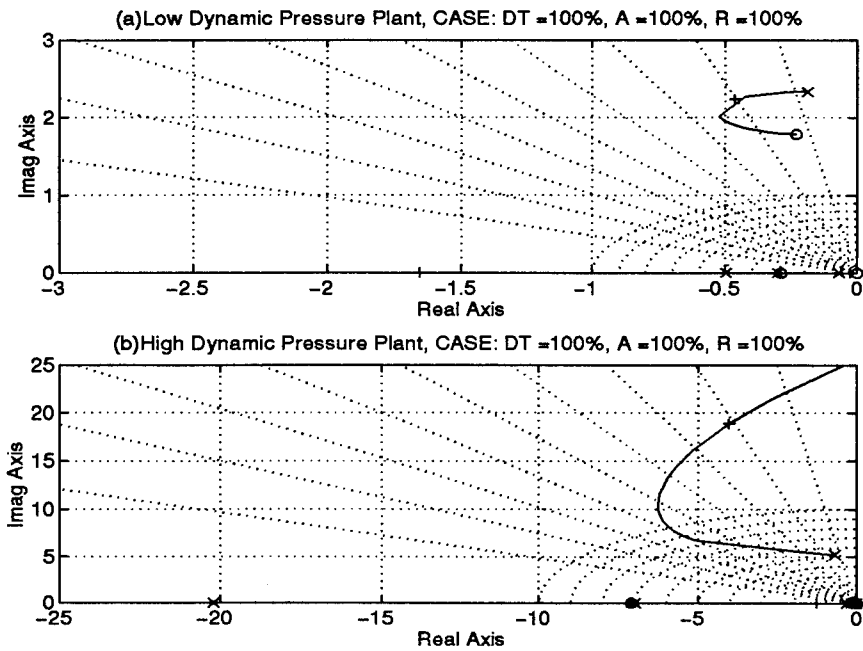


Figure 6.4 Root Locus Plots and Closed Loop Poles for Healthy Aircraft with Dutch Roll Damping Loop

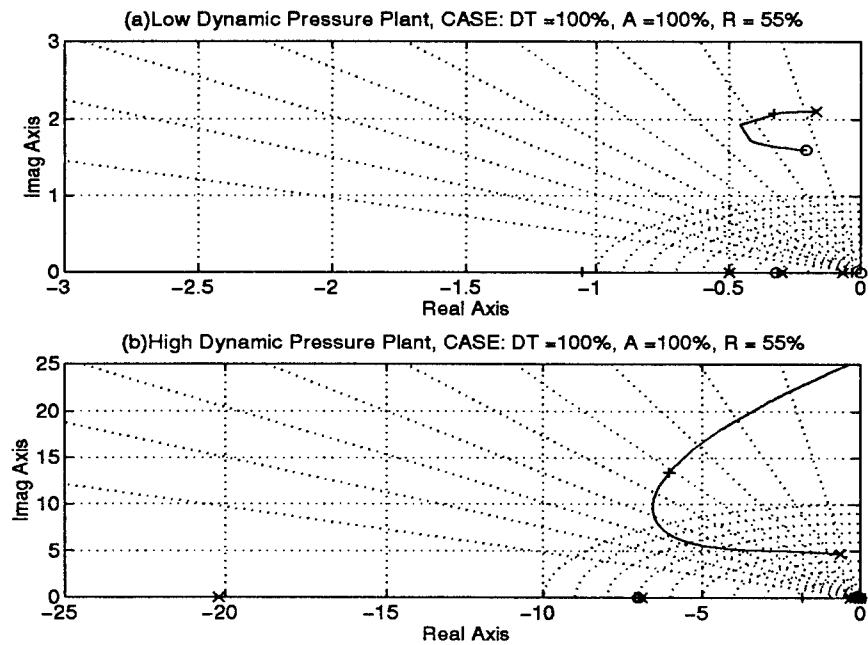


Figure 6.5 Root Locus Plots and Closed Loop Poles for 45% Rudder Failure with Dutch Roll Damping Loop

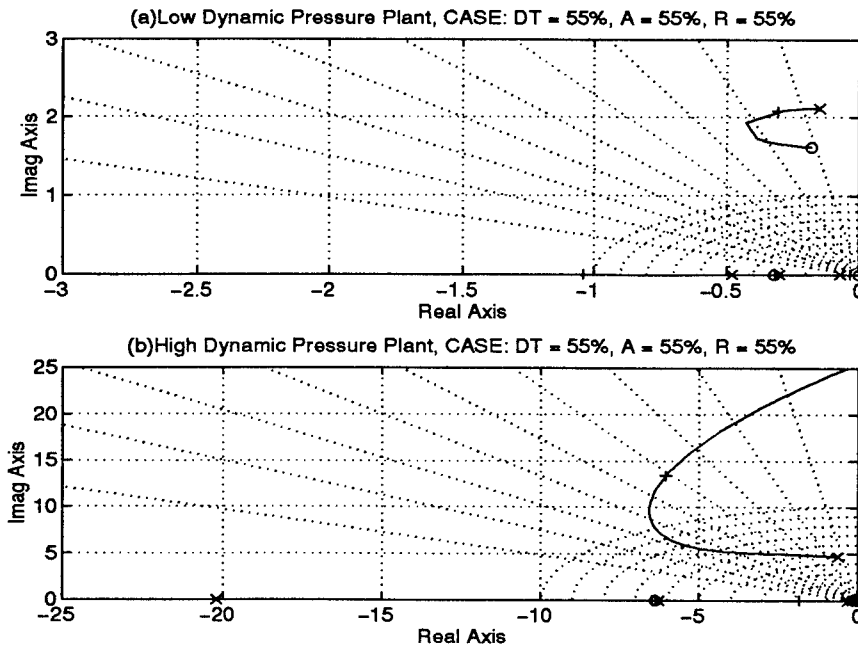


Figure 6.6 Root Locus Plots and Closed Loop Poles for 45% Stabilator, 45% Aileron, and 45% Rudder Failures with Dutch Roll Damping Loop

*6.1.1.1 Weighting Matrix.* In this research the weighting matrix represents the distribution of roll command authority between the ailerons and the differential tail. Since the differential tail can only exhibit approximately a third of the aileron deflection, the selected weighting matrix (See Eq. (6.2)) reflects this limitation. Also, to achieve 'feet-on-the-floor' turn coordination an aileron/rudder interconnect is traditionally included in the weighting matrix. However, this interconnect is not included for a couple of reasons. First, Reynolds explored various weighting matrices in his attempt to construct a full subsonic envelope compensator for the VISTA, and he found that the aileron/rudder interconnect actually degrades the command response. From his research the aileron/rudder interconnect introduced a high frequency 'ringing' into both the roll-rate and sideslip output[16]. Second, there is an effective aileron/rudder interconnect already built into the MIMO QFT structure chosen for this design. By rejecting the cross-coupling disturbances each equivalent MISO case in the MIMO structure is effectively decoupled. Since the feedback variables are roll rate  $p$  and sideslip  $\beta$ , QFT decoupling translates into turn coordination.

Class	LEVEL		
IV CAT A	1	2	3
	1.0	1.4	10

Table 6.1 MILSTD 1797A Recommended Roll Mode Time Constants(seconds)

$$\begin{bmatrix} \delta_{aftail(cmd)} \\ \delta_{ail(cmd)} \\ \delta_{rud(ref)} \end{bmatrix} = W * \begin{bmatrix} p_{cmd} \\ \beta_{cmd} \end{bmatrix} = \begin{bmatrix} 0.294 & 0 \\ 1 & 0 \\ 0 & 1 \end{bmatrix} \begin{bmatrix} p_{cmd} \\ \beta_{cmd} \end{bmatrix} \quad (6.2)$$

**6.1.2 Lateral Specifications.** In addition to the tracking, external disturbance, and stability performance specifications developed for the longitudinal channel, the cross-coupling specifications must also be defined for the lateral/directional design. All of these requirements are developed in the following sections.

**6.1.2.1 Tracking Specifications.** The majority of roll tracking specifications dictated by the MILSTD 1797A are in terms of time domain requirement such as minimum time to roll and maximum time to settle. The only specification that lends itself to frequency model generation is the roll mode time constants  $\tau$  found in Table 6.1. Assuming the system settles within 4 time constants, the Level 1 specification can be interpreted as a 4 second settling time. Since the MILSTD does not directly specify a damping ratio  $\zeta$  for the upper tracking bound  $T_{RU_p}$ , 0.5 is arbitrarily chosen. With this value of  $\zeta$  and the Level 1 settling time specification, the two percent settling time formula

$$T_{settle} = \frac{4}{\zeta\omega_n} \quad (6.3)$$

found in Eq. (6.3) is used to identify  $\omega_n = 2 \text{ rps}$  as the undamped natural frequency for the upper tracking bound. [5]

Given this value of natural frequency and a 0.5 damping ratio, Phillips placed a zero in the upper tracking model (Eq. (6.4)) to establish a 5 rps system bandwidth.

$$T_{RU_p} = \frac{4(s+1)}{s^2 + 2s + 4} \quad (6.4)$$

Settling Times <sup>1</sup>		
Level	Spec	Model
1	4	3.89
2	6.4	6.23
3	40	9.91

Table 6.2 Model settling times(seconds)

He also included an additional pole to the underdamped lower tracking bound,  $T_{RL1}$ , (Eq. 6.5). The purpose of this pole is to insure that the settling time does not exceed the 4 second limit for Level 1 roll tracking.

$$T_{RL1_p} = \frac{2.5}{(s + 1.25)(s + 2)} \quad (6.5)$$

Only the Level 2 and 3 lower tracking models require development in this design, since, like the longitudinal channel, the failed aircraft does not respond as quickly as the healthy aircraft. The Level 2 and 3 lower tracking models are developed following a similar modeling procedure established in Phillips' thesis. [15] The degraded roll mode time constants are transformed into settling time specifications and then the two percent settling time formula for a second-order model is applied. Additional poles are added to adjust the settling time of the system until it satisfies the MILSTD Level 2 and 3 time domain specifications. The models are found in Eqs. (6.6) and (6.7).

$$T_{RL2_p} = \frac{1.05}{(s + 0.75)(s + 1.4)} \quad (6.6)$$

$$T_{RL3_p} = \frac{0.375}{(s + 0.5)(s + 0.75)} \quad (6.7)$$

Finally, the frequency and step responses of the system are generated (Fig. 6.7) and the settling time data is gathered (See Table 6.2) to validate the tracking models.

The MILSTD does not impose boundaries on the  $\beta$  tracking response, since the pilot rarely attempts to track a sideslip angle except in refueling or terminal flight situations which are not considered in this design. Following Phillips' example, the upper and lower

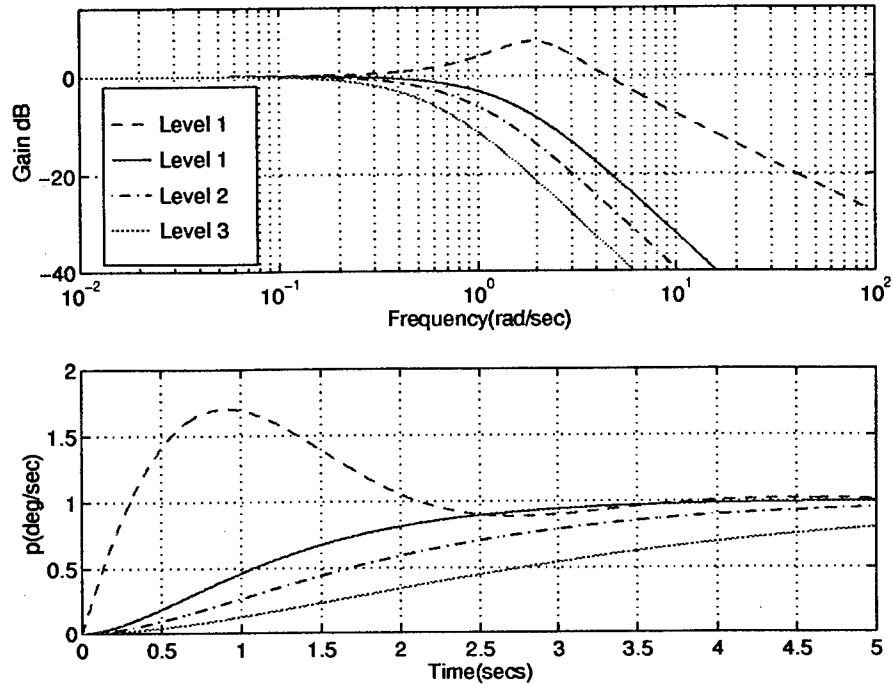


Figure 6.7 Roll Channel Level 1, 2 and 3 Tracking Specifications

boundaries (Eqs. (6.8) and (6.9)) are arbitrarily selected for the  $\beta$  response.

$$T_{RU_\beta} = \frac{4(s+1)}{s^2 + 2s + 4} \quad (6.8)$$

$$T_{RL_\beta} = \frac{1}{(s+1)^2} \quad (6.9)$$

**6.1.2.2 Cross-coupling Specifications.** The MILSTD does not provide a lucid and complete requirement for the development of QFT cross-coupling specifications. This ambiguity has lead previous designers to develop their own 'robust' specifications based upon either personal flight experience or time simulation analysis. From these developments two specific QFT cross-coupling specifications have been implemented. First, it is assumed that  $\beta$  is commanded so rarely that the coupling of  $\beta_{cmd}$  to  $p$  is not a major design consideration. If there is significant cross-coupling of the sideslip channel into the roll channel then this will appear during time simulations and corrected at that point in the design. The second cross-coupling specification places limitations on the  $\beta$  cross-coupling due to a  $p_{cmd}$  input. Unlike the  $p/\beta_{cmd}$  cross-coupling,  $\beta/p_{cmd}$  coupling is of

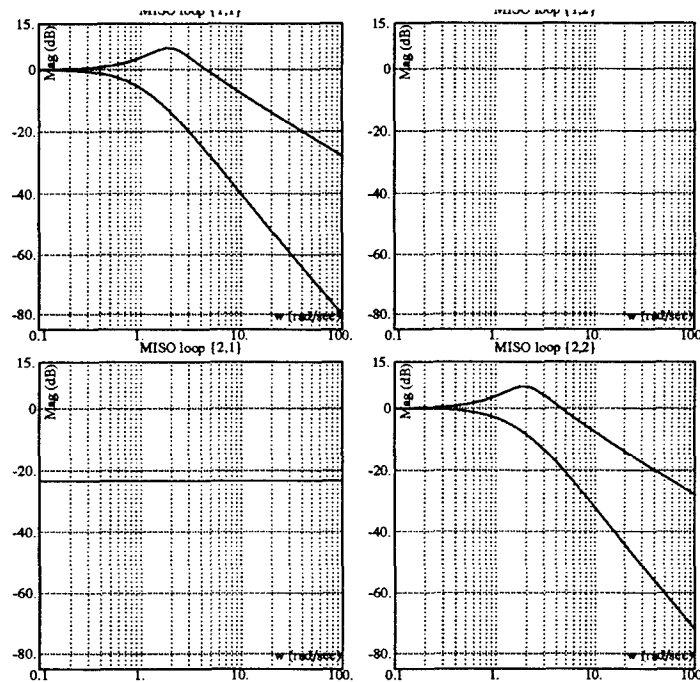


Figure 6.8 Lateral Channel Tracking and Cross-coupling Specifications

primary importance to a successful lateral/directional flight control system. To satisfy the  $\beta$  cross-coupling specifications, the aircraft must exhibit less than 0.067 degrees of sideslip for a unit step roll command at lower energy states (low  $\bar{q}$ ) or 0.022 degrees of sideslip for a unit step roll command at higher energy states (high  $\bar{q}$ ). Finally, there is also a 6 degree absolute maximum allowable sideslip limit levied on the maximum roll command input. The tracking and cross-coupling specifications are found in Fig. 6.8.

**6.1.2.3 Stability Specifications.** The same stability gain and phase margins employed in the longitudinal channel apply to the lateral/directional channel. Therefore the phase margin angle must be at least 30 degrees and the gain margin must be greater than 6 dB.

**6.1.2.4 External Disturbance Rejection Specifications.** Due primarily to the lessons learned in the longitudinal channel a -11 dB limit is arbitrarily placed on the systems external disturbance rejection response. However, like the longitudinal channel the external disturbance specifications are left to be validated in the time domain. Figure 6.9

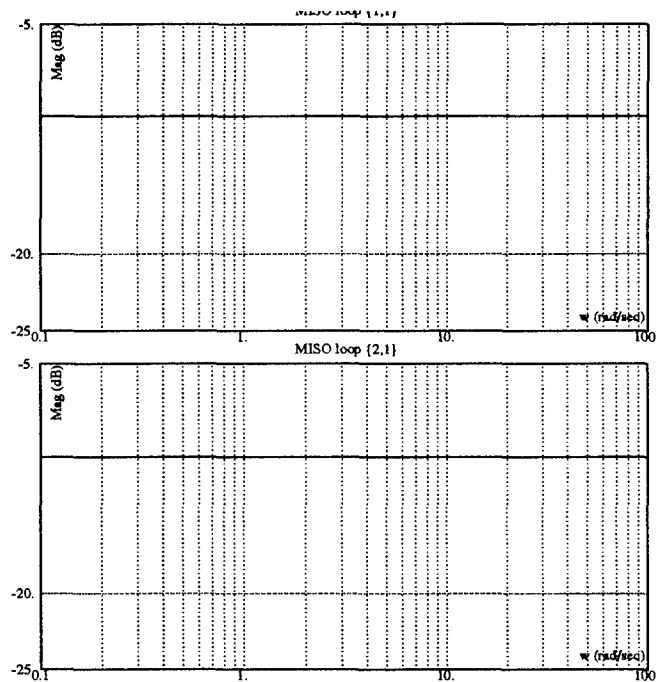


Figure 6.9 Lateral Channel Disturbance Rejection Specifications

displays the specification for both the roll (MISO loop(1,1)) and sideslip (MISO loop(2,2)) channels.

*6.1.2.5 Performance Benchmarks.* The performance specifications are dominated by the MILSTD roll angle requirements. These specifications like the cross-coupling requirements are not applicable to the entire subsonic envelope, instead they are dependent on the aircraft's forward velocity,  $U$ . This dependency is expressed in Table 6.3, where the speed range symbols are defined in Table 6.4.

Level	Speed Range	90 deg	360 deg
1	L	1.4	4.1
	M	1.0	2.8
2	L		
	M	1.3	3.4

Table 6.3 Roll Performance Specifications for MIL STD 1797A Class IV Aircraft

Speed Range Symbol	Equivalent Airspeed Range
L	$V_{min} + 20 \text{ KTS} \leq V < 1.4 V_{min}$
M	$1.4 V_{min} \leq V < 0.7 V_{max}$

Table 6.4 Speed Range for MIL STD 1797A Class IV Aircraft

Level 3 handling qualities are excluded from consideration in the roll performance requirements (Table 6.3), since this level is reserved for especially disabled aircraft where stability is the only applicable specification.

*6.1.3 Loaded and Effective Plants.* With the 3 tank configuration plants eliminated from consideration in the longitudinal design it is pointless to include this configuration in the lateral/directional channel. The remaining 199 healthy plants are once again obtained from Phillips' data files in the form of state-space **A** and **B** matrices, and subjected to the failure modeling process detailed in Chap. IV. This failure modeling process in the lateral/directional channel is complicated by yet another factor, multiple control effectors. Now in addition to the plant parameter variation inherent in the healthy plants and the damage levels experienced in the longitudinal design, each plant can also experience single, double, or triple control failures. For each damage level selected, including the healthy case, there are eight possible failure combinations translating into 1592 failure plants.

A similar procedure to the one used in the longitudinal channel is applied to the selection of damage levels in the lateral/directional channel. From previous research it appears that the longitudinal channel due to its inherent instability is more sensitive to control effector failures than the lateral/directional channel. This difference in sensitivity is manifested in the increased level of failure imposed on the lateral/directional channel. Keating found that the URV with a 50% triple control effector failure could still maintain stability. However, he did not include in his analysis the limitations imposed by rate and deflection saturations that created some difficulties in successfully designing the longitudinal compensator. Considering these saturation limitations, a 45% damage level is selected with the 25% damage level as the backup plant set.

	$\delta_{dt}$	$\delta_a$	$\delta_r$	Disturbance
$\beta$	$\beta/\delta_{dt}$	$\beta/\delta_a$	$\beta/\delta_r$	$\beta/dist$
$p$	$p/\delta_{dt}$	$p/\delta_a$	$p/\delta_r$	$p/dist$

Table 6.5 MIMO Plant Transfer Function Description

With the feedback structure defined in previous sections, and slightly greater than 3000 plants (1592 45% failed plants + 1592 25% failed plants) generated via the failure modeling process, a *Matlab* macro is employed to develop the associated QFT tracking and external disturbance transfer functions denoted in Table 6.5. The loaded plant matrix augmented with the dutch roll damper, discussed in Section 6.1.1, is 2X3 and the loaded disturbance plant matrix is 2x1. These plant matrices are formatted for input into *Mathematica* and consequently loaded into QFTCAD. The frequency responses for the 45% triple failure plant set and external disturbance plants are located in Figs. 6.10 and 6.11, respectively. The MISO loop(1,1) on Fig. 6.10 corresponds to the  $\beta/\delta_{dt}$  transfer function found on Table 6.5, while MISO loop(2,3) on this figure corresponds to the  $p/\delta_r$  transfer function. The other MISO loops correspond similarly to this table, including the disturbance transfer functions found in Fig. 6.11.

Ultimately, the weighting matrix described in Eq. (6.2) and the actuator dynamics found in Eq. (3.13) are placed in series with each loaded plant and the 2x2 effective plant matrix is generated via QFTCAD. The frequency response of these effective plant models can be found in Fig. 6.12, where the MISO loops correspond to the following variables:

- MISO loop (1,1) -  $\beta/\beta_{cmd}$
- MISO loop (1,2) -  $\beta/p_{cmd}$
- MISO loop (2,1) -  $p/\beta_{cmd}$
- MISO loop (2,2) -  $p/p_{cmd}$

**6.1.3.1 Diagonal Dominance.** The  $\mathbf{Q}$  matrices are generated and the verification of the diagonal dominance condition (as  $\omega \rightarrow \infty$ )

$$|q_{11}(j\omega)q_{22}(j\omega)| > |q_{12}(j\omega)q_{21}(j\omega)| \quad (6.10)$$

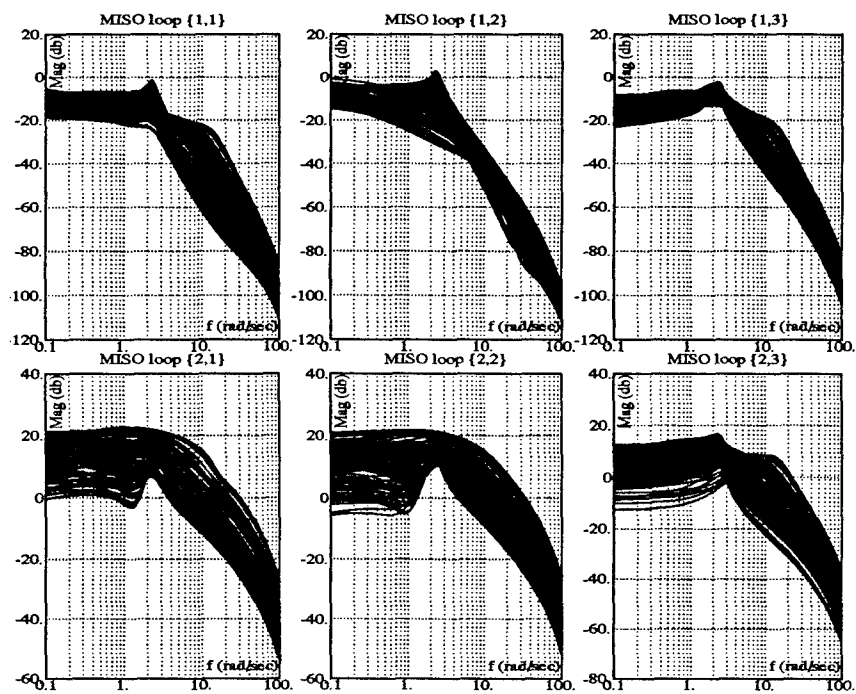


Figure 6.10 Frequency Response of Loaded Plant Models ( $P_L$ )

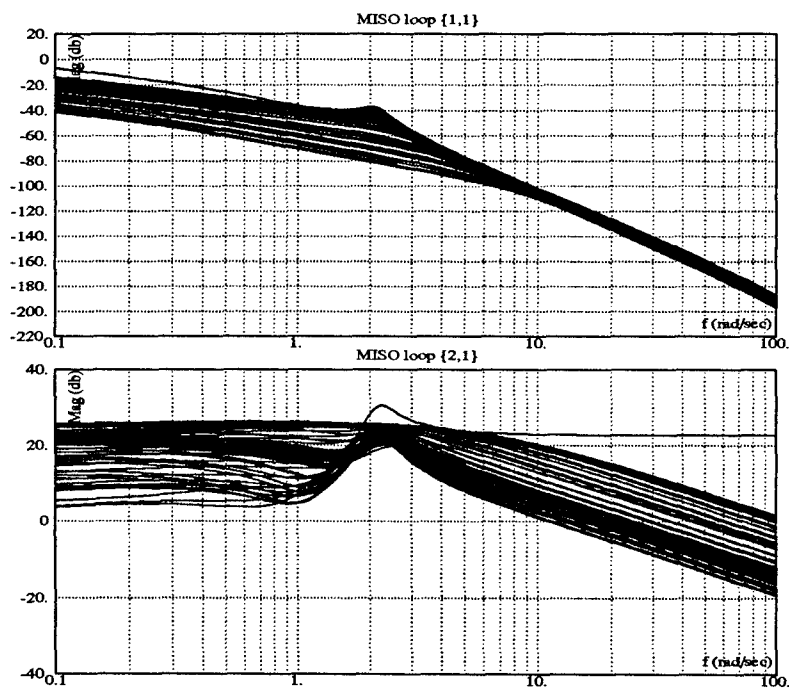


Figure 6.11 Frequency Response of External Disturbance Plant Models ( $P_D$ )

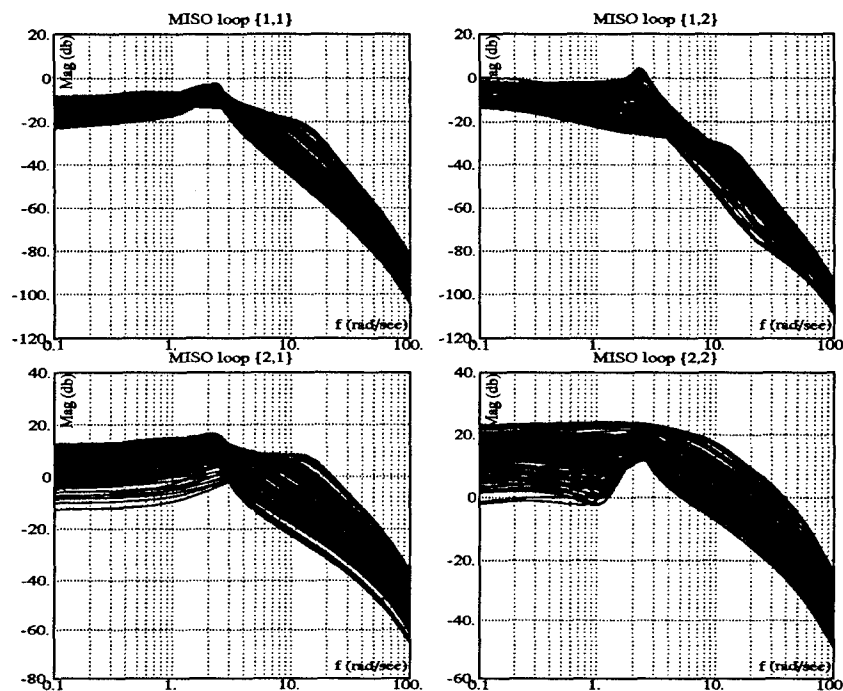


Figure 6.12 Frequency Response of Effective Plant Models ( $P_e$ )

is readily determined by QFTCAD. The diagonal dominance plot is found in Fig. 6.13. Though the responses are negative over a large portion of the bandwidth, the condition is satisfied as  $\omega$  approaches infinity. With diagonal dominance a Method 1 MIMO QFT design can be accomplished as previously discussed in Chap. II.

**6.1.4 Frequency templates.** After the plant cases and external disturbance plants are loaded, and manipulated to form the  $P$ ,  $P_e$ ,  $P_D$ , and  $Q$  matrices the QFTCAD 'Temp' option automatically generates the frequency templates for each of the two lateral/directional channels. These  $\beta$  and  $p$  templates are developed over the same range of frequencies (See Eq. (5.7)) utilized in the longitudinal design.

**6.1.4.1 Healthy Aircraft Templates.** Phillips' templates are used to benchmark the healthy aircraft models developed in this research. This comparison of healthy plant templates serves as an important milestone in the research. If the templates match, then it assures that the several *Matlab* routines employed to generate the models are working correctly, and that there is sufficient reason to assume the failure templates are correct

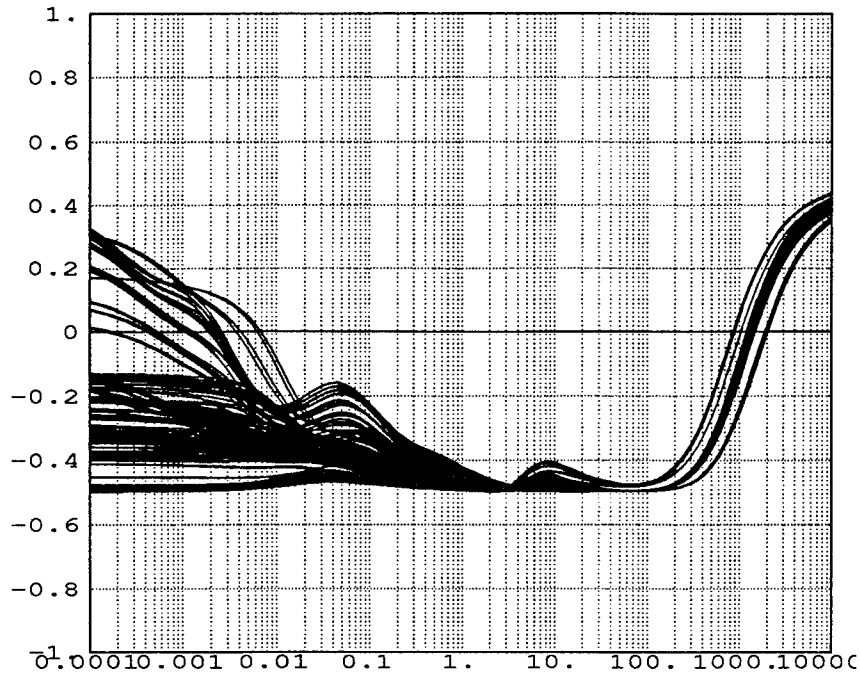


Figure 6.13 Diagonal Dominance Validation

as well. Fortunately, in the lateral/directional channel the healthy plant models from the previous design match identically with those generated in this design. Unlike the longitudinal channel, Matlab's *linmod* function provided the identical transfer functions as those developed by closing the dutch roll damper via matrix manipulation. The discrepancy found in the longitudinal channel appears to be caused by the non linear weighting scheme in the simulation diagram, and is discussed further in Appendix E.

The healthy plant frequency templates for the  $\beta$  and  $p$  channels can be found in Figs. 6.14 and 6.15. These figures provide a basis of comparison for the failed templates which are discussed in the following section.

*6.1.4.2 Failed Aircraft Templates.* The single failure templates are displayed in Figs. 6.16 through 6.23. To aid in the comparison of healthy versus failed plant cases, the healthy plant templates are superimposed on the failure templates. These figures convey considerable information about the effects of failures on the aircraft. First, each control surface failure effects the related aircraft mode. For example, a 45% aileron failure has little effect on the  $\beta$  templates found in Fig. 6.16, while resulting in a 5 dB expansion

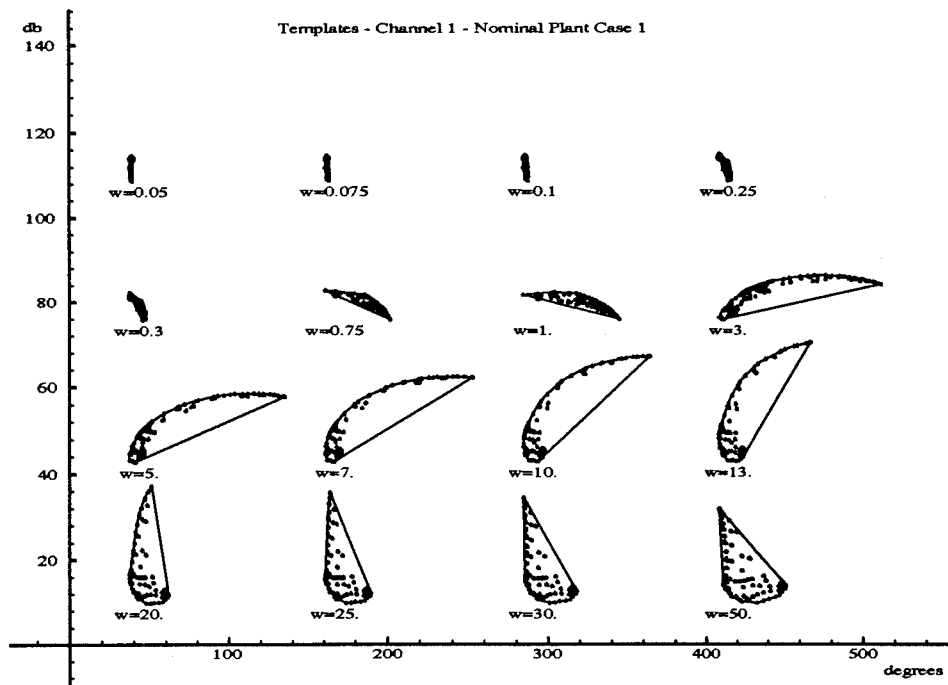


Figure 6.14 Healthy Aircraft, Beta Templates

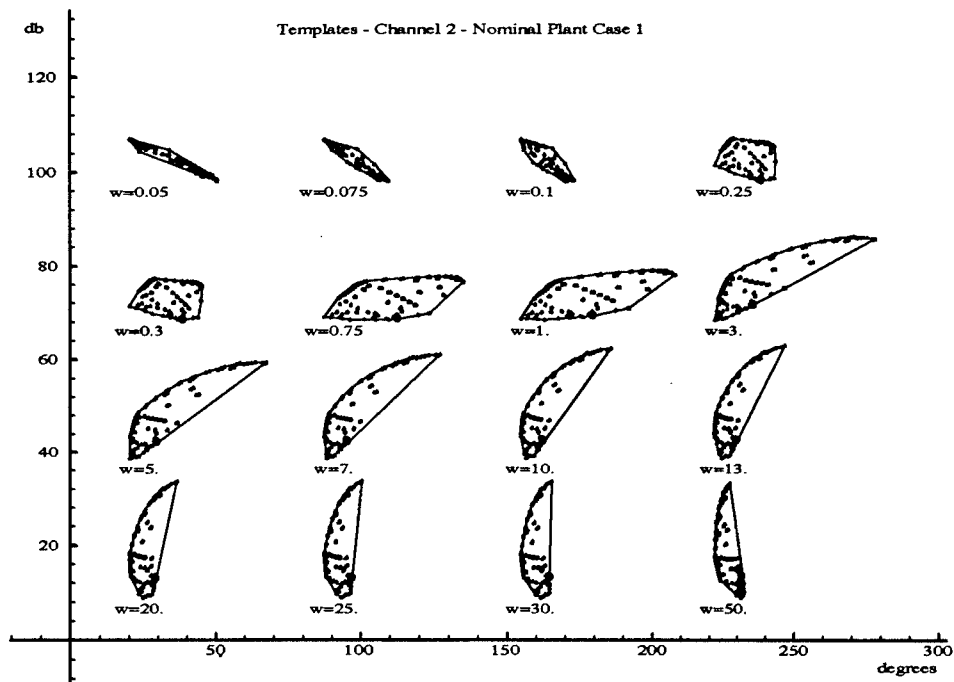


Figure 6.15 Healthy Aircraft, Roll Templates

of the  $p$  templates found in Fig. 6.17 and enlarged in Fig. 6.18. Similarly, a 45% rudder failure displays a 5 dB expansion of the  $\beta$  templates in Fig. 6.19 and Fig. 6.20, but has little effect on the  $p$  templates in Fig. 6.21. This isolation of failure effects agrees with the relationships developed in Chap. IV, and the physical laws governing the aircraft's failure response.

In addition to failure isolation, the failed templates exhibit another curious relationship. Like the longitudinal failure templates, the lateral/directional templates increase primarily in magnitude. It appears from the analysis of Figs 6.16 through 6.23, that the control derivatives, which have the greatest impact on the system gain, are most effected by the control effector failures. Though this finding seems to justify modifying only the state-space  $\mathbf{B}$  matrix in control effector failure analysis, the compensator design proves otherwise.

Finally, since  $C_{lpF}$  is the only stability derivative involving multiple control effector failures in its formulation, the multiple failure cases are simply composites of the worst case single failure templates (largest magnitude and phase template cases) identified in the single failure analysis (See Figs. 6.24 and 6.25). These composite failure plant sets justify the use of only the 199 triple failure cases to adequately represent the entire failed parameter space. If a clear relationship between multiple control effector failures and template growth could not be established, then a list of plants lying on the perimeter of each failure case, for each frequency, would have to be assembled. Fortunately, the 45% triple failure case is applied as the basic plant set for the remainder of the lateral/directional design. If a successful QFT design can not be accomplished for the 45% triple failure template design, then the backup 25% triple failure set will be implemented.

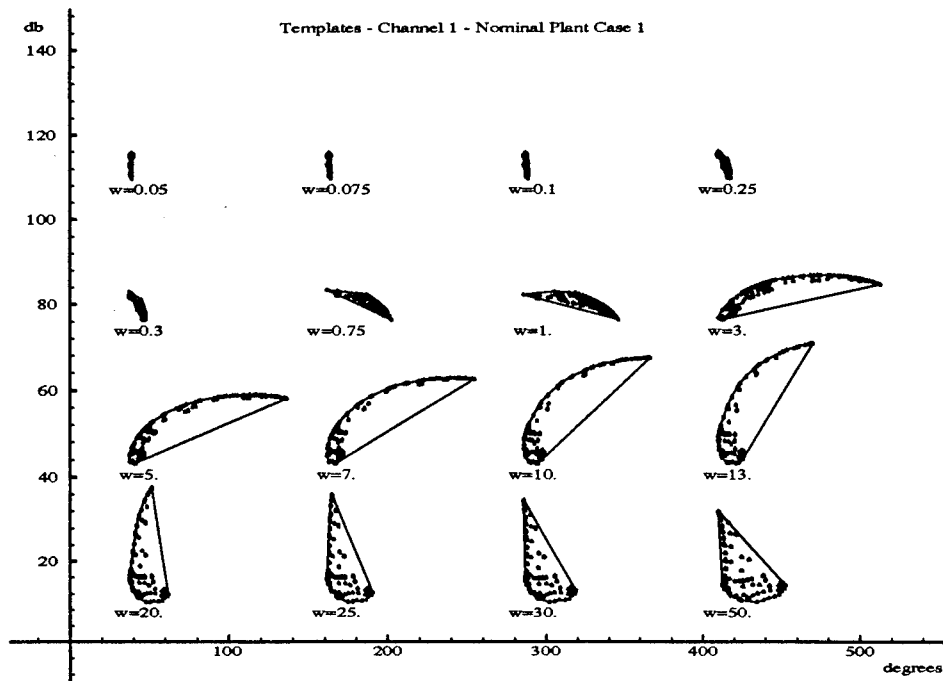


Figure 6.16 45% Aileron Failure, Beta ( $\beta$ ) Templates

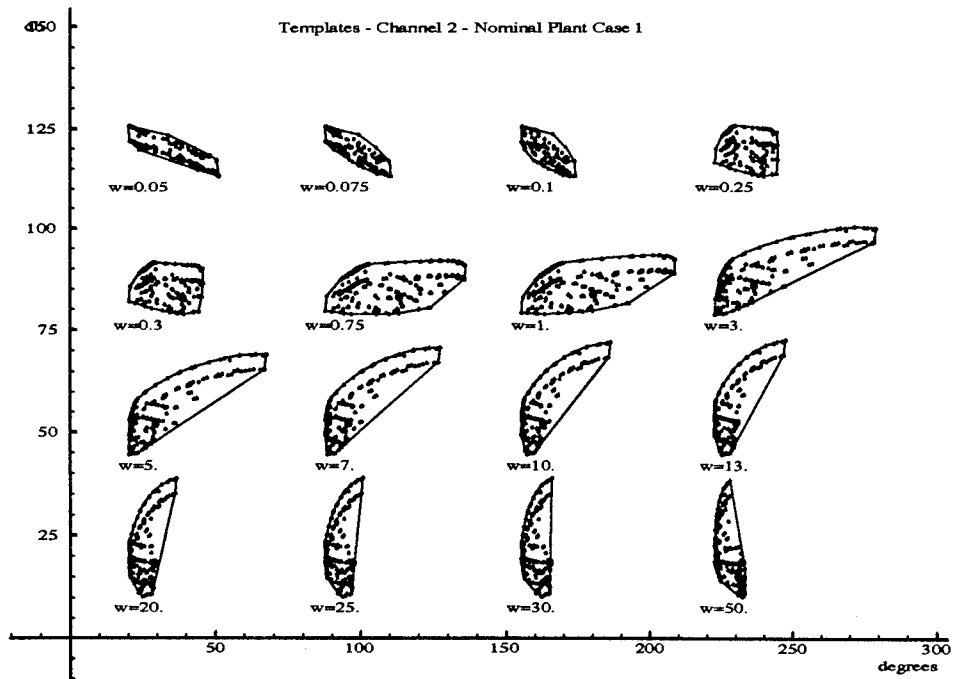


Figure 6.17 45% Aileron Failure, Roll ( $p$ ) Templates

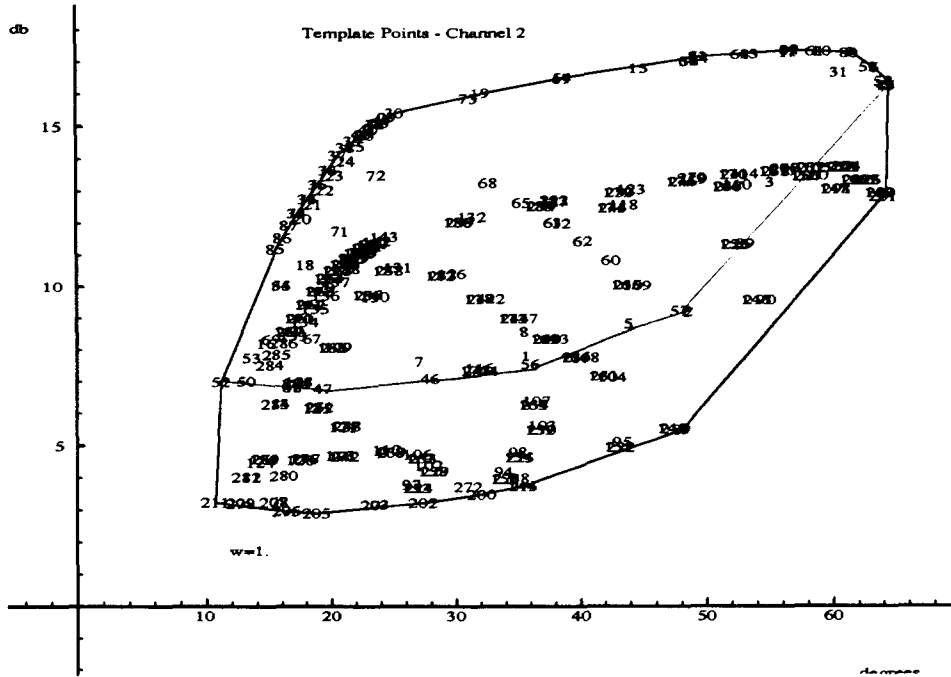


Figure 6.18 45% Aileron Failure, Roll ( $p$ ) Template for  $\omega = 1$  rps

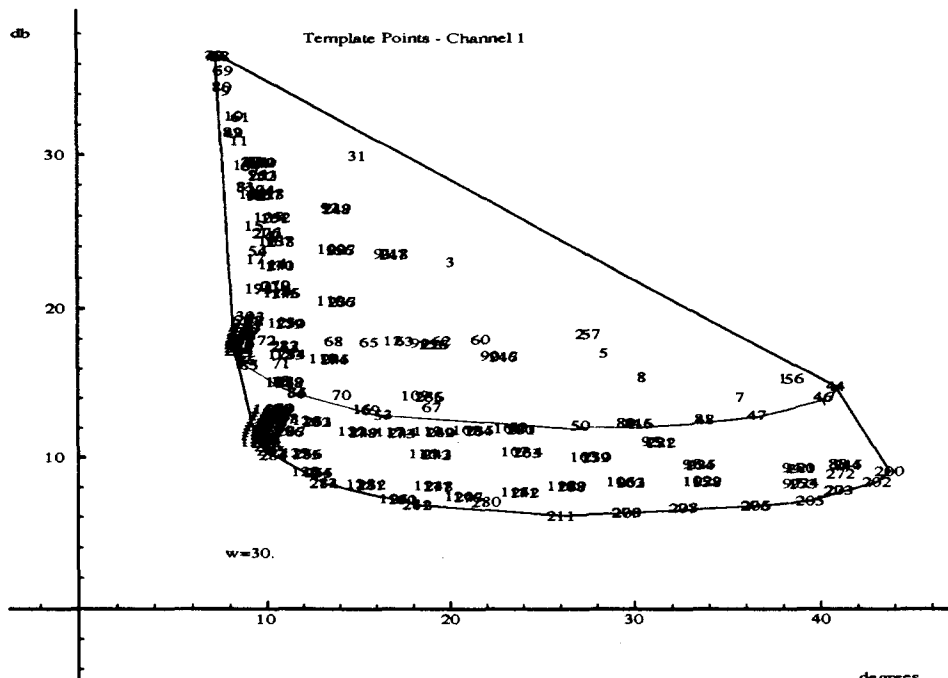


Figure 6.19 45% Rudder Failure, Beta ( $\beta$ ) Template for  $\omega = 30$  rps

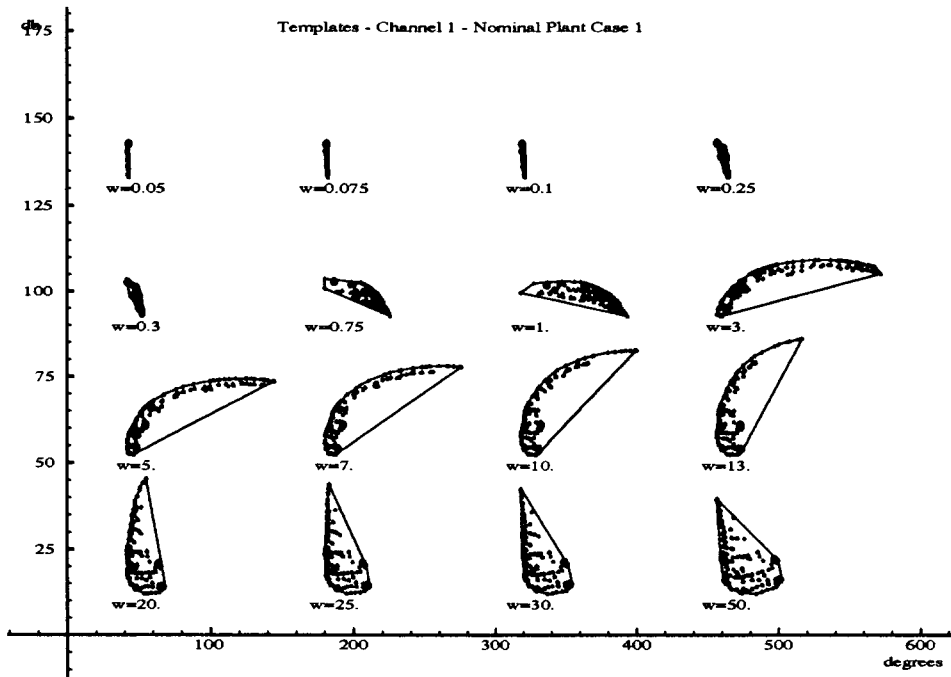


Figure 6.20 45% Rudder Failure, Beta ( $\beta$ ) Templates

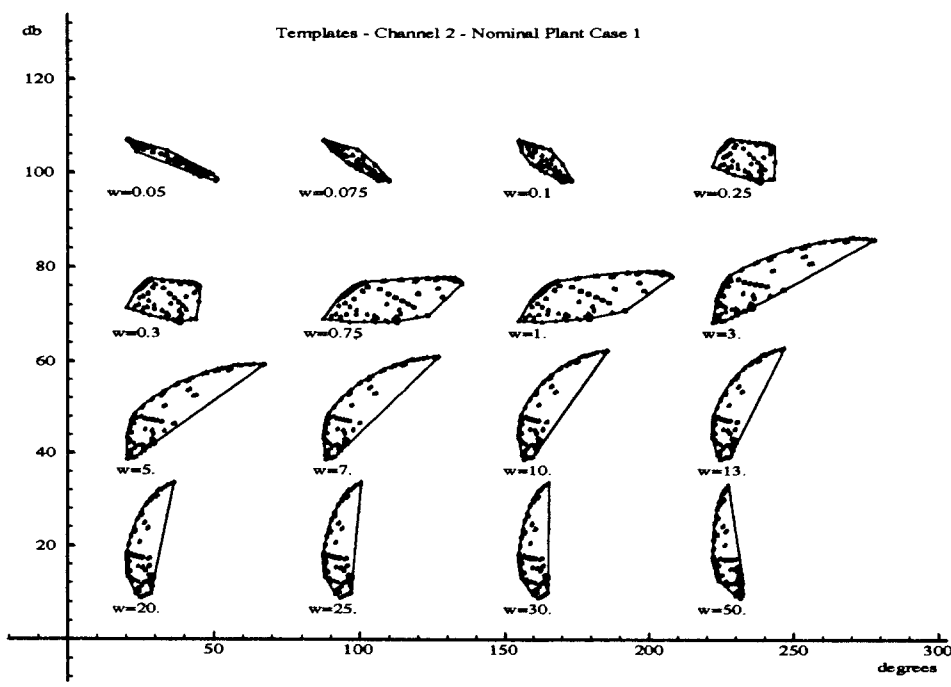


Figure 6.21 45% Rudder Failure, Roll ( $\rho$ ) Templates

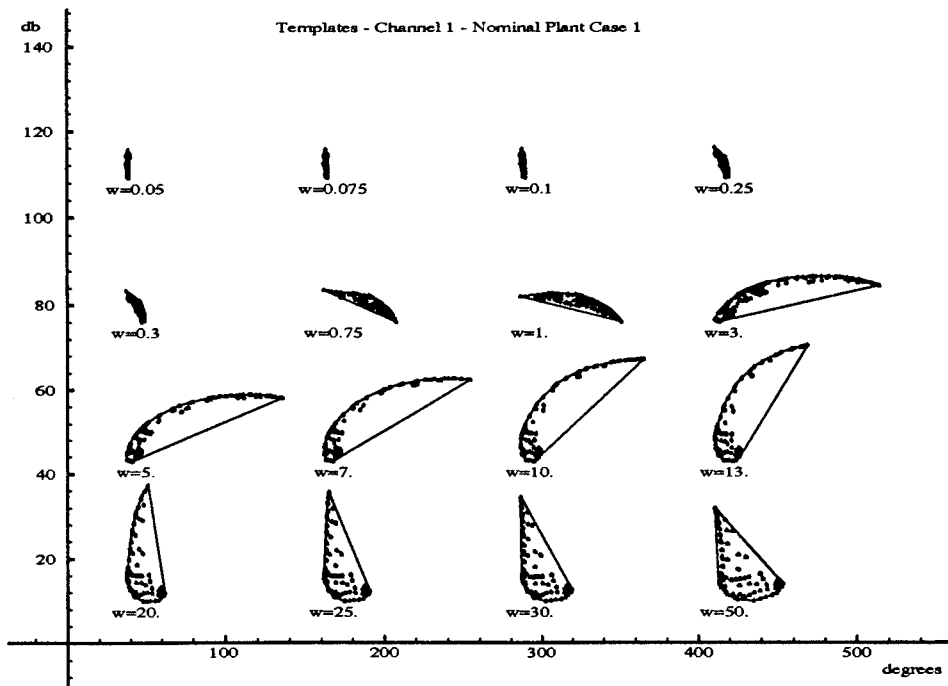


Figure 6.22 45% Differential Stabilator Failure, Beta ( $\beta$ ) Templates

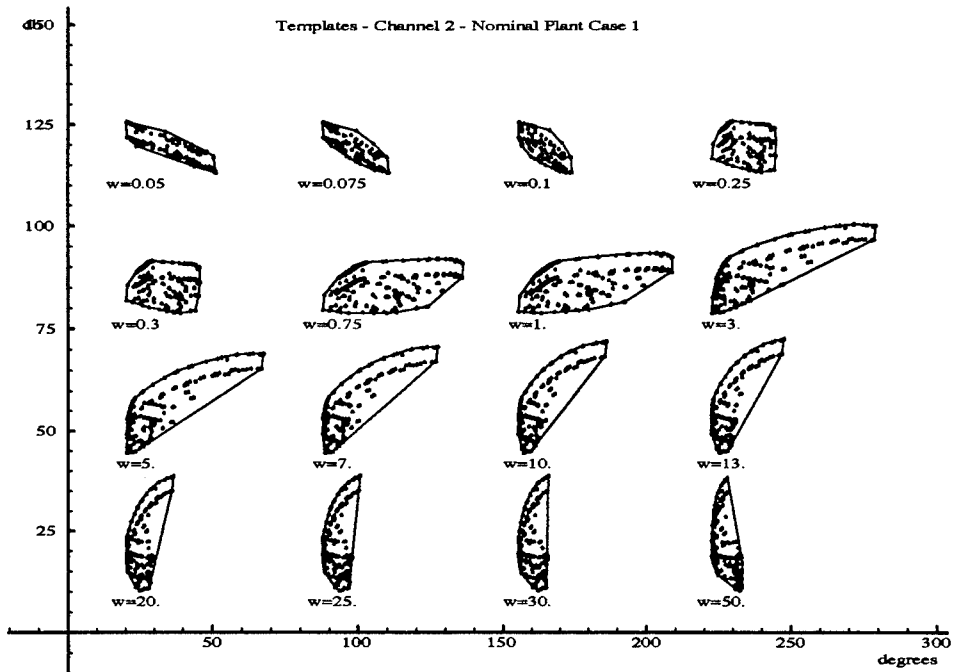


Figure 6.23 45% Differential Stabilator Failure, Roll ( $p$ ) Templates

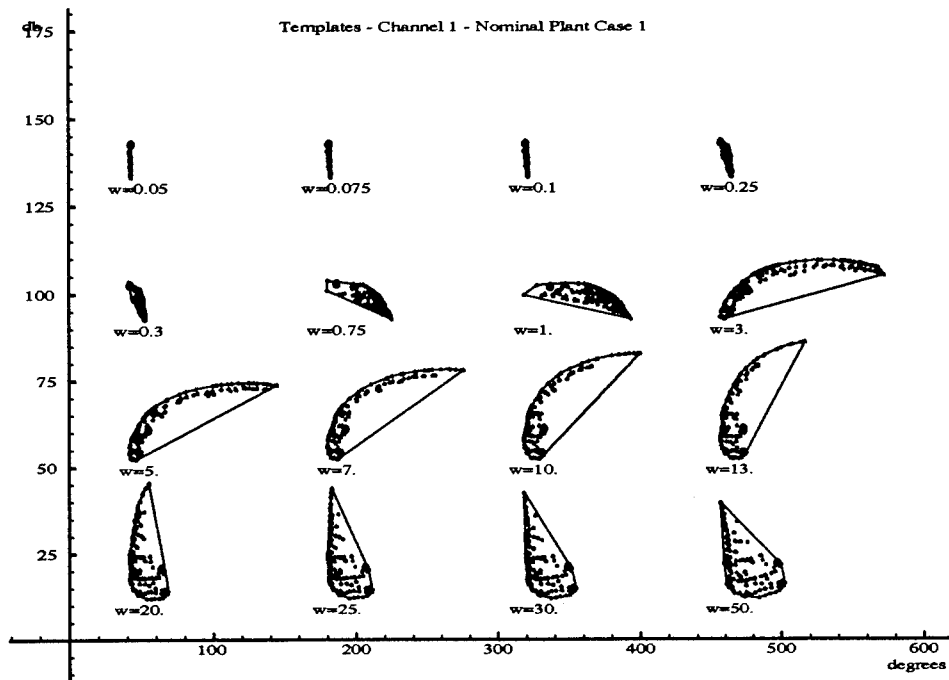


Figure 6.24 45% Triple Failure, Beta ( $\beta$ ) Templates

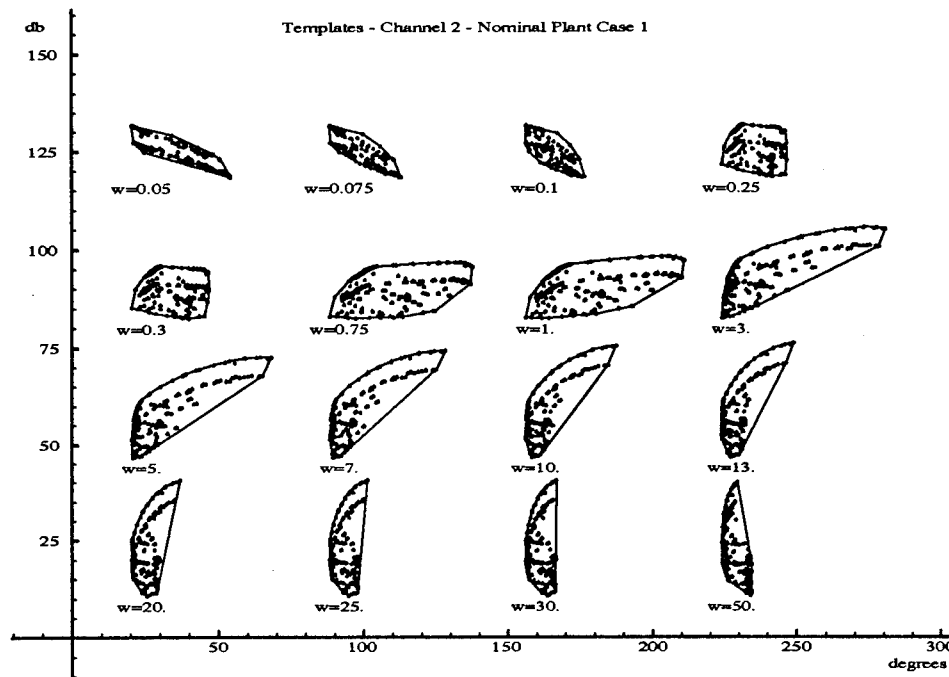


Figure 6.25 45% Triple Failure, Roll ( $p$ ) Templates

*6.1.5 QFT Generated Bounds.* The nominal plants for both the roll and beta channels are selected on top of the 30 rps frequency templates. The nominal plant for the roll channel is SRF plant #4, corresponding to the 50,000 ft Mach 0.9 trim condition, and the nominal plant for the beta channel is SRF plant #89, corresponding to the 10,000 ft Mach 0.85 trim condition. With these nominal plants, as well as the  $\mathbf{Q}$  matrices and all QFT tracking and disturbance models previously identified, the QFT bounds for tracking, cross-coupling, stability, and external disturbance are formed.

*6.1.5.1 Tracking and Stability Bounds.* The low frequency roll tracking bounds in the range of 0.05 to 0.1 rps are extremely restrictive requiring a gain increase in excess of 45 dB, however the boundaries in the bandwidth of the pilot are achievable with significantly less gain. Therefore, the lower frequency bounds are selectively disregarded and the focus is concentrated on satisfying the bounds within the pilots bandwidth. Fortunately, as previously mentioned, Phillips' lateral/directional models match identically to the healthy models developed in this research. These healthy models (See Figs. 6.26 and 6.28) provide yet another opportunity to evaluate failure effects on the system's tracking response. It is anticipated that the tracking bounds are more restrictive for the failure case, since more control effector authority is required to perform a particular tracking task. This expectation is confirmed in evaluation of Figs. 6.26 and 6.27, where the failed tracking bounds are approximately 5 dB greater than the healthy bounds at 0.75 rps. These more restrictive tracking bounds are the result of the taller(increased gain) failure templates. Finally, though the failed stability bounds demonstrate an increase in gain commensurate with the damage level there is not an appreciable difference in phase between the healthy and failed cases.

The sideslip ( $\beta$ ) channel tracking and stability bounds show similar effects to the roll channel bounds. The failed aircraft boundaries shown in Fig. 6.29 are approximately 7 dB greater than the healthy bounds at 0.75 rps. These enlarged boundaries are once again the result of the failed aircraft's taller stability bounds. These stability bounds are unlike the roll channel stability bounds, since they show both an increase in magnitude and phase when compared to the healthy boundaries found in Fig. 6.28. This increase in phase can

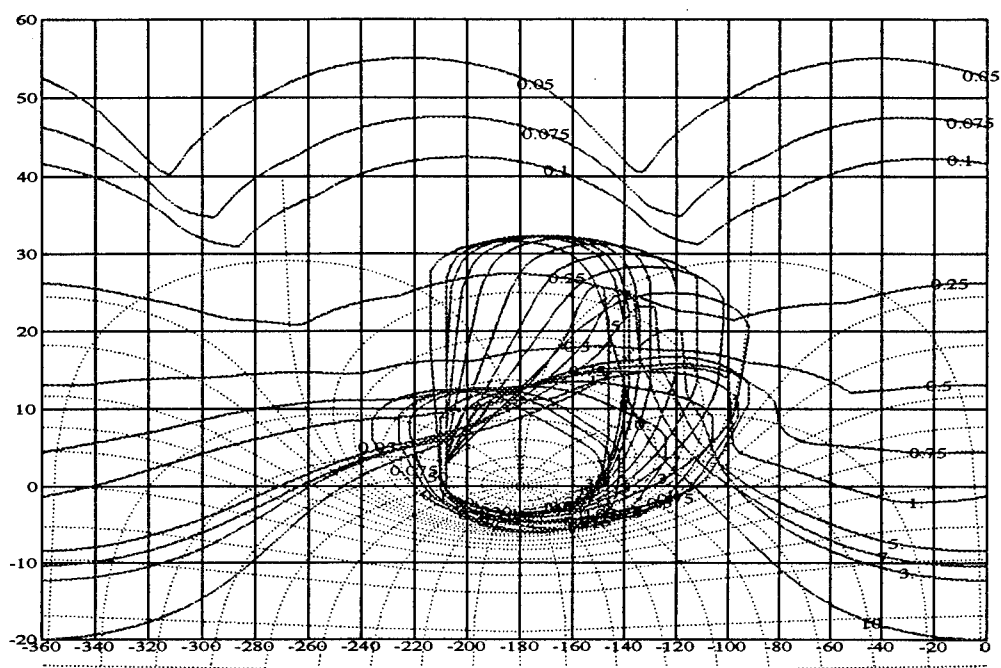


Figure 6.26 QFTCAD Stability and Tracking Bounds for the Roll Channel of the Healthy VISTA F-16

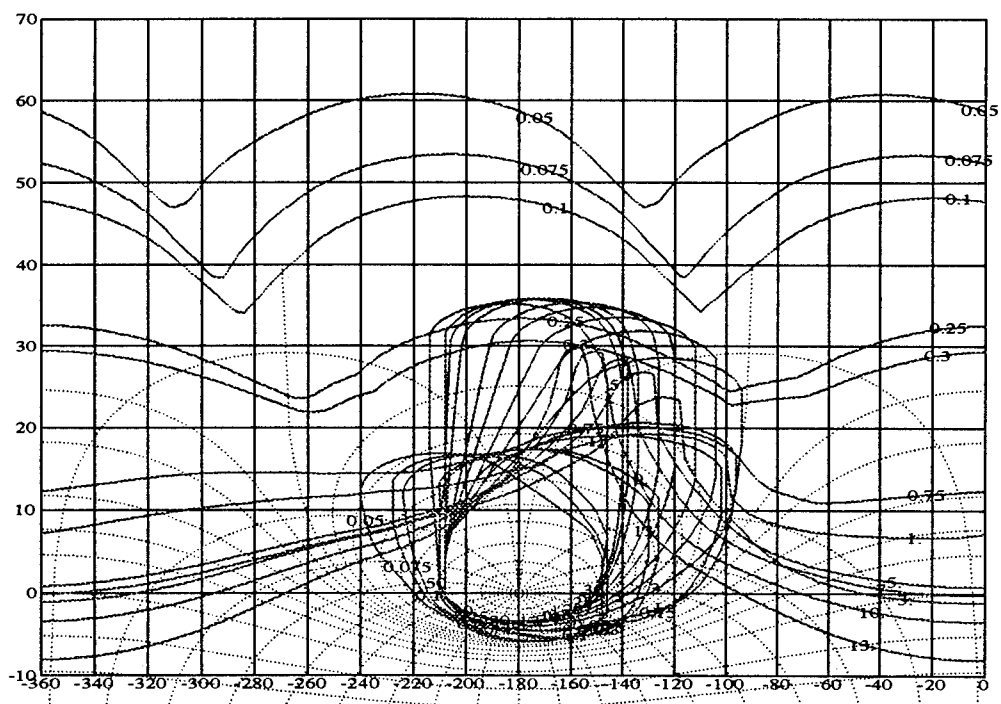


Figure 6.27 QFTCAD Stability and Tracking Bounds for the Roll Channel of VISTA F-16 Experiencing a 45% Triple Failure

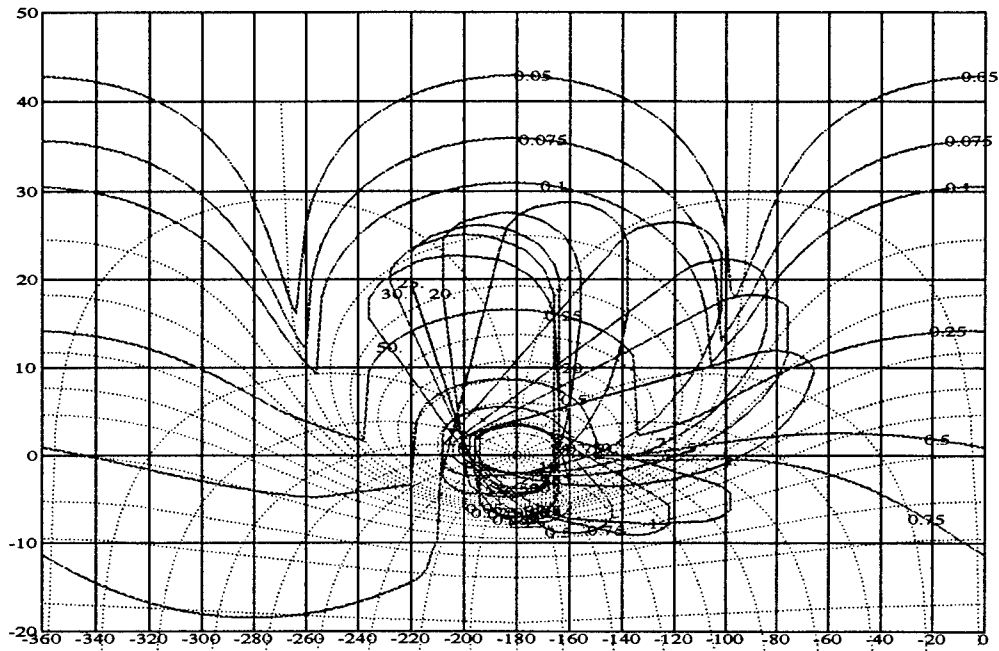


Figure 6.28 QFTCAD Stability and Tracking Bounds for the Beta Channel of the Healthy VISTA F-16

be traced to the failure modeling discussed in Chap. IV. The roll channel failures have the greatest impact on the control derivatives of the system, while the beta channel failures have an appreciable effect on both the stability and control derivatives.

*6.1.5.2 External Disturbance Bounds.* The external disturbance bounds (See Figs. 6.30 and 6.31) for both the roll and beta channels are both too restrictive to achieve. These bounds are selectively removed from the composite boundary and time simulations are evaluated to determine whether the responses require additional disturbance rejection.

*6.1.6 Compensator Design.* The same constraints identified in Chap. II apply to the lateral/directional design as well. Fortunately, the lateral/directional channel is inherently stable reducing the restrictions encountered in the longitudinal FCS design. The development of the roll  $p$  and sideslip  $\beta$  compensators follows.

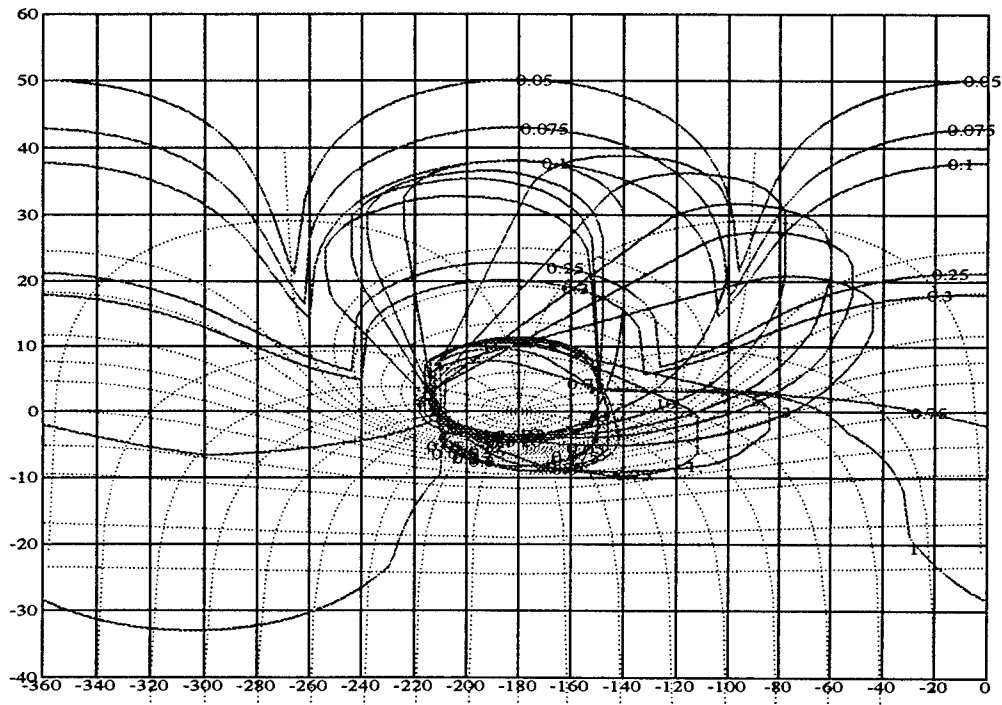


Figure 6.29 QFTCAD Stability and Tracking Bounds for the Beta Channel of the VISTA F-16 Experiencing a 45% Triple Failure

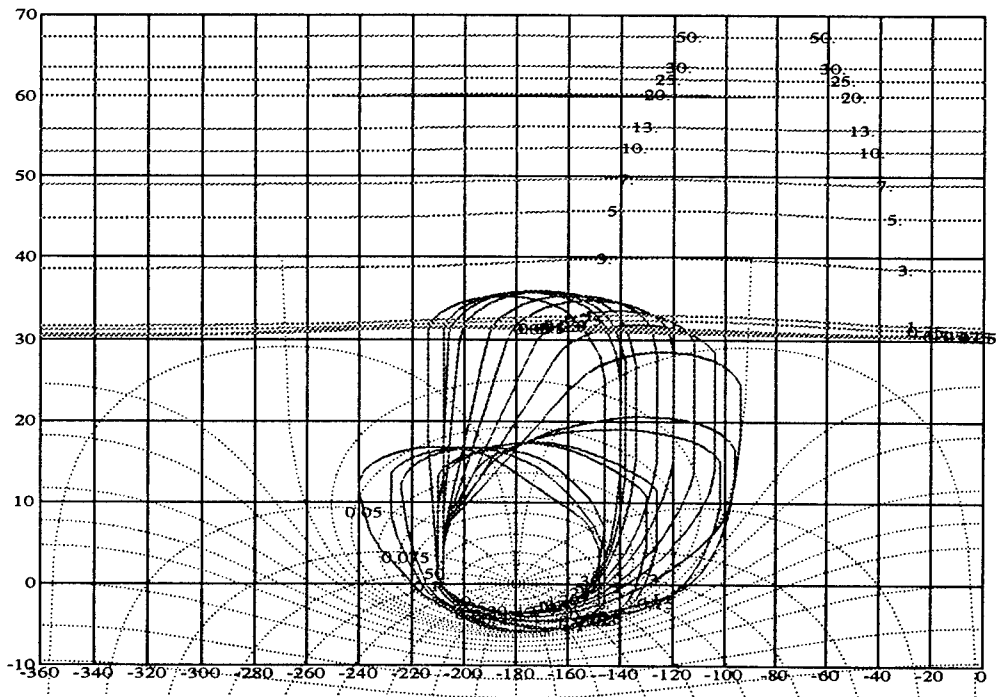


Figure 6.30 QFT External Disturbance Bounds for Roll Channel

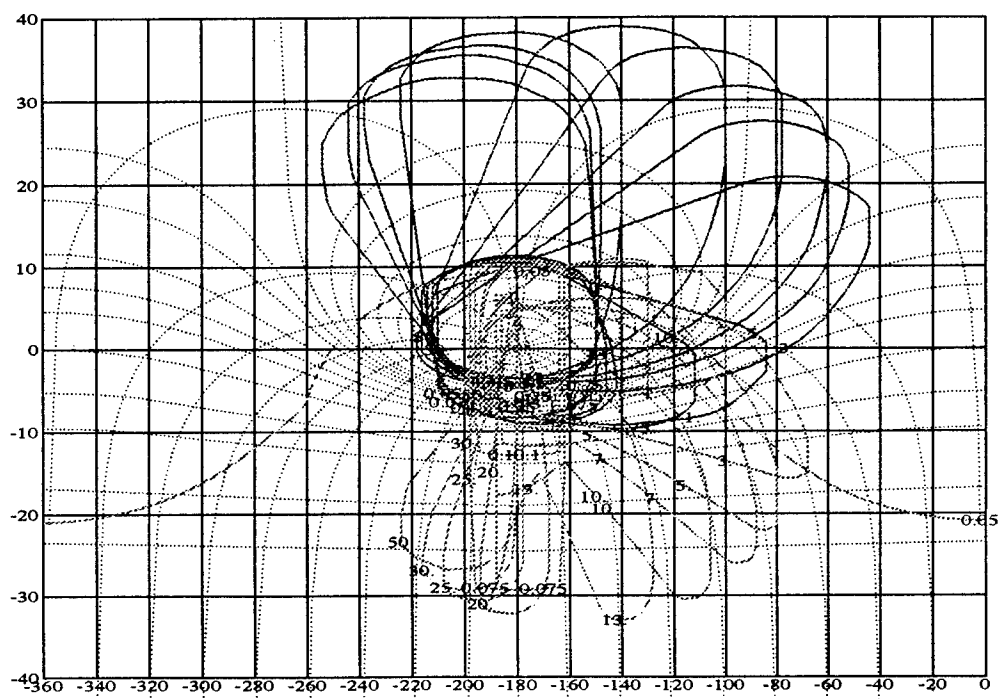


Figure 6.31 QFT External Disturbances Bounds for Beta Channel

*6.1.6.1 Roll Channel.* One of the goals of this fault tolerant control law enumerated in Chap. II is to generate a system that can maintain nominal performance without control effector failures and maintain stability with failures. Since Phillips's compensator already guarantees that the former condition is satisfied then if the design can be manipulated only enough to provide stability and Level 3 tracking response for the failed plants, then the specified design criteria will be satisfied. Thus, as a starting point, Phillips' compensator is loaded and evaluated.

Since the major contribution of the control effector failures is to increase the gain required to achieve a particular level of tracking response, it is assumed that Phillips' compensator would require some additional gain. However his compensator nearly met all tracking and stability bounds due to some inherent overdesign in his compensator. Only the lower  $\bar{q}$  plants of the failed plant set violated the associated stability bounds. To satisfy these exceptional plants, the roll compensator zero is adjusted from 3.5 rps to 4 rps. The final roll compensator  $G_p$  is found in Eq. (6.11), and on Fig. 6.32.

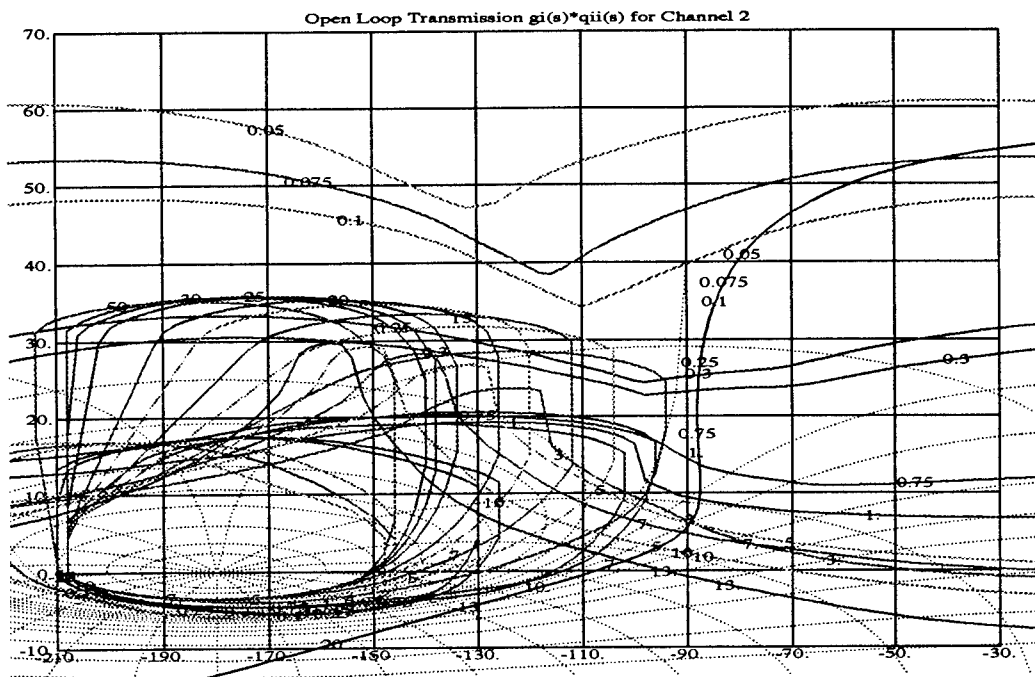


Figure 6.32 QFTCAD Tracking Bounds and Nominal Loop for Roll Channel with 45% Triple Failure

$$G_p = \frac{0.10(s + 4)}{s} \quad (6.11)$$

6.1.6.2 *Sideslip Channel.* In an effort to reduce the design restrictions on the beta compensator only satisfaction of the stability bounds is attempted. Following a similar line of reasoning established in the roll compensator design, Phillips' compensator is initially loaded and evaluated in this design.

Once again his compensator nearly satisfies all the stability requirements for the failed plant as well as the healthy plant set. However, it is apparent from initial roll response simulations that the sideslip angle cross-coupling does not meet specifications, and that gain scheduling must be utilized in order to achieve the desired cross-coupling. As in Phillips' design, 150 lbs/ft<sup>2</sup> appears to be a natural division among the plants cases identified on the sideslip frequency templates. Therefore the gain for  $\bar{q} \leq 150$  lbs/ft<sup>2</sup> is adjusted to 60 and for  $\bar{q} > 150$  lbs/ft<sup>2</sup> it is set at 110. The increase in the low  $\bar{q}$  gain however causes some of these plants to violated the QFT stability bounds. As a

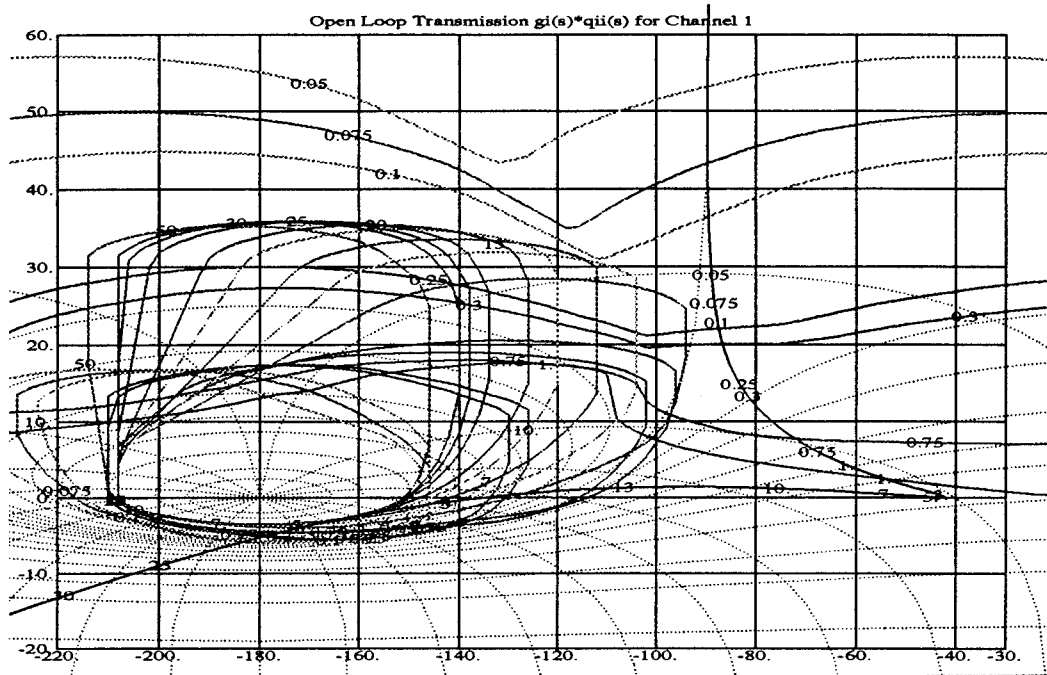


Figure 6.33 QFTCAD Tracking Bounds and Nominal Loop for Beta Channel with 45% Triple Failure

final adjustment the zero at 1.7 rps is shifted lower in frequency to 1.35 rps providing additional increase in phase necessary to circumvent the lower frequency stability bounds. The nominal loop in Fig. 6.33 clearly satisfies all of the stability bounds and the tracking bounds within the higher frequency range of the pilots bandwidth. The final compensator is listed in Eq. (6.12).

$$G_{\beta} = \frac{K_{\beta}(s + 1.35)(s + 2)}{s(s + 60)} \quad (6.12)$$

where  $K_{\beta} = -60$  for  $\bar{q} \leq 150 \text{ lbs/ft}^2$  and  $K_{\beta} = -110$  for  $\bar{q} > 150 \text{ lbs/ft}^2$

**6.1.7 Prefilter Design.** The final component necessary to successfully complete the QFT design process is the prefilter  $F$ . The purpose of the prefilter is especially important in this MIMO FCS design, for a properly designed prefilter can insure the desired tracking response as well as reduce the inherent cross-coupling between the two channels. The roll channel prefilter is designed first and the beta channel prefilter thereafter.

*6.1.7.1 Roll Channel.* A pole is introduced to limit the system response within the pilot's bandwidth, however it is apparent that a zero is necessary to position the tracking response within the Level 3 tracking bounds. The dutch roll damper has a deleterious effect on the low frequency tracking response of the low  $\bar{q}$  plants. It appears that the dutch roll damper slows the roll responses within this frequency range creating a droop in the tracking response. The introduction of a second pole is then warranted to mitigate the effects of this zero on the higher frequency tracking response. The prefilter found in Eq. (6.13) guarantees that the Level 1, 2 and 3 roll tracking specifications are satisfied.

$$F_p = \frac{7.58(s+2)}{(s+1.1)(s+15)} \quad (6.13)$$

*6.1.7.2 Sideslip Channel.* The removal of the beta tracking bounds from consideration in the sideslip channel design appears to obviate the need for a sideslip channel prefilter. Though beta tracking is not a primary design objective, the nominal loop in Fig. 6.33 clearly shows that the system has the robustness required to track a  $\beta_{cmd}$  within the desired specifications. Consequently, the first prefilter design is employed to position the beta tracking responses within the tracking boundaries. However after some preliminary tracking validation plots, a curious relationship became apparent. The cross-coupling of the roll response to a  $\beta_{cmd}$  input became more severe as the prefilter is adjusted to fit within the tracking bounds. In light of this relationship and the fact that the beta tracking models are arbitrarily generated, the compensator in Eq. (6.14) is applied to achieve the best beta tracking response while minimizing the effect of roll on the beta cross-coupling.

$$F_\beta = \frac{3.5}{(s+3.5)} \quad (6.14)$$

## 6.2 Time Simulations

The purpose of the time simulations is to determine if the compensated system satisfies the time domain specifications. In addition to verifying specifications, the simulation data is employed to construct a maximum command gradient for both roll and sideslip channels.

*6.2.1 Tracking.* Similar to the longitudinal design (page 5-20) a sample of 20 tracking responses is presented over a specified  $\bar{q}$  region, where the solid lines represent the healthy aircraft and the dashed lines represent the failed aircraft responses.

*6.2.1.1 Roll Tracking Responses.* Dynamic pressure  $\bar{q}$  has the most significant impact among all other plant parameters including control effector failures. The low  $\bar{q}$  time responses in Figs. 6.34, 6.35, and 6.36 clearly represent the worst case design scenarios. The low  $\bar{q}$  responses exhibit the greatest roll  $p$  settling times, the worst beta  $\beta$  cross-coupling, and a noticeable increase in control surface deflection. Yet despite their inherent shortcomings these responses satisfy the primary lateral design criteria. The simulations demonstrate that all healthy aircraft responses meet Level 1 tracking specifications, the failed aircraft responses are within Level 1 or Level 2 tracking specifications, and the beta cross-coupling response (See Fig. 6.35) does not exceed the 0.067 limit for low  $\bar{q}$  plants. The low  $\bar{q}$  time responses also demonstrate the domination of the available control authority by the failed plants. The consequences of this domination become a factor later in the design when the rate and deflection saturation nonlinearities are applied.

The high  $\bar{q}$  time responses illustrated in Figs. 6.37, 6.38, and 6.39 show a dramatic improvement in overall performance when compared to the low  $\bar{q}$  plants. All the plants, healthy as well as those experiencing 45% triple failure, meet or exceed Level 1 roll tracking specifications. The high  $\bar{q}$  plants exhibit significant robustness especially evident in the roll angle  $\phi$  and sideslip angle  $\beta$  responses. The gain scheduling introduced to satisfy the 0.067 sideslip angle limit for the low  $\bar{q}$  plants enabled the design to achieve the more restrictive 0.022 sideslip limit for the high  $\bar{q}$  cases as well. The satisfaction of the sideslip angle requirements is found on Fig. 6.38, and in the complete tabular listing of all lateral time responses in Appendix D.

*6.2.1.2 Sideslip Tracking Responses.* The unit sideslip step responses in Figs. 6.40, 6.41, and 6.42 reflect the design emphasis placed on roll performance and turn coordination over sideslip tracking. In other words, the compensated system satisfies the roll angle and sideslip cross-coupling specifications at the expense of sideslip tracking performance. Though the compensated system tracks the sideslip command input  $\beta_{cmd}$

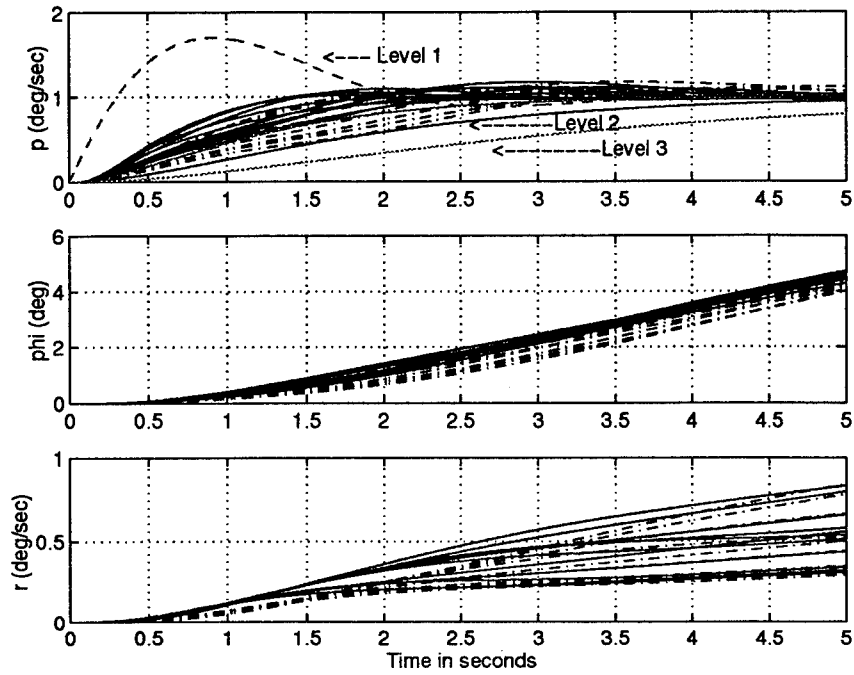


Figure 6.34 Roll Unit Step Response of Compensated System Healthy Aircraft and 45% Triple Failure Plants ( $\bar{q} < 150 \text{ lbs/ft}^2$ ) [1 of 3]

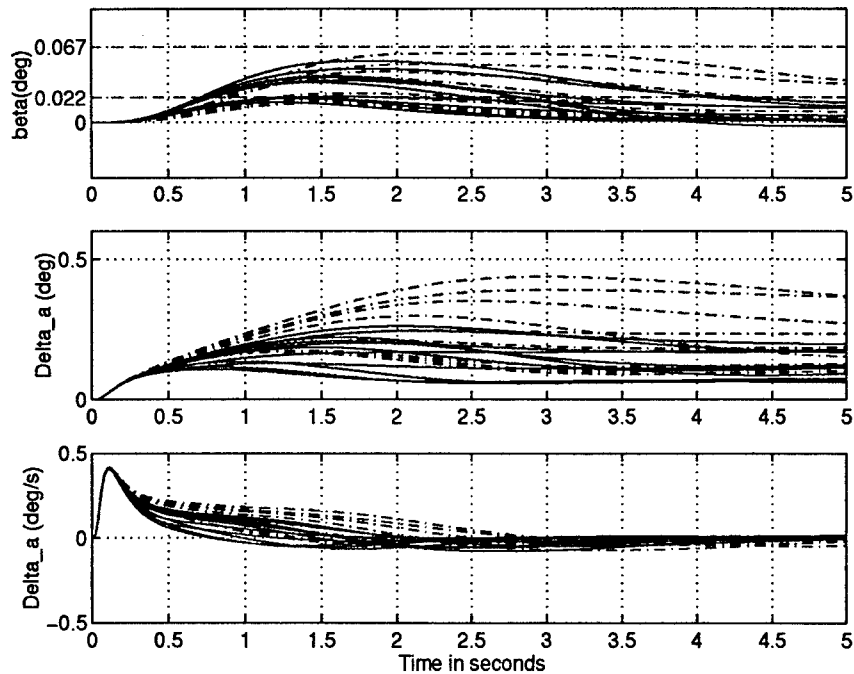


Figure 6.35 Unit Roll Step Response of Compensated System Healthy Aircraft and 45% Triple Failure Plants ( $\bar{q} < 150 \text{ lbs/ft}^2$ ) [2 of 3]

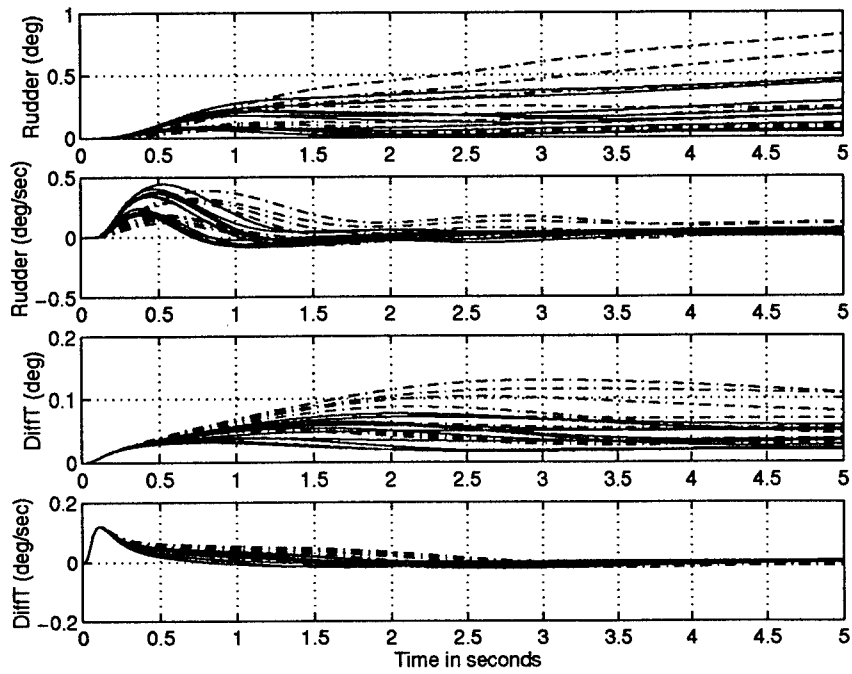


Figure 6.36 Unit Roll Step Response of Compensated System Healthy Aircraft and 45% Triple Failure Plants ( $\bar{q} < 150 \text{ lbs/ft}^2$ ) [3 of 3]

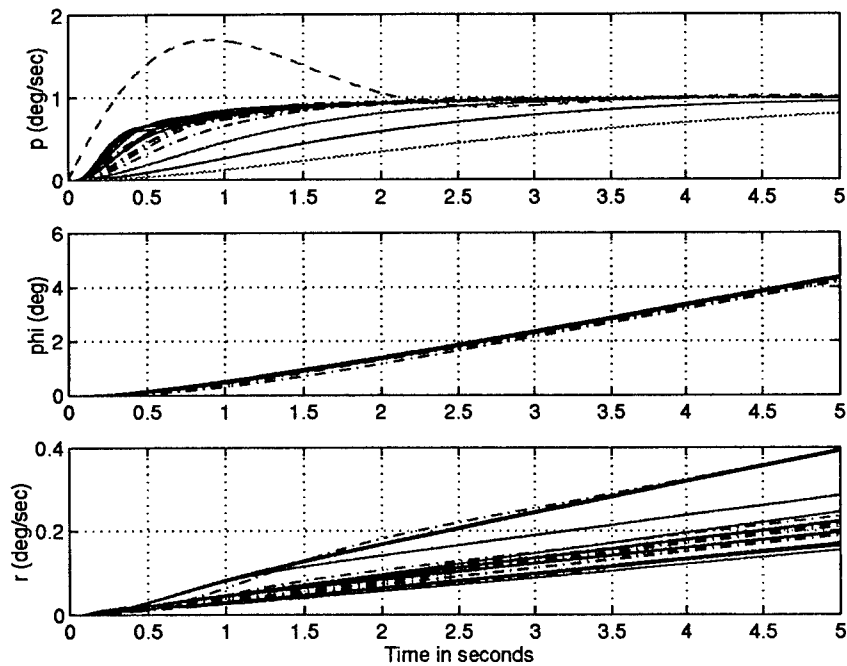


Figure 6.37 Unit Roll Step Response of Compensated System Healthy Aircraft and 45% Triple Failure Plants ( $\bar{q} > 150 \text{ lbs/ft}^2$ ) [1 of 3]

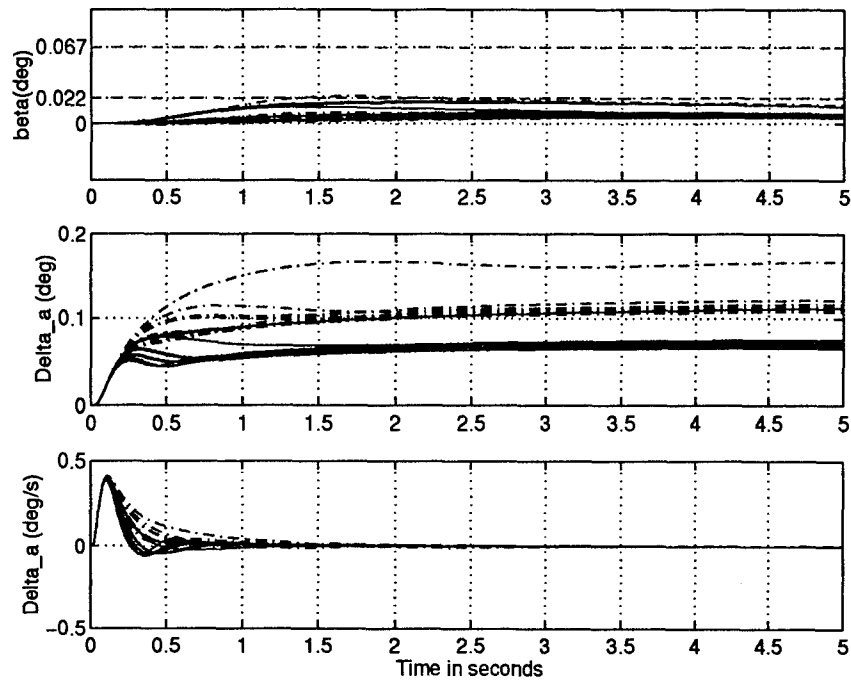


Figure 6.38 Unit Roll Step Response of Compensated System Healthy Aircraft and 45% Triple Failure Plants ( $\bar{q} > 150 \text{ lbs}/ft^2$ ) [2 of 3]

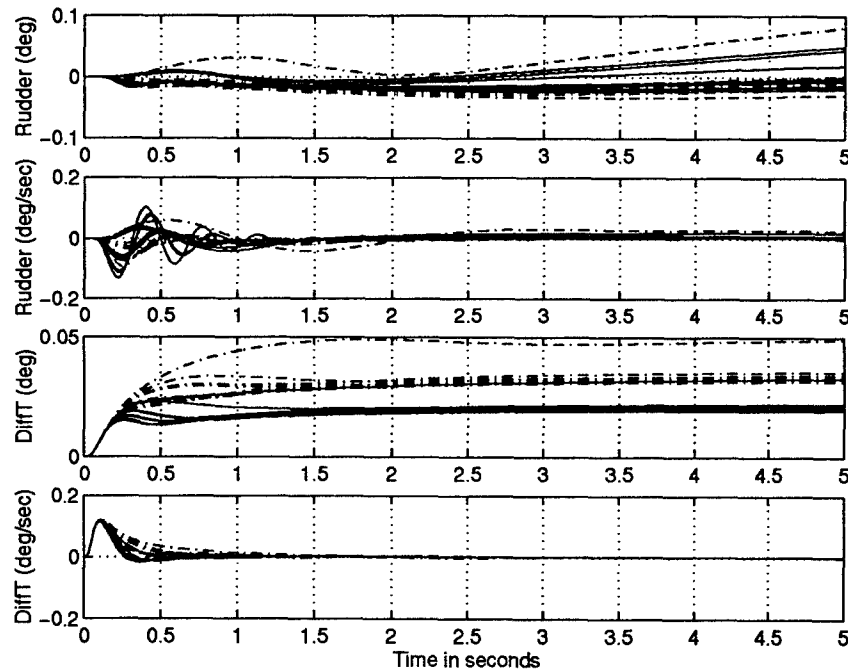


Figure 6.39 Unit Roll Step Response of Compensated System Healthy Aircraft and 45% Triple Failure Plants ( $\bar{q} > 150 \text{ lbs}/ft^2$ ) [3 of 3]

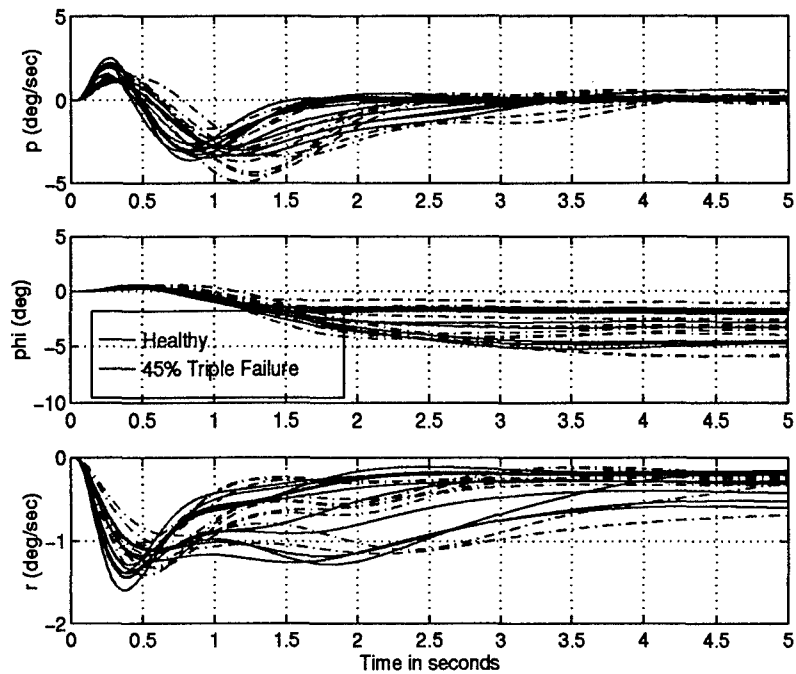


Figure 6.40 Unit Beta Step Response of Compensated System Healthy Aircraft and 45% Triple Failure Plants [1 of 3]

with zero steady-state error, these responses are sluggish. However, this sluggishness is accepted for a few reasons: first, the pilot rarely commands a sideslip angle so the necessity of a fast  $\beta$  response is mitigated, and second, deleterious  $\beta$  cross-coupling is accentuated given a faster  $\beta$  response.

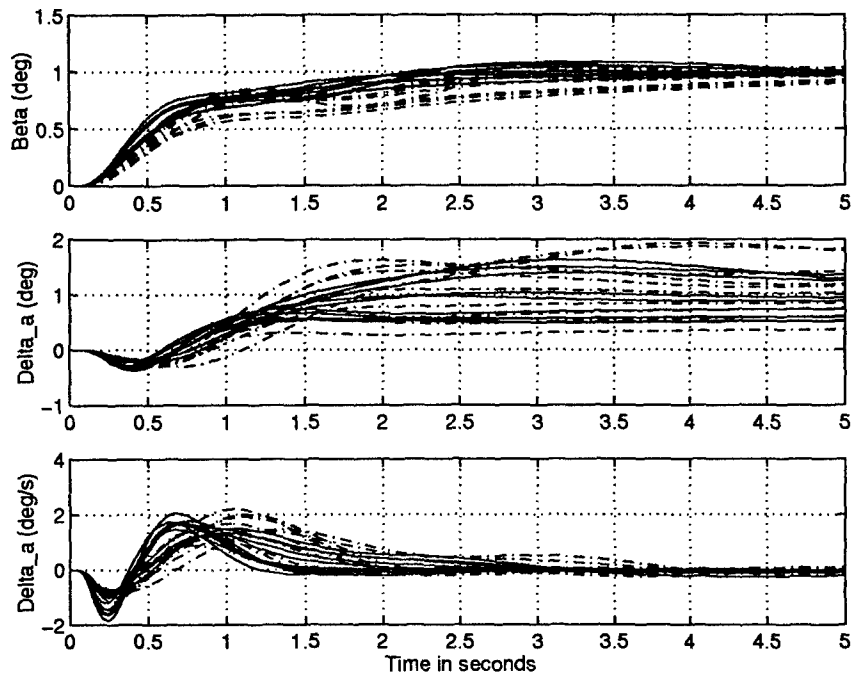


Figure 6.41 Unit Beta Step Response of Compensated System Healthy Aircraft and 45% Triple Failure Plants [2 of 3]

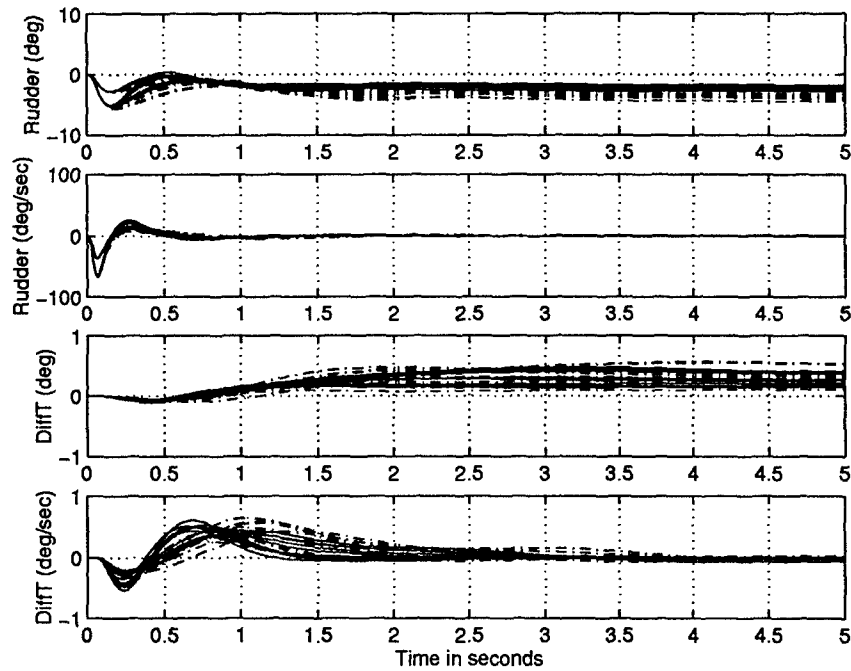


Figure 6.42 Unit Beta Step Response of Compensated System Healthy Aircraft and 45% Triple Failure Plants [3 of 3]

6.2.2 *Maximum Command Gradients.* Equations (6.15) through (6.20) determine the maximum allowable command input without causing rate and deflection saturations, while Eqs. (6.21) and (6.22) represent the minimum command input necessary to satisfy the roll angle performance criteria. The unit step responses found in Figs. (6.34) through (6.42) provide the data necessary to generate the maximum command gradients for the roll and sideslip channels. These gradients are found in Figs. 6.43 and 6.44.

$$\frac{60}{\delta_{ail_{max}}} \quad (6.15)$$

$$\frac{60}{\delta_{rud_{max}}} \quad (6.16)$$

$$\frac{60}{\delta_{DT_{max}}} \quad (6.17)$$

$$\frac{20}{\delta_{ail_{max}}} \quad (6.18)$$

$$\frac{30}{\delta_{rud_{max}}} \quad (6.19)$$

$$\frac{20}{\delta_{DT_{max}}} \quad (6.20)$$

$$\frac{360}{\phi_{(2.8sec)}} \quad (6.21)$$

$$\frac{60}{\phi_{(1sec)}} \quad (6.22)$$

The maximum roll command gradient boundaries (See Fig. 6.43) are conspicuously more restrictive than the gradient proposed by Phillips. The rudder and differential tail, rate and deflection saturation restrictions are not limiting factors in the overall roll gradient design. The aileron saturation restrictions, however, prove to be dominant and consequently are the only saturation boundaries identified on the figure. The aileron experiences rate and deflection saturation before achieving the 90 degree roll performance requirement. Though Phillips manipulated the maximum command gradient under the saturation boundaries and above the roll performance restrictions, in this design a more aggressive approach is taken. The maximum roll command gradient noted by the solid line on Fig. 6.43 violates

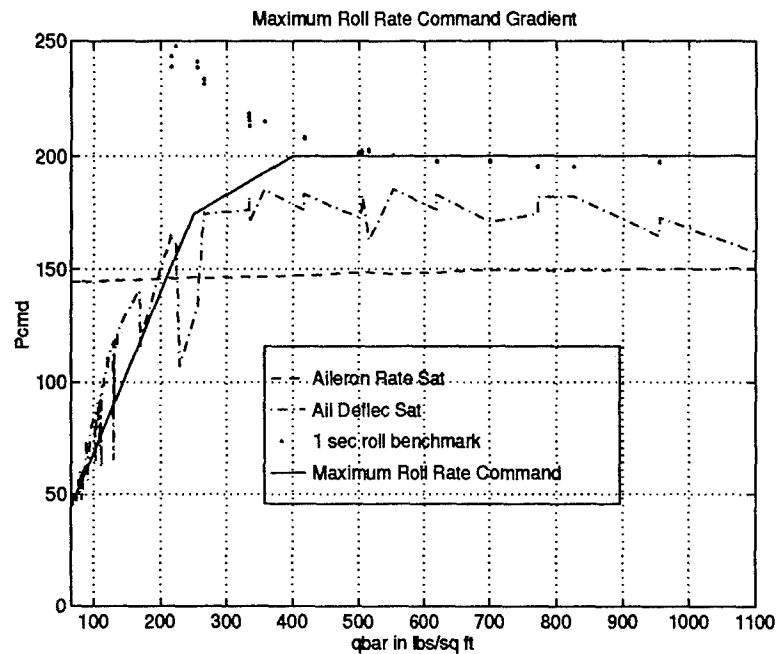


Figure 6.43 Maximum Roll Command Gradient

the rate saturation limits over most of the dynamic pressure range and violates the deflection saturation limits for dynamic pressures in excess of  $150 \text{ lbs/ft}^2$ . These boundaries are selectively either intersected or ignored in an attempt to improve the roll performance of the aircraft. However, it is vital for the sanctity of feedback to limit the duration of control effector saturation. If the system remains in saturation long enough, the feedback path is eliminated causing the system to go 'open-loop', and possibly unstable. Simulations of the lateral design with the maximum command gradients in place are employed to settle these performance and stability issues.

As anticipated from the unit sideslip time response analysis, the rudder rate and deflection saturation limits dominated the maximum sideslip command gradient boundaries. Since the rudder rate saturates for such a relatively small command input and previous attempts at violating the rate limits have been successful, the maximum command gradient denoted by the solid line in Fig. 6.44 is designed to exceed the rudder rate limits. Like the roll input gradient, the performance and stability issues are settled via the time simulations.

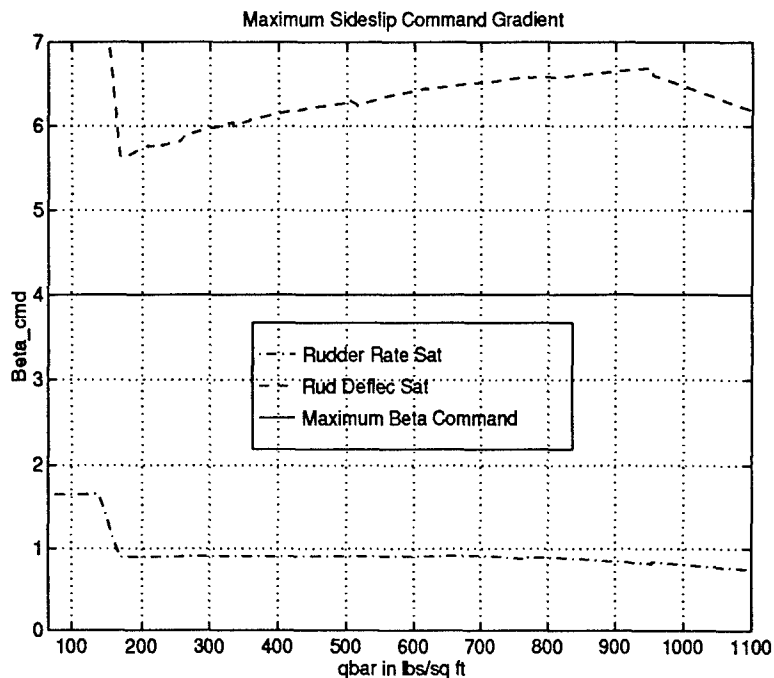


Figure 6.44 Maximum Sideslip Command Gradient

### 6.3 Design Validation

The final step in the lateral/directional design process is to verify that the compensated system satisfies the frequency and time domain stability, tracking, and external disturbance specifications established earlier in this chapter.

#### 6.3.1 Stability Validation.

**6.3.1.1 Sideslip Channel.** None of the 398 open loop sideslip transmission functions in Fig. 6.45 transect the 6 dB constant magnitude contour, consequently the stability criteria for the sideslip channel is satisfied.

**6.3.1.2 Roll Channel.** The roll compensator satisfies the 6 dB stability contour with ease in Fig. 6.46. Though the gain can be increased approximately 10 dB without violating the contour, the rate and deflection saturation limits impose more restrictive requirements on the compensator gain.

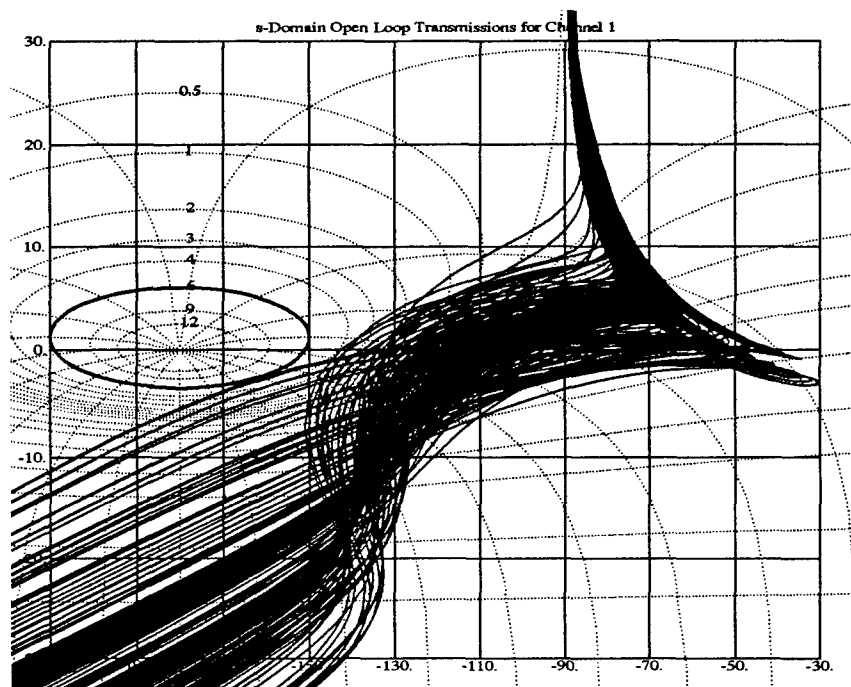


Figure 6.45 QFT Stability Validation for the Sideslip ( $\beta$ ) Channel

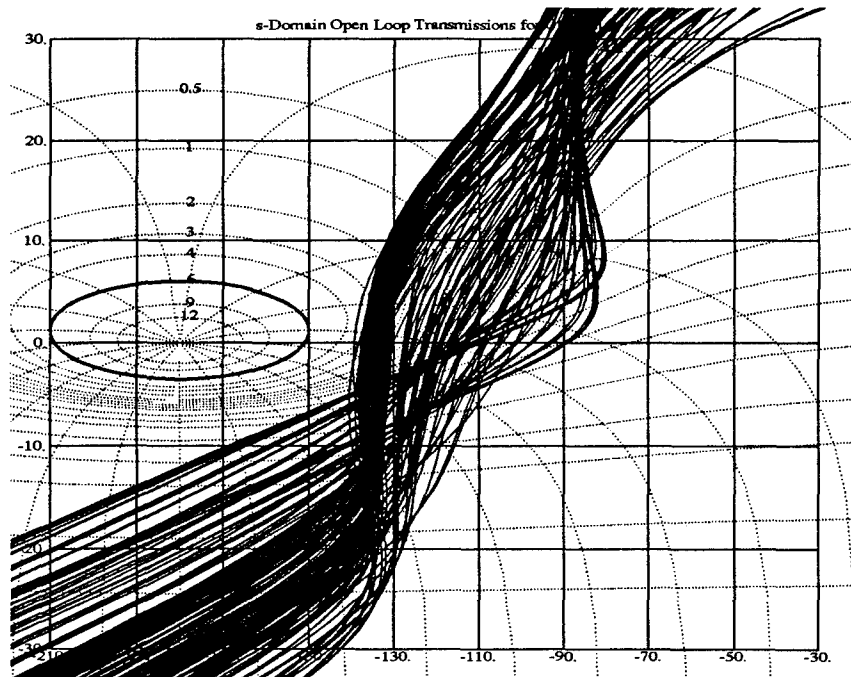


Figure 6.46 QFT Stability Validation for the Roll ( $p$ ) Channel

6.3.2 *Tracking Validation.* The tracking validation plots found in Figs. 6.47 and 6.48 represent the culmination of MILSTD 1797A specifications and the utilization of engineering judgement into achieving a viable full envelop robust control design for the VISTA F-16 experiencing control effector failures. The tracking specifications for the  $Beta_{out}/Beta_{cmd}$  MISO equivalent system are arbitrarily selected to satisfy QFTCAD as discussed in section 6.1.2.1. The time simulations, therefore, are relied upon to determine if the design provides suitable tracking for this system.  $Beta_{out}/Roll_{cmd}$  MISO system meets the 0.0607 degree cross-coupling specification for all of the high dynamic pressure plants in Fig. 6.48 and for the vast majority of the low dynamic pressure plants in Fig. 6.47. The  $Roll_{out}/Beta_{cmd}$  system however does not meet the -11 dB specification in either the low or high  $\bar{q}$  ranges, and validation of this system is left for the time responses. Finally, the  $Roll_{out}/Roll_{cmd}$  MISO system meets or exceeds all applicable specifications defined in section 6.1.2.1. The majority of the healthy plants identified by the solid lines in both figures meet the Level 1 tracking specification, while only the low  $\bar{q}$  failed plants in Fig. 6.48 violate the Level 2 tracking bounds. This droop in the roll tracking response can be attributed to the interaction of the dutch roll damper and sideslip feedback at low dynamic pressures. In general, all the plants, healthy and failed, low as well as high dynamic pressure meet or exceed the Level 3 tracking requirement.

6.3.3 *External Disturbance Rejection Validation.* The external disturbance validation plots in Fig. 6.49 are deceiving due to a subtlety of the external disturbance modeling process (Chap. IV). Traditionally the external disturbance rejection plot represents how the system responds to a unit step external disturbance input. However in this design, the external disturbance magnitude is enhanced by the model (See Eqs. (4.72) and (4.74)). So a unit step external disturbance input in this design, represents the effect of applying a 5 degree stabilator deflection. In other words, the external disturbance rejection plots in Fig. 6.49 are approximately 14 dB greater than they should be. After reducing each of these figures by 14 dB, the  $\beta$  responses (MISO(1,1)) are within acceptable limits, while some  $p$  responses (MISO(2,1)) remain outside acceptable limits. Finally, the external disturbance simulations are necessary to determine if the trouble plants can be controlled by a human pilot.

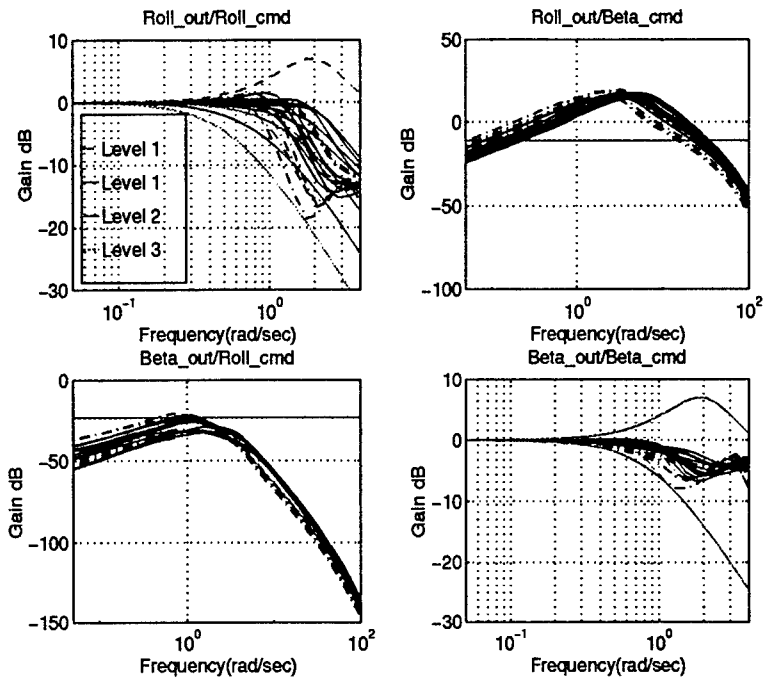


Figure 6.47 QFT Tracking Validation for the Lateral/Directional Channel ( $\bar{q} < 150$  lbs/ft<sup>2</sup>)

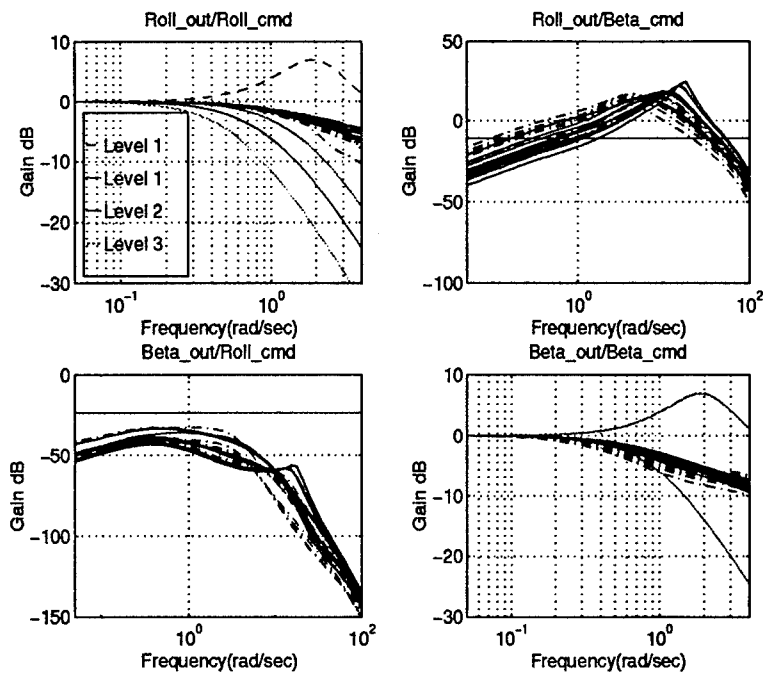


Figure 6.48 QFT Tracking Validation for the Lateral/Directional Channel ( $\bar{q} > 150$  lbs/ft<sup>2</sup>)

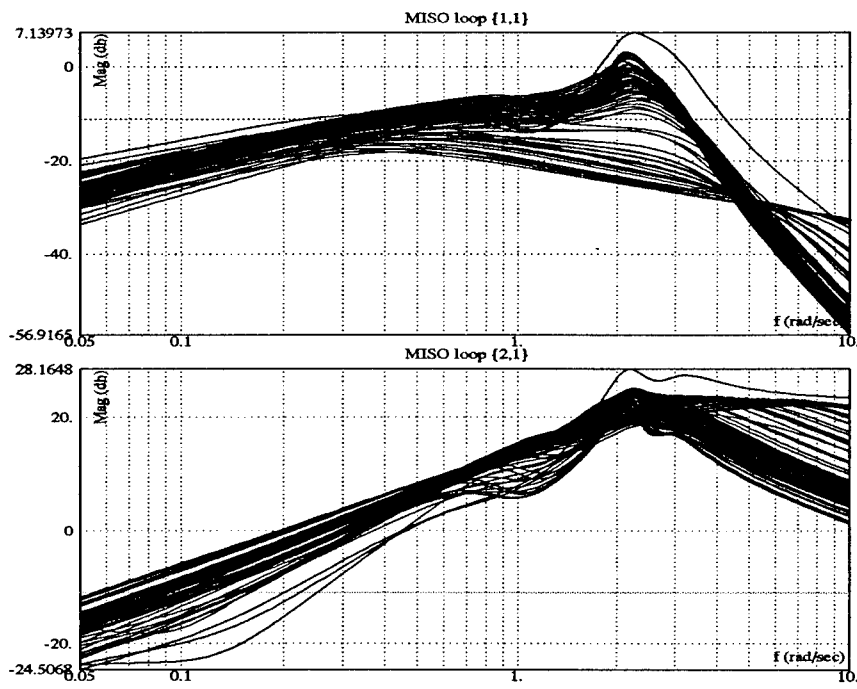


Figure 6.49 QFT External Disturbance Validation

*6.3.4 Time Domain Validation.* The time domain validation verifies that the FCS can meet time domain specifications when realistically high amplitude inputs, and rate and deflection saturation limitations are applied. The roll and sideslip tracking, and external disturbance responses are examined in the following sections, and the tabular data associated with these plots can be found in Appendix D.

*6.3.4.1 Roll Tracking Responses.* Figures 6.50 through 6.55 demonstrate that the system does indeed maintain stability, even though the extreme low  $\bar{q}$  failed plants saturate the aileron deflection. The low  $\bar{q}$  cases however do not meet the roll angle performance criteria identified on Fig. 6.50. There is simply insufficient control authority available at low dynamic pressure to adhere to these MILSTD specifications. Though this is disconcerting, Phillips was also unable to achieve these performance specifications and he was only concerned with the healthy plant set. Furthermore, Fig. 6.51 indicates that the 6 degree sideslip specification has been satisfied, while it also confirms the authenticity of the command gradient boundaries. Recall that for dynamic pressure less than 150 lbs/ft<sup>2</sup> the maximum roll command input does not exceed the aileron rate limits.

The high dynamic pressure plants found in Figs. 6.53 through 6.55 also verify that the system can maintain stability despite aileron and differential tail saturation. The high dynamic pressure plants also demonstrate enhanced roll performance and beta decoupling. The majority of the plants including the failure plants satisfy the 360 degree roll angle requirement, and all of the plants meet the 6 degree maximum sideslip specification. The roll command gradient proves that the 90 degree roll angle requirements are the most difficult restriction to satisfy. However, as Appendix C supports, a majority of the healthy plants met or exceeded this criteria as well.

*6.3.4.2 Sideslip Tracking Responses.* Unlike the roll tracking responses, both the low and high  $\bar{q}$  plants are grouped together on Figs. 6.56, 6.56, and 6.56. The failed sideslip tracking simulations in Fig. 6.56 are clearly less responsive than the healthy aircraft plants identified by the solid lines. Also, the rudder deflection remains within the saturation limits for all plant cases, while the rudder rate does saturate. For some

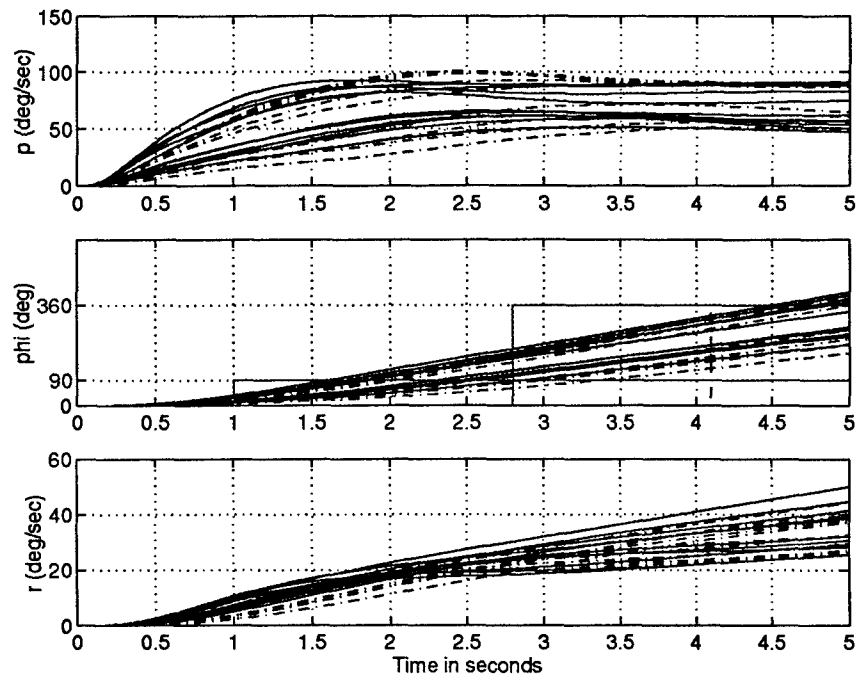


Figure 6.50 Maximum Roll Gradient Step Response of Compensated System, Healthy Aircraft and 45% Triple Failure Plants ( $\bar{q} < 150 \text{ lbs}/ft^2$ ) [1 of 3]

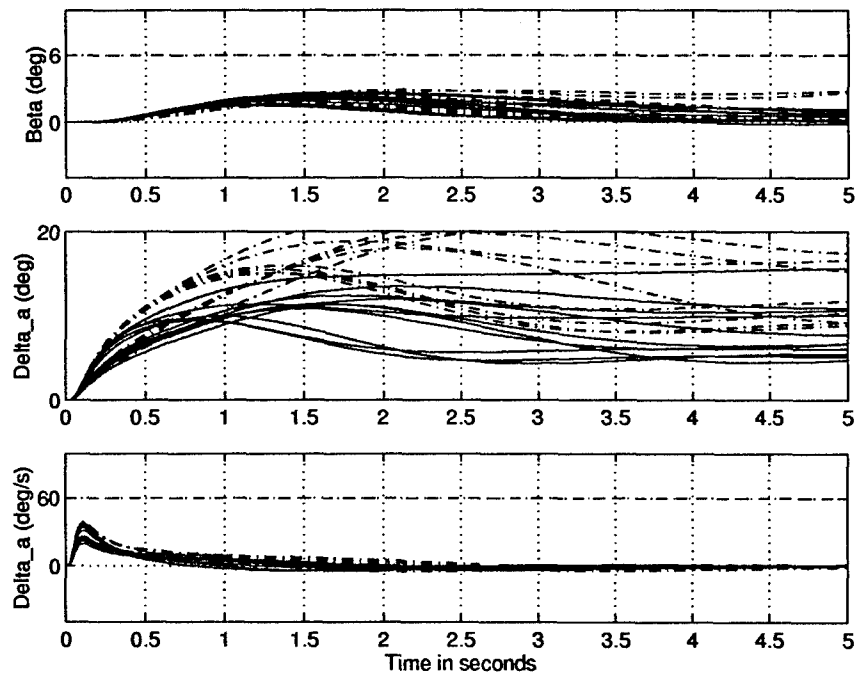


Figure 6.51 Maximum Roll Gradient Step Response of Compensated System, Healthy Aircraft and 45% Triple Failure Plants ( $\bar{q} < 150 \text{ lbs}/ft^2$ ) [2 of 3]

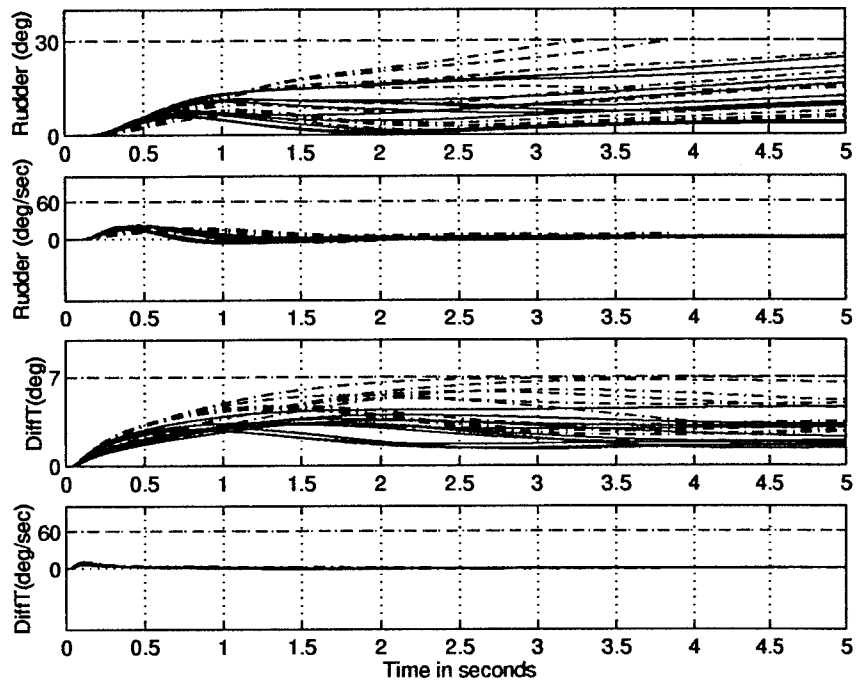


Figure 6.52 Maximum Roll Gradient Step Response of Compensated System, Healthy Aircraft and 45% Triple Failure Plants ( $\bar{q} < 150 \text{ lbs/ft}^2$ ) [3 of 3]

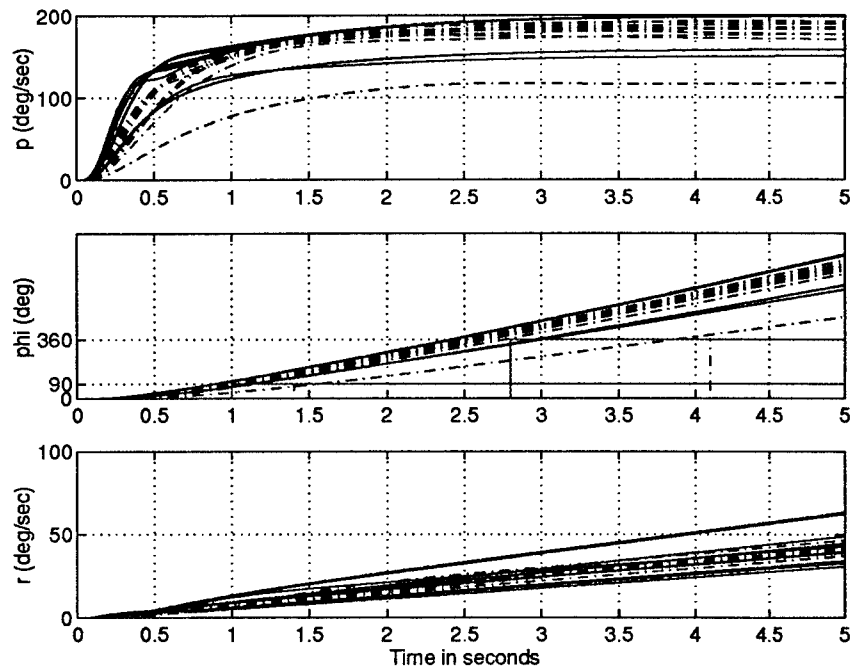


Figure 6.53 Maximum Roll Gradient Step Response of Compensated System, Healthy Aircraft and 45% Triple Failure Plants ( $\bar{q} > 150 \text{ lbs/ft}^2$ ) [1 of 3]

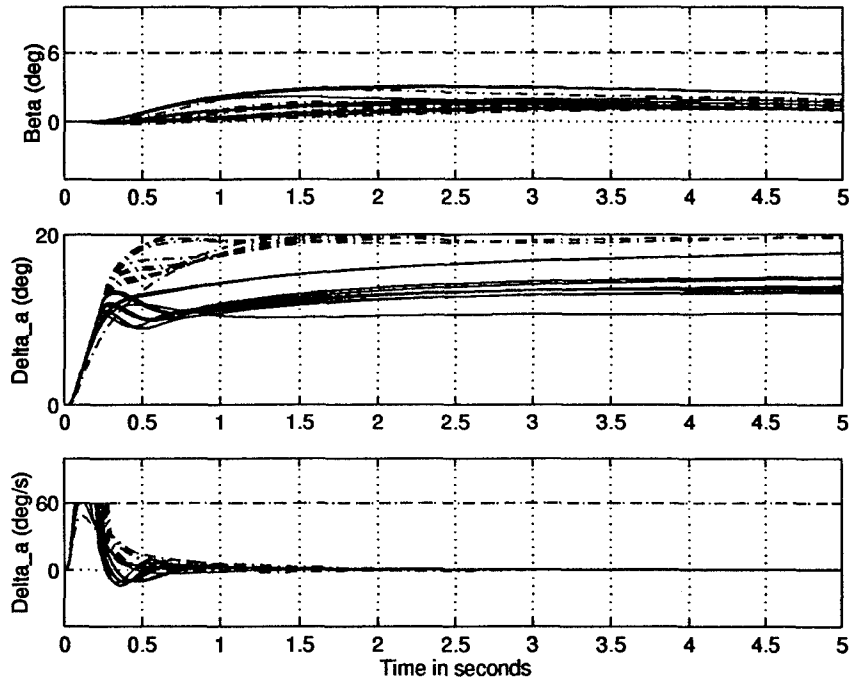


Figure 6.54 Maximum Roll Gradient Step Response of Compensated System, Healthy Aircraft and 45% Triple Failure Plants ( $\bar{q} > 150 \text{ lbs}/ft^2$ ) [2 of 3]

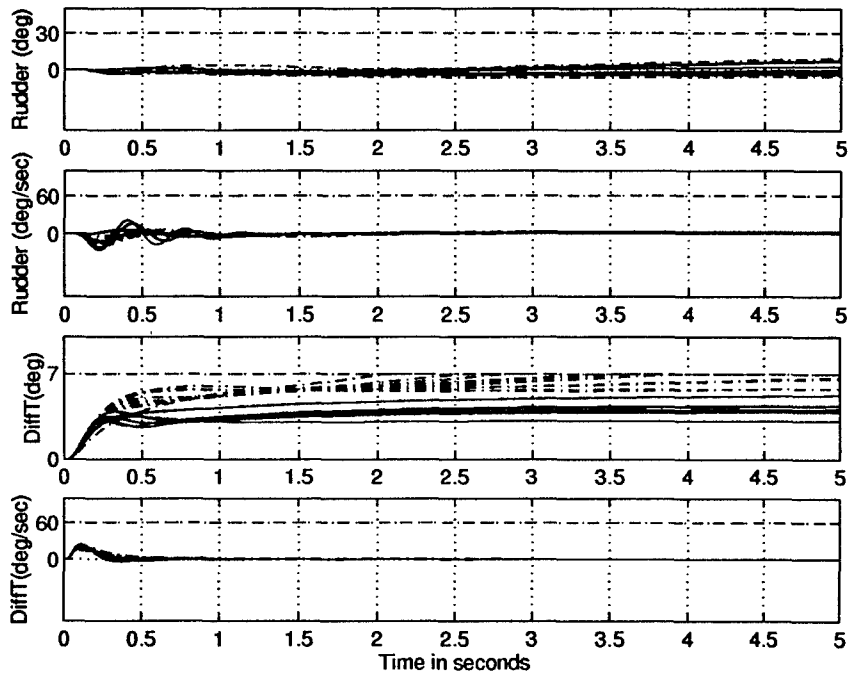


Figure 6.55 Maximum Roll Gradient Step Response of Compensated System, Healthy Aircraft and 45% Triple Failure Plants ( $\bar{q} > 150 \text{ lbs}/ft^2$ ) [3 of 3]

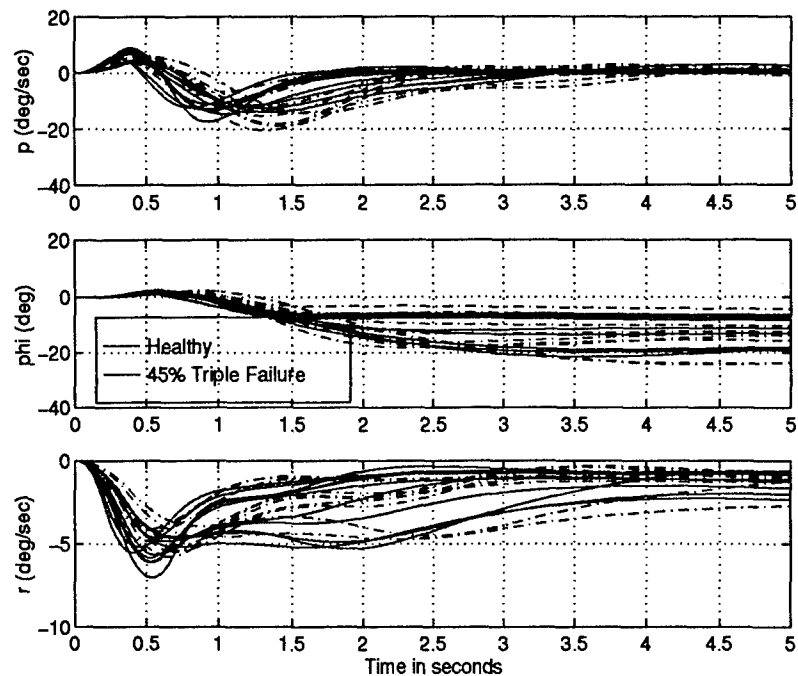


Figure 6.56 Maximum Sideslip Gradient Step Response of Compensated System, Healthy Aircraft and 45% Triple Failure Plants [1 of 3]

plants this saturation exceeds 0.5 seconds. Fortunately, the system maintains stability, and verifies that the aggressive  $\beta$  command gradient is warranted.

*6.3.4.3 External Disturbance.* Time domain external disturbance analysis is imperative to validate the disturbance models, and to determine how the disturbance effects the entire system. Recall that the external disturbance is introduced to appropriately model the asymmetric horizontal stabilator deflection problem created from an elevator failure. If the system is wired correctly then the aileron and differential tail should deflect in the negative direction (based on the sign convention established in Chap. III) to counter a positive roll- rate. Also, the rudder should deflect in the positive direction to counter a positive sideslip angle disturbance. The simulations found in Figs. 6.59 through 6.64, indeed confirm that the system responds appropriately to the external disturbance.

Since the external disturbance specifications are not achieved in the design of the QFT compensator, the disturbance rejection simulations are particularly important to settle some pertinent stability and control issues. Acceptable disturbance rejection requires

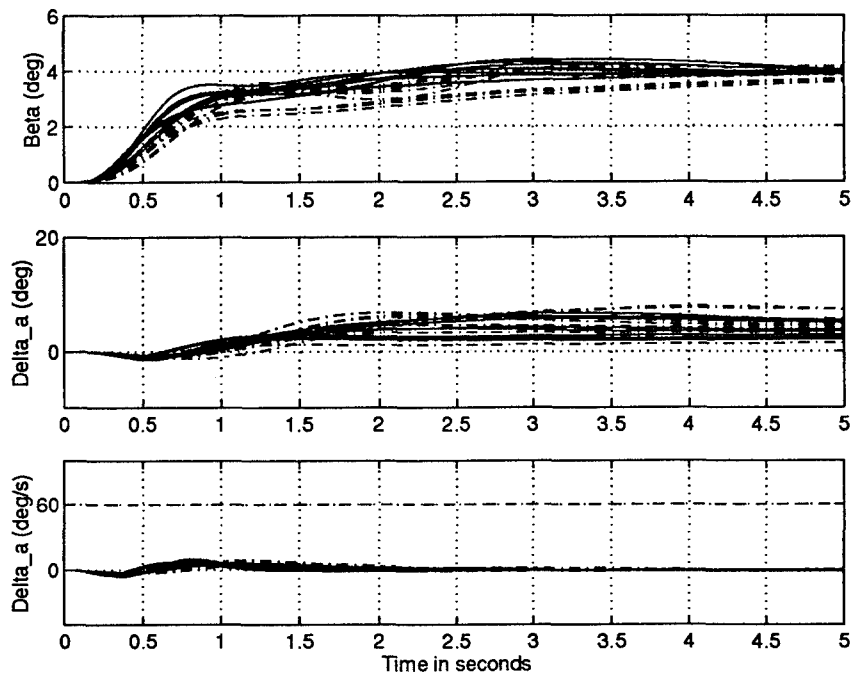


Figure 6.57 Maximum Sideslip Gradient Step Response of Compensated System, Healthy Aircraft and 45% Triple Failure Plants [2 of 3]

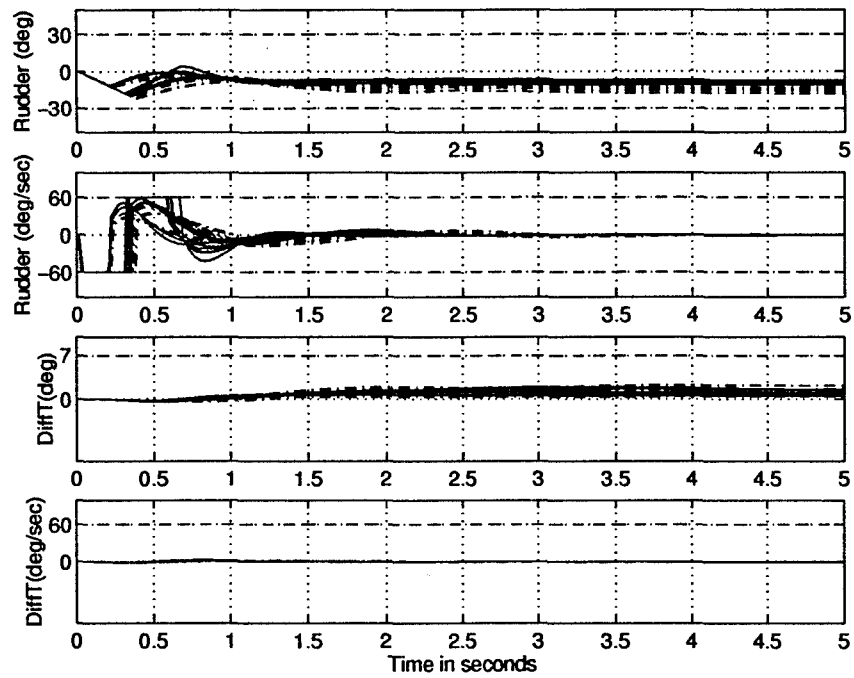


Figure 6.58 Maximum Sideslip Gradient Step Response of Compensated System, Healthy Aircraft and 45% Triple Failure Plants [3 of 3]

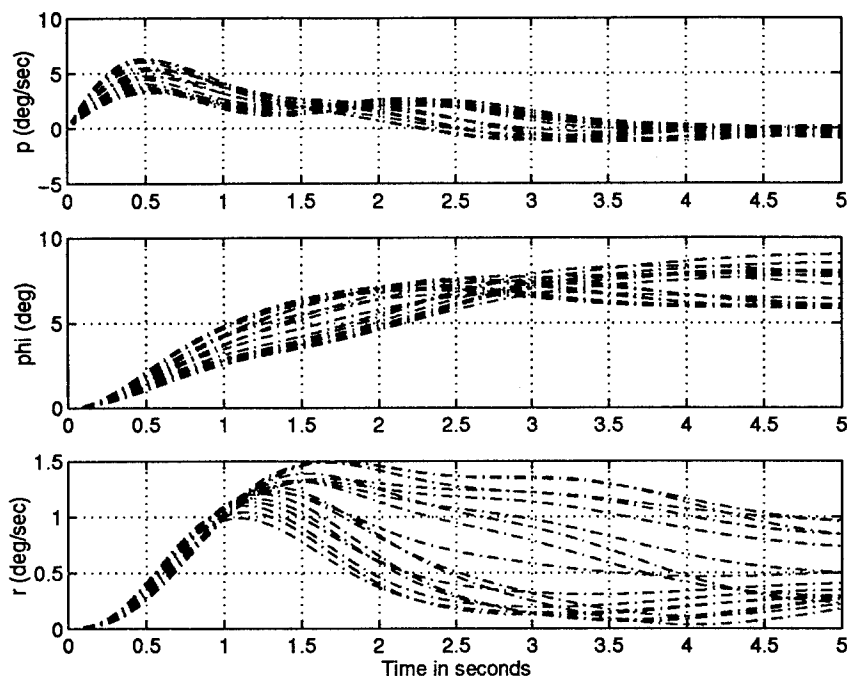


Figure 6.59 Disturbance Step Response of Compensated System, 45% Triple Failure Plants ( $\bar{q} < 150 \text{ lbs}/ft^2$ ) [1 of 3]

that the system maintain stability, the commanded responses settle within the five second time period of interest, and the control effectors avoid rate and deflection saturation limits. The external disturbance rejection simulations for the low dynamic pressure found in Figs. 6.59, 6.60, and 6.61 clearly meet these rejection requirements.

The commanded variables, roll rate  $p$  and sideslip  $\beta$ , are the only variables expected to settle to zero in steady-state. The other aircraft states and control effector deflection must be evaluated in the time domain to determine if the responses are within acceptable limits. Among the most crucial of all uncontrolled states is the roll angle  $\phi$ . Even if the roll-rate settles to zero the system may achieve a significant roll angle before the pilot can counter the disturbance. From Fig. 6.59,  $\phi$  approaches only 9 degrees which is tolerable considering a 45% reduction in the horizontal stabilator area.

The high dynamic pressure external disturbance time responses in Figs. 6.62, 6.63, and 6.64 exhibit superior rejection in comparison to the low  $\bar{q}$  plants. These high  $\bar{q}$  plants easily satisfy the disturbance rejection settling, stability, and saturation requirements.

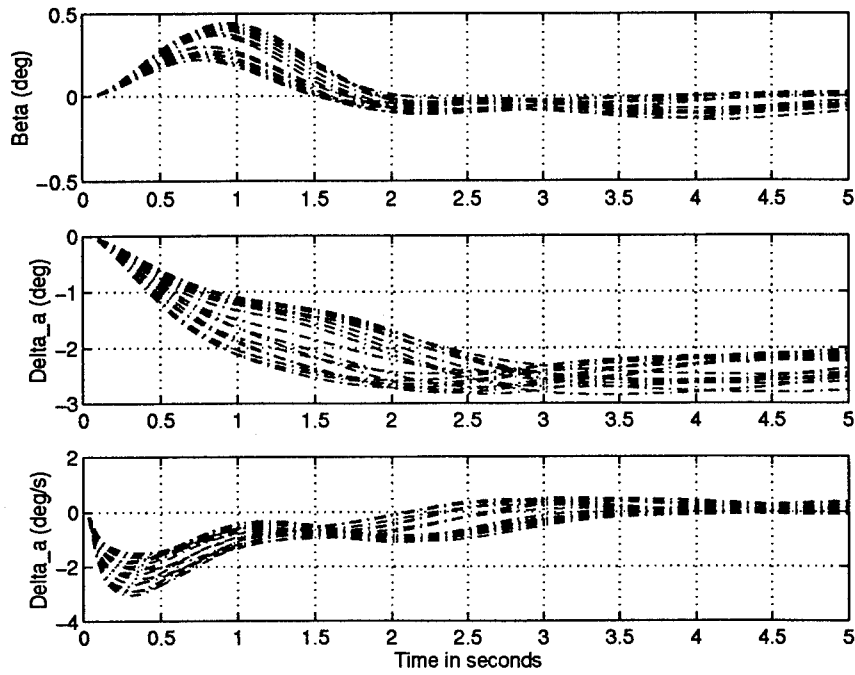


Figure 6.60 Disturbance Step Response of Compensated System, 45% Triple Failure Plants ( $\bar{q} < 150 \text{ lbs/ft}^2$ ) [2 of 3]

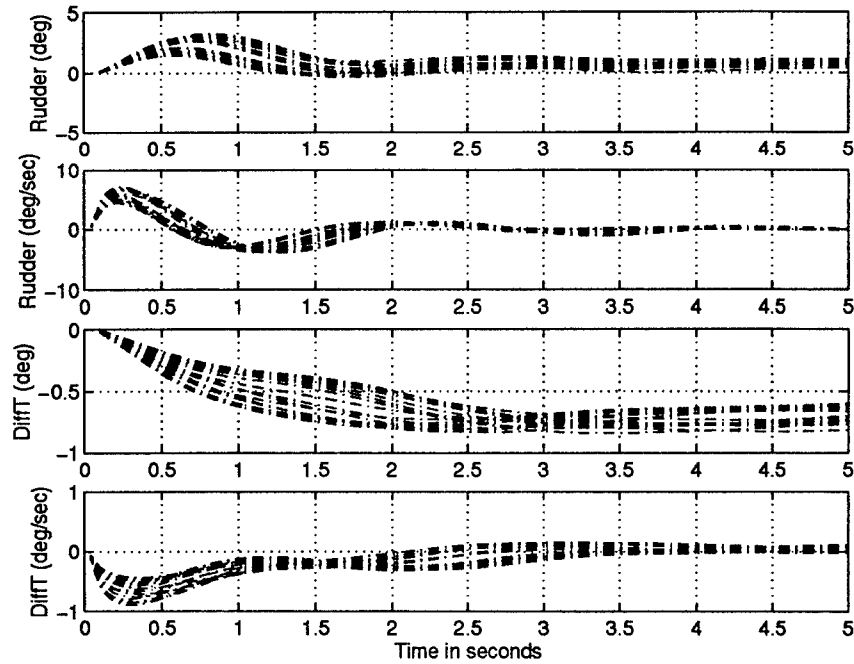


Figure 6.61 Disturbance Step Response of Compensated System, 45% Triple Failure Plants ( $\bar{q} < 150 \text{ lbs/ft}^2$ ) [3 of 3]

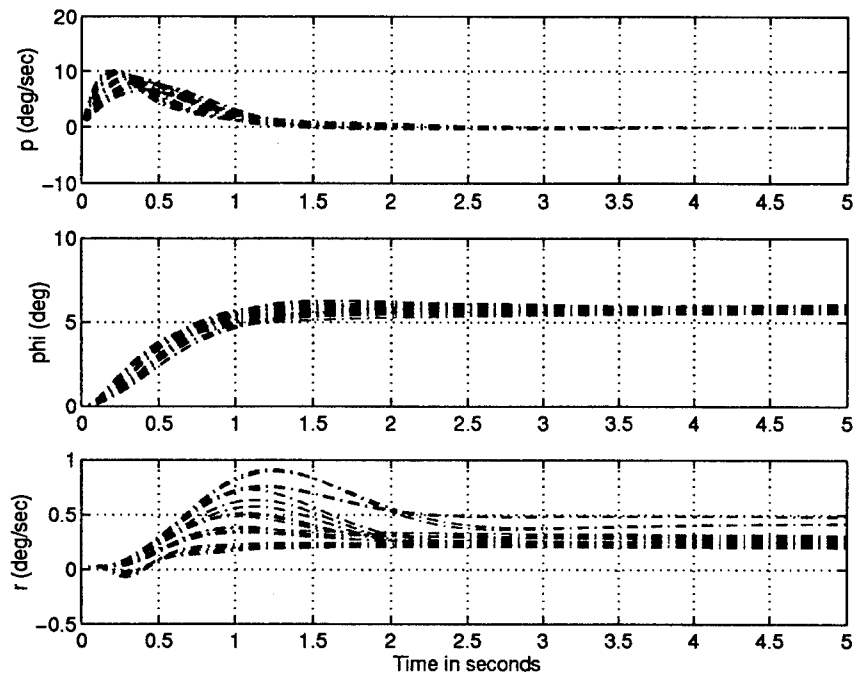


Figure 6.62 Disturbance Step Response of Compensated System, 45% Triple Failure Plants ( $\bar{q} > 150 \text{ lbs/ft}^2$ ) [1 of 3]

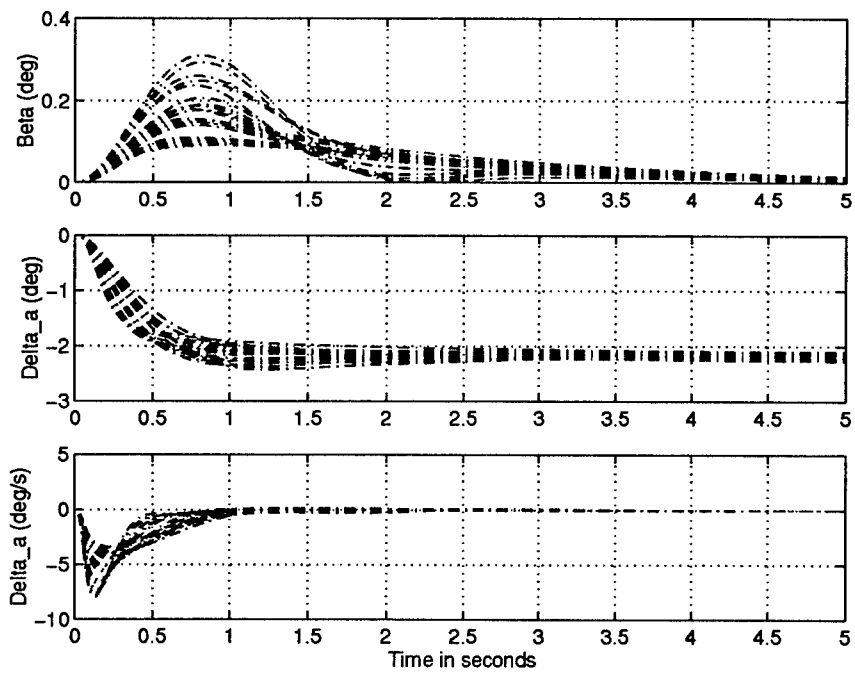


Figure 6.63 Disturbance Step Response of Compensated System, 45% Triple Failure Plants ( $\bar{q} > 150 \text{ lbs/ft}^2$ ) [2 of 3]

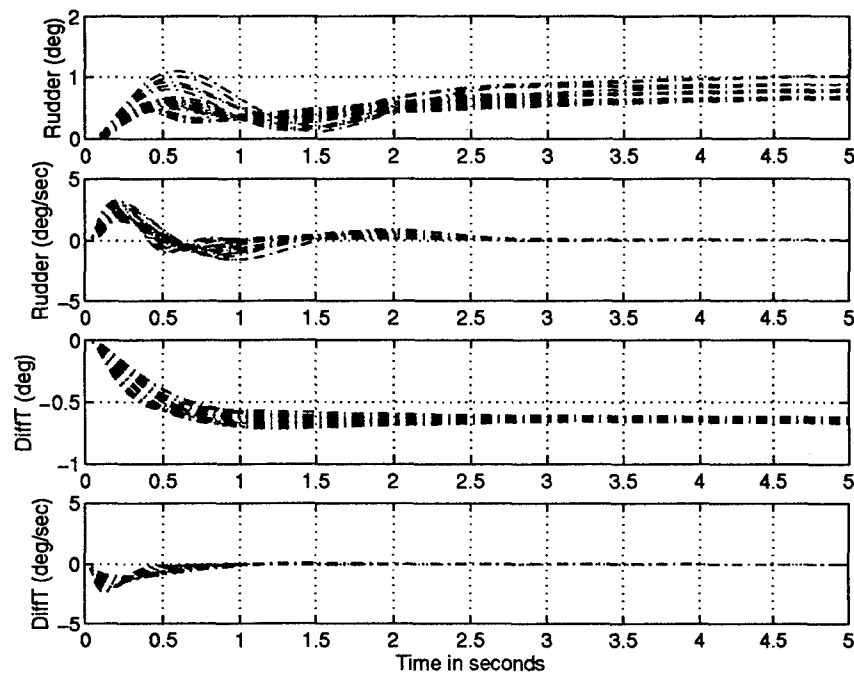


Figure 6.64 Disturbance Step Response of Compensated System, 45% Triple Failure Plants ( $\bar{q} > 150 \text{ lbs/ft}^2$ ) [3 of 3]

#### 6.4 Lateral/Directional Design Summary

This chapter covered the complete lateral/directional channel design process. The 2X2 MIMO QFT structure is discussed including the dutch roll damper circuit and weighting matrix  $W$ . A root locus approach is taken to determine the coefficients of the washout filter, and then the focus is shifted to the development of the tracking, external disturbance, and performance specifications. From these specifications the appropriate models are generated and the failure analysis is initiated. A 45% triple failure design set is selected and the QFTCAD program is applied to form the effective plants and subsequent frequency templates. Since Phillips' plants matched the healthy plants from this design, some additional comparisons are drawn between the healthy and failed plant sets. Given these templates, the QFT bounds are formed and the failure effects on tracking, cross-coupling, and stability are examined. These boundaries guided the development of the QFT roll and sideslip compensators. Time simulations are applied to this FCS design, the responses are discussed, and the maximum command gradients are formed. Finally, the lateral/directional FCS in Fig 6.65 is validated with realistic command inputs and satura-

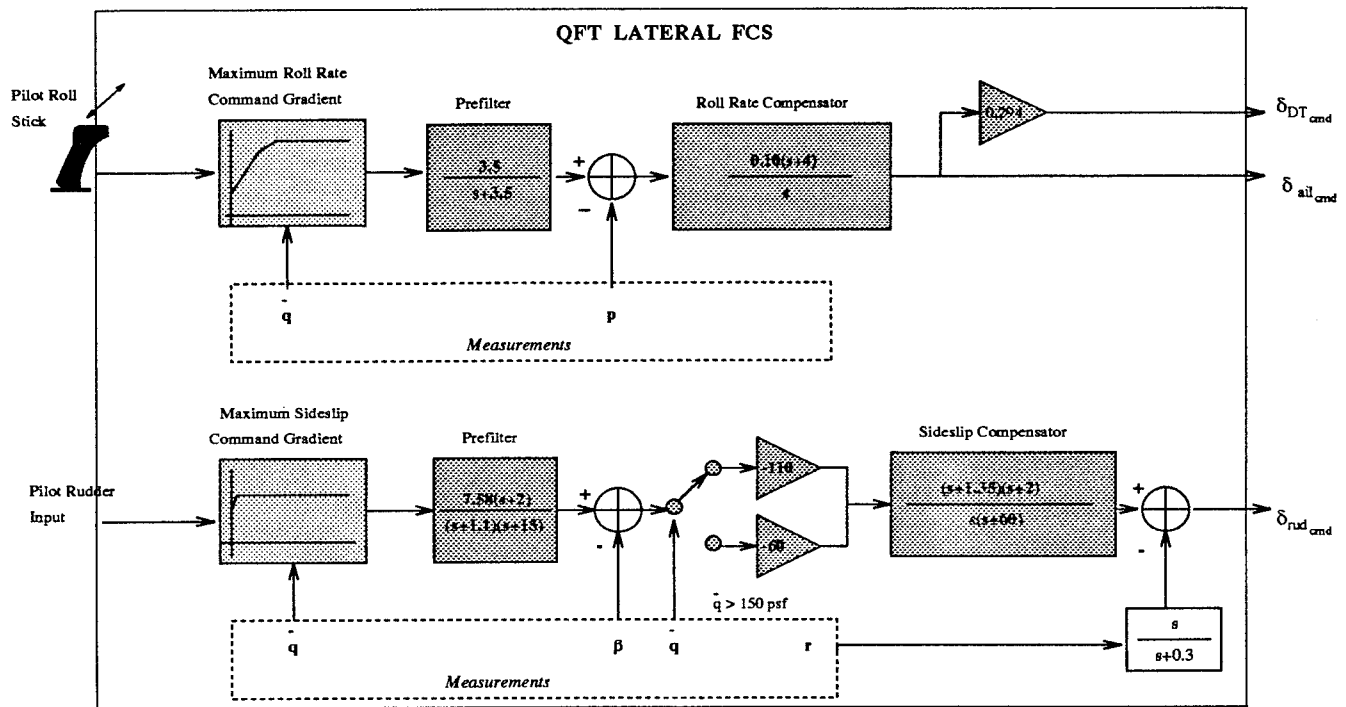


Figure 6.65 Final QFT Lateral FCS

tion limitations. A more complete evaluation of the design objectives and failure analysis follows in Chap. VII.

## *VII. Conclusions and Recommendations*

This chapter provides closure for this research effort by presenting overall design conclusions and recommendations for future exploration.

### *7.1 Conclusions*

The primary and secondary goals established in Chap. I have been achieved. Specifically, a realistic robust FCS for the full subsonic envelope of the VISTA F-16 has been developed which is tolerant to flight control effector failures from the outset. Furthermore, the maximum control effector failure level that a successful QFT design can accommodate has been determined.

Thus, the compensated system clearly met the MILSTD Level 1 flying qualities specifications for the unimpaired aircraft at high dynamic pressure flight conditions in both the longitudinal and lateral/directional channels, which is tantamount to maintaining nominal flight control. Furthermore, for 25% stabilator failure in the longitudinal channel, and the 45% triple effector failure cases in the lateral/directional channel at least Level 3 flying qualities specifications were achieved. The majority of the impaired aircraft for the high dynamic pressure flight conditions exhibit Level 1 or 2 flying qualities, while only the worst case low dynamic pressure failed plants exhibit Level 3 flying qualities.

The secondary goal was to determine the maximum control effector failure level the proposed QFT design could incur. In general, it was more difficult to achieve the performance specifications in the longitudinal channel than in the lateral/directional channel. The static instability of the VISTA F-16, coupled with the restrictions placed on the compensator, required significant attention in the longitudinal design. Though Phillips [15] was able to avoid saturating the control surfaces while simultaneously achieving the performance benchmarks, a more aggressive approach was necessary in this design. The command gradient was designed to violate the stabilator saturation rate limits, while avoiding the deflection limits. The stabilator deflection limits were uncompromising. If they were violated then the system becomes unstable. This instability indicated that a successful QFT FCS design for damage levels greater than 25% is unattainable, which coincides

with the difficulties encountered during the loop shaping process. The lateral/directional channel, however, did not demonstrate the same instability, or loop shaping difficulties experienced in the longitudinal design. A more aggressive command gradient was required for both the roll and sideslip compensators, but the system maintained stability for both control effector deflection and rate saturation. The only constraint limiting the accommodation of higher failure levels in the lateral/directional channel is sideslip angle tracking and disturbance rejection. If stability was the only applicable requirement, a successful QFT FCS design for a damage level in excess of 45% triple failure may be attainable.

The compensators for both channels (repeated in Eqs. 7.1, 7.2, and 7.3) adhere to the guidelines established in Chap II. The longitudinal and lateral/directional compensators are both second-order transfer functions, with bandwidths less than 60 rps, and physically realizable steady-state gains. In addition, gain scheduling was applied discriminately. Scheduling was only necessary to achieve the required turn coordination specifications in the directional channel. Overall, the three compensators and prefilters are remarkably elegant considering the extent of the uncertainty inherent in this problem.

$$G_{C^*} = \frac{4.45(s + 2.3)(s + 12.5)}{s(s + 43)} \quad F_{C^*} = \frac{0.25(s + 6)}{s + 1.5} \quad (7.1)$$

$$G_p = \frac{0.10(s + 4)}{s} \quad F_p = \frac{7.58(s + 2)}{(s + 1.1)(s + 15)} \quad (7.2)$$

$$G_\beta = \frac{K_\beta(s + 1.35)(s + 2)}{s(s + 60)} \quad F_\beta = \frac{3.5}{(s + 3.5)} \quad (7.3)$$

This research further promotes the  $C^*$  controlled variable concept in order to embed flying quality specifications into the design, and enhance system performance. Properly selecting the blending of the  $q$  and  $N_z$  components of  $C^*$  proves to be extremely important. The "asymptotic" gradient, which more accurately represents the pilot's tracking tendencies, has been proven to actually decrease the equivalent plant uncertainty witnessed on the QFT frequency templates. Also, the  $C^*$  blending has demonstrated an intimate connection with the size and geometry of the templates for the failed plants. This connection has been thoroughly investigated in this thesis and is referred to as the "swirl effect."

Finally, it should be noted that this design has undergone extensive testing and evaluation in both the frequency and time domains. Despite actuator saturation limitations and compensator restrictions, the design achieves the 9g and 25° angle-of-attack performance benchmarks in the longitudinal channel and the roll angle requirements for nearly all plant cases in the lateral/directional channel. In addition, the compensated system was able to maintain “feet-on-the-floor” turn coordination over the entire flight envelope.

## 7.2 Recommendations

The following recommendations are made:

- First, Phillips’ FCS design for the unimpaired aircraft should be compared to the current F-16 Block 40 flight control system. Then, this comparison should be employed to further evaluate the performance of the fault tolerant system developed in this research. It is expected that this analysis will endorse QFT as a robust design over the Block 40’s gain scheduling “point design” approach.
- The failures effected the aircraft as anticipated. The failed aircraft models required a gain increase to track a step input, while responding with greater overshoot, onset delay, and settling time than the healthy aircraft models. However, the insignificant difference between the 15% and 25% failure templates, and the relatively benign disturbance responses, imply that the failure modeling analysis may be too conservative. The failure analysis was conducted on aircraft models trimmed about a level flight condition, which may not represent the worst case failure scenario. Therefore, it is suggested that the failure modeling generated in this research should be validated with wind tunnel data, and encoded into the SRF simulation routine. Full non linear simulations can then be conducted on this fault tolerant design, and the design reevaluated.
- The  $C^*$  variable has been shown to have a dramatic and beneficial impact on both the healthy and failed FCS design process. This finding warrants additional research in developing an “optimal”  $C^*$  blend.

- Some additional time domain analysis may be appropriate for this fault tolerant system. Traditionally, only step tracking and disturbance responses are independently generated. However, a step response may not mimic a pilot's command input as well as a ramp or doublet response, and the saturation limits imposed on the control effectors may invalidate the linearity condition that allows for independent observation of the tracking and disturbance responses. Therefore, tracking simulations should be conducted with a variety of realistic command inputs while simultaneously introducing an external disturbance.
- The following enhancements are suggested for the QFTCAD program:
  1. To readily determine the difference between various plant sets, it would have been helpful in this design for QFTCAD to store and overlay frequency templates from various plant sets.
  2. In line with the previous suggestion, if a composite listing of boundary plants from each frequency template could be generated automatically, and the design continued only with this boundary set, the computational burden encountered in this design would have been reduced considerably.
  3. QFTCAD's *Mathematica* based plot functions provide little flexibility for customization, and therefore could use some improvements.
  4. A direct interface with *Matlab* to load and manipulate plant files would have obviated the need for the elaborate modeling scheme developed in Chap IV.
- The FCS developed in this research has proven that QFT can manage the level of uncertainty inherent in a fault tolerant FCS, while yielding a control system capable of maintaining nearly nominal flight performance without failures and stabilization with failures. However this robustness negatively impacts the performance of the healthy aircraft. In essence the fault tolerant FCS is designed to favor a worst case scenario, that may never occur, over the performance of the healthy aircraft. Surely the uncertainty in the design would be reduced and greater nominal performance could be achieved, if some failure detection and isolation (FDI) scheme was applied

in conjunction with the QFT approach. Thus, further research should be conducted bringing this marriage of QFT and a FDI scheme to fruition.

## Appendix A. Failure Model Generation Macro

### %PURPOSE

The Purpose of this program is to implement control effector failures on the VISTA F-16 AC models generated by Major Scott Phillips in his thesis. This algorithm was developed by Keating in his study of the Lambda test aircraft with minor modifications made due to the structural differences between the VISTA and the Lambda aircraft.

### %ORGANIZATION

This program loads a particular AC plant from Phillips' database located in the edit\_plants directory then it modifies the appropriate stability derivatives and outputs these plants to mF#.m located in the failed\_plants dir where # corresponds to the SRF number of the unfailed plant.

### %CONSTANTS DEFINED

nu = 0.90;  
Se = 63.7;            %Sq ft Surface area of fully functional elevator  
Sr = 11.65;          %Sq ft Surface area of fully functional rudder  
Sa = 26.56;          %Sq ft Surface area of fully functional aileron  
Sf = 54.8;           %Sq ft Surface area of fully functional VTail  
St = 63.7;           %Sq ft Surface area of fully functional HTail  
Sw = 323.2;          %Sq ft Surface area of fully functional wing  
lt = 15.86;          %length from tail to Nominal Cg at FS320.654  
k = 0.33;            %Aerodynamic constant

### %SELECT DAMAGE LEVEL

Zeta\_e = .25;  
Zeta\_r = 1;  
Zeta\_a = 1;  
Zeta\_rp = ((Zeta\_r - 1)\*Sr + Sf)/Sf ;  
Zeta\_ar = ((Zeta\_e - 1)\*St + (Zeta\_a - 1)\*Sa + (Zeta\_r - 1)\*Sr  
          + Sw + Sf + St)/(Sw + Sf + St) ;

### %INPUT PLANTS

cd /eng1/vcacciat/Thesis/PLANTS  
for u = 1:282;  
    cd /eng1/vcacciat/Thesis/PLANTS/edited\_plants  
eval(['m' num2str(u) 'e']);

### %Define Variables Necessary for Stability Derivative Modeling

A = A\_VISTA;  
B = B\_VISTA ;  
Delta\_Xcg = XCG/12;

```

at = CLQ/ALPHA;
aw = CLQ/ALPHA;

%Define Variables Necessary for Disturbance Modeling
Kn = IXZ/IZZ;
Lambda = 1-((IXZ)^2/(IXX*IZZ));
MaxELEV = 21;
Trim=.20*MaxELEV;
Ldelta_a = B(7,4);
Zdelta_e = B(3,1);
Zalpha_dot = A(3,4);
Mdelta_e = B(2,1);
Malpha_dot = A(4,4);
k1 = U - Zalpha_dot;
k2 = (1 - Zeta_e)/Zeta_e;

%MODIFY Stability Derivatives

%%LONGITUDINAL
%%Cma
%%%%%%%%%Note that Delta_MA/MA is negative and the F-16 is unstable
%%%%%%%%%so the failed Cma should be of greater value then the healthy
Delta_MA =(Zeta_e-1)*nu*St*at*lt*(1-k);
MA = Sw*aw*Delta_Xcg - Zeta_e*nu*St*at*lt*(1-k);
A(4,3) = A(4,3)*(1 - (Delta_MA/MA));

%%Cmq
A(4,4) = A(4,4)*Zeta_e;

%%Cmdeltae
B(4,1) = B(4,1)*Zeta_e;

%%Cza
Delta_ZA =(1-Zeta_e)*nu*St*at*(1 - k);
ZA = Sw*aw + Zeta_e*nu*St*at*(1 - k);
A(3,3) = A(3,3)*(1 - (Delta_ZA/ZA));

%%Czq
A(3,4) = A(3,4)*Zeta_e;

%%Czdeltae
B(3,1) = B(3,1)*Zeta_e;

%%LATERAL/DIRECTIONAL
%%CyB

```

```

A(6,6) = A(6,6)*Zeta_rp;

%%%Cyp
A(6,7) = A(6,7)*Zeta_rp;

%%%Cyr
A(6,8) = A(6,8)*Zeta_rp;

%%%Cydeltaa
B(6,4) = B(6,4)*Zeta_a;

%%%Cydeltar
B(6,5) = B(6,5)*Zeta_r;

%%%CydeltaDFtail
B(6,2) = B(6,2)*Zeta_e;

%%%Clp
A(7,7) = A(7,7)*Zeta_ar;

%%%Clr
A(7,8) = A(7,8)*Zeta_rp;

%%%ClB
A(7,6) = A(7,6)*Zeta_rp;

%%%Cldeltaa
B(7,4) = B(7,4)*Zeta_a;

%%%Cldeltar
B(7,5) = B(7,5)*Zeta_r;

%%%CldeltaDFtail
B(7,2) = B(7,2)*Zeta_e;

%%%CnB
A(8,6) = A(8,6)*Zeta_rp;

%%%Cnp
A(8,7) = A(8,7)*Zeta_rp;

%%%Cnr
A(8,8) = A(8,8)*Zeta_rp;

%%%Cndeltaa

```

```

B(8,4) = B(8,4)*Zeta_a;

%%%Cndeltar
B(8,5) = B(8,5)*Zeta_r;

%%%CndeltaDFtail
B(8,2) = B(8,2)*Zeta_e;

%Define Cross Coupling Disturbance Models
Gamma_lat = zeros(4,1);
Gamma_lat(3,1) = (((1-Zeta_e)*Ldelta_a)/(6*Lambda));
Gamma_lat(4,1) = ((Kn*(1-Zeta_e)*Ldelta_a)/(6*Lambda));

Gamma_long = zeros(4,1);
Gamma_long(3,1) = (k2*Zdelta_e)/(Zeta_e*k1);
Gamma_long(4,1) = k2*(Mdelta_e*k1 + Malpha_dot*Zdelta_e)/k1;

Gamma_lat = -MaxELEV*Gamma_lat;
Gamma_long = Trim*Gamma_long;

%STORE NEW PLANTS and Disturbance Inputs
cd /eng1/vcacciat/Thesis/PLANTS/failed_plants
fid = fopen(['mF' num2str(u) 'e.m'],'w');
fprintf(fid,['%%Failure Case #' num2str(u)]);
fprintf(fid,'\nZeta_e =%3.2f; Zeta_a =%3.2f;
          Zeta_r =%3.2f;',Zeta_e,Zeta_a,Zeta_r);
fprintf(fid,'\nU = %f;',U);
fprintf(fid,' qbar = %f;',qbar);
fprintf(fid,['\n \nA_VISTA_F = [']);
fprintf(fid,'%f,%f,%f,%f,%f,%f,%f,%f;',A');
fprintf(fid,[' ]; ']);
fprintf(fid,['\n \nB_VISTA_F = [']);
fprintf(fid,'%f, %f, %f, %f, %f;',B');
fprintf(fid,[' ]; ']);
fprintf(fid,['\n \nGamma_long = [']);
fprintf(fid,'%f;', Gamma_long);
fprintf(fid,[' ]; ']);
fprintf(fid,['\n \nGamma_lat = [']);
fprintf(fid,'%f;', Gamma_lat);
fprintf(fid,[' ]; ']);
status = fclose(fid);
end

```

*Appendix B. Parameter Space Data Points*

This appendix contains a list of all of the data points for which LTI aircraft models are generated by the SRF.

#	U(ft/sec)	Mach	Alt(ft)	Tanks	$q(\text{lb}/\text{ft}^2)$
1	356.3108	0.38	30000	3	63.6460
2	306.8269	0.31	20000	1	65.4696
3	306.8179	0.31	20000	0	65.4696
4	282.6290	0.28	15000	1	65.5666
5	371.1044	0.39	30000	1	67.0399
6	371.0953	0.39	30000	0	67.0399
7	340.3061	0.35	25000	1	67.4267
8	340.2972	0.35	25000	0	67.4267
9	409.8783	0.44	35000	1	67.6717
10	407.3858	0.44	35000	3	67.6717
11	268.5053	0.26	10000	1	68.8746
12	268.4976	0.26	10000	0	68.8746
13	233.5497	0.22	1000	3	69.1382
14	316.8115	0.32	20000	3	69.7616
15	292.9719	0.29	15000	3	70.3335
16	252.9760	0.24	5000	1	70.9929
17	251.7848	0.24	5000	3	70.9929
18	349.9148	0.36	25000	3	71.3347
19	279.4878	0.27	10000	2	74.2746
20	280.3498	0.27	10000	1	74.2746
21	279.1366	0.27	10000	3	74.2746
22	280.3444	0.27	10000	0	74.2746
23	246.9440	0.23	1000	1	75.5664
24	264.9703	0.25	5000	0	77.0323
25	442.3595	0.47	35000	0	77.2143
26	496.4158	0.53	40000	1	77.2914
27	494.0463	0.53	40000	3	77.2914
28	496.4142	0.53	40000	0	77.2914
29	505.9001	0.54	40000	2	80.2356
30	507.2213	0.54	40000	1	80.2356
31	504.8485	0.54	40000	3	80.2356
32	507.2212	0.54	40000	0	80.2356
33	316.8614	0.31	15000	2	80.3692
34	317.7535	0.31	15000	1	80.3692
35	316.4457	0.31	15000	3	80.3692
36	317.7506	0.31	15000	0	80.3692
37	451.9645	0.48	35000	2	80.5349
38	453.1725	0.48	35000	1	80.5349
39	451.1247	0.48	35000	3	80.5349
40	453.1725	0.48	35000	0	80.5349
41	414.1389	0.43	30000	2	81.4969
42	415.2408	0.43	30000	1	81.4969
43	413.4491	0.43	30000	3	81.4969
44	415.2395	0.43	30000	0	81.4969
45	258.3013	0.24	1000	2	82.2802
46	258.9648	0.24	1000	1	82.2802
47	258.0598	0.24	1000	3	82.2802

#	U(ft/sec)	Mach	Alt(ft)	Tanks	$q(\text{lb}/\text{ft}^2)$
48	258.9626	0.24	1000	0	82.2802
49	276.1144	0.26	5000	2	83.3181
50	276.8024	0.26	5000	1	83.3181
51	275.8478	0.26	5000	3	83.3181
52	276.8001	0.26	5000	0	83.3181
53	351.7636	0.35	20000	2	83.4550
54	352.6862	0.35	20000	1	83.4550
55	351.2820	0.35	20000	3	83.4550
56	352.6857	0.35	20000	0	83.4550
57	384.2509	0.39	25000	2	83.7192
58	385.2349	0.39	25000	1	83.7192
59	383.6765	0.39	25000	3	83.7192
60	385.2340	0.39	25000	0	83.7192
61	473.5181	0.50	35000	2	87.3860
62	474.5858	0.50	35000	1	87.3860
63	472.6632	0.50	35000	3	87.3860
64	474.5876	0.50	35000	0	87.3860
65	605.7848	0.64	45000	1	88.7159
66	605.7899	0.64	45000	0	88.7159
67	435.3305	0.45	30000	3	89.2543
68	538.1724	0.57	40000	2	89.3983
69	539.2541	0.57	40000	1	89.3983
70	537.0843	0.57	40000	3	89.3983
71	539.2568	0.57	40000	0	89.3983
72	314.4668	0.30	10000	2	91.6970
73	315.2011	0.30	10000	1	91.6970
74	314.1575	0.30	10000	3	91.6970
75	315.2010	0.30	10000	0	91.6970
76	625.6518	0.66	45000	2	94.3473
77	626.6525	0.66	45000	1	94.3473
78	626.6591	0.66	45000	0	94.3473
79	734.2271	0.77	50000	0	101.0962
80	362.6436	0.35	15000	2	102.4478
81	363.2888	0.35	15000	1	102.4478
82	362.1963	0.35	15000	3	102.4478
83	363.2904	0.35	15000	0	102.4478
84	655.5445	0.69	45000	3	103.1193
85	744.5969	0.78	50000	0	103.7392
86	667.0249	0.70	45000	2	106.1299
87	667.9643	0.70	45000	1	106.1299
88	665.8376	0.70	45000	3	106.1299
89	667.9745	0.70	45000	0	106.1299
90	754.9666	0.79	50000	0	106.4162
91	407.6037	0.40	20000	2	109.0025
92	408.2125	0.40	20000	1	109.0025
93	407.0826	0.40	20000	3	109.0025
94	408.2147	0.40	20000	0	109.0025

#	U(ft/sec)	Mach	Alt(ft)	Tanks	$\bar{q}$ (lb/ft <sup>2</sup> )
95	764.1132	0.80	50000	2	109.1273
96	765.2863	0.80	50000	1	109.1273
97	765.3006	0.80	50000	0	109.1273
98	489.3799	0.50	30000	2	110.1905
99	490.0036	0.50	30000	1	110.1905
100	488.6942	0.50	30000	3	110.1905
101	490.0065	0.50	30000	0	110.1905
102	323.1903	0.30	5000	2	110.9265
103	323.7697	0.30	5000	1	110.9265
104	322.7902	0.30	5000	3	110.9265
105	323.7712	0.30	5000	0	110.9265
106	774.5156	0.81	50000	2	111.8726
107	775.6357	0.81	50000	1	111.8726
108	775.6498	0.81	50000	0	111.8726
109	784.8859	0.82	50000	2	114.6519
110	785.9575	0.82	50000	1	114.6519
111	785.9714	0.82	50000	0	114.6519
112	795.2271	0.83	50000	2	117.4653
113	796.2540	0.83	50000	1	117.4653
114	796.2675	0.83	50000	0	117.4653
115	805.5421	0.84	50000	2	120.3129
116	806.5272	0.84	50000	1	120.3129
117	803.9543	0.84	50000	3	120.3129
118	806.5403	0.84	50000	0	120.3129
119	718.4875	0.75	45000	2	121.8328
120	719.3352	0.75	45000	1	121.8328
121	717.1732	0.75	45000	3	121.8328
122	719.3445	0.75	45000	0	121.8328
123	815.8332	0.85	50000	2	123.1945
124	816.6036	0.85	50000	1	123.1945
125	814.2523	0.85	50000	3	123.1945
126	816.6129	0.85	50000	0	123.1945
127	825.9927	0.86	50000	2	126.1103
128	826.6674	0.86	50000	1	126.1103
129	824.5324	0.86	50000	3	126.1103
130	826.6767	0.86	50000	0	126.1103
131	836.0692	0.87	50000	2	129.0601
132	836.7357	0.87	50000	1	129.0601
133	834.7814	0.87	50000	3	129.0601
134	836.7450	0.87	50000	0	129.0601
135	330.6034	0.30	1000	2	129.4213
136	331.0931	0.30	1000	1	129.4213
137	330.2076	0.30	1000	3	129.4213
138	331.0943	0.30	1000	0	129.4213
139	411.7170	0.39	15000	2	129.8252
140	412.2256	0.39	15000	1	129.8252
141	411.1960	0.39	15000	3	129.8252

#	U(ft/sec)	Mach	Alt(ft)	Tanks	$\bar{q}$ (lb/ft <sup>2</sup> )
142	412.2274	0.39	15000	0	129.8252
143	534.4108	0.54	30000	2	129.9582
144	534.9595	0.54	30000	1	129.9582
145	533.6214	0.54	30000	3	129.9582
146	534.9625	0.54	30000	0	129.9582
147	488.3471	0.49	25000	2	130.0074
148	488.8853	0.49	25000	1	130.0074
149	487.6650	0.49	25000	3	130.0074
150	488.8876	0.49	25000	0	130.0074
151	587.5572	0.61	35000	2	130.0653
152	588.1083	0.61	35000	1	130.0653
153	586.6335	0.61	35000	3	130.0653
154	588.1118	0.61	35000	0	130.0653
155	447.9792	0.44	20000	2	130.1006
156	448.5037	0.44	20000	1	130.1006
157	447.3843	0.44	20000	3	130.1006
158	448.5057	0.44	20000	0	130.1006
159	749.0121	0.78	45000	2	131.7744
160	749.5445	0.78	45000	1	131.7744
161	747.7755	0.78	45000	3	131.7744
162	749.5507	0.78	45000	0	131.7744
163	846.1508	0.88	50000	2	132.0441
164	846.8071	0.88	50000	1	132.0441
165	844.9784	0.88	50000	3	132.0441
166	846.8163	0.88	50000	0	132.0441
167	671.9930	0.70	40000	2	134.8266
168	672.4916	0.70	40000	1	134.8266
169	670.9288	0.70	40000	3	134.8266
170	672.4959	0.70	40000	0	134.8266
171	856.2359	0.89	50000	2	135.0621
172	856.8798	0.89	50000	1	135.0621
173	855.0580	0.89	50000	3	135.0621
174	856.8889	0.89	50000	0	135.0621
175	461.4592	0.45	20000	3	137.9562
176	866.3225	0.90	50000	2	138.1142
177	866.9518	0.90	50000	1	138.1142
178	865.1412	0.90	50000	3	138.1142
179	866.9608	0.90	50000	0	138.1142
180	592.3990	0.60	30000	3	158.6743
181	427.6254	0.40	10000	3	163.0169
182	848.8048	0.88	45000	2	167.7286
183	849.1861	0.88	45000	1	167.7286
184	847.9139	0.88	45000	3	167.7286
185	849.1904	0.88	45000	0	167.7286
186	515.3699	0.50	20000	2	170.3164
187	515.6489	0.50	20000	1	170.3164
188	514.9072	0.50	20000	3	170.3164

#	U(ft/sec)	Mach	Alt(ft)	Tanks	$\bar{q}$ (lb/ft <sup>2</sup> )
189	515.6502	0.50	20000	0	170.3164
190	643.1663	0.65	30000	3	186.2219
191	567.6104	0.55	20000	3	206.0828
192	482.4902	0.45	10000	3	206.3182
193	840.2690	0.87	40000	2	208.2658
194	840.5090	0.87	40000	1	208.2658
195	839.7098	0.87	40000	3	208.2658
196	840.5118	0.87	40000	0	208.2658
197	694.1871	0.70	30000	2	215.9733
198	694.4091	0.70	30000	1	215.9733
199	693.6675	0.70	30000	3	215.9733
200	694.4109	0.70	30000	0	215.9733
201	869.9337	0.90	40000	1	222.8766
202	869.2272	0.90	40000	3	222.8766
203	869.9363	0.90	40000	0	222.8766
204	443.5660	0.40	1000	2	228.5562
205	443.7502	0.40	1000	1	228.5562
206	443.2620	0.40	1000	3	228.5562
207	443.7508	0.40	1000	0	228.5562
208	620.0384	0.60	20000	3	245.2556
209	743.9712	0.75	30000	3	247.9286
210	537.3339	0.50	10000	2	254.7139
211	537.4980	0.50	10000	1	254.7139
212	536.9779	0.50	10000	3	254.7139
213	537.4987	0.50	10000	0	254.7139
214	845.4997	0.87	35000	2	264.5698
215	845.6716	0.87	35000	1	264.5698
216	845.0479	0.87	35000	3	264.5698
217	845.6735	0.87	35000	0	264.5698
218	794.1589	0.80	30000	3	282.0876
219	672.3800	0.65	20000	3	287.8346
220	591.2659	0.55	10000	3	308.2038
221	864.8840	0.87	30000	2	333.6127
222	865.0098	0.87	30000	1	333.6127
223	864.5085	0.87	30000	3	333.6127
224	865.0110	0.87	30000	0	333.6127
225	724.9935	0.70	20000	2	333.8201
226	725.1219	0.70	20000	1	333.8201
227	724.5963	0.70	20000	3	333.8201
228	725.1229	0.70	20000	0	333.8201
229	894.9976	0.90	30000	1	357.0172
230	894.5495	0.90	30000	3	357.0172
231	894.9987	0.90	30000	0	357.0172
232	645.4193	0.60	10000	3	366.7880
233	776.7334	0.75	20000	3	383.2118
234	883.6877	0.87	25000	2	416.6143
235	883.7897	0.87	25000	1	416.6143

#	U(ft/sec)	Mach	Alt(ft)	Tanks	$\bar{q}$ (lb/ft <sup>2</sup> )
236	883.3687	0.87	25000	3	416.6143
237	883.7905	0.87	25000	0	416.6143
238	699.5460	0.65	10000	3	430.4664
239	828.8166	0.80	20000	3	436.0099
240	753.9324	0.70	10000	2	499.2391
241	754.0159	0.70	10000	1	499.2391
242	753.6174	0.70	10000	3	499.2391
243	754.0165	0.70	10000	0	499.2391
244	891.6245	0.86	20000	2	503.8640
245	891.7075	0.86	20000	1	503.8640
246	891.3319	0.86	20000	3	503.8640
247	891.7080	0.86	20000	0	503.8640
248	667.3123	0.60	1000	2	514.2514
249	667.3877	0.60	1000	1	514.2514
250	667.0334	0.60	1000	3	514.2514
251	667.3881	0.60	1000	0	514.2514
252	933.2764	0.90	20000	1	551.8250
253	932.9374	0.90	20000	3	551.8250
254	933.2769	0.90	20000	0	551.8250
255	807.6479	0.75	10000	3	573.1062
256	909.3434	0.86	15000	2	618.5337
257	909.4110	0.86	15000	1	618.5337
258	909.0850	0.86	15000	3	618.5337
259	909.4115	0.86	15000	0	618.5337
260	861.6325	0.80	10000	3	652.0676
261	778.8329	0.70	1000	2	699.9532
262	778.8885	0.70	1000	1	699.9532
263	778.5750	0.70	1000	3	699.9532
264	778.8887	0.70	1000	0	699.9532
265	937.4568	0.87	10000	2	771.1717
266	937.5140	0.87	10000	1	771.1717
267	937.2269	0.87	10000	3	771.1717
268	937.5142	0.87	10000	0	771.1717
269	969.8751	0.90	10000	1	825.2729
270	969.6061	0.90	10000	3	825.2729
271	969.8754	0.90	10000	0	825.2729
272	965.6384	0.88	5000	2	954.4603
273	965.6884	0.88	5000	1	954.4603
274	965.4279	0.88	5000	3	954.4603
275	965.6886	0.88	5000	0	954.4603
276	979.3263	0.88	1000	2	1106.2120
277	979.3723	0.88	1000	1	1106.2120
278	979.1241	0.88	1000	3	1106.2120
279	979.3725	0.88	1000	0	1106.2120
280	1001.6410	0.90	1000	1	1157.0650
281	1001.4010	0.90	1000	3	1157.0650
282	1001.6410	0.90	1000	0	1157.0650

*Appendix C. Longitudinal Channel Time Response*

Variable	Units
$\bar{q}$	<i>lbs/ft<sup>2</sup></i>
$t_1$	seconds
$\Delta_t$	seconds
$\dot{\delta}_{elev}$	deg/sec
$\delta_{elev}$	degrees
$g_{pil}$	g's
$\alpha$	degrees

C.1 Longitudinal Unit  $C^*_{cmd}$  Step Input Time Response (Healthy)

#	srf#	$\bar{q}$	$t_1$	$\Delta t_{minL1}$	$\Delta t$	$\Delta t_{maxL1}$	$\Delta t_{maxL2}$	$\frac{\Delta q_2}{\Delta q_1}$	$\delta_{elev(max)}$	$\delta_{elev(max)}$	$g_{pil(ss)}$	$\alpha_{ss}$
1	119	65.4696	0.048	0.029	0.980	1.630	5.215	0.000	7.388	0.462	2.196	20.240
2	253	65.4696	0.087	0.029	1.102	1.630	5.215	0.848	7.407	0.353	2.196	20.249
3	118	65.5666	0.048	0.032	0.985	1.769	5.661	0.000	7.388	0.494	2.182	20.037
4	122	67.0399	0.087	0.024	1.083	1.347	4.311	0.425	7.407	0.492	2.234	20.316
5	256	67.0399	0.086	0.024	1.083	1.347	4.312	0.846	7.406	0.229	2.234	20.319
6	121	67.4267	0.087	0.026	1.091	1.469	4.702	0.576	7.407	0.528	2.217	20.010
7	255	67.4267	0.086	0.026	1.090	1.469	4.702	1.219	7.407	0.264	2.217	20.014
8	124	67.6717	0.086	0.022	1.075	1.220	3.904	0.754	7.406	0.429	2.255	20.435
9	116	68.8746	0.084	0.034	1.117	1.862	5.959	2.449	7.407	0.554	2.177	19.117
10	251	68.8746	0.083	0.034	1.116	1.862	5.959	0.000	7.407	0.292	2.177	19.123
11	115	70.9929	0.082	0.036	1.123	1.976	6.325	0.000	7.406	0.502	2.169	18.507
12	10	74.2746	0.075	0.032	1.100	1.789	5.725	0.000	7.403	-1.334	2.188	18.716
13	66	74.2746	0.080	0.032	1.108	1.783	5.707	3.376	7.405	0.323	2.189	18.039
14	202	74.2746	0.079	0.032	1.108	1.784	5.707	0.000	7.405	0.079	2.189	18.044
15	113	75.5664	0.078	0.036	1.126	2.025	6.479	0.000	7.405	0.349	2.169	17.501
16	250	77.0323	0.077	0.034	1.114	1.887	6.038	0.000	7.404	0.028	2.181	17.379
17	258	77.2143	0.081	0.020	1.044	1.130	3.617	0.000	7.402	0.153	2.286	18.694
18	125	77.2914	0.081	0.018	1.039	1.007	3.223	0.000	7.402	0.390	2.311	19.068
19	259	77.2914	0.080	0.018	1.039	1.007	3.223	0.000	7.401	0.164	2.311	19.064
20	37	80.2356	0.076	0.018	1.036	0.988	3.163	0.000	7.400	-0.359	2.319	19.092
21	93	80.2356	0.077	0.018	1.033	0.986	3.154	0.000	7.400	0.399	2.321	18.460
22	229	80.2356	0.076	0.018	1.033	0.986	3.154	0.000	7.400	0.184	2.321	18.455
23	15	80.3692	0.077	0.028	1.059	1.578	5.050	0.000	7.401	-1.054	2.218	17.693
24	71	80.3692	0.081	0.028	1.058	1.574	5.035	0.000	7.402	0.365	2.219	17.017
25	207	80.3692	0.080	0.028	1.059	1.574	5.035	0.000	7.402	0.142	2.219	17.020
26	33	80.5349	0.076	0.020	1.040	1.106	3.540	0.000	7.400	-0.592	2.294	18.686
27	89	80.5349	0.078	0.020	1.037	1.103	3.531	0.000	7.400	0.341	2.296	18.036
28	225	80.5349	0.077	0.020	1.037	1.103	3.531	0.000	7.400	0.125	2.296	18.034
29	28	81.4969	0.075	0.022	1.042	1.207	3.863	0.000	7.400	-0.759	2.276	18.219
30	84	81.4969	0.078	0.022	1.040	1.204	3.853	0.000	7.400	0.303	2.277	17.567
31	220	81.4969	0.077	0.022	1.040	1.204	3.853	0.000	7.400	0.087	2.277	17.566
32	1	82.2802	0.075	0.035	1.068	1.936	6.194	0.000	7.401	-1.642	2.182	16.987
33	57	82.2802	0.080	0.035	1.067	1.931	6.178	0.000	7.402	-0.157	2.182	16.355
34	193	82.2802	0.079	0.035	1.068	1.931	6.178	0.000	7.402	-0.377	2.182	16.359
35	7	83.3181	0.075	0.033	1.059	1.811	5.795	0.000	7.400	-1.666	2.194	16.974
36	63	83.3181	0.080	0.033	1.057	1.806	5.780	0.000	7.401	-0.255	2.195	16.352
37	199	83.3181	0.078	0.033	1.059	1.806	5.780	0.000	7.401	-0.471	2.195	16.356
38	19	83.4550	0.074	0.026	1.048	1.421	4.549	0.000	7.399	-1.027	2.242	17.376
39	75	83.4550	0.077	0.026	1.048	1.418	4.537	0.000	7.400	0.250	2.243	16.718
40	211	83.4550	0.076	0.026	1.048	1.418	4.537	0.000	7.400	0.038	2.243	16.719

#	srf#	$\bar{q}$	$t_1$	$\Delta t_{minL1}$	$\Delta t$	$\Delta t_{maxL1}$	$\Delta t_{maxL2}$	$\frac{\Delta q_2}{\Delta q_1}$	$\delta_{elev(max)}$	$\delta_{elev(max)}$	$g_{pil(ss)}$	$\alpha_{ss}$
42	81	83.7192	0.076	0.023	1.041	1.298	4.153	0.000	7.400	0.258	2.263	16.914
43	217	83.7192	0.075	0.023	1.042	1.298	4.153	0.000	7.399	0.048	2.263	16.914
44	34	87.3860	0.069	0.019	1.026	1.056	3.379	0.000	7.396	-0.468	2.315	17.410
45	90	87.3860	0.070	0.019	1.024	1.054	3.371	0.000	7.397	0.335	2.317	16.802
46	226	87.3860	0.069	0.019	1.024	1.054	3.371	0.000	7.396	0.139	2.317	16.799
47	127	88.7159	0.071	0.015	0.967	0.825	2.641	0.000	7.393	0.392	2.397	16.771
48	261	88.7159	0.070	0.015	0.968	0.825	2.641	0.000	7.393	0.209	2.397	16.764
49	38	89.3983	0.067	0.017	1.016	0.929	2.973	0.000	7.395	-0.106	2.349	17.357
50	94	89.3983	0.076	0.017	0.973	0.927	2.967	0.000	7.395	0.411	2.363	16.532
51	230	89.3983	0.075	0.017	0.974	0.927	2.967	0.000	7.394	0.222	2.363	16.527
52	11	91.6970	0.068	0.029	1.038	1.590	5.088	0.000	7.395	-2.047	2.227	16.011
53	67	91.6970	0.071	0.029	1.039	1.586	5.076	0.000	7.397	-0.707	2.227	15.385
54	203	91.6970	0.070	0.029	1.040	1.586	5.076	0.000	7.396	-0.900	2.227	15.386
55	41	94.3473	0.064	0.014	0.958	0.799	2.557	0.000	7.389	-0.229	2.415	16.398
56	97	94.3473	0.065	0.014	0.955	0.798	2.553	0.000	7.389	0.188	2.417	15.877
57	233	94.3473	0.064	0.014	0.956	0.798	2.553	0.000	7.389	0.020	2.417	15.870
58	262	101.0962	0.050	0.012	0.934	0.681	2.179	0.000	7.379	-0.085	2.477	14.955
59	16	102.4478	0.061	0.025	1.005	1.379	4.412	0.000	7.390	-1.262	2.269	14.491
60	72	102.4478	0.065	0.025	1.001	1.376	4.404	0.000	7.391	-0.227	2.269	13.908
61	208	102.4478	0.064	0.025	1.002	1.376	4.404	0.000	7.391	-0.395	2.269	13.907
62	263	103.7392	0.050	0.012	0.920	0.672	2.149	0.000	7.377	-0.146	2.484	15.343
63	42	106.1299	0.053	0.013	0.934	0.750	2.399	0.000	7.380	-0.567	2.455	14.795
64	98	106.1299	0.054	0.013	0.935	0.749	2.395	0.000	7.381	-0.109	2.451	14.922
65	234	106.1299	0.053	0.013	0.935	0.749	2.395	0.000	7.380	-0.252	2.451	14.910
66	264	106.4162	0.047	0.012	0.908	0.662	2.119	0.000	7.375	-0.214	2.494	14.955
67	20	109.0025	0.058	0.022	0.983	1.227	3.925	0.000	7.386	-1.227	2.305	13.842
68	76	109.0025	0.061	0.022	0.980	1.225	3.920	0.000	7.387	-0.393	2.306	13.308
69	212	109.0025	0.060	0.022	0.981	1.225	3.920	0.000	7.387	-0.547	2.306	13.306
70	46	109.1273	0.047	0.012	0.892	0.654	2.094	0.000	7.372	-0.695	2.496	15.232
71	102	109.1273	0.047	0.012	0.893	0.653	2.091	0.000	7.373	-0.149	2.504	14.592
72	238	109.1273	0.047	0.012	0.889	0.653	2.091	0.000	7.372	-0.278	2.503	14.575
73	29	110.1905	0.059	0.018	0.960	1.022	3.269	0.000	7.385	-0.890	2.359	13.952
74	85	110.1905	0.060	0.018	0.957	1.020	3.265	0.000	7.385	-0.360	2.360	13.471
75	221	110.1905	0.059	0.018	0.958	1.020	3.265	0.000	7.385	-0.511	2.360	13.468
76	8	110.9265	0.055	0.028	1.013	1.547	4.951	0.000	7.386	-2.218	2.249	13.553
77	64	110.9265	0.058	0.028	1.012	1.544	4.942	0.000	7.388	-0.986	2.250	12.936
78	200	110.9265	0.057	0.028	1.013	1.544	4.942	0.000	7.388	-1.141	2.250	12.934
79	47	111.8726	0.046	0.012	0.876	0.646	2.066	0.000	7.370	-0.960	2.504	14.783
80	103	111.8726	0.046	0.012	0.874	0.645	2.063	0.000	7.370	-0.426	2.512	14.159
81	239	111.8726	0.046	0.012	0.870	0.645	2.063	0.000	7.370	-0.549	2.511	14.142
82	48	114.6519	0.046	0.011	0.858	0.637	2.039	0.000	7.368	-1.189	2.512	14.348

#	srf#	$\bar{q}$	$t_1$	$\Delta t_{minL1}$	$\Delta t$	$\Delta t_{maxL1}$	$\Delta t_{maxL2}$	$\frac{\Delta q_2}{\Delta q_1}$	$\delta_{elev(max)}$	$\delta_{elev(max)}$	$g_{pil(ss)}$	$\alpha_{ss}$
83	104	114.6519	0.046	0.011	0.854	0.636	2.036	0.000	7.367	-0.667	2.520	13.737
84	240	114.6519	0.046	0.011	0.850	0.636	2.036	0.000	7.367	-0.785	2.519	13.719
85	49	117.4653	0.046	0.011	0.839	0.629	2.012	0.000	7.365	-1.384	2.520	13.924
86	105	117.4653	0.046	0.011	0.834	0.628	2.009	0.000	7.365	-0.876	2.527	13.324
87	241	117.4653	0.046	0.011	0.830	0.628	2.009	0.000	7.364	-0.989	2.527	13.307
88	50	120.3129	0.046	0.011	0.820	0.621	1.986	0.000	7.362	-1.549	2.528	13.511
89	106	120.3129	0.046	0.011	0.813	0.620	1.984	0.000	7.362	-1.056	2.535	12.921
90	242	120.3129	0.046	0.011	0.810	0.620	1.984	0.000	7.361	-1.164	2.535	12.903
91	43	121.8328	0.046	0.013	0.868	0.696	2.227	0.000	7.368	-0.834	2.498	13.591
92	99	121.8328	0.046	0.013	0.869	0.695	2.224	0.000	7.369	-0.426	2.502	13.021
93	235	121.8328	0.046	0.013	0.865	0.695	2.224	0.000	7.368	-0.543	2.502	13.009
94	51	123.1945	0.045	0.011	0.802	0.613	1.961	0.000	7.359	-1.688	2.536	13.108
95	107	123.1945	0.045	0.011	0.790	0.612	1.959	0.000	7.359	-1.236	2.564	11.570
96	243	123.1945	0.045	0.011	0.787	0.612	1.959	0.000	7.358	-1.341	2.564	11.561
97	52	126.1103	0.045	0.011	0.780	0.605	1.937	0.000	7.356	-1.807	2.570	11.816
98	108	126.1103	0.045	0.011	0.775	0.605	1.935	0.000	7.356	-1.420	2.573	11.344
99	244	126.1103	0.045	0.011	0.772	0.605	1.935	0.000	7.356	-1.521	2.573	11.334
100	53	129.0601	0.045	0.011	0.766	0.598	1.914	0.000	7.353	-1.967	2.579	11.589
101	109	129.0601	0.045	0.011	0.761	0.598	1.912	0.000	7.353	-1.606	2.582	11.110
102	245	129.0601	0.045	0.011	0.758	0.598	1.912	0.000	7.353	-1.704	2.581	11.100
103	2	129.4213	0.046	0.027	0.988	1.512	4.840	0.000	7.379	-2.247	2.270	11.849
104	58	129.4213	0.049	0.027	1.008	1.510	4.832	0.000	7.381	-1.082	2.270	11.280
105	194	129.4213	0.046	0.027	1.007	1.510	4.832	0.000	7.381	-1.214	2.270	11.277
106	17	129.8252	0.046	0.022	0.970	1.214	3.886	0.000	7.378	-1.490	2.327	12.019
107	73	129.8252	0.050	0.022	0.978	1.213	3.881	0.000	7.380	-0.686	2.328	11.501
108	209	129.8252	0.049	0.022	0.979	1.213	3.881	0.000	7.379	-0.816	2.328	11.497
109	30	129.9582	0.046	0.017	0.949	0.936	2.994	0.000	7.376	-0.940	2.407	12.389
110	86	129.9582	0.049	0.017	0.950	0.935	2.991	0.000	7.377	-0.559	2.408	11.925
111	222	129.9582	0.047	0.017	0.948	0.935	2.991	0.000	7.377	-0.684	2.408	11.920
112	26	130.0074	0.046	0.018	0.956	1.024	3.276	0.000	7.377	-1.162	2.378	12.257
113	82	130.0074	0.049	0.018	0.960	1.023	3.273	0.000	7.378	-0.621	2.379	11.773
114	218	130.0074	0.048	0.018	0.960	1.023	3.273	0.000	7.378	-0.749	2.379	11.769
115	35	130.0653	0.046	0.015	0.934	0.851	2.723	0.000	7.375	-0.727	2.439	12.506
116	91	130.0653	0.046	0.015	0.935	0.850	2.721	0.000	7.375	-0.485	2.440	12.064
117	227	130.0653	0.046	0.015	0.931	0.850	2.721	0.000	7.375	-0.608	2.440	12.058
118	21	130.1006	0.046	0.020	0.963	1.116	3.572	0.000	7.377	-1.344	2.352	12.119
119	77	130.1006	0.049	0.020	0.969	1.115	3.567	0.000	7.379	-0.664	2.353	11.616
120	213	130.1006	0.049	0.020	0.969	1.115	3.567	0.000	7.379	-0.792	2.353	11.612
121	44	131.7744	0.045	0.012	0.811	0.668	2.136	0.000	7.360	-0.934	2.538	11.208
122	100	131.7744	0.045	0.012	0.812	0.667	2.135	0.000	7.361	-0.579	2.539	10.793
123	236	131.7744	0.045	0.012	0.809	0.667	2.135	0.000	7.360	-0.683	2.539	10.786

#	srf#	$\bar{q}$	$t_1$	$\Delta_{t_{min}L1}$	$\Delta_t$	$\Delta_{t_{max}L1}$	$\Delta_{t_{max}L2}$	$\frac{\Delta_{q2}}{\Delta_{q1}}$	$\delta_{elev(max)}$	$\delta_{elev(max)}$	$g_{pil(ss)}$	$\alpha_{ss}$
124	54	132.0441	0.045	0.011	0.753	0.591	1.891	0.000	7.351	-2.131	2.588	11.353
125	110	132.0441	0.045	0.011	0.747	0.590	1.889	0.000	7.351	-1.796	2.590	10.866
126	246	132.0441	0.045	0.011	0.744	0.590	1.889	0.000	7.350	-1.891	2.590	10.856
127	39	134.8266	0.046	0.013	0.858	0.744	2.381	0.000	7.365	-0.901	2.492	12.204
128	95	134.8266	0.046	0.013	0.853	0.744	2.379	0.000	7.366	-0.611	2.498	10.630
129	231	134.8266	0.046	0.013	0.849	0.743	2.379	0.000	7.366	-0.719	2.498	10.626
130	55	135.0621	0.045	0.011	0.740	0.584	1.869	0.000	7.348	-2.298	2.596	11.107
131	111	135.0621	0.045	0.011	0.735	0.584	1.867	0.000	7.348	-1.989	2.599	10.613
132	247	135.0621	0.045	0.011	0.732	0.584	1.867	0.000	7.347	-2.081	2.599	10.603
133	56	138.1142	0.044	0.010	0.729	0.577	1.847	0.000	7.345	-2.469	2.605	10.853
134	112	138.1142	0.044	0.010	0.724	0.577	1.846	0.000	7.345	-2.184	2.607	10.351
135	248	138.1142	0.044	0.010	0.721	0.577	1.846	0.000	7.344	-2.274	2.607	10.341
136	45	167.7286	0.043	0.011	0.684	0.589	1.885	0.000	7.330	-2.447	2.626	8.977
137	101	167.7286	0.043	0.011	0.687	0.589	1.884	0.000	7.330	-2.212	2.625	7.767
138	237	167.7286	0.043	0.011	0.684	0.589	1.884	0.000	7.330	-2.284	2.625	7.761
139	22	170.3164	0.045	0.017	0.859	0.970	3.105	0.000	7.361	-1.465	2.434	9.053
140	78	170.3164	0.045	0.017	0.864	0.970	3.103	0.000	7.362	-1.085	2.435	8.715
141	214	170.3164	0.045	0.017	0.860	0.970	3.103	0.000	7.362	-1.179	2.435	8.713
142	40	208.2658	0.041	0.011	0.645	0.595	1.904	0.000	7.309	-2.190	2.652	6.819
143	96	208.2658	0.042	0.011	0.647	0.595	1.904	0.000	7.311	-1.979	2.653	6.521
144	232	208.2658	0.041	0.011	0.645	0.595	1.904	0.000	7.310	-2.037	2.653	6.517
145	31	215.9733	0.042	0.013	0.715	0.720	2.305	0.000	7.327	-1.460	2.581	7.462
146	87	215.9733	0.042	0.013	0.717	0.720	2.304	0.000	7.329	-1.290	2.581	7.179
147	223	215.9733	0.042	0.013	0.714	0.720	2.304	0.000	7.328	-1.354	2.581	7.176
148	126	222.8766	0.041	0.010	0.625	0.575	1.839	0.000	7.299	-2.194	2.677	5.854
149	260	222.8766	0.041	0.010	0.623	0.575	1.839	0.000	7.299	-2.248	2.677	5.849
150	3	228.5562	0.042	0.020	0.807	1.127	3.607	0.000	7.341	-2.165	2.431	6.960
151	59	228.5562	0.042	0.020	0.817	1.127	3.606	0.000	7.345	-1.508	2.431	6.632
152	195	228.5562	0.042	0.020	0.814	1.127	3.606	0.000	7.344	-1.578	2.431	6.631
153	12	254.7139	0.041	0.017	0.759	0.931	2.978	0.000	7.329	-1.824	2.514	6.505
154	68	254.7139	0.042	0.017	0.762	0.930	2.977	0.000	7.331	-1.456	2.514	6.226
155	204	254.7139	0.042	0.017	0.759	0.930	2.977	0.000	7.330	-1.517	2.514	6.224
156	36	264.5698	0.039	0.011	0.606	0.591	1.892	0.000	7.280	-2.009	2.691	5.564
157	92	264.5698	0.039	0.011	0.609	0.591	1.892	0.000	7.283	-1.877	2.691	5.304
158	228	264.5698	0.039	0.011	0.607	0.591	1.892	0.000	7.282	-1.923	2.691	5.300
159	32	333.6127	0.037	0.010	0.571	0.578	1.850	0.000	7.257	-1.894	2.734	4.594
160	88	333.6127	0.037	0.010	0.575	0.578	1.850	0.000	7.259	-1.868	2.734	4.366
161	224	333.6127	0.037	0.010	0.573	0.578	1.850	0.000	7.259	-1.905	2.734	4.363
162	23	333.8201	0.038	0.012	0.637	0.690	2.207	0.000	7.277	-1.401	2.669	5.255
163	79	333.8201	0.038	0.012	0.638	0.690	2.207	0.000	7.280	-1.340	2.669	5.023
164	215	333.8201	0.038	0.012	0.636	0.690	2.207	0.000	7.279	-1.381	2.669	5.021

#	srf#	$\bar{q}$	$t_1$	$\Delta_{t_{min}L1}$	$\Delta_t$	$\Delta_{t_{max}L1}$	$\Delta_{t_{max}L2}$	$\frac{\Delta_{q2}}{\Delta_{q1}}$	$\delta_{elev(max)}$	$\delta_{elev(max)}$	$g_{pil(ss)}$	$\alpha_{ss}$
165	123	357.0172	0.036	0.010	0.558	0.559	1.788	0.000	7.253	-2.196	2.756	4.038
166	257	357.0172	0.036	0.010	0.556	0.559	1.788	0.000	7.253	-2.230	2.756	4.035
167	27	416.6143	0.035	0.010	0.543	0.566	1.811	0.000	7.243	-1.915	2.773	3.904
168	83	416.6143	0.035	0.010	0.547	0.566	1.810	0.000	7.245	-1.929	2.773	3.686
169	219	416.6143	0.035	0.010	0.545	0.566	1.810	0.000	7.244	-1.958	2.773	3.684
170	13	499.2391	0.034	0.012	0.584	0.663	2.122	0.000	7.244	-1.392	2.747	3.840
171	69	499.2391	0.034	0.012	0.585	0.663	2.122	0.000	7.246	-1.381	2.747	3.631
172	205	499.2391	0.034	0.012	0.583	0.663	2.122	0.000	7.245	-1.408	2.747	3.630
173	24	503.8640	0.033	0.010	0.520	0.561	1.794	0.000	7.228	-1.829	2.801	3.385
174	80	503.8640	0.033	0.010	0.524	0.561	1.794	0.000	7.231	-1.878	2.801	3.182
175	216	503.8640	0.033	0.010	0.522	0.561	1.794	0.000	7.230	-1.903	2.801	3.180
176	4	514.2514	0.035	0.013	0.626	0.749	2.398	0.000	7.252	-1.511	2.713	3.871
177	60	514.2514	0.035	0.013	0.625	0.749	2.397	0.000	7.253	-1.436	2.713	3.672
178	196	514.2514	0.035	0.013	0.623	0.749	2.397	0.000	7.252	-1.464	2.713	3.671
179	120	551.8250	0.032	0.010	0.499	0.536	1.714	0.000	7.218	-2.263	2.826	2.821
180	254	551.8250	0.032	0.010	0.497	0.536	1.714	0.000	7.218	-2.285	2.826	2.819
181	18	618.5337	0.030	0.010	0.494	0.550	1.760	0.000	7.208	-1.845	2.833	2.873
182	74	618.5337	0.031	0.010	0.496	0.550	1.759	0.000	7.211	-1.921	2.833	2.683
183	210	618.5337	0.031	0.010	0.494	0.550	1.759	0.000	7.210	-1.941	2.833	2.681
184	5	699.9532	0.030	0.012	0.539	0.642	2.054	0.000	7.216	-1.467	2.806	2.930
185	61	699.9532	0.031	0.012	0.539	0.642	2.054	0.000	7.218	-1.523	2.806	2.750
186	197	699.9532	0.031	0.012	0.537	0.642	2.054	0.000	7.218	-1.542	2.806	2.749
187	14	771.1717	0.028	0.010	0.452	0.533	1.707	0.000	7.179	-2.320	2.865	2.431
188	70	771.1717	0.029	0.010	0.455	0.533	1.707	0.000	7.184	-2.415	2.865	2.256
189	206	771.1717	0.029	0.010	0.454	0.533	1.707	0.000	7.183	-2.431	2.865	2.254
190	117	825.2729	0.028	0.009	0.434	0.516	1.650	0.000	7.170	-2.696	2.879	2.071
191	252	825.2729	0.028	0.009	0.432	0.516	1.650	0.000	7.169	-2.711	2.879	2.069
192	9	954.4603	0.026	0.009	0.411	0.518	1.657	0.000	7.145	-2.466	2.891	2.078
193	65	954.4603	0.027	0.009	0.417	0.518	1.657	0.000	7.151	-2.576	2.891	1.910
194	201	954.4603	0.027	0.009	0.415	0.518	1.657	0.000	7.150	-2.589	2.891	1.908
195	6	1106.2120	0.025	0.009	0.381	0.511	1.634	0.000	7.118	-2.507	2.906	1.886
196	62	1106.2120	0.026	0.009	0.386	0.511	1.634	0.000	7.125	-2.629	2.906	1.720
197	198	1106.2120	0.026	0.009	0.385	0.511	1.634	0.000	7.124	-2.640	2.906	1.719
198	114	1157.0650	0.025	0.009	0.371	0.499	1.597	0.000	7.112	-2.810	2.913	1.635
199	249	1157.0650	0.025	0.009	0.369	0.499	1.597	0.000	7.110	-2.820	2.913	1.634

C.2 Longitudinal Unit  $C^*_{cmd}$  Step Input Time Response (25% Stabilator Failure)

#	srf#	$\bar{q}$	$t_1$	$\Delta t_{minL1}$	$\Delta t$	$\Delta t_{maxL1}$	$\Delta t_{maxL2}$	$\frac{\Delta q_2}{\Delta q_1}$	$\delta_{elev(max)}$	$\delta_{elev(max)}$	$g_{pil(ss)}$	$\alpha_{ss}$
1	119	65.4696	0.123	0.029	1.122	1.630	5.215	0.020	7.414	0.705	2.197	19.044
2	253	65.4696	0.186	0.029	1.232	1.630	5.215	0.017	7.425	0.673	2.197	19.050
3	118	65.5666	0.122	0.032	1.130	1.769	5.661	0.081	7.414	0.739	2.183	18.919
4	122	67.0399	0.184	0.024	1.213	1.347	4.311	0.015	7.424	0.805	2.237	18.920
5	256	67.0399	0.183	0.024	1.213	1.347	4.312	0.014	7.424	0.540	2.237	18.925
6	121	67.4267	0.184	0.026	1.220	1.469	4.702	0.013	7.425	0.843	2.219	18.712
7	255	67.4267	0.183	0.026	1.220	1.469	4.702	0.017	7.424	0.578	2.219	18.717
8	124	67.6717	0.182	0.022	1.205	1.220	3.904	0.013	7.424	0.737	2.259	18.921
9	116	68.8746	0.182	0.034	1.245	1.862	5.959	0.016	7.425	0.874	2.177	18.066
10	251	68.8746	0.181	0.034	1.245	1.862	5.959	0.018	7.425	0.611	2.177	18.073
11	115	70.9929	0.179	0.036	1.251	1.976	6.325	0.016	7.424	0.821	2.169	17.521
12	10	74.2746	0.168	0.032	1.228	1.789	5.725	0.015	7.423	-1.030	2.189	17.643
13	66	74.2746	0.176	0.032	1.233	1.783	5.707	0.012	7.424	0.633	2.189	16.988
14	202	74.2746	0.175	0.032	1.233	1.784	5.707	0.016	7.424	0.388	2.189	16.993
15	113	75.5664	0.174	0.036	1.251	2.025	6.479	0.016	7.424	0.661	2.169	16.564
16	250	77.0323	0.171	0.034	1.240	1.887	6.038	0.017	7.423	0.335	2.182	16.394
17	258	77.2143	0.178	0.020	1.150	1.130	3.617	0.000	7.422	0.432	2.291	17.020
18	125	77.2914	0.175	0.018	1.150	1.007	3.223	0.000	7.421	0.666	2.320	17.195
19	259	77.2914	0.174	0.018	1.151	1.007	3.223	0.000	7.421	0.440	2.320	17.194
20	37	80.2356	0.167	0.018	1.149	0.988	3.163	0.000	7.420	-0.089	2.328	17.187
21	93	80.2356	0.169	0.018	1.142	0.986	3.154	0.000	7.420	0.668	2.330	16.575
22	229	80.2356	0.167	0.018	1.144	0.986	3.154	0.000	7.420	0.452	2.330	16.573
23	15	80.3692	0.176	0.028	1.152	1.578	5.050	0.002	7.421	-0.775	2.219	16.494
24	71	80.3692	0.184	0.028	1.144	1.574	5.035	0.004	7.422	0.647	2.219	15.838
25	207	80.3692	0.182	0.028	1.146	1.574	5.035	0.004	7.422	0.423	2.219	15.842
26	33	80.5349	0.169	0.020	1.149	1.106	3.540	0.000	7.420	-0.319	2.299	16.977
27	89	80.5349	0.173	0.020	1.140	1.103	3.531	0.000	7.421	0.613	2.301	16.348
28	225	80.5349	0.171	0.020	1.143	1.103	3.531	0.000	7.421	0.396	2.301	16.348
29	28	81.4969	0.169	0.022	1.147	1.207	3.863	0.000	7.420	-0.487	2.279	16.662
30	84	81.4969	0.174	0.022	1.139	1.204	3.853	0.000	7.421	0.575	2.281	16.030
31	220	81.4969	0.172	0.022	1.141	1.204	3.853	0.000	7.421	0.359	2.281	16.031
32	1	82.2802	0.178	0.035	1.145	1.936	6.194	0.008	7.421	-1.366	2.182	16.023
33	57	82.2802	0.189	0.035	1.131	1.931	6.178	0.008	7.422	0.121	2.182	15.412
34	193	82.2802	0.187	0.035	1.134	1.931	6.178	0.009	7.422	-0.100	2.182	15.416
35	7	83.3181	0.177	0.033	1.138	1.811	5.795	0.006	7.421	-1.393	2.194	15.951
36	63	83.3181	0.187	0.033	1.124	1.806	5.780	0.006	7.421	0.020	2.195	15.351
37	199	83.3181	0.185	0.033	1.127	1.806	5.780	0.007	7.421	-0.197	2.195	15.355
38	19	83.4550	0.169	0.026	1.146	1.421	4.549	0.000	7.420	-0.755	2.244	16.067
39	75	83.4550	0.175	0.026	1.139	1.418	4.537	0.000	7.421	0.523	2.244	15.429
40	211	83.4550	0.173	0.026	1.142	1.418	4.537	0.000	7.421	0.311	2.244	15.432

#	srf#	$\bar{q}$	$t_1$	$\Delta_{t_{min}L1}$	$\Delta_t$	$\Delta_{t_{max}L1}$	$\Delta_{t_{max}L2}$	$\frac{\Delta_{q2}}{\Delta_{q1}}$	$\delta_{elev(max)}$	$\delta_{elev(max)}$	$g_{pil(ss)}$	$\alpha_{ss}$
42	81	83.7191	0.173	0.023	1.135	1.298	4.153	0.000	7.420	0.528	2.265	15.507
43	217	83.7191	0.171	0.023	1.138	1.298	4.153	0.000	7.420	0.318	2.265	15.509
44	34	87.3860	0.157	0.019	1.133	1.056	3.379	0.000	7.418	-0.211	2.320	15.682
45	90	87.3860	0.160	0.019	1.125	1.054	3.371	0.000	7.418	0.590	2.322	15.095
46	226	87.3860	0.158	0.019	1.127	1.054	3.371	0.000	7.418	0.395	2.322	15.094
47	127	88.7159	0.168	0.015	1.029	0.825	2.641	0.000	7.416	0.618	2.406	14.778
48	261	88.7159	0.166	0.015	1.032	0.825	2.641	0.000	7.416	0.435	2.406	14.775
49	38	89.3983	0.150	0.017	1.127	0.929	2.973	0.000	7.417	0.142	2.358	15.413
50	94	89.3983	0.178	0.017	1.024	0.927	2.967	0.000	7.417	0.644	2.368	14.692
51	230	89.3983	0.176	0.017	1.027	0.927	2.967	0.000	7.417	0.455	2.368	14.690
52	11	91.6970	0.163	0.029	1.118	1.590	5.088	0.002	7.418	-1.790	2.227	14.904
53	67	91.6970	0.171	0.029	1.110	1.586	5.076	0.005	7.419	-0.449	2.228	14.298
54	203	91.6970	0.168	0.029	1.114	1.586	5.076	0.003	7.419	-0.642	2.228	14.300
55	41	94.3473	0.155	0.014	1.023	0.799	2.557	0.000	7.413	-0.015	2.424	14.393
56	97	94.3473	0.155	0.014	1.019	0.798	2.553	0.000	7.413	0.401	2.425	13.904
57	233	94.3473	0.154	0.014	1.021	0.798	2.553	0.000	7.413	0.233	2.425	13.900
58	262	101.0962	0.123	0.012	1.021	0.681	2.179	0.000	7.407	0.103	2.489	12.825
59	16	102.4478	0.155	0.025	1.068	1.379	4.412	0.000	7.414	-1.030	2.269	13.231
60	72	102.4478	0.163	0.025	1.054	1.376	4.404	0.003	7.415	0.006	2.270	12.676
61	208	102.4478	0.160	0.025	1.058	1.376	4.404	0.003	7.415	-0.163	2.270	12.675
62	263	103.7392	0.130	0.012	0.982	0.672	2.149	0.000	7.406	0.029	2.502	12.856
63	42	106.1299	0.133	0.013	1.001	0.750	2.399	0.000	7.408	-0.377	2.462	12.825
64	98	106.1299	0.136	0.013	0.998	0.749	2.395	0.000	7.408	0.080	2.462	12.683
65	234	106.1299	0.134	0.013	1.000	0.749	2.395	0.000	7.408	-0.064	2.462	12.675
66	264	106.4162	0.125	0.012	0.976	0.662	2.119	0.000	7.404	-0.050	2.511	12.472
67	20	109.0025	0.149	0.022	1.042	1.227	3.925	0.000	7.412	-1.009	2.306	12.503
68	76	109.0025	0.155	0.022	1.030	1.225	3.920	0.001	7.413	-0.174	2.306	11.997
69	212	109.0025	0.153	0.022	1.033	1.225	3.920	0.000	7.413	-0.329	2.306	11.996
70	46	109.1273	0.115	0.012	0.994	0.654	2.094	0.000	7.403	-0.537	2.515	12.710
71	102	109.1273	0.121	0.012	0.970	0.653	2.091	0.000	7.403	0.006	2.520	12.110
72	238	109.1273	0.120	0.012	0.971	0.653	2.091	0.000	7.403	-0.124	2.520	12.098
73	29	110.1905	0.149	0.018	1.012	1.022	3.269	0.000	7.411	-0.682	2.360	12.408
74	85	110.1905	0.153	0.018	1.002	1.020	3.265	0.000	7.411	-0.153	2.361	11.957
75	221	110.1905	0.151	0.018	1.005	1.020	3.265	0.000	7.411	-0.304	2.361	11.955
76	8	110.9265	0.144	0.028	1.079	1.547	4.951	0.001	7.412	-1.992	2.250	12.446
77	64	110.9265	0.153	0.028	1.065	1.544	4.942	0.005	7.413	-0.759	2.250	11.856
78	200	110.9265	0.150	0.028	1.069	1.544	4.942	0.005	7.413	-0.914	2.250	11.856
79	47	111.8726	0.108	0.012	0.998	0.646	2.066	0.000	7.401	-0.811	2.522	12.291
80	103	111.8726	0.113	0.012	0.975	0.645	2.063	0.000	7.401	-0.281	2.527	11.705
81	239	111.8726	0.112	0.012	0.976	0.645	2.063	0.000	7.401	-0.405	2.527	11.693
82	48	114.6519	0.101	0.011	1.000	0.637	2.039	0.000	7.400	-1.048	2.529	11.882

#	srf#	$\bar{q}$	$t_1$	$\Delta t_{minL1}$	$\Delta t$	$\Delta t_{maxL1}$	$\Delta t_{maxL2}$	$\frac{\Delta q_2}{\Delta q_1}$	$\delta_{elev(max)}$	$\delta_{elev(max)}$	$g_{pil(ss)}$	$\alpha_{ss}$
83	104	114.6519	0.106	0.011	0.978	0.636	2.036	0.000	7.400	-0.531	2.535	11.308
84	240	114.6519	0.104	0.011	0.980	0.636	2.036	0.000	7.399	-0.651	2.534	11.296
85	49	117.4653	0.095	0.011	1.001	0.629	2.012	0.000	7.398	-1.252	2.535	11.483
86	105	117.4653	0.099	0.011	0.980	0.628	2.009	0.000	7.398	-0.750	2.542	10.919
87	241	117.4653	0.097	0.011	0.982	0.628	2.009	0.000	7.397	-0.864	2.541	10.906
88	50	120.3129	0.089	0.011	1.000	0.621	1.986	0.000	7.396	-1.427	2.542	11.091
89	106	120.3129	0.092	0.011	0.980	0.620	1.984	0.000	7.396	-0.940	2.549	10.536
90	242	120.3129	0.091	0.011	0.982	0.620	1.984	0.000	7.395	-1.050	2.548	10.523
91	43	121.8328	0.108	0.013	0.982	0.696	2.227	0.000	7.400	-0.689	2.507	11.321
92	99	121.8328	0.113	0.013	0.962	0.695	2.224	0.000	7.400	-0.284	2.510	10.787
93	235	121.8328	0.112	0.013	0.964	0.695	2.224	0.000	7.400	-0.402	2.510	10.780
94	51	123.1945	0.083	0.011	0.999	0.613	1.961	0.000	7.394	-1.575	2.549	10.708
95	107	123.1945	0.103	0.011	0.903	0.612	1.959	0.000	7.394	-1.138	2.567	9.668
96	243	123.1945	0.101	0.011	0.906	0.612	1.959	0.000	7.394	-1.244	2.567	9.661
97	52	126.1103	0.094	0.011	0.922	0.605	1.937	0.000	7.392	-1.713	2.575	9.866
98	108	126.1103	0.099	0.011	0.896	0.605	1.935	0.000	7.392	-1.330	2.576	9.427
99	244	126.1103	0.098	0.011	0.898	0.605	1.935	0.000	7.392	-1.432	2.576	9.420
100	53	129.0601	0.091	0.011	0.915	0.598	1.914	0.000	7.390	-1.882	2.583	9.625
101	109	129.0601	0.096	0.011	0.889	0.598	1.912	0.000	7.390	-1.525	2.584	9.179
102	245	129.0601	0.095	0.011	0.891	0.598	1.912	0.000	7.390	-1.624	2.584	9.172
103	2	129.4213	0.125	0.027	1.079	1.512	4.840	0.000	7.408	-2.037	2.270	10.750
104	58	129.4213	0.134	0.027	1.068	1.510	4.832	0.003	7.409	-0.870	2.270	10.190
105	194	129.4213	0.132	0.027	1.071	1.510	4.832	0.003	7.409	-1.003	2.270	10.189
106	17	129.8252	0.126	0.022	1.045	1.214	3.886	0.000	7.407	-1.290	2.328	10.668
107	73	129.8252	0.132	0.022	1.037	1.213	3.881	0.000	7.408	-0.485	2.328	10.168
108	209	129.8252	0.131	0.022	1.039	1.213	3.881	0.000	7.408	-0.615	2.328	10.167
109	30	129.9582	0.124	0.017	1.017	0.936	2.994	0.000	7.405	-0.754	2.409	10.710
110	86	129.9582	0.127	0.017	1.009	0.935	2.991	0.000	7.406	-0.373	2.409	10.269
111	222	129.9582	0.125	0.017	1.012	0.935	2.991	0.000	7.406	-0.498	2.409	10.266
112	26	130.0074	0.125	0.018	1.026	1.024	3.276	0.000	7.406	-0.970	2.379	10.699
113	82	130.0074	0.129	0.018	1.018	1.023	3.273	0.000	7.407	-0.430	2.380	10.236
114	218	130.0074	0.127	0.018	1.021	1.023	3.273	0.000	7.407	-0.557	2.380	10.234
115	35	130.0653	0.121	0.015	1.006	0.851	2.723	0.000	7.404	-0.547	2.442	10.685
116	91	130.0653	0.124	0.015	0.997	0.850	2.721	0.000	7.405	-0.306	2.442	10.268
117	227	130.0653	0.122	0.015	1.000	0.850	2.721	0.000	7.404	-0.429	2.442	10.265
118	21	130.1006	0.125	0.020	1.036	1.116	3.572	0.000	7.406	-1.148	2.353	10.670
119	77	130.1006	0.131	0.020	1.027	1.115	3.567	0.000	7.407	-0.467	2.353	10.187
120	213	130.1006	0.129	0.020	1.030	1.115	3.567	0.000	7.407	-0.595	2.353	10.185
121	44	131.7744	0.100	0.012	0.934	0.668	2.136	0.000	7.395	-0.823	2.539	9.571
122	100	131.7744	0.108	0.012	0.907	0.667	2.135	0.000	7.395	-0.470	2.539	9.186
123	236	131.7744	0.106	0.012	0.910	0.667	2.135	0.000	7.395	-0.576	2.539	9.182

#	srf#	$\bar{q}$	$t_1$	$\Delta t_{minL1}$	$\Delta t$	$\Delta t_{maxL1}$	$\Delta t_{maxL2}$	$\frac{\Delta q_2}{\Delta q_1}$	$\delta_{elev(max)}$	$\delta_{elev(max)}$	$g_{pil(ss)}$	$\alpha_{ss}$
124	54	132.0441	0.088	0.011	0.908	0.591	1.891	0.000	7.388	-2.053	2.592	9.375
125	110	132.0441	0.093	0.011	0.882	0.590	1.889	0.000	7.388	-1.722	2.593	8.923
126	246	132.0441	0.091	0.011	0.885	0.590	1.889	0.000	7.388	-1.818	2.593	8.916
127	39	134.8266	0.105	0.013	0.976	0.744	2.381	0.000	7.398	-0.763	2.496	10.173
128	95	134.8266	0.118	0.013	0.920	0.744	2.379	0.000	7.398	-0.479	2.498	9.145
129	231	134.8266	0.116	0.013	0.923	0.743	2.379	0.000	7.398	-0.589	2.498	9.143
130	55	135.0621	0.085	0.011	0.901	0.584	1.869	0.000	7.387	-2.228	2.600	9.117
131	111	135.0621	0.090	0.011	0.876	0.584	1.867	0.000	7.386	-1.922	2.601	8.660
132	247	135.0621	0.089	0.011	0.877	0.584	1.867	0.000	7.386	-2.015	2.601	8.653
133	56	138.1142	0.082	0.010	0.894	0.577	1.847	0.000	7.385	-2.407	2.608	8.853
134	112	138.1142	0.087	0.010	0.869	0.577	1.846	0.000	7.384	-2.125	2.609	8.389
135	248	138.1142	0.086	0.010	0.871	0.577	1.846	0.000	7.384	-2.215	2.609	8.382
136	45	167.7286	0.069	0.011	0.866	0.589	1.885	0.000	7.374	-2.413	2.626	7.292
137	101	167.7286	0.053	0.011	0.942	0.589	1.884	0.000	7.374	-2.171	2.625	6.539
138	237	167.7286	0.052	0.011	0.944	0.589	1.884	0.000	7.374	-2.244	2.625	6.535
139	22	170.3164	0.112	0.017	0.942	0.970	3.105	0.006	7.395	-1.330	2.434	7.916
140	78	170.3164	0.116	0.017	0.930	0.970	3.103	0.007	7.396	-0.950	2.434	7.600
141	214	170.3164	0.114	0.017	0.934	0.970	3.103	0.007	7.396	-1.045	2.434	7.600
142	40	208.2658	0.044	0.011	0.886	0.595	1.904	0.000	7.359	-2.168	2.652	5.737
143	96	208.2658	0.045	0.011	0.887	0.595	1.904	0.000	7.360	-1.957	2.653	5.463
144	232	208.2658	0.045	0.011	0.884	0.595	1.904	0.000	7.360	-2.015	2.653	5.460
145	31	215.9733	0.056	0.013	0.944	0.720	2.305	0.000	7.372	-1.413	2.581	6.348
146	87	215.9733	0.060	0.013	0.929	0.720	2.304	0.000	7.373	-1.244	2.581	6.085
147	223	215.9733	0.058	0.013	0.933	0.720	2.304	0.000	7.372	-1.309	2.581	6.084
148	126	222.8766	0.044	0.010	0.842	0.575	1.839	0.000	7.352	-2.174	2.677	4.901
149	260	222.8766	0.044	0.010	0.839	0.575	1.839	0.000	7.351	-2.227	2.677	4.899
150	3	228.5562	0.069	0.020	1.038	1.127	3.607	0.006	7.383	-2.048	2.431	6.107
151	59	228.5562	0.073	0.020	1.029	1.127	3.606	0.005	7.385	-1.389	2.431	5.794
152	195	228.5562	0.072	0.020	1.032	1.127	3.606	0.006	7.385	-1.460	2.431	5.794
153	12	254.7139	0.060	0.017	0.982	0.931	2.978	0.000	7.374	-1.753	2.514	5.609
154	68	254.7139	0.063	0.017	0.973	0.930	2.977	0.002	7.375	-1.385	2.514	5.346
155	204	254.7139	0.062	0.017	0.976	0.930	2.977	0.001	7.375	-1.446	2.514	5.346
156	36	264.5698	0.043	0.011	0.786	0.591	1.892	0.000	7.338	-1.989	2.691	4.658
157	92	264.5698	0.043	0.011	0.790	0.591	1.892	0.000	7.340	-1.858	2.691	4.416
158	228	264.5698	0.043	0.011	0.787	0.591	1.892	0.000	7.339	-1.904	2.691	4.414
159	32	333.6127	0.041	0.010	0.696	0.578	1.850	0.000	7.312	-1.876	2.734	3.826
160	88	333.6127	0.041	0.010	0.700	0.578	1.850	0.000	7.314	-1.851	2.734	3.614
161	224	333.6127	0.041	0.010	0.698	0.578	1.850	0.000	7.314	-1.888	2.734	3.612
162	23	333.8201	0.042	0.012	0.804	0.690	2.207	0.000	7.335	-1.382	2.669	4.395
163	79	333.8201	0.042	0.012	0.805	0.690	2.207	0.002	7.337	-1.322	2.669	4.180
164	215	333.8201	0.042	0.012	0.802	0.690	2.207	0.002	7.336	-1.363	2.669	4.179

#	srf#	$\bar{q}$	$t_1$	$\Delta t_{minL1}$	$\Delta t$	$\Delta t_{maxL1}$	$\Delta t_{maxL2}$	$\frac{\Delta g_2}{\Delta g_1}$	$\delta_{elev(max)}$	$\delta_{elev(max)}$	$g_{pil(ss)}$	$\alpha_{ss}$
165	123	357.0172	0.040	0.010	0.662	0.559	1.788	0.000	7.301	-2.179	2.756	3.328
166	257	357.0172	0.040	0.010	0.659	0.559	1.788	0.000	7.301	-2.213	2.756	3.326
167	27	416.6143	0.039	0.010	0.618	0.566	1.811	0.000	7.280	-1.899	2.773	3.225
168	83	416.6143	0.039	0.010	0.621	0.566	1.810	0.000	7.283	-1.913	2.773	3.021
169	219	416.6143	0.039	0.010	0.619	0.566	1.810	0.000	7.282	-1.943	2.773	3.020
170	13	499.2391	0.039	0.012	0.653	0.663	2.122	0.000	7.285	-1.376	2.747	3.157
171	69	499.2391	0.039	0.012	0.654	0.663	2.122	0.000	7.287	-1.365	2.747	2.961
172	205	499.2391	0.039	0.012	0.652	0.663	2.122	0.000	7.286	-1.393	2.747	2.961
173	24	503.8640	0.038	0.010	0.557	0.561	1.794	0.000	7.259	-1.817	2.801	2.785
174	80	503.8640	0.038	0.010	0.561	0.561	1.794	0.000	7.260	-1.866	2.801	2.595
175	216	503.8640	0.038	0.010	0.559	0.561	1.794	0.000	7.260	-1.890	2.801	2.594
176	4	514.2514	0.039	0.013	0.716	0.749	2.398	0.000	7.301	-1.495	2.713	3.200
177	60	514.2514	0.039	0.013	0.716	0.749	2.397	0.000	7.303	-1.420	2.713	3.013
178	196	514.2514	0.039	0.013	0.713	0.749	2.397	0.000	7.302	-1.449	2.713	3.013
179	120	551.8250	0.037	0.010	0.514	0.536	1.714	0.000	7.251	-2.251	2.826	2.308
180	254	551.8250	0.037	0.010	0.512	0.536	1.714	0.000	7.251	-2.273	2.826	2.307
181	18	618.5337	0.036	0.010	0.493	0.550	1.760	0.000	7.244	-1.833	2.833	2.358
182	74	618.5337	0.036	0.010	0.496	0.550	1.759	0.000	7.246	-1.910	2.833	2.179
183	210	618.5337	0.036	0.010	0.494	0.550	1.759	0.000	7.246	-1.930	2.833	2.178
184	5	699.9532	0.036	0.012	0.540	0.642	2.054	0.000	7.250	-1.456	2.806	2.388
185	61	699.9532	0.037	0.012	0.539	0.642	2.054	0.000	7.252	-1.512	2.806	2.219
186	197	699.9532	0.036	0.012	0.538	0.642	2.054	0.000	7.251	-1.531	2.806	2.219
187	14	771.1717	0.035	0.010	0.421	0.533	1.707	0.000	7.223	-2.309	2.865	2.010
188	70	771.1717	0.035	0.010	0.425	0.533	1.707	0.000	7.226	-2.405	2.865	1.844
189	206	771.1717	0.035	0.010	0.423	0.533	1.707	0.000	7.225	-2.421	2.865	1.843
190	117	825.2729	0.034	0.009	0.395	0.516	1.650	0.000	7.215	-2.686	2.879	1.701
191	252	825.2729	0.034	0.009	0.393	0.516	1.650	0.000	7.215	-2.701	2.879	1.700
192	9	954.4603	0.033	0.009	0.362	0.518	1.657	0.000	7.198	-2.457	2.891	1.725
193	65	954.4603	0.034	0.009	0.364	0.518	1.657	0.000	7.201	-2.567	2.891	1.564
194	201	954.4603	0.034	0.009	0.363	0.518	1.657	0.000	7.201	-2.580	2.891	1.563
195	6	1106.2120	0.032	0.009	0.328	0.511	1.634	0.000	7.178	-2.498	2.906	1.569
196	62	1106.2120	0.033	0.009	0.329	0.511	1.634	0.000	7.182	-2.621	2.906	1.410
197	198	1106.2120	0.033	0.009	0.328	0.511	1.634	0.000	7.181	-2.632	2.906	1.409
198	114	1157.0650	0.032	0.009	0.313	0.499	1.597	0.000	7.172	-2.802	2.913	1.347
199	249	1157.0650	0.032	0.009	0.312	0.499	1.597	0.000	7.171	-2.812	2.913	1.346

C.3 Longitudinal Maximum  $C_{cmd}$  Step Input Time Response (Healthy)

#	srf#	$\bar{q}$	$\delta_{elev(max)}$	$\delta_{elev(max)}$	$g_{pil_{max}}$	$\alpha_{max}$
1	119	65.4696	38.786	2.348	3.030	32.195
2	253	65.4696	38.889	2.324	3.030	32.223
3	118	65.5666	38.787	2.393	2.956	31.228
4	122	67.0399	38.885	2.861	3.229	34.202
5	256	67.0399	38.883	2.595	3.228	34.199
6	121	67.4267	38.885	2.974	3.142	32.943
7	255	67.4267	38.884	2.708	3.141	32.946
8	124	67.6717	38.882	2.872	3.339	35.473
9	116	68.8746	38.886	3.108	2.928	29.624
10	251	68.8746	38.885	2.837	2.927	29.633
11	115	70.9929	38.884	3.060	2.887	28.367
12	10	74.2746	38.867	1.090	2.987	29.458
13	66	74.2746	38.877	2.815	2.991	28.544
14	202	74.2746	38.875	2.563	2.991	28.550
15	113	75.5664	38.876	2.880	2.886	26.879
16	250	77.0323	38.872	2.512	2.953	27.236
17	258	77.2143	38.861	2.455	3.499	35.166
18	125	77.2914	38.859	2.673	3.635	37.464
19	259	77.2914	38.857	2.440	3.633	37.441
20	37	80.2356	38.849	1.876	3.674	37.808
21	93	80.2356	38.850	2.633	3.688	36.964
22	229	80.2356	38.848	2.410	3.686	36.938
23	15	80.3692	38.855	1.260	3.143	29.460
24	71	80.3692	38.861	2.712	3.148	28.535
25	207	80.3692	38.860	2.482	3.148	28.543
26	33	80.5349	38.850	1.657	3.543	35.516
27	89	80.5349	38.852	2.597	3.555	34.632
28	225	80.5349	38.851	2.374	3.553	34.620
29	28	81.4969	38.849	1.492	3.448	33.569
30	84	81.4969	38.852	2.567	3.457	32.682
31	220	81.4969	38.851	2.345	3.456	32.675
32	1	82.2802	38.853	0.685	2.954	26.362
33	57	82.2802	38.860	2.210	2.957	25.459
34	193	82.2802	38.859	1.983	2.957	25.470
35	7	83.3181	38.849	0.632	3.020	26.929
36	63	83.3181	38.857	2.081	3.023	26.030
37	199	83.3181	38.855	1.857	3.023	26.041
38	19	83.4550	38.846	1.229	3.272	30.259
39	75	83.4550	38.851	2.531	3.277	29.351
40	211	83.4550	38.849	2.312	3.277	29.356
41	25	83.7192	38.844	1.324	3.374	31.647

#	srf#	$\bar{q}$	$\delta_{elev(max)}$	$\delta_{elev(max)}$	$g_{pitmax}$	$\alpha_{max}$
42	81	83.7192	38.848	2.513	3.382	30.730
43	217	83.7192	38.847	2.296	3.381	30.729
44	34	87.3860	38.830	1.683	3.655	34.422
45	90	87.3860	38.832	2.490	3.665	33.582
46	226	87.3860	38.830	2.288	3.664	33.565
47	127	88.7159	38.812	2.407	4.084	36.088
48	261	88.7159	38.811	2.218	4.082	36.063
49	38	89.3983	38.822	1.998	3.834	36.415
50	94	89.3983	38.822	2.480	3.906	34.266
51	230	89.3983	38.821	2.285	3.905	34.248
52	11	91.6970	38.826	0.131	3.191	26.806
53	67	91.6970	38.833	1.502	3.194	25.947
54	203	91.6970	38.832	1.303	3.194	25.953
55	41	94.3473	38.791	1.710	4.180	35.844
56	97	94.3473	38.792	2.125	4.189	35.005
57	233	94.3473	38.790	1.951	4.187	34.977
58	262	101.0962	38.741	1.687	4.507	35.655
59	16	102.4478	38.796	0.773	3.411	26.676
60	72	102.4478	38.803	1.829	3.415	25.771
61	208	102.4478	38.801	1.655	3.415	25.768
62	263	103.7392	38.729	1.605	4.540	39.257
63	42	106.1299	38.746	1.233	4.391	33.896
64	98	106.1299	38.748	1.694	4.368	36.489
65	234	106.1299	38.746	1.545	4.366	36.446
66	264	106.4162	38.717	1.530	4.591	38.802
67	20	109.0025	38.777	0.730	3.602	26.773
68	76	109.0025	38.783	1.581	3.605	25.917
69	212	109.0025	38.782	1.420	3.605	25.913
70	46	109.1273	38.704	1.043	4.605	39.470
71	102	109.1273	38.707	1.590	4.645	38.402
72	238	109.1273	38.705	1.460	4.642	38.341
73	29	110.1905	38.770	1.019	3.885	28.810
74	85	110.1905	38.773	1.555	3.889	27.999
75	221	110.1905	38.772	1.398	3.889	27.991
76	8	110.9265	38.777	-0.217	3.309	24.275
77	64	110.9265	38.786	1.041	3.312	23.330
78	200	110.9265	38.785	0.881	3.312	23.327
79	47	111.8726	38.692	0.772	4.647	38.745
80	103	111.8726	38.694	1.306	4.686	37.721
81	239	111.8726	38.692	1.181	4.683	37.657
82	48	114.6519	38.679	0.537	4.688	38.050

#	srf#	$\bar{q}$	$\delta_{elev(max)}$	$\delta_{elev(max)}$	$g_{pil,max}$	$\alpha_{max}$
83	104	114.6519	38.679	1.057	4.728	37.062
84	240	114.6519	38.677	0.938	4.725	37.000
85	49	117.4653	38.666	0.334	4.730	37.388
86	105	117.4653	38.664	0.841	4.769	36.434
87	241	117.4653	38.662	0.727	4.766	36.372
88	50	120.3129	38.651	0.163	4.772	36.756
89	106	120.3129	38.648	0.654	4.811	35.831
90	242	120.3129	38.646	0.545	4.808	35.769
91	43	121.8328	38.682	0.895	4.612	35.430
92	99	121.8328	38.686	1.304	4.635	34.422
93	235	121.8328	38.684	1.185	4.633	34.383
94	51	123.1945	38.635	0.018	4.814	36.154
95	107	123.1945	38.634	0.468	4.963	29.833
96	243	123.1945	38.631	0.362	4.962	29.802
97	52	126.1103	38.620	-0.107	4.994	30.624
98	108	126.1103	38.619	0.279	5.008	29.719
99	244	126.1103	38.617	0.177	5.007	29.688
100	53	129.0601	38.606	-0.272	5.040	30.510
101	109	129.0601	38.605	0.087	5.054	29.584
102	245	129.0601	38.602	-0.012	5.053	29.555
103	2	129.4213	38.737	-0.344	3.418	22.531
104	58	129.4213	38.752	0.857	3.420	21.803
105	194	129.4213	38.750	0.719	3.420	21.794
106	17	129.8252	38.733	0.361	3.719	25.104
107	73	129.8252	38.743	1.189	3.721	24.346
108	209	129.8252	38.741	1.054	3.721	24.334
109	30	129.9582	38.726	0.859	4.137	28.636
110	86	129.9582	38.730	1.247	4.141	27.898
111	222	129.9582	38.728	1.116	4.141	27.881
112	26	130.0074	38.728	0.655	3.985	27.342
113	82	130.0074	38.735	1.208	3.989	26.594
114	218	130.0074	38.733	1.075	3.989	26.580
115	35	130.0653	38.718	1.044	4.305	30.097
116	91	130.0653	38.721	1.287	4.311	29.364
117	227	130.0653	38.719	1.158	4.310	29.344
118	21	130.1006	38.730	0.489	3.848	26.152
119	77	130.1006	38.739	1.188	3.851	25.396
120	213	130.1006	38.737	1.054	3.851	25.385
121	44	131.7744	38.639	0.776	4.822	27.071
122	100	131.7744	38.644	1.132	4.829	26.239
123	236	131.7744	38.642	1.026	4.828	26.218

#	srf#	$\bar{q}$	$\delta_{elev(max)}$	$\delta_{elev(max)}$	$g_{pil,max}$	$\alpha_{max}$
124	54	132.0441	38.592	-0.442	5.086	30.373
125	110	132.0441	38.590	-0.108	5.099	29.429
126	246	132.0441	38.588	-0.204	5.098	29.399
127	39	134.8266	38.668	0.822	4.583	31.763
128	95	134.8266	38.671	1.114	4.616	24.882
129	231	134.8266	38.669	1.004	4.616	24.869
130	55	135.0621	38.577	-0.615	5.131	30.214
131	111	135.0621	38.576	-0.306	5.144	29.247
132	247	135.0621	38.573	-0.399	5.143	29.217
133	56	138.1142	38.562	-0.791	5.176	30.032
134	112	138.1142	38.561	-0.507	5.188	29.042
135	248	138.1142	38.558	-0.598	5.187	29.011
136	45	167.7286	49.207	-0.223	6.200	30.683
137	101	167.7286	49.212	0.013	6.197	24.225
138	237	167.7286	49.208	-0.061	6.197	24.206
139	22	170.3164	50.422	0.902	4.975	24.058
140	78	170.3164	50.431	1.285	4.977	23.377
141	214	170.3164	50.428	1.189	4.977	23.371
142	40	208.2658	60.000	0.832	7.776	26.903
143	96	208.2658	60.000	1.047	7.778	26.042
144	232	208.2658	60.000	0.986	7.778	26.023
145	31	215.9733	60.000	1.779	7.381	28.892
146	87	215.9733	60.000	1.953	7.383	28.083
147	223	215.9733	60.000	1.886	7.383	28.075
148	126	222.8766	60.000	1.119	8.514	25.296
149	260	222.8766	60.000	1.063	8.514	25.275
150	3	228.5562	60.000	1.412	6.272	24.770
151	59	228.5562	60.000	2.080	6.274	24.027
152	195	228.5562	60.000	2.007	6.274	24.022
153	12	254.7139	60.000	1.745	7.138	25.258
154	68	254.7139	60.000	2.119	7.139	24.556
155	204	254.7139	60.000	2.055	7.139	24.550
156	36	264.5698	60.000	1.418	8.907	24.881
157	92	264.5698	60.000	1.556	8.908	24.083
158	228	264.5698	60.000	1.507	8.908	24.065
159	32	333.6127	60.000	1.465	9.338	20.975
160	88	333.6127	60.000	1.500	9.338	20.295
161	224	333.6127	60.000	1.460	9.338	20.280
162	23	333.8201	60.000	2.034	8.692	23.212
163	79	333.8201	60.000	2.100	8.692	22.549
164	215	333.8201	60.000	2.056	8.692	22.540

#	srf#	$\bar{q}$	$\delta_{elev(max)}$	$\delta_{elev(max)}$	$g_{pilmax}$	$\alpha_{max}$
165	123	357.0172	60.000	1.138	9.559	19.142
166	257	357.0172	60.000	1.101	9.559	19.128
167	27	416.6143	60.000	1.374	9.730	18.401
168	83	416.6143	60.000	1.368	9.730	17.765
169	219	416.6143	60.000	1.336	9.730	17.752
170	13	499.2391	60.000	1.924	9.474	18.178
171	69	499.2391	60.000	1.941	9.474	17.602
172	205	499.2391	60.000	1.911	9.474	17.594
173	24	503.8640	60.000	1.408	10.014	16.158
174	80	503.8640	60.000	1.368	10.014	15.587
175	216	503.8640	60.000	1.341	10.014	15.576
176	4	514.2514	60.000	1.855	9.131	17.932
177	60	514.2514	60.000	1.934	9.131	17.439
178	196	514.2514	60.000	1.903	9.131	17.433
179	120	551.8250	60.000	0.936	10.264	13.722
180	254	551.8250	60.000	0.912	10.264	13.711
181	18	618.5337	60.000	1.320	10.326	13.819
182	74	618.5337	60.000	1.256	10.326	13.315
183	210	618.5337	60.000	1.233	10.326	13.306
184	5	699.9532	60.000	1.744	10.059	14.277
185	61	699.9532	60.000	1.696	10.060	13.794
186	197	699.9532	60.000	1.673	10.060	13.788
187	14	771.1717	60.000	0.746	10.646	11.383
188	70	771.1717	60.000	0.666	10.646	10.952
189	206	771.1717	60.000	0.646	10.646	10.944
190	117	825.2729	60.000	0.333	10.791	9.910
191	252	825.2729	60.000	0.315	10.791	9.902
192	9	954.4603	60.000	0.495	10.913	9.584
193	65	954.4603	60.000	0.399	10.913	9.201
194	201	954.4603	60.000	0.384	10.913	9.194
195	6	1106.2120	60.000	0.391	11.061	8.603
196	62	1106.2120	60.000	0.285	11.061	8.245
197	198	1106.2120	60.000	0.271	11.061	8.239
198	114	1157.0650	60.000	0.071	11.134	7.716
199	249	1157.0650	60.000	0.057	11.134	7.710

C.4 Longitudinal Maximum  $C^*_{cmd}$  Step Input Time Response (25% Stabilator Failure)

#	srf#	$\bar{q}$	$\dot{\delta}_{elev(max)}$	$\delta_{elev(max)}$	$g_{pil_{max}}$	$\alpha_{max}$
1	119	65.4696	38.924	2.590	3.036	25.921
2	253	65.4696	38.982	2.324	3.039	25.997
3	118	65.5666	38.925	2.643	2.960	25.364
4	122	67.0399	38.979	2.861	3.243	26.903
5	256	67.0399	38.978	2.595	3.243	26.907
6	121	67.4267	38.979	2.974	3.152	26.152
7	255	67.4267	38.978	2.708	3.151	26.160
8	124	67.6717	38.977	2.957	3.361	27.546
9	116	68.8746	38.980	3.308	2.931	24.114
10	251	68.8746	38.979	3.043	2.930	24.126
11	115	70.9929	38.979	3.714	2.888	23.196
12	10	74.2746	38.969	1.907	2.990	23.829
13	66	74.2746	38.974	4.168	2.994	23.025
14	202	74.2746	38.974	3.922	2.994	23.036
15	113	75.5664	38.974	4.459	2.887	21.960
16	250	77.0323	38.971	4.126	2.954	22.066
17	258	77.2143	38.964	3.923	3.527	26.377
18	125	77.2914	38.962	4.124	3.681	27.632
19	259	77.2914	38.961	3.889	3.679	27.622
20	37	80.2356	38.956	3.294	3.721	27.805
21	93	80.2356	38.957	4.044	3.733	27.069
22	229	80.2356	38.956	3.819	3.731	27.058
23	15	80.3692	38.962	2.728	3.147	23.164
24	71	80.3692	38.965	4.188	3.151	22.346
25	207	80.3692	38.964	3.956	3.151	22.359
26	33	80.5349	38.957	3.088	3.572	26.545
27	89	80.5349	38.958	4.024	3.582	25.772
28	225	80.5349	38.958	3.799	3.581	25.770
29	28	81.4969	38.957	2.923	3.466	25.391
30	84	81.4969	38.959	3.998	3.474	24.610
31	220	81.4969	38.958	3.774	3.473	24.613
32	1	82.2802	38.961	2.134	2.954	21.300
33	57	82.2802	38.965	3.668	2.956	20.511
34	193	82.2802	38.964	3.439	2.957	20.524
35	7	83.3181	38.959	2.066	3.021	21.559
36	63	83.3181	38.963	3.522	3.023	20.776
37	199	83.3181	38.962	3.297	3.023	20.790
38	19	83.4550	38.956	2.658	3.279	23.387
39	75	83.4550	38.959	3.966	3.283	22.587
40	211	83.4550	38.958	3.745	3.283	22.598
41	25	83.7191	38.954	2.741	3.385	24.145

#	srf#	$\bar{q}$	$\delta_{elev(max)}$	$\delta_{elev(max)}$	$g_{pl_{max}}$	$\alpha_{max}$
42	81	83.7191	38.957	3.931	3.392	23.344
43	217	83.7191	38.956	3.712	3.391	23.351
44	34	87.3860	38.945	3.031	3.682	25.348
45	90	87.3860	38.946	3.834	3.691	24.619
46	226	87.3860	38.945	3.629	3.690	24.615
47	127	88.7159	38.933	3.593	4.130	25.626
48	261	88.7159	38.932	3.402	4.129	25.618
49	38	89.3983	38.939	3.302	3.879	26.209
50	94	89.3983	38.940	3.704	3.932	24.607
51	230	89.3983	38.939	3.507	3.932	24.605
52	11	91.6970	38.945	1.476	3.192	20.995
53	67	91.6970	38.948	2.858	3.195	20.240
54	203	91.6970	38.948	2.657	3.195	20.250
55	41	94.3473	38.920	2.833	4.226	25.318
56	97	94.3473	38.920	3.245	4.231	24.646
57	233	94.3473	38.919	3.068	4.230	24.635
58	262	101.0962	38.887	2.676	4.569	24.474
59	16	102.4478	38.926	1.992	3.413	20.064
60	72	102.4478	38.930	3.051	3.416	19.299
61	208	102.4478	38.929	2.875	3.416	19.303
62	263	103.7392	38.880	2.523	4.633	26.200
63	42	106.1299	38.891	2.230	4.427	23.554
64	98	106.1299	38.892	2.688	4.425	24.735
65	234	106.1299	38.891	2.536	4.424	24.714
66	264	106.4162	38.872	2.391	4.681	25.768
67	20	109.0025	38.914	1.877	3.604	19.744
68	76	109.0025	38.917	2.729	3.606	19.031
69	212	109.0025	38.916	2.566	3.606	19.035
70	46	109.1273	38.864	1.869	4.703	26.233
71	102	109.1273	38.866	2.402	4.730	25.371
72	238	109.1273	38.864	2.265	4.728	25.337
73	29	110.1905	38.908	2.109	3.891	20.707
74	85	110.1905	38.910	2.643	3.894	20.050
75	221	110.1905	38.909	2.485	3.894	20.052
76	8	110.9265	38.915	0.973	3.310	18.464
77	64	110.9265	38.920	2.235	3.312	17.663
78	200	110.9265	38.919	2.073	3.312	17.667
79	47	111.8726	38.856	1.554	4.739	25.660
80	103	111.8726	38.857	2.068	4.768	24.837
81	239	111.8726	38.856	1.937	4.766	24.801
82	48	114.6519	38.848	1.275	4.775	25.104

#	srf#	$\bar{q}$	$\delta_{elev(max)}$	$\delta_{elev(max)}$	$g_{pit_{max}}$	$\alpha_{max}$
83	104	114.6519	38.848	1.769	4.806	24.313
84	240	114.6519	38.846	1.643	4.804	24.277
85	49	117.4653	38.839	1.026	4.811	24.568
86	105	117.4653	38.838	1.501	4.844	23.804
87	241	117.4653	38.836	1.381	4.841	23.769
88	50	120.3129	38.829	0.805	4.847	24.050
89	106	120.3129	38.827	1.261	4.881	23.311
90	242	120.3129	38.826	1.145	4.878	23.274
91	43	121.8328	38.850	1.653	4.663	23.511
92	99	121.8328	38.852	2.052	4.678	22.698
93	235	121.8328	38.850	1.927	4.677	22.679
94	51	123.1945	38.819	0.608	4.882	23.552
95	107	123.1945	38.818	0.984	4.978	19.843
96	243	123.1945	38.816	0.873	4.978	19.831
97	52	126.1103	38.808	0.384	5.016	20.387
98	108	126.1103	38.808	0.749	5.023	19.652
99	244	126.1103	38.807	0.641	5.023	19.639
100	53	129.0601	38.799	0.175	5.061	20.196
101	109	129.0601	38.798	0.514	5.067	19.447
102	245	129.0601	38.797	0.409	5.067	19.434
103	2	129.4213	38.891	0.759	3.418	16.762
104	58	129.4213	38.899	1.968	3.420	16.081
105	194	129.4213	38.898	1.828	3.420	16.081
106	17	129.8252	38.886	1.410	3.721	18.012
107	73	129.8252	38.892	2.245	3.723	17.351
108	209	129.8252	38.891	2.108	3.723	17.351
109	30	129.9582	38.879	1.840	4.146	19.818
110	86	129.9582	38.881	2.227	4.149	19.202
111	222	129.9582	38.880	2.094	4.148	19.199
112	26	130.0074	38.881	1.661	3.991	19.161
113	82	130.0074	38.885	2.216	3.994	18.525
114	218	130.0074	38.884	2.081	3.993	18.525
115	35	130.0653	38.873	1.989	4.319	20.535
116	91	130.0653	38.875	2.228	4.323	19.936
117	227	130.0653	38.873	2.097	4.322	19.931
118	21	130.1006	38.884	1.517	3.851	18.544
119	77	130.1006	38.889	2.220	3.854	17.893
120	213	130.1006	38.888	2.085	3.854	17.893
121	44	131.7744	38.821	1.356	4.829	18.476
122	100	131.7744	38.824	1.704	4.832	17.803
123	236	131.7744	38.823	1.592	4.832	17.797

#	srf#	$\bar{q}$	$\delta_{elev(max)}$	$\delta_{elev(max)}$	$g_{pil,max}$	$\alpha_{max}$
124	54	132.0441	38.789	-0.036	5.106	19.989
125	110	132.0441	38.788	0.278	5.111	19.228
126	246	132.0441	38.787	0.177	5.111	19.215
127	39	134.8266	38.840	1.549	4.606	21.099
128	95	134.8266	38.842	1.804	4.617	17.085
129	231	134.8266	38.841	1.689	4.617	17.084
130	55	135.0621	38.779	-0.248	5.150	19.768
131	111	135.0621	38.778	0.042	5.154	18.992
132	247	135.0621	38.777	-0.057	5.154	18.979
133	56	138.1142	38.769	-0.461	5.193	19.533
134	112	138.1142	38.768	-0.195	5.197	18.742
135	248	138.1142	38.767	-0.291	5.197	18.728
136	45	167.7286	49.503	0.004	6.202	19.367
137	101	167.7286	49.507	0.287	6.195	15.983
138	237	167.7286	49.504	0.208	6.194	15.978
139	22	170.3164	50.659	1.823	4.975	16.270
140	78	170.3164	50.664	2.209	4.975	15.738
141	214	170.3164	50.662	2.106	4.976	15.743
142	40	208.2658	60.000	1.027	7.773	17.328
143	96	208.2658	60.000	1.242	7.777	16.673
144	232	208.2658	60.000	1.181	7.777	16.672
145	31	215.9733	60.000	2.203	7.381	18.575
146	87	215.9733	60.000	2.368	7.383	17.954
147	223	215.9733	60.000	2.293	7.383	17.962
148	126	222.8766	60.000	1.316	8.513	16.129
149	260	222.8766	60.000	1.260	8.513	16.128
150	3	228.5562	60.000	2.553	6.272	16.301
151	59	228.5562	60.000	3.244	6.274	15.711
152	195	228.5562	60.000	3.165	6.274	15.721
153	12	254.7139	60.000	2.441	7.138	16.299
154	68	254.7139	60.000	2.816	7.139	15.764
155	204	254.7139	60.000	2.745	7.139	15.774
156	36	264.5698	60.000	1.611	8.906	15.821
157	92	264.5698	60.000	1.748	8.908	15.208
158	228	264.5698	60.000	1.700	8.908	15.208
159	32	333.6127	60.000	1.634	9.338	13.294
160	88	333.6127	60.000	1.667	9.338	12.768
161	224	333.6127	60.000	1.627	9.338	12.768
162	23	333.8201	60.000	2.220	8.692	14.619
163	79	333.8201	60.000	2.284	8.692	14.111
164	215	333.8201	60.000	2.241	8.692	14.116

#	srf#	$\bar{q}$	$\delta_{elev(max)}$	$\delta_{elev(max)}$	$g_{pilmax}$	$\alpha_{max}$
165	123	357.0172	60.000	1.304	9.559	12.037
166	257	357.0172	60.000	1.268	9.559	12.038
167	27	416.6143	60.000	1.532	9.730	11.608
168	83	416.6143	60.000	1.526	9.730	11.112
169	219	416.6143	60.000	1.494	9.730	11.113
170	13	499.2391	60.000	2.078	9.474	11.343
171	69	499.2391	60.000	2.093	9.474	10.902
172	205	499.2391	60.000	2.063	9.474	10.906
173	24	503.8640	60.000	1.540	10.014	10.162
174	80	503.8640	60.000	1.499	10.014	9.713
175	216	503.8640	60.000	1.472	10.014	9.714
176	4	514.2514	60.000	2.004	9.131	11.218
177	60	514.2514	60.000	2.082	9.131	10.851
178	196	514.2514	60.000	2.051	9.131	10.857
179	120	551.8250	60.000	1.052	10.264	8.591
180	254	551.8250	60.000	1.028	10.264	8.591
181	18	618.5337	60.000	1.436	10.326	8.675
182	74	618.5337	60.000	1.368	10.326	8.276
183	210	618.5337	60.000	1.346	10.326	8.277
184	5	699.9532	60.000	1.854	10.059	8.856
185	61	699.9532	60.000	1.804	10.060	8.485
186	197	699.9532	60.000	1.781	10.060	8.488
187	14	771.1717	60.000	0.855	10.646	7.176
188	70	771.1717	60.000	0.771	10.646	6.830
189	206	771.1717	60.000	0.752	10.646	6.831
190	117	825.2729	60.000	0.435	10.791	6.213
191	252	825.2729	60.000	0.417	10.791	6.213
192	9	954.4603	60.000	0.580	10.913	6.053
193	65	954.4603	60.000	0.484	10.913	5.742
194	201	954.4603	60.000	0.467	10.913	5.741
195	6	1106.2120	60.000	0.475	11.061	5.436
196	62	1106.2120	60.000	0.364	11.061	5.142
197	198	1106.2120	60.000	0.351	11.061	5.142
198	114	1157.0650	60.000	0.150	11.134	4.833
199	249	1157.0650	60.000	0.137	11.134	4.833

*C.5 Longitudinal Channel Disturbance Time Response*

#	srf#	$\bar{q}$	$t_{settle}$	$Dist_{max}$
1	119	65.4696	1.155	0.087
2	253	65.4696	1.140	0.197
3	118	65.5666	1.155	0.084
4	122	67.0399	1.130	0.198
5	256	67.0399	1.120	0.197
6	121	67.4267	1.135	0.209
7	255	67.4267	1.130	0.209
8	124	67.6717	1.120	0.196
9	116	68.8746	1.155	0.237
10	251	68.8746	1.155	0.236
11	115	70.9929	1.160	0.259
12	10	74.2746	1.140	0.247
13	66	74.2746	1.150	0.285
14	202	74.2746	1.150	0.284
15	113	75.5664	1.170	0.302
16	250	77.0323	1.160	0.313
17	258	77.2143	1.145	0.298
18	125	77.2914	1.135	0.293
19	259	77.2914	1.130	0.292
20	37	80.2356	1.120	0.288
21	93	80.2356	1.130	0.318
22	229	80.2356	1.125	0.317
23	15	80.3692	1.160	0.308
24	71	80.3692	1.170	0.327
25	207	80.3692	1.165	0.326
26	33	80.5349	1.135	0.293
27	89	80.5349	1.145	0.321
28	225	80.5349	1.140	0.320
29	28	81.4969	1.145	0.302
30	84	81.4969	1.150	0.327
31	220	81.4969	1.150	0.327
32	1	82.2802	1.165	0.317
33	57	82.2802	1.170	0.333
34	193	82.2802	1.170	0.332
35	7	83.3181	1.165	0.317
36	63	83.3181	1.170	0.335
37	199	83.3181	1.170	0.334
38	19	83.4550	1.150	0.313
39	75	83.4550	1.160	0.336
40	211	83.4550	1.160	0.336
41	25	83.7191	1.145	0.313

#	srf#	$\bar{q}$	$t_{settle}$	$Dist_{max}$
42	81	83.7191	1.155	0.338
43	217	83.7191	1.150	0.337
44	34	87.3860	1.125	0.339
45	90	87.3860	1.135	0.370
46	226	87.3860	1.130	0.369
47	127	88.7159	1.200	0.404
48	261	88.7159	1.200	0.403
49	38	89.3983	1.110	0.366
50	94	89.3983	1.220	0.412
51	230	89.3983	1.210	0.411
52	11	91.6970	1.155	0.333
53	67	91.6970	1.160	0.356
54	203	91.6970	1.165	0.355
55	41	94.3473	1.190	0.401
56	97	94.3473	1.190	0.420
57	233	94.3473	1.190	0.419
58	262	101.0962	1.140	0.413
59	16	102.4478	1.170	0.364
60	72	102.4478	1.170	0.378
61	208	102.4478	1.165	0.377
62	263	103.7392	1.235	0.435
63	42	106.1299	1.175	0.429
64	98	106.1299	1.210	0.455
65	234	106.1299	1.205	0.454
66	264	106.4162	1.230	0.450
67	20	109.0025	1.165	0.384
68	76	109.0025	1.170	0.401
69	212	109.0025	1.170	0.400
70	46	109.1273	1.195	0.425
71	102	109.1273	1.235	0.466
72	238	109.1273	1.230	0.465
73	29	110.1905	1.180	0.428
74	85	110.1905	1.185	0.448
75	221	110.1905	1.180	0.447
76	8	110.9265	1.160	0.347
77	64	110.9265	1.160	0.359
78	200	110.9265	1.160	0.358
79	47	111.8726	1.175	0.435
80	103	111.8726	1.215	0.477
81	239	111.8726	1.205	0.476
82	48	114.6519	1.150	0.449

#	srf#	$\bar{q}$	$t_{settle}$	$Dist_{max}$
83	104	114.6519	1.190	0.491
84	240	114.6519	1.190	0.491
85	49	117.4653	1.140	0.465
86	105	117.4653	1.180	0.508
87	241	117.4653	1.170	0.507
88	50	120.3129	1.120	0.483
89	106	120.3129	1.160	0.527
90	242	120.3129	1.155	0.526
91	43	121.8328	1.190	0.490
92	99	121.8328	1.215	0.526
93	235	121.8328	1.210	0.525
94	51	123.1945	1.110	0.503
95	107	123.1945	1.220	0.558
96	243	123.1945	1.215	0.556
97	52	126.1103	1.200	0.541
98	108	126.1103	1.225	0.570
99	244	126.1103	1.220	0.569
100	53	129.0601	1.205	0.553
101	109	129.0601	1.230	0.583
102	245	129.0601	1.235	0.581
103	2	129.4213	1.155	0.343
104	58	129.4213	1.160	0.358
105	194	129.4213	1.155	0.357
106	17	129.8252	1.160	0.399
107	73	129.8252	1.160	0.419
108	209	129.8252	1.160	0.417
109	30	129.9582	1.165	0.495
110	86	129.9582	1.170	0.520
111	222	129.9582	1.170	0.519
112	26	130.0074	1.165	0.458
113	82	130.0074	1.170	0.481
114	218	130.0074	1.165	0.479
115	35	130.0653	1.175	0.534
116	91	130.0653	1.175	0.560
117	227	130.0653	1.175	0.559
118	21	130.1006	1.160	0.426
119	77	130.1006	1.160	0.448
120	213	130.1006	1.160	0.446
121	44	131.7744	1.160	0.532
122	100	131.7744	1.175	0.564
123	236	131.7744	1.170	0.563

#	srf#	$\bar{q}$	$t_{settle}$	$Dist_{max}$
124	54	132.0441	1.220	0.566
125	110	132.0441	1.240	0.595
126	246	132.0441	1.240	0.594
127	39	134.8266	1.185	0.541
128	95	134.8266	1.160	0.579
129	231	134.8266	1.160	0.578
130	55	135.0621	1.220	0.579
131	111	135.0621	1.245	0.609
132	247	135.0621	1.245	0.607
133	56	138.1142	1.230	0.592
134	112	138.1142	1.250	0.622
135	248	138.1142	1.245	0.621
136	45	167.7286	1.190	0.640
137	101	167.7286	1.095	0.630
138	237	167.7286	1.100	0.628
139	22	170.3164	1.100	0.545
140	78	170.3164	1.095	0.570
141	214	170.3164	1.095	0.568
142	40	208.2658	1.155	0.633
143	96	208.2658	1.115	0.661
144	232	208.2658	1.120	0.659
145	31	215.9733	1.095	0.624
146	87	215.9733	1.085	0.645
147	223	215.9733	1.090	0.643
148	126	222.8766	1.170	0.685
149	260	222.8766	1.190	0.683
150	3	228.5562	1.145	0.497
151	59	228.5562	1.120	0.529
152	195	228.5562	1.130	0.527
153	12	254.7139	1.100	0.586
154	68	254.7139	1.085	0.610
155	204	254.7139	1.090	0.608
156	36	264.5698	1.250	0.666
157	92	264.5698	1.135	0.697
158	228	264.5698	1.145	0.695
159	32	333.6127	1.430	0.697
160	88	333.6127	1.155	0.730
161	224	333.6127	1.180	0.728
162	23	333.8201	1.070	0.656
163	79	333.8201	1.040	0.678
164	215	333.8201	1.045	0.676

#	srf#	$\bar{q}$	$t_{settle}$	$Dist_{max}$
165	123	357.0172	1.295	0.758
166	257	357.0172	1.375	0.755
167	27	416.6143	4.805	0.721
168	83	416.6143	1.210	0.754
169	219	416.6143	1.260	0.751
170	13	499.2391	1.110	0.676
171	69	499.2391	1.040	0.699
172	205	499.2391	1.060	0.696
173	24	503.8640	4.830	0.734
174	80	503.8640	1.235	0.768
175	216	503.8640	1.290	0.765
176	4	514.2514	1.105	0.662
177	60	514.2514	1.080	0.673
178	196	514.2514	1.095	0.671
179	120	551.8250	4.845	0.806
180	254	551.8250	4.845	0.804
181	18	618.5337	4.855	0.759
182	74	618.5337	1.400	0.794
183	210	618.5337	1.530	0.791
184	5	699.9532	1.165	0.697
185	61	699.9532	1.055	0.721
186	197	699.9532	1.080	0.719
187	14	771.1717	4.890	0.801
188	70	771.1717	4.885	0.836
189	206	771.1717	4.885	0.835

*Appendix D. Lateral Channel Time Response*

Variable	Units
$\bar{q}$	<i>lbs/ft<sup>2</sup></i>
$t_1$	seconds
$\phi$	degrees
$\beta$	degrees
$\dot{\delta}_{ail}$	deg/sec
$\delta_{ail}$	degrees
$\dot{\delta}_{rud}$	deg/sec
$\delta_{rud}$	degrees
$\dot{\delta}_{elev}$	deg/sec
$\delta_{elev}$	degrees

D.1 Lateral Unit  $P_{cmd}$  Step Input Time Response (Healthy)

#	srf#	$\bar{q}$	$\phi_{1sec}$	$\phi_{2.8sec}$	$\beta_{max}$	$\delta_{a_{max}}$	$\delta_{a_{max}}$	$\delta_{r_{max}}$	$\delta_{r_{max}}$	$\delta_{elev_{max}}$	$\delta_{elev_{max}}$
1	119	65.4696	0.224	1.917	0.056	0.414	0.266	0.462	0.400	0.122	0.078
2	253	65.4696	0.224	1.918	0.056	0.414	0.265	0.461	0.399	0.122	0.078
3	118	65.5666	0.224	1.893	0.057	0.414	0.270	0.462	0.452	0.122	0.079
4	122	67.0399	0.228	1.974	0.052	0.414	0.253	0.446	0.314	0.122	0.074
5	256	67.0399	0.227	1.975	0.052	0.414	0.253	0.446	0.313	0.122	0.074
6	121	67.4267	0.229	1.957	0.053	0.414	0.254	0.447	0.334	0.122	0.075
7	255	67.4267	0.229	1.957	0.053	0.414	0.254	0.447	0.333	0.122	0.075
8	124	67.6717	0.228	1.998	0.051	0.414	0.249	0.438	0.294	0.122	0.073
9	116	68.8746	0.233	1.902	0.054	0.414	0.260	0.444	0.466	0.122	0.076
10	251	68.8746	0.233	1.902	0.054	0.414	0.260	0.444	0.464	0.122	0.076
11	115	70.9929	0.238	1.894	0.053	0.414	0.257	0.432	0.492	0.122	0.075
12	10	74.2746	0.243	1.893	0.052	0.413	0.256	0.445	0.432	0.122	0.075
13	66	74.2746	0.247	1.945	0.050	0.414	0.239	0.416	0.409	0.122	0.070
14	202	74.2746	0.247	1.945	0.050	0.414	0.239	0.416	0.408	0.122	0.070
15	113	75.5664	0.248	1.907	0.050	0.414	0.245	0.407	0.478	0.122	0.072
16	250	77.0323	0.252	1.936	0.048	0.413	0.235	0.401	0.426	0.122	0.069
17	258	77.2143	0.248	2.047	0.042	0.414	0.221	0.382	0.224	0.122	0.065
18	125	77.2914	0.247	2.069	0.041	0.414	0.219	0.377	0.218	0.122	0.064
19	259	77.2914	0.247	2.070	0.041	0.414	0.219	0.377	0.217	0.122	0.064
20	37	80.2356	0.255	2.066	0.041	0.413	0.217	0.389	0.216	0.122	0.064
21	93	80.2356	0.260	2.104	0.039	0.414	0.206	0.368	0.204	0.122	0.061
22	229	80.2356	0.260	2.104	0.039	0.414	0.206	0.369	0.204	0.122	0.060
23	15	80.3692	0.256	1.944	0.045	0.413	0.234	0.407	0.333	0.121	0.069
24	71	80.3692	0.259	1.977	0.043	0.413	0.222	0.377	0.318	0.122	0.065
25	207	80.3692	0.259	1.978	0.043	0.413	0.222	0.377	0.317	0.122	0.065
26	33	80.5349	0.256	2.040	0.041	0.413	0.219	0.393	0.220	0.122	0.064
27	89	80.5349	0.261	2.077	0.040	0.413	0.208	0.370	0.208	0.122	0.061
28	225	80.5349	0.261	2.077	0.040	0.413	0.208	0.370	0.207	0.122	0.061
29	28	81.4969	0.260	2.024	0.042	0.413	0.219	0.394	0.224	0.121	0.064
30	84	81.4969	0.264	2.059	0.040	0.413	0.207	0.369	0.220	0.122	0.061
31	220	81.4969	0.264	2.060	0.040	0.413	0.207	0.369	0.219	0.122	0.061
32	1	82.2802	0.259	1.893	0.048	0.413	0.242	0.404	0.439	0.121	0.071
33	57	82.2802	0.260	1.926	0.045	0.413	0.229	0.374	0.414	0.121	0.067
34	193	82.2802	0.260	1.926	0.045	0.413	0.229	0.374	0.413	0.121	0.067
35	7	83.3181	0.262	1.920	0.046	0.413	0.234	0.401	0.396	0.121	0.069
36	63	83.3181	0.264	1.952	0.043	0.413	0.222	0.371	0.375	0.121	0.065
37	199	83.3181	0.263	1.952	0.043	0.413	0.222	0.371	0.374	0.121	0.065
38	19	83.4550	0.264	1.985	0.042	0.413	0.220	0.391	0.278	0.121	0.065
39	75	83.4550	0.267	2.016	0.040	0.413	0.209	0.363	0.267	0.121	0.062
40	211	83.4550	0.267	2.016	0.040	0.413	0.209	0.363	0.266	0.121	0.062
41	25	83.7192	0.266	2.013	0.041	0.413	0.215	0.388	0.245	0.121	0.063

#	srf#	$\bar{q}$	$\phi_{1sec}$	$\phi_{2.8sec}$	$\beta_{max}$	$\delta_{amax}$	$\delta_{amax}$	$\delta_{rmax}$	$\delta_{rmax}$	$\delta_{elevmax}$	$\delta_{elevmax}$
42	81	83.7192	0.269	2.045	0.039	0.413	0.204	0.362	0.237	0.121	0.060
43	217	83.7192	0.269	2.046	0.039	0.413	0.204	0.362	0.236	0.121	0.060
44	34	87.3860	0.281	2.098	0.037	0.413	0.193	0.372	0.190	0.121	0.057
45	90	87.3860	0.286	2.127	0.036	0.413	0.184	0.349	0.179	0.121	0.054
46	226	87.3860	0.286	2.127	0.035	0.413	0.184	0.349	0.178	0.121	0.054
47	127	88.7159	0.297	2.206	0.033	0.413	0.170	0.328	0.162	0.121	0.050
48	261	88.7159	0.297	2.206	0.033	0.413	0.170	0.328	0.161	0.121	0.050
49	38	89.3983	0.294	2.153	0.035	0.412	0.179	0.366	0.179	0.121	0.053
50	94	89.3983	0.299	2.175	0.034	0.413	0.172	0.342	0.168	0.121	0.051
51	230	89.3983	0.299	2.175	0.034	0.413	0.172	0.343	0.167	0.121	0.051
52	11	91.6970	0.280	1.981	0.040	0.412	0.208	0.370	0.304	0.121	0.061
53	67	91.6970	0.281	2.001	0.037	0.413	0.199	0.340	0.287	0.121	0.059
54	203	91.6970	0.281	2.001	0.037	0.413	0.199	0.340	0.287	0.121	0.059
55	41	94.3473	0.309	2.201	0.031	0.412	0.163	0.326	0.152	0.121	0.048
56	97	94.3473	0.311	2.219	0.030	0.413	0.158	0.300	0.142	0.121	0.047
57	233	94.3473	0.311	2.219	0.030	0.413	0.158	0.301	0.141	0.121	0.047
58	262	101.0962	0.319	2.247	0.025	0.413	0.149	0.243	0.109	0.121	0.044
59	16	102.4478	0.301	2.018	0.032	0.412	0.184	0.316	0.218	0.121	0.054
60	72	102.4478	0.301	2.028	0.030	0.412	0.179	0.287	0.206	0.121	0.052
61	208	102.4478	0.301	2.028	0.030	0.412	0.178	0.288	0.205	0.121	0.052
62	263	103.7392	0.328	2.252	0.024	0.413	0.144	0.234	0.103	0.121	0.042
63	42	106.1299	0.336	2.218	0.026	0.412	0.143	0.277	0.118	0.121	0.042
64	98	106.1299	0.337	2.229	0.024	0.412	0.140	0.252	0.108	0.121	0.041
65	234	106.1299	0.337	2.229	0.024	0.412	0.140	0.252	0.108	0.121	0.041
66	264	106.4162	0.337	2.256	0.023	0.412	0.139	0.226	0.097	0.121	0.041
67	20	109.0025	0.318	2.062	0.028	0.411	0.166	0.295	0.173	0.121	0.049
68	76	109.0025	0.318	2.069	0.027	0.412	0.162	0.267	0.163	0.121	0.048
69	212	109.0025	0.318	2.069	0.027	0.412	0.162	0.268	0.162	0.121	0.048
70	46	109.1273	0.342	2.249	0.024	0.412	0.137	0.239	0.101	0.121	0.040
71	102	109.1273	0.347	2.258	0.022	0.412	0.134	0.217	0.091	0.121	0.039
72	238	109.1273	0.347	2.258	0.022	0.412	0.134	0.218	0.091	0.121	0.039
73	29	110.1905	0.335	2.130	0.027	0.411	0.150	0.294	0.133	0.121	0.044
74	85	110.1905	0.335	2.138	0.025	0.412	0.147	0.268	0.126	0.121	0.043
75	221	110.1905	0.335	2.138	0.025	0.412	0.147	0.269	0.126	0.121	0.043
76	8	110.9265	0.303	1.970	0.030	0.411	0.188	0.289	0.237	0.121	0.055
77	64	110.9265	0.302	1.974	0.028	0.412	0.184	0.260	0.221	0.121	0.054
78	200	110.9265	0.302	1.974	0.028	0.412	0.184	0.260	0.221	0.121	0.054
79	47	111.8726	0.353	2.250	0.022	0.412	0.132	0.231	0.095	0.121	0.039
80	103	111.8726	0.358	2.257	0.021	0.412	0.129	0.209	0.085	0.121	0.038
81	239	111.8726	0.358	2.257	0.021	0.412	0.129	0.209	0.085	0.121	0.038
82	48	114.6519	0.364	2.251	0.021	0.412	0.126	0.223	0.089	0.121	0.037

#	srf#	$\bar{q}$	$\phi_{1sec}$	$\phi_{2.8sec}$	$\beta_{max}$	$\delta_{amax}$	$\delta_{amax}$	$\delta_{rmax}$	$\delta_{rmax}$	$\delta_{elevmax}$	$\delta_{elevmax}$
83	104	114.6519	0.369	2.255	0.020	0.412	0.124	0.201	0.080	0.121	0.036
84	240	114.6519	0.369	2.255	0.020	0.412	0.124	0.201	0.080	0.121	0.036
85	49	117.4653	0.375	2.250	0.020	0.411	0.121	0.214	0.083	0.121	0.036
86	105	117.4653	0.380	2.253	0.019	0.411	0.119	0.193	0.075	0.121	0.035
87	241	117.4653	0.380	2.253	0.019	0.411	0.119	0.194	0.075	0.121	0.035
88	50	120.3129	0.387	2.249	0.019	0.411	0.116	0.206	0.078	0.121	0.034
89	106	120.3129	0.392	2.252	0.018	0.411	0.115	0.185	0.070	0.121	0.034
90	242	120.3129	0.392	2.252	0.018	0.411	0.115	0.186	0.070	0.121	0.034
91	43	121.8328	0.383	2.235	0.021	0.411	0.118	0.226	0.085	0.121	0.035
92	99	121.8328	0.384	2.237	0.019	0.411	0.117	0.202	0.077	0.121	0.035
93	235	121.8328	0.384	2.237	0.019	0.411	0.117	0.203	0.077	0.121	0.035
94	51	123.1945	0.399	2.248	0.018	0.411	0.112	0.199	0.073	0.121	0.033
95	107	123.1945	0.398	2.249	0.017	0.411	0.112	0.176	0.065	0.121	0.033
96	243	123.1945	0.398	2.249	0.017	0.411	0.112	0.177	0.065	0.121	0.033
97	52	126.1103	0.407	2.246	0.017	0.411	0.108	0.190	0.068	0.121	0.032
98	108	126.1103	0.404	2.246	0.016	0.411	0.110	0.167	0.061	0.121	0.032
99	244	126.1103	0.404	2.245	0.016	0.411	0.110	0.167	0.061	0.121	0.032
100	53	129.0601	0.412	2.242	0.016	0.410	0.106	0.180	0.063	0.121	0.031
101	109	129.0601	0.409	2.242	0.015	0.411	0.108	0.157	0.056	0.121	0.032
102	245	129.0601	0.409	2.242	0.015	0.411	0.108	0.157	0.056	0.121	0.032
103	2	129.4213	0.326	1.977	0.024	0.410	0.179	0.234	0.192	0.121	0.053
104	58	129.4213	0.327	1.986	0.023	0.411	0.176	0.210	0.181	0.121	0.052
105	194	129.4213	0.327	1.986	0.023	0.411	0.176	0.211	0.180	0.121	0.052
106	17	129.8252	0.351	2.069	0.022	0.410	0.143	0.237	0.139	0.121	0.042
107	73	129.8252	0.352	2.077	0.021	0.411	0.139	0.213	0.130	0.121	0.041
108	209	129.8252	0.352	2.077	0.021	0.411	0.139	0.213	0.130	0.121	0.041
109	30	129.9582	0.381	2.160	0.021	0.410	0.121	0.243	0.095	0.121	0.036
110	86	129.9582	0.382	2.166	0.020	0.410	0.119	0.218	0.089	0.121	0.035
111	222	129.9582	0.382	2.166	0.020	0.410	0.119	0.219	0.089	0.121	0.035
112	26	130.0074	0.370	2.131	0.021	0.410	0.128	0.241	0.108	0.121	0.038
113	82	130.0074	0.371	2.137	0.020	0.410	0.125	0.216	0.102	0.121	0.037
114	218	130.0074	0.371	2.137	0.020	0.410	0.125	0.217	0.101	0.121	0.037
115	35	130.0653	0.391	2.187	0.020	0.410	0.115	0.241	0.086	0.120	0.034
116	91	130.0653	0.393	2.192	0.019	0.410	0.114	0.216	0.078	0.121	0.033
117	227	130.0653	0.393	2.192	0.019	0.410	0.114	0.217	0.078	0.121	0.034
118	21	130.1006	0.361	2.101	0.022	0.410	0.135	0.238	0.122	0.121	0.040
119	77	130.1006	0.362	2.107	0.020	0.410	0.132	0.214	0.115	0.121	0.039
120	213	130.1006	0.362	2.108	0.020	0.410	0.132	0.215	0.115	0.121	0.039
121	44	131.7744	0.413	2.237	0.018	0.410	0.106	0.198	0.070	0.121	0.031
122	100	131.7744	0.407	2.234	0.017	0.411	0.109	0.176	0.062	0.121	0.032
123	236	131.7744	0.407	2.234	0.016	0.411	0.109	0.177	0.062	0.121	0.032

#	srf#	$\bar{q}$	$\phi_{1sec}$	$\phi_{2.8sec}$	$\beta_{max}$	$\delta_{amax}$	$\delta_{amax}$	$\delta_{rmax}$	$\delta_{rmax}$	$\delta_{elevmax}$	$\delta_{elevmax}$
124	54	132.0441	0.417	2.239	0.015	0.410	0.105	0.170	0.059	0.121	0.031
125	110	132.0441	0.415	2.239	0.014	0.411	0.106	0.146	0.051	0.121	0.031
126	246	132.0441	0.415	2.239	0.014	0.411	0.106	0.147	0.051	0.121	0.031
127	39	134.8266	0.411	2.215	0.018	0.410	0.106	0.208	0.072	0.120	0.031
128	95	134.8266	0.409	2.215	0.017	0.410	0.107	0.186	0.065	0.121	0.032
129	231	134.8266	0.409	2.215	0.017	0.410	0.107	0.187	0.065	0.121	0.032
130	55	135.0621	0.422	2.235	0.015	0.410	0.103	0.159	0.054	0.121	0.030
131	111	135.0621	0.420	2.236	0.014	0.410	0.105	0.135	0.047	0.121	0.031
132	247	135.0621	0.420	2.236	0.014	0.410	0.105	0.136	0.047	0.121	0.031
133	56	138.1142	0.426	2.232	0.014	0.410	0.102	0.147	0.049	0.121	0.030
134	112	138.1142	0.424	2.233	0.013	0.410	0.103	0.124	0.042	0.121	0.030
135	248	138.1142	0.424	2.233	0.013	0.410	0.103	0.124	0.042	0.121	0.030
136	45	167.7286	0.458	2.199	0.017	0.409	0.090	0.051	0.017	0.120	0.027
137	101	167.7286	0.456	2.204	0.016	0.409	0.092	0.039	0.014	0.120	0.027
138	237	167.7286	0.456	2.204	0.016	0.409	0.092	0.040	0.014	0.120	0.027
139	22	170.3164	0.433	2.136	0.023	0.407	0.101	0.091	0.060	0.120	0.030
140	78	170.3164	0.433	2.141	0.022	0.408	0.099	0.077	0.053	0.120	0.029
141	214	170.3164	0.433	2.141	0.022	0.408	0.099	0.078	0.052	0.120	0.029
142	40	208.2658	0.484	2.192	0.013	0.407	0.082	0.025	0.011	0.120	0.024
143	96	208.2658	0.483	2.196	0.012	0.407	0.084	0.016	0.008	0.120	0.025
144	232	208.2658	0.482	2.196	0.012	0.407	0.084	0.017	0.008	0.120	0.025
145	31	215.9733	0.494	2.194	0.016	0.405	0.076	0.048	0.023	0.119	0.022
146	87	215.9733	0.490	2.192	0.014	0.406	0.079	0.036	0.019	0.119	0.023
147	223	215.9733	0.490	2.192	0.014	0.406	0.079	0.037	0.019	0.119	0.023
148	126	222.8766	0.490	2.197	0.011	0.407	0.082	0.007	0.004	0.120	0.024
149	260	222.8766	0.490	2.197	0.011	0.407	0.082	0.007	0.004	0.120	0.024
150	3	228.5562	0.452	2.108	0.019	0.404	0.112	0.041	0.050	0.119	0.033
151	59	228.5562	0.449	2.106	0.018	0.405	0.112	0.030	0.044	0.119	0.033
152	195	228.5562	0.449	2.106	0.018	0.405	0.112	0.031	0.044	0.119	0.033
153	12	254.7139	0.485	2.152	0.016	0.402	0.090	0.029	0.031	0.118	0.026
154	68	254.7139	0.483	2.151	0.015	0.403	0.090	0.019	0.026	0.119	0.026
155	204	254.7139	0.483	2.151	0.015	0.403	0.090	0.020	0.025	0.119	0.026
156	36	264.5698	0.505	2.187	0.010	0.405	0.074	0.007	0.004	0.119	0.022
157	92	264.5698	0.505	2.193	0.010	0.405	0.076	0.006	0.001	0.119	0.022
158	228	264.5698	0.505	2.193	0.010	0.405	0.076	0.006	0.001	0.119	0.022
159	32	333.6127	0.519	2.186	0.009	0.402	0.068	0.009	0.000	0.118	0.020
160	88	333.6127	0.520	2.193	0.008	0.403	0.070	0.011	0.000	0.118	0.021
161	224	333.6127	0.520	2.193	0.008	0.403	0.070	0.010	0.000	0.118	0.021
162	23	333.8201	0.521	2.188	0.011	0.400	0.070	0.008	0.008	0.118	0.021
163	79	333.8201	0.519	2.187	0.010	0.401	0.070	0.008	0.004	0.118	0.021
164	215	333.8201	0.519	2.187	0.010	0.401	0.070	0.008	0.004	0.118	0.021

#	srf#	$\bar{q}$	$\phi_{1sec}$	$\phi_{2.8sec}$	$\beta_{max}$	$\delta_{amax}$	$\delta_{amax}$	$\delta_{rmax}$	$\delta_{rmax}$	$\delta_{elevmax}$	$\delta_{elevmax}$
165	123	357.0172	0.524	2.194	0.008	0.402	0.069	0.015	0.000	0.118	0.020
166	257	357.0172	0.524	2.194	0.008	0.402	0.069	0.014	0.000	0.118	0.020
167	27	416.6143	0.527	2.185	0.008	0.399	0.068	0.021	0.000	0.117	0.020
168	83	416.6143	0.529	2.192	0.007	0.400	0.066	0.024	0.000	0.118	0.019
169	219	416.6143	0.529	2.192	0.007	0.400	0.066	0.022	0.000	0.118	0.019
170	13	499.2391	0.531	2.186	0.009	0.396	0.070	0.028	0.000	0.116	0.021
171	69	499.2391	0.531	2.186	0.009	0.396	0.070	0.032	0.000	0.117	0.020
172	205	499.2391	0.531	2.186	0.009	0.396	0.070	0.031	0.000	0.117	0.020
173	24	503.8640	0.531	2.185	0.007	0.397	0.068	0.034	0.000	0.117	0.020
174	80	503.8640	0.533	2.191	0.007	0.398	0.066	0.038	0.000	0.117	0.019
175	216	503.8640	0.533	2.191	0.007	0.398	0.066	0.036	0.000	0.117	0.019
176	4	514.2514	0.527	2.179	0.010	0.394	0.074	0.025	0.003	0.116	0.022
177	60	514.2514	0.527	2.178	0.010	0.395	0.074	0.029	0.000	0.116	0.022
178	196	514.2514	0.527	2.178	0.010	0.395	0.074	0.027	0.000	0.116	0.022
179	120	551.8250	0.535	2.193	0.006	0.397	0.065	0.046	0.000	0.117	0.019
180	254	551.8250	0.535	2.193	0.006	0.397	0.065	0.044	0.000	0.117	0.019
181	18	618.5337	0.534	2.185	0.007	0.395	0.068	0.052	0.000	0.116	0.020
182	74	618.5337	0.536	2.191	0.007	0.396	0.066	0.056	0.000	0.116	0.020
183	210	618.5337	0.536	2.191	0.007	0.396	0.066	0.055	0.000	0.116	0.020
184	5	699.9532	0.533	2.182	0.008	0.391	0.071	0.057	0.000	0.115	0.021
185	61	699.9532	0.533	2.182	0.008	0.392	0.071	0.063	0.000	0.115	0.021
186	197	699.9532	0.533	2.182	0.008	0.392	0.071	0.061	0.000	0.115	0.021
187	14	771.1717	0.536	2.183	0.006	0.392	0.069	0.071	0.000	0.115	0.020
188	70	771.1717	0.537	2.189	0.006	0.393	0.067	0.076	0.000	0.116	0.020
189	206	771.1717	0.537	2.189	0.006	0.393	0.067	0.074	0.000	0.116	0.020
190	117	825.2729	0.537	2.189	0.006	0.393	0.067	0.083	0.000	0.115	0.020
191	252	825.2729	0.537	2.189	0.006	0.393	0.067	0.081	0.000	0.115	0.020
192	9	954.4603	0.531	2.172	0.006	0.390	0.074	0.088	0.000	0.115	0.022
193	65	954.4603	0.532	2.180	0.006	0.391	0.071	0.093	0.000	0.115	0.021
194	201	954.4603	0.532	2.180	0.006	0.391	0.071	0.091	0.000	0.115	0.021
195	6	1106.2120	0.526	2.163	0.006	0.389	0.077	0.098	0.000	0.114	0.023
196	62	1106.2120	0.527	2.171	0.006	0.390	0.074	0.103	0.000	0.115	0.022
197	198	1106.2120	0.527	2.171	0.006	0.390	0.074	0.101	0.000	0.115	0.022
198	114	1157.0650	0.525	2.168	0.005	0.390	0.075	0.105	0.000	0.115	0.022
199	249	1157.0650	0.525	2.168	0.005	0.390	0.075	0.103	0.000	0.115	0.022

D.2 Lateral Unit  $P_{cmd}$  Step Input Time Response (45% Triple Failure)

#	sr#	$\bar{q}$	$\phi_{1sec}$	$\phi_{2.8sec}$	$\beta_{max}$	$\delta_{amax}$	$\delta_{amax}$	$\delta_{rmax}$	$\delta_{rmax}$	$\delta_{elevmax}$	$\delta_{elevmax}$
1	119	65.4696	0.145	1.339	0.062	0.416	0.442	0.408	0.765	0.122	0.130
2	253	65.4696	0.145	1.339	0.061	0.416	0.442	0.407	0.763	0.122	0.130
3	118	65.5666	0.145	1.319	0.063	0.416	0.452	0.408	0.836	0.122	0.133
4	122	67.0399	0.147	1.397	0.058	0.416	0.417	0.393	0.590	0.122	0.122
5	256	67.0399	0.147	1.398	0.058	0.416	0.416	0.392	0.589	0.122	0.122
6	121	67.4267	0.148	1.385	0.059	0.416	0.421	0.393	0.648	0.122	0.124
7	255	67.4267	0.148	1.386	0.058	0.416	0.421	0.392	0.646	0.122	0.124
8	124	67.6717	0.147	1.420	0.056	0.416	0.407	0.385	0.529	0.122	0.120
9	116	68.8746	0.151	1.351	0.061	0.416	0.438	0.392	0.823	0.122	0.129
10	251	68.8746	0.151	1.352	0.061	0.416	0.438	0.391	0.821	0.122	0.129
11	115	70.9929	0.154	1.359	0.060	0.416	0.435	0.382	0.844	0.122	0.128
12	10	74.2746	0.160	1.343	0.060	0.415	0.439	0.389	0.788	0.122	0.129
13	66	74.2746	0.161	1.426	0.056	0.415	0.404	0.365	0.708	0.122	0.119
14	202	74.2746	0.160	1.426	0.056	0.415	0.404	0.364	0.705	0.122	0.119
15	113	75.5664	0.162	1.400	0.058	0.415	0.417	0.359	0.802	0.122	0.123
16	250	77.0323	0.165	1.436	0.055	0.415	0.400	0.352	0.720	0.122	0.117
17	258	77.2143	0.163	1.530	0.047	0.416	0.362	0.327	0.375	0.122	0.106
18	125	77.2914	0.163	1.549	0.046	0.416	0.356	0.323	0.341	0.122	0.105
19	259	77.2914	0.163	1.550	0.045	0.416	0.356	0.322	0.340	0.122	0.105
20	37	80.2356	0.169	1.545	0.045	0.415	0.356	0.330	0.349	0.122	0.105
21	93	80.2356	0.172	1.610	0.044	0.415	0.335	0.313	0.304	0.122	0.098
22	229	80.2356	0.172	1.610	0.044	0.415	0.335	0.313	0.303	0.122	0.098
23	15	80.3692	0.169	1.426	0.051	0.415	0.399	0.348	0.599	0.122	0.117
24	71	80.3692	0.170	1.490	0.048	0.415	0.373	0.323	0.543	0.122	0.110
25	207	80.3692	0.170	1.490	0.048	0.415	0.373	0.323	0.541	0.122	0.110
26	33	80.5349	0.170	1.521	0.046	0.415	0.363	0.334	0.377	0.122	0.107
27	89	80.5349	0.172	1.586	0.045	0.415	0.341	0.315	0.340	0.122	0.100
28	225	80.5349	0.172	1.586	0.044	0.415	0.341	0.315	0.339	0.122	0.100
29	28	81.4969	0.172	1.513	0.047	0.415	0.365	0.334	0.412	0.122	0.107
30	84	81.4969	0.174	1.576	0.045	0.415	0.342	0.314	0.377	0.122	0.101
31	220	81.4969	0.174	1.576	0.045	0.415	0.342	0.314	0.376	0.122	0.101
32	1	82.2802	0.171	1.390	0.055	0.415	0.420	0.350	0.755	0.122	0.124
33	57	82.2802	0.171	1.453	0.052	0.415	0.391	0.325	0.686	0.122	0.115
34	193	82.2802	0.171	1.454	0.051	0.415	0.391	0.325	0.684	0.122	0.115
35	7	83.3181	0.173	1.421	0.053	0.415	0.404	0.346	0.686	0.122	0.119
36	63	83.3181	0.173	1.484	0.050	0.415	0.377	0.321	0.625	0.122	0.111
37	199	83.3181	0.173	1.484	0.050	0.415	0.377	0.321	0.623	0.122	0.111
38	19	83.4550	0.175	1.486	0.048	0.415	0.373	0.332	0.496	0.122	0.110
39	75	83.4550	0.176	1.546	0.045	0.415	0.350	0.309	0.453	0.122	0.103
40	211	83.4550	0.176	1.546	0.045	0.415	0.350	0.308	0.452	0.122	0.103
41	25	83.7191	0.177	1.516	0.046	0.415	0.362	0.328	0.438	0.122	0.106

#	srf#	$\bar{q}$	$\phi_{1sec}$	$\phi_{2.8sec}$	$\beta_{max}$	$\delta_{a_{max}}$	$\delta_{a_{max}}$	$\delta_{r_{max}}$	$\delta_{r_{max}}$	$\delta_{elev_{max}}$	$\delta_{elev_{max}}$
42	81	83.7191	0.178	1.578	0.044	0.415	0.340	0.307	0.402	0.122	0.100
43	217	83.7191	0.178	1.578	0.044	0.415	0.339	0.307	0.401	0.122	0.100
44	34	87.3860	0.189	1.636	0.042	0.415	0.321	0.312	0.304	0.122	0.094
45	90	87.3860	0.191	1.693	0.040	0.415	0.302	0.292	0.285	0.122	0.089
46	226	87.3860	0.191	1.694	0.040	0.415	0.302	0.292	0.284	0.122	0.089
47	127	88.7159	0.198	1.800	0.038	0.415	0.275	0.275	0.221	0.122	0.081
48	261	88.7159	0.198	1.801	0.037	0.415	0.275	0.275	0.220	0.122	0.081
49	38	89.3983	0.199	1.717	0.040	0.415	0.296	0.305	0.250	0.122	0.087
50	94	89.3983	0.200	1.767	0.038	0.415	0.281	0.285	0.230	0.122	0.083
51	230	89.3983	0.200	1.768	0.038	0.415	0.281	0.285	0.230	0.122	0.083
52	11	91.6970	0.187	1.528	0.046	0.415	0.356	0.312	0.519	0.122	0.105
53	67	91.6970	0.187	1.575	0.043	0.415	0.336	0.287	0.476	0.122	0.099
54	203	91.6970	0.187	1.575	0.043	0.415	0.336	0.286	0.474	0.122	0.099
55	41	94.3473	0.208	1.810	0.036	0.415	0.268	0.272	0.213	0.122	0.079
56	97	94.3473	0.207	1.857	0.034	0.415	0.256	0.250	0.193	0.122	0.075
57	233	94.3473	0.207	1.857	0.034	0.415	0.256	0.250	0.192	0.122	0.075
58	262	101.0962	0.211	1.931	0.029	0.415	0.237	0.202	0.149	0.122	0.070
59	16	102.4478	0.204	1.620	0.037	0.414	0.313	0.259	0.367	0.122	0.092
60	72	102.4478	0.202	1.649	0.034	0.415	0.301	0.236	0.340	0.122	0.089
61	208	102.4478	0.202	1.650	0.034	0.415	0.301	0.236	0.339	0.122	0.089
62	263	103.7392	0.217	1.957	0.027	0.415	0.228	0.194	0.140	0.122	0.067
63	42	106.1299	0.227	1.906	0.030	0.415	0.235	0.228	0.165	0.122	0.069
64	98	106.1299	0.226	1.942	0.028	0.415	0.226	0.206	0.146	0.122	0.066
65	234	106.1299	0.226	1.943	0.028	0.415	0.226	0.206	0.145	0.122	0.066
66	264	106.4162	0.224	1.985	0.026	0.415	0.220	0.186	0.132	0.122	0.065
67	20	109.0025	0.216	1.701	0.033	0.414	0.282	0.239	0.290	0.122	0.083
68	76	109.0025	0.214	1.726	0.031	0.414	0.273	0.217	0.270	0.122	0.080
69	212	109.0025	0.214	1.726	0.030	0.414	0.273	0.217	0.269	0.122	0.080
70	46	109.1273	0.229	1.972	0.027	0.415	0.220	0.199	0.142	0.122	0.065
71	102	109.1273	0.231	2.010	0.025	0.415	0.211	0.179	0.124	0.122	0.062
72	238	109.1273	0.231	2.010	0.025	0.415	0.211	0.179	0.124	0.122	0.062
73	29	110.1905	0.229	1.802	0.031	0.414	0.253	0.238	0.223	0.122	0.074
74	85	110.1905	0.227	1.829	0.029	0.414	0.244	0.216	0.210	0.122	0.072
75	221	110.1905	0.227	1.829	0.029	0.414	0.244	0.216	0.209	0.122	0.072
76	8	110.9265	0.206	1.589	0.035	0.414	0.324	0.234	0.393	0.122	0.095
77	64	110.9265	0.203	1.608	0.032	0.414	0.314	0.211	0.362	0.122	0.092
78	200	110.9265	0.203	1.609	0.032	0.414	0.314	0.211	0.361	0.122	0.092
79	47	111.8726	0.237	1.997	0.026	0.415	0.211	0.190	0.132	0.122	0.062
80	103	111.8726	0.239	2.030	0.024	0.415	0.204	0.171	0.116	0.122	0.060
81	239	111.8726	0.239	2.030	0.024	0.415	0.204	0.171	0.116	0.122	0.060
82	48	114.6519	0.245	2.021	0.025	0.414	0.202	0.182	0.123	0.122	0.059

#	sr#	$\bar{q}$	$\phi_{1sec}$	$\phi_{2.8sec}$	$\beta_{max}$	$\delta_{a_{max}}$	$\delta_{\alpha_{max}}$	$\delta_{r_{max}}$	$\delta_{r_{max}}$	$\delta_{elev_{max}}$	$\delta_{elev_{max}}$
83	104	114.6519	0.247	2.049	0.023	0.414	0.196	0.164	0.108	0.122	0.058
84	240	114.6519	0.247	2.049	0.023	0.414	0.196	0.164	0.108	0.122	0.058
85	49	117.4653	0.254	2.042	0.024	0.414	0.194	0.174	0.114	0.122	0.057
86	105	117.4653	0.256	2.067	0.022	0.414	0.188	0.156	0.100	0.122	0.055
87	241	117.4653	0.256	2.067	0.022	0.414	0.188	0.157	0.100	0.122	0.055
88	50	120.3129	0.263	2.061	0.022	0.414	0.186	0.167	0.106	0.122	0.055
89	106	120.3129	0.266	2.084	0.021	0.414	0.181	0.149	0.093	0.122	0.053
90	242	120.3129	0.266	2.085	0.020	0.414	0.181	0.150	0.093	0.122	0.053
91	43	121.8328	0.262	2.034	0.024	0.414	0.190	0.183	0.119	0.122	0.056
92	99	121.8328	0.262	2.051	0.022	0.414	0.186	0.163	0.103	0.122	0.055
93	235	121.8328	0.262	2.051	0.022	0.414	0.187	0.163	0.103	0.122	0.055
94	51	123.1945	0.273	2.079	0.021	0.414	0.178	0.160	0.098	0.122	0.052
95	107	123.1945	0.271	2.092	0.020	0.414	0.177	0.142	0.087	0.122	0.052
96	243	123.1945	0.271	2.092	0.019	0.414	0.177	0.142	0.087	0.122	0.052
97	52	126.1103	0.280	2.089	0.020	0.414	0.173	0.152	0.092	0.122	0.051
98	108	126.1103	0.275	2.097	0.019	0.414	0.173	0.134	0.080	0.122	0.051
99	244	126.1103	0.275	2.097	0.019	0.414	0.173	0.134	0.080	0.122	0.051
100	53	129.0601	0.284	2.092	0.019	0.414	0.170	0.144	0.085	0.122	0.050
101	109	129.0601	0.280	2.102	0.018	0.414	0.170	0.126	0.074	0.122	0.050
102	245	129.0601	0.280	2.102	0.018	0.414	0.170	0.126	0.074	0.122	0.050
103	2	129.4213	0.223	1.647	0.028	0.414	0.306	0.185	0.316	0.122	0.090
104	58	129.4213	0.223	1.667	0.026	0.414	0.297	0.168	0.295	0.122	0.087
105	194	129.4213	0.223	1.668	0.026	0.414	0.297	0.168	0.294	0.122	0.087
106	17	129.8252	0.243	1.779	0.026	0.414	0.245	0.187	0.234	0.122	0.072
107	73	129.8252	0.242	1.799	0.024	0.414	0.237	0.169	0.218	0.122	0.070
108	209	129.8252	0.242	1.799	0.024	0.414	0.236	0.170	0.217	0.122	0.070
109	30	129.9582	0.266	1.923	0.025	0.413	0.205	0.192	0.165	0.122	0.060
110	86	129.9582	0.265	1.945	0.023	0.414	0.198	0.173	0.154	0.122	0.058
111	222	129.9582	0.265	1.946	0.023	0.414	0.198	0.173	0.153	0.122	0.058
112	26	130.0074	0.257	1.874	0.025	0.413	0.217	0.191	0.186	0.122	0.064
113	82	130.0074	0.257	1.896	0.023	0.414	0.210	0.171	0.173	0.122	0.062
114	218	130.0074	0.256	1.896	0.023	0.414	0.210	0.172	0.172	0.122	0.062
115	35	130.0653	0.274	1.972	0.024	0.413	0.193	0.191	0.144	0.122	0.057
116	91	130.0653	0.273	1.994	0.022	0.414	0.187	0.171	0.134	0.122	0.055
117	227	130.0653	0.273	1.995	0.022	0.414	0.187	0.171	0.133	0.122	0.055
118	21	130.1006	0.250	1.827	0.025	0.414	0.230	0.189	0.208	0.122	0.068
119	77	130.1006	0.249	1.848	0.024	0.414	0.222	0.170	0.194	0.122	0.065
120	213	130.1006	0.249	1.848	0.024	0.414	0.222	0.170	0.193	0.122	0.065
121	44	131.7744	0.287	2.088	0.021	0.414	0.168	0.159	0.096	0.122	0.050
122	100	131.7744	0.280	2.085	0.019	0.414	0.171	0.141	0.084	0.122	0.050
123	236	131.7744	0.280	2.085	0.019	0.414	0.171	0.141	0.084	0.122	0.050

#	srf#	$\bar{q}$	$\phi_{1sec}$	$\phi_{2.8sec}$	$\beta_{max}$	$\delta_{amax}$	$\delta_{amax}$	$\delta_{rmax}$	$\delta_{rmax}$	$\delta_{elevmax}$	$\delta_{elevmax}$
124	54	132.0441	0.288	2.095	0.018	0.414	0.167	0.135	0.078	0.122	0.049
125	110	132.0441	0.284	2.106	0.017	0.414	0.166	0.117	0.068	0.122	0.049
126	246	132.0441	0.284	2.106	0.017	0.414	0.166	0.117	0.068	0.122	0.049
127	39	134.8266	0.288	2.047	0.022	0.413	0.172	0.166	0.105	0.122	0.051
128	95	134.8266	0.284	2.055	0.020	0.414	0.172	0.148	0.098	0.122	0.051
129	231	134.8266	0.284	2.055	0.020	0.414	0.172	0.148	0.098	0.122	0.051
130	55	135.0621	0.292	2.096	0.017	0.414	0.164	0.126	0.071	0.122	0.048
131	111	135.0621	0.288	2.109	0.016	0.414	0.163	0.108	0.062	0.122	0.048
132	247	135.0621	0.288	2.109	0.016	0.414	0.163	0.109	0.062	0.122	0.048
133	56	138.1142	0.296	2.098	0.016	0.413	0.161	0.117	0.065	0.122	0.047
134	112	138.1142	0.292	2.112	0.015	0.414	0.161	0.099	0.056	0.122	0.047
135	248	138.1142	0.292	2.112	0.015	0.414	0.161	0.100	0.056	0.122	0.047
136	45	167.7286	0.330	2.066	0.018	0.413	0.142	0.041	0.030	0.121	0.042
137	101	167.7286	0.325	2.083	0.017	0.413	0.142	0.031	0.025	0.121	0.042
138	237	167.7286	0.325	2.083	0.017	0.413	0.142	0.032	0.024	0.121	0.042
139	22	170.3164	0.316	1.947	0.026	0.412	0.172	0.071	0.096	0.121	0.051
140	78	170.3164	0.314	1.962	0.024	0.412	0.167	0.060	0.082	0.121	0.049
141	214	170.3164	0.314	1.962	0.024	0.412	0.167	0.060	0.082	0.121	0.049
142	40	208.2658	0.360	2.070	0.014	0.412	0.126	0.020	0.018	0.121	0.037
143	96	208.2658	0.355	2.083	0.013	0.412	0.128	0.015	0.013	0.121	0.038
144	232	208.2658	0.355	2.083	0.013	0.412	0.128	0.015	0.013	0.121	0.038
145	31	215.9733	0.377	2.072	0.017	0.411	0.120	0.037	0.038	0.121	0.035
146	87	215.9733	0.370	2.070	0.016	0.411	0.123	0.028	0.030	0.121	0.036
147	223	215.9733	0.370	2.070	0.016	0.411	0.123	0.028	0.030	0.121	0.036
148	126	222.8766	0.363	2.087	0.011	0.412	0.124	0.012	0.006	0.121	0.036
149	260	222.8766	0.363	2.088	0.011	0.412	0.124	0.012	0.006	0.121	0.036
150	3	228.5562	0.341	1.930	0.022	0.410	0.186	0.032	0.078	0.121	0.055
151	59	228.5562	0.337	1.927	0.021	0.411	0.187	0.032	0.067	0.121	0.055
152	195	228.5562	0.337	1.927	0.021	0.411	0.187	0.032	0.067	0.121	0.055
153	12	254.7139	0.377	2.006	0.017	0.409	0.150	0.023	0.049	0.120	0.044
154	68	254.7139	0.373	2.006	0.016	0.410	0.150	0.023	0.039	0.120	0.044
155	204	254.7139	0.373	2.006	0.016	0.410	0.150	0.023	0.038	0.120	0.044
156	36	264.5698	0.389	2.069	0.011	0.410	0.114	0.009	0.007	0.121	0.033
157	92	264.5698	0.385	2.081	0.010	0.411	0.115	0.009	0.002	0.121	0.034
158	228	264.5698	0.385	2.081	0.010	0.411	0.115	0.009	0.002	0.121	0.034
159	32	333.6127	0.415	2.072	0.009	0.409	0.113	0.008	0.000	0.120	0.033
160	88	333.6127	0.412	2.083	0.008	0.409	0.110	0.008	0.000	0.120	0.032
161	224	333.6127	0.412	2.083	0.008	0.409	0.110	0.008	0.000	0.120	0.032
162	23	333.8201	0.422	2.073	0.011	0.408	0.117	0.012	0.012	0.120	0.034
163	79	333.8201	0.418	2.072	0.010	0.408	0.117	0.012	0.006	0.120	0.034
164	215	333.8201	0.418	2.072	0.010	0.408	0.117	0.012	0.006	0.120	0.034

#	srf#	$\bar{q}$	$\phi_{1sec}$	$\phi_{2.8sec}$	$\beta_{max}$	$\delta_{a_{max}}$	$\delta_{a_{max}}$	$\delta_{r_{max}}$	$\delta_{r_{max}}$	$\delta_{elev_{max}}$	$\delta_{elev_{max}}$
165	123	357.0172	0.419	2.088	0.008	0.409	0.108	0.007	0.000	0.120	0.032
166	257	357.0172	0.418	2.088	0.008	0.409	0.108	0.007	0.000	0.120	0.032
167	27	416.6143	0.434	2.073	0.008	0.407	0.113	0.007	0.000	0.120	0.033
168	83	416.6143	0.432	2.085	0.007	0.408	0.109	0.007	0.000	0.120	0.032
169	219	416.6143	0.432	2.085	0.007	0.408	0.109	0.007	0.000	0.120	0.032
170	13	499.2391	0.448	2.075	0.010	0.404	0.116	0.010	0.000	0.119	0.034
171	69	499.2391	0.446	2.076	0.009	0.405	0.115	0.010	0.000	0.119	0.034
172	205	499.2391	0.446	2.076	0.009	0.405	0.115	0.010	0.000	0.119	0.034
173	24	503.8640	0.446	2.075	0.007	0.406	0.113	0.007	0.000	0.119	0.033
174	80	503.8640	0.445	2.085	0.007	0.406	0.109	0.007	0.000	0.119	0.032
175	216	503.8640	0.445	2.085	0.007	0.406	0.109	0.007	0.000	0.119	0.032
176	4	514.2514	0.445	2.063	0.011	0.403	0.122	0.014	0.004	0.118	0.036
177	60	514.2514	0.443	2.062	0.011	0.404	0.123	0.014	0.000	0.119	0.036
178	196	514.2514	0.443	2.062	0.011	0.404	0.123	0.014	0.000	0.119	0.036
179	120	551.8250	0.449	2.088	0.007	0.406	0.108	0.009	0.000	0.119	0.032
180	254	551.8250	0.449	2.088	0.007	0.406	0.108	0.008	0.000	0.119	0.032
181	18	618.5337	0.455	2.076	0.007	0.404	0.113	0.011	0.000	0.119	0.033
182	74	618.5337	0.454	2.085	0.007	0.404	0.109	0.013	0.000	0.119	0.032
183	210	618.5337	0.454	2.085	0.007	0.404	0.109	0.012	0.000	0.119	0.032
184	5	699.9532	0.455	2.071	0.009	0.400	0.117	0.011	0.000	0.118	0.034
185	61	699.9532	0.454	2.071	0.008	0.401	0.117	0.014	0.000	0.118	0.034
186	197	699.9532	0.454	2.071	0.008	0.401	0.117	0.013	0.000	0.118	0.034
187	14	771.1717	0.461	2.074	0.007	0.401	0.114	0.018	0.000	0.118	0.034
188	70	771.1717	0.460	2.084	0.006	0.402	0.110	0.021	0.000	0.118	0.032
189	206	771.1717	0.460	2.084	0.006	0.402	0.110	0.020	0.000	0.118	0.032
190	117	825.2729	0.460	2.084	0.006	0.402	0.110	0.023	0.000	0.118	0.032
191	252	825.2729	0.460	2.084	0.006	0.402	0.110	0.022	0.000	0.118	0.032
192	9	954.4603	0.456	2.059	0.006	0.399	0.121	0.023	0.000	0.117	0.036
193	65	954.4603	0.455	2.069	0.006	0.400	0.116	0.027	0.000	0.118	0.034
194	201	954.4603	0.455	2.069	0.006	0.400	0.116	0.026	0.000	0.118	0.034
195	6	1106.2120	0.451	2.045	0.006	0.399	0.127	0.026	0.000	0.117	0.037
196	62	1106.2120	0.449	2.055	0.006	0.399	0.121	0.031	0.000	0.117	0.036
197	198	1106.2120	0.449	2.055	0.006	0.399	0.121	0.030	0.000	0.117	0.036
198	114	1157.0650	0.447	2.051	0.005	0.399	0.123	0.032	0.000	0.117	0.036
199	249	1157.0650	0.447	2.051	0.005	0.399	0.123	0.031	0.000	0.117	0.036



D.3 Lateral Maximum  $P_{cmd}$  Step Input Time Response (Healthy)

#	srf#	$\bar{q}$	$\phi_{1sec}$	$\phi_{2.8sec}$	$\beta_{max}$	$\delta_{amax}$	$\delta_{amax}$	$\delta_{rmax}$	$\delta_{rmax}$	$\delta_{elevmax}$	$\delta_{elevmax}$
1	119	65.4696	9.848	84.197	2.448	18.191	11.659	20.271	17.555	5.348	3.428
2	253	65.4696	9.843	84.215	2.442	18.191	11.657	20.255	17.516	5.348	3.427
3	118	65.5666	9.856	83.255	2.488	18.218	11.866	20.329	19.892	5.356	3.488
4	122	67.0399	10.245	88.908	2.360	18.654	11.386	20.092	14.134	5.484	3.348
5	256	67.0399	10.240	88.928	2.354	18.654	11.384	20.082	14.090	5.484	3.347
6	121	67.4267	10.377	88.645	2.394	18.765	11.518	20.253	15.110	5.517	3.386
7	255	67.4267	10.372	88.665	2.388	18.764	11.515	20.242	15.079	5.517	3.386
8	124	67.6717	10.362	90.844	2.316	18.841	11.310	19.907	13.382	5.539	3.325
9	116	68.8746	10.785	88.114	2.518	19.180	12.037	20.565	21.568	5.639	3.539
10	251	68.8746	10.779	88.130	2.512	19.180	12.034	20.553	21.519	5.639	3.538
11	115	70.9929	11.365	90.623	2.553	19.796	12.271	20.658	23.515	5.820	3.608
12	10	74.2746	12.197	94.991	2.620	20.743	12.859	22.335	21.664	6.098	3.781
13	66	74.2746	12.382	97.560	2.491	20.753	12.005	20.858	20.522	6.101	3.530
14	202	74.2746	12.376	97.574	2.485	20.752	12.003	20.851	20.475	6.101	3.529
15	113	75.5664	12.685	97.403	2.563	21.125	12.491	20.815	24.405	6.211	3.672
16	250	77.0323	13.160	100.912	2.511	21.552	12.271	20.921	22.196	6.336	3.608
17	258	77.2143	12.984	106.967	2.189	21.621	11.555	19.963	11.681	6.357	3.397
18	125	77.2914	12.944	108.249	2.145	21.646	11.473	19.710	11.416	6.364	3.373
19	259	77.2914	12.938	108.268	2.140	21.646	11.471	19.714	11.372	6.364	3.373
20	37	80.2356	13.851	112.388	2.212	22.492	11.795	21.157	11.725	6.613	3.468
21	93	80.2356	14.161	114.471	2.128	22.497	11.196	20.043	11.124	6.614	3.292
22	229	80.2356	14.155	114.490	2.123	22.496	11.194	20.053	11.083	6.614	3.291
23	15	80.3692	13.968	105.949	2.461	22.515	12.754	22.166	18.160	6.619	3.750
24	71	80.3692	14.100	107.763	2.325	22.526	12.096	20.537	17.329	6.623	3.556
25	207	80.3692	14.094	107.778	2.320	22.525	12.093	20.541	17.289	6.622	3.555
26	33	80.5349	13.972	111.390	2.262	22.575	11.974	21.471	12.039	6.637	3.520
27	89	80.5349	14.244	113.435	2.168	22.582	11.358	20.221	11.342	6.639	3.339
28	225	80.5349	14.238	113.452	2.163	22.581	11.356	20.228	11.298	6.639	3.339
29	28	81.4969	14.353	111.948	2.304	22.851	12.086	21.798	12.404	6.718	3.553
30	84	81.4969	14.586	113.878	2.199	22.858	11.473	20.410	12.140	6.720	3.373
31	220	81.4969	14.580	113.894	2.194	22.858	11.472	20.418	12.116	6.720	3.373
32	1	82.2802	14.442	105.752	2.655	23.063	13.542	22.593	24.513	6.780	3.981
33	57	82.2802	14.532	107.590	2.500	23.075	12.813	20.903	23.128	6.784	3.767
34	193	82.2802	14.527	107.603	2.494	23.075	12.809	20.902	23.072	6.784	3.766
35	7	83.3181	14.811	108.634	2.602	23.366	13.268	22.692	22.403	6.870	3.901
36	63	83.3181	14.915	110.461	2.456	23.378	12.566	21.020	21.219	6.873	3.694
37	199	83.3181	14.910	110.474	2.450	23.378	12.563	21.022	21.168	6.873	3.693
38	19	83.4550	14.970	112.530	2.377	23.411	12.498	22.169	15.752	6.883	3.674
39	75	83.4550	15.141	114.275	2.253	23.422	11.876	20.575	15.124	6.886	3.492
40	211	83.4550	15.136	114.289	2.247	23.421	11.873	20.583	15.089	6.886	3.491
41	25	83.7192	15.109	114.507	2.329	23.490	12.236	22.088	13.921	6.906	3.597

#	srf#	$\bar{q}$	$\phi_{1sec}$	$\phi_{2.8sec}$	$\beta_{max}$	$\delta_{amax}$	$\delta_{amax}$	$\delta_{rmax}$	$\delta_{rmax}$	$\delta_{elevmax}$	$\delta_{elevmax}$
42	81	83.7192	15.321	116.333	2.216	23.500	11.620	20.581	13.476	6.909	3.416
43	217	83.7192	15.315	116.348	2.211	23.499	11.618	20.591	13.446	6.909	3.416
44	34	87.3860	16.738	124.819	2.213	24.550	11.474	22.129	11.317	7.218	3.373
45	90	87.3860	17.033	126.492	2.113	24.558	10.931	20.735	10.635	7.220	3.214
46	226	87.3860	17.027	126.508	2.108	24.557	10.929	20.757	10.598	7.220	3.213
47	127	88.7159	17.945	133.285	1.983	24.949	10.249	19.803	9.788	7.335	3.013
48	261	88.7159	17.939	133.297	1.979	24.949	10.250	19.828	9.758	7.335	3.014
49	38	89.3983	17.932	131.116	2.147	25.124	10.908	22.296	10.879	7.387	3.207
50	94	89.3983	18.189	132.482	2.050	25.134	10.466	20.844	10.232	7.390	3.077
51	230	89.3983	18.182	132.495	2.045	25.134	10.466	20.869	10.200	7.389	3.077
52	11	91.6970	17.509	123.894	2.484	25.792	13.015	23.115	18.999	7.583	3.827
53	67	91.6970	17.606	125.154	2.332	25.806	12.462	21.257	17.980	7.587	3.664
54	203	91.6970	17.600	125.164	2.326	25.806	12.459	21.270	17.937	7.587	3.663
55	41	94.3473	19.919	141.797	2.019	26.570	10.496	20.992	9.822	7.812	3.086
56	97	94.3473	20.029	142.987	1.919	26.586	10.191	19.344	9.127	7.816	2.996
57	233	94.3473	20.024	142.995	1.915	26.586	10.193	19.374	9.101	7.816	2.997
58	262	101.0962	22.090	155.562	1.727	28.574	10.318	16.814	7.548	8.401	3.034
59	16	102.4478	21.142	141.631	2.227	28.896	12.890	22.153	15.268	8.495	3.790
60	72	102.4478	21.117	142.319	2.091	28.919	12.529	20.149	14.427	8.502	3.684
61	208	102.4478	21.111	142.326	2.086	28.918	12.527	20.182	14.391	8.502	3.683
62	263	103.7392	23.297	160.097	1.698	29.337	10.244	16.648	7.300	8.625	3.012
63	42	106.1299	24.461	161.457	1.899	29.986	10.416	20.145	8.621	8.816	3.062
64	98	106.1299	24.567	162.242	1.781	30.004	10.217	18.326	7.860	8.821	3.004
65	234	106.1299	24.565	162.248	1.776	30.003	10.218	18.369	7.843	8.821	3.004
66	264	106.4162	24.628	164.670	1.667	30.108	10.133	16.484	7.051	8.852	2.979
67	20	109.0025	23.811	154.280	2.118	30.786	12.426	22.041	12.911	9.051	3.653
68	76	109.0025	23.779	154.818	1.989	30.811	12.140	20.014	12.191	9.058	3.569
69	212	109.0025	23.772	154.824	1.985	30.810	12.139	20.056	12.160	9.058	3.569
70	46	109.1273	25.631	168.491	1.764	30.880	10.280	17.941	7.548	9.079	3.022
71	102	109.1273	26.008	169.186	1.639	30.888	10.031	16.252	6.815	9.081	2.949
72	238	109.1273	26.011	169.190	1.635	30.888	10.030	16.302	6.803	9.081	2.949
73	29	110.1905	25.338	161.212	2.037	31.121	11.354	22.280	10.065	9.150	3.338
74	85	110.1905	25.349	161.816	1.918	31.146	11.112	20.305	9.532	9.157	3.267
75	221	110.1905	25.342	161.821	1.914	31.145	11.113	20.353	9.507	9.157	3.267
76	8	110.9265	23.105	150.152	2.274	31.344	14.345	22.020	18.024	9.215	4.217
77	64	110.9265	23.002	150.444	2.120	31.371	14.019	19.806	16.875	9.223	4.122
78	200	110.9265	22.996	150.450	2.116	31.371	14.016	19.840	16.833	9.223	4.121
79	47	111.8726	27.139	172.989	1.721	31.666	10.118	17.747	7.275	9.310	2.975
80	103	111.8726	27.500	173.490	1.597	31.674	9.907	16.045	6.561	9.312	2.913
81	239	111.8726	27.504	173.493	1.593	31.673	9.906	16.098	6.551	9.312	2.912
82	48	114.6519	28.714	177.459	1.675	32.459	9.958	17.545	7.002	9.543	2.928

#	srf#	$\bar{q}$	$\phi_{1sec}$	$\phi_{2.8sec}$	$\beta_{max}$	$\delta_{a_{max}}$	$\delta_{a_{max}}$	$\delta_{r_{max}}$	$\delta_{r_{max}}$	$\delta_{elev_{max}}$	$\delta_{elev_{max}}$
83	104	114.6519	29.072	177.821	1.554	32.468	9.776	15.820	6.307	9.545	2.874
84	240	114.6519	29.076	177.823	1.550	32.467	9.774	15.877	6.300	9.545	2.874
85	49	117.4653	30.357	181.923	1.628	33.260	9.798	17.335	6.730	9.778	2.881
86	105	117.4653	30.726	182.191	1.509	33.268	9.638	15.584	6.053	9.781	2.834
87	241	117.4653	30.730	182.192	1.506	33.267	9.636	15.649	6.048	9.781	2.833
88	50	120.3129	32.071	186.403	1.579	34.067	9.639	17.104	6.459	10.016	2.834
89	106	120.3129	32.463	186.608	1.464	34.076	9.496	15.332	5.800	10.018	2.792
90	242	120.3129	32.468	186.609	1.461	34.075	9.494	15.401	5.797	10.018	2.791
91	43	121.8328	32.150	187.673	1.726	34.497	9.917	18.936	7.174	10.142	2.916
92	99	121.8328	32.262	187.798	1.599	34.514	9.857	16.950	6.435	10.147	2.898
93	235	121.8328	32.261	187.799	1.595	34.514	9.858	17.016	6.431	10.147	2.898
94	51	123.1945	33.858	190.917	1.529	34.881	9.479	16.868	6.191	10.255	2.787
95	107	123.1945	33.815	190.960	1.430	34.904	9.522	14.949	5.548	10.262	2.800
96	243	123.1945	33.810	190.958	1.426	34.903	9.524	15.021	5.548	10.261	2.800
97	52	126.1103	35.441	195.391	1.488	35.710	9.421	16.563	5.938	10.499	2.770
98	108	126.1103	35.139	195.339	1.394	35.742	9.574	14.489	5.279	10.508	2.815
99	244	126.1103	35.134	195.336	1.390	35.742	9.575	14.564	5.281	10.508	2.815
100	53	129.0601	36.745	199.775	1.447	36.557	9.479	16.066	5.651	10.748	2.787
101	109	129.0601	36.474	199.757	1.355	36.591	9.633	13.945	4.992	10.758	2.832
102	245	129.0601	36.469	199.754	1.352	36.590	9.635	14.021	4.995	10.757	2.833
103	2	129.4213	29.100	176.673	2.153	36.662	16.034	20.935	17.144	10.779	4.714
104	58	129.4213	29.223	177.437	2.027	36.692	15.724	18.781	16.144	10.787	4.623
105	194	129.4213	29.217	177.444	2.024	36.691	15.723	18.842	16.104	10.787	4.623
106	17	129.8252	31.467	185.478	1.989	36.763	12.801	21.228	12.414	10.808	3.764
107	73	129.8252	31.565	186.120	1.868	36.794	12.471	19.056	11.680	10.817	3.667
108	209	129.8252	31.559	186.125	1.864	36.793	12.470	19.126	11.650	10.817	3.666
109	30	129.9582	34.174	193.790	1.877	36.775	10.873	21.792	8.559	10.812	3.197
110	86	129.9582	34.274	194.316	1.754	36.807	10.703	19.564	8.022	10.821	3.147
111	222	129.9582	34.267	194.319	1.751	36.806	10.706	19.648	8.001	10.821	3.147
112	26	130.0074	33.237	191.252	1.912	36.801	11.473	21.613	9.730	10.819	3.373
113	82	130.0074	33.332	191.815	1.790	36.832	11.252	19.397	9.132	10.829	3.308
114	218	130.0074	33.326	191.819	1.787	36.831	11.254	19.475	9.107	10.828	3.309
115	35	130.0653	35.155	196.357	1.829	36.799	10.345	21.599	7.754	10.819	3.041
116	91	130.0653	35.260	196.841	1.707	36.830	10.231	19.400	7.000	10.828	3.008
117	227	130.0653	35.253	196.844	1.704	36.830	10.235	19.488	6.997	10.828	3.009
118	21	130.1006	32.407	188.709	1.946	36.836	12.101	21.402	10.985	10.830	3.558
119	77	130.1006	32.502	189.305	1.825	36.867	11.830	19.198	10.320	10.839	3.478
120	213	130.1006	32.495	189.309	1.821	36.866	11.831	19.272	10.293	10.839	3.478
121	44	131.7744	37.545	203.620	1.609	37.331	9.692	18.025	6.332	10.975	2.849
122	100	131.7744	37.068	203.328	1.502	37.364	9.882	16.005	5.672	10.985	2.905
123	236	131.7744	37.062	203.326	1.499	37.363	9.884	16.092	5.674	10.985	2.906

#	srf#	$\bar{q}$	$\phi_{1sec}$	$\phi_{2.8sec}$	$\beta_{max}$	$\delta_{amax}$	$\delta_{amax}$	$\delta_{rmax}$	$\delta_{rmax}$	$\delta_{elevmax}$	$\delta_{elevmax}$
124	54	132.0441	38.058	204.199	1.404	37.413	9.545	15.484	5.345	10.999	2.806
125	110	132.0441	37.821	204.218	1.314	37.449	9.702	13.314	4.685	11.010	2.852
126	246	132.0441	37.815	204.215	1.311	37.448	9.703	13.392	4.690	11.010	2.853
127	39	134.8266	38.283	206.404	1.683	38.182	9.910	19.413	6.753	11.226	2.913
128	95	134.8266	38.089	206.416	1.571	38.215	10.004	17.340	6.066	11.235	2.941
129	231	134.8266	38.083	206.416	1.568	38.214	10.007	17.432	6.068	11.235	2.942
130	55	135.0621	39.379	208.663	1.359	38.280	9.620	14.809	5.021	11.254	2.828
131	111	135.0621	39.178	208.725	1.272	38.318	9.779	12.597	4.361	11.265	2.875
132	247	135.0621	39.172	208.722	1.269	38.317	9.780	12.680	4.368	11.265	2.875
133	56	138.1142	40.710	213.170	1.313	39.156	9.702	14.042	4.681	11.512	2.852
134	112	138.1142	40.545	213.280	1.227	39.196	9.865	11.801	4.021	11.524	2.900
135	248	138.1142	40.540	213.277	1.224	39.195	9.866	11.888	4.029	11.523	2.901
136	45	167.7286	53.348	256.314	1.967	47.614	10.509	5.932	2.018	13.999	3.090
137	101	167.7286	53.172	256.843	1.842	47.672	10.758	4.547	1.682	14.015	3.163
138	237	167.7286	53.160	256.845	1.837	47.671	10.757	4.629	1.669	14.015	3.163
139	22	170.3164	51.241	252.886	2.769	48.229	11.929	10.740	7.114	14.179	3.507
140	78	170.3164	51.259	253.527	2.560	48.283	11.714	9.151	6.228	14.195	3.444
141	214	170.3164	51.247	253.532	2.554	48.282	11.713	9.247	6.201	14.195	3.444
142	40	208.2658	70.319	318.593	1.915	59.123	11.895	3.679	1.559	17.382	3.497
143	96	208.2658	70.133	319.242	1.795	59.212	12.203	2.396	1.166	17.408	3.588
144	232	208.2658	70.119	319.243	1.790	59.210	12.201	2.462	1.150	17.408	3.587
145	31	215.9733	74.471	330.990	2.365	60.000	11.532	7.218	3.503	17.957	3.390
146	87	215.9733	73.852	330.579	2.179	60.000	11.850	5.454	2.858	17.988	3.484
147	223	215.9733	73.838	330.578	2.173	60.000	11.848	5.579	2.837	17.988	3.483
148	126	222.8766	76.324	342.121	1.683	60.000	12.814	1.124	0.605	18.636	3.767
149	260	222.8766	76.310	342.122	1.678	60.000	12.812	1.128	0.590	18.635	3.767
150	3	228.5562	72.151	336.858	3.085	60.000	17.869	6.587	8.013	18.983	5.253
151	59	228.5562	71.801	336.396	2.951	60.000	17.887	4.851	7.097	19.015	5.259
152	195	228.5562	71.791	336.399	2.946	60.000	17.886	4.958	7.059	19.015	5.259
153	12	254.7139	85.195	378.355	2.763	60.000	15.802	5.401	5.530	20.805	4.646
154	68	254.7139	84.897	378.188	2.593	60.000	15.778	3.614	4.505	20.846	4.639
155	204	254.7139	84.886	378.190	2.588	60.000	15.777	3.713	4.473	20.845	4.639
156	36	264.5698	89.483	388.044	1.831	60.000	13.345	1.439	0.736	21.109	3.923
157	92	264.5698	89.508	389.041	1.710	60.000	13.671	1.054	0.262	21.146	4.019
158	228	264.5698	89.494	389.042	1.706	60.000	13.669	1.052	0.246	21.145	4.019
159	32	333.6127	98.002	413.065	1.640	60.000	13.187	2.121	0.000	22.341	3.877
160	88	333.6127	98.198	414.248	1.541	60.000	13.491	2.392	0.000	22.387	3.966
161	224	333.6127	98.188	414.248	1.538	60.000	13.488	2.183	0.000	22.386	3.965
162	23	333.8201	98.357	413.505	2.032	60.000	13.269	1.598	1.425	22.227	3.901
163	79	333.8201	98.072	413.315	1.910	60.000	13.293	1.482	0.757	22.280	3.908
164	215	333.8201	98.064	413.315	1.906	60.000	13.294	1.446	0.737	22.279	3.908

#	srf#	$\bar{q}$	$\phi_{1sec}$	$\phi_{2.8sec}$	$\beta_{max}$	$\delta_{a_{max}}$	$\delta_{a_{max}}$	$\delta_{r_{max}}$	$\delta_{r_{max}}$	$\delta_{elev_{max}}$	$\delta_{elev_{max}}$
165	123	357.0172	100.992	423.158	1.451	60.000	13.586	3.321	0.000	22.823	3.994
166	257	357.0172	100.984	423.159	1.448	60.000	13.583	3.094	0.000	22.822	3.993
167	27	416.6143	105.294	437.079	1.547	60.000	13.600	4.856	0.000	23.494	3.998
168	83	416.6143	105.668	438.483	1.466	60.000	13.404	5.426	0.000	23.547	3.941
169	219	416.6143	105.664	438.484	1.463	60.000	13.400	5.153	0.000	23.546	3.940
170	13	499.2391	106.162	437.211	1.783	60.000	13.985	6.316	0.000	23.271	4.111
171	69	499.2391	106.077	437.212	1.711	60.000	13.945	7.235	0.000	23.316	4.100
172	205	499.2391	106.077	437.212	1.709	60.000	13.945	6.902	0.000	23.315	4.100
173	24	503.8640	106.179	437.078	1.454	60.000	13.634	7.613	0.000	23.373	4.008
174	80	503.8640	106.474	438.289	1.387	60.000	13.240	8.336	0.000	23.413	3.893
175	216	503.8640	106.474	438.290	1.385	60.000	13.240	8.027	0.000	23.412	3.893
176	4	514.2514	105.443	435.827	2.039	60.000	14.838	5.728	0.607	23.187	4.362
177	60	514.2514	105.261	435.588	1.950	60.000	14.875	6.581	0.000	23.236	4.373
178	196	514.2514	105.260	435.588	1.947	60.000	14.875	6.236	0.000	23.235	4.373
179	120	551.8250	106.868	438.548	1.274	60.000	13.094	9.973	0.000	23.380	3.850
180	254	551.8250	106.868	438.548	1.272	60.000	13.093	9.653	0.000	23.379	3.849
181	18	618.5337	106.840	436.967	1.366	60.000	13.685	11.233	0.000	23.234	4.024
182	74	618.5337	107.072	438.139	1.307	60.000	13.274	12.078	0.000	23.280	3.903
183	210	618.5337	107.072	438.139	1.305	60.000	13.274	11.729	0.000	23.279	3.903
184	5	699.9532	106.595	436.452	1.623	60.000	14.215	12.314	0.000	23.025	4.179
185	61	699.9532	106.472	436.305	1.569	60.000	14.232	13.440	0.000	23.081	4.184
186	197	699.9532	106.471	436.304	1.567	60.000	14.232	13.046	0.000	23.080	4.184
187	14	771.1717	107.186	436.517	1.278	60.000	13.865	15.185	0.000	23.072	4.076
188	70	771.1717	107.402	437.832	1.223	60.000	13.377	16.077	0.000	23.126	3.933
189	206	771.1717	107.400	437.832	1.222	60.000	13.377	15.690	0.000	23.125	3.933
190	117	825.2729	107.425	437.783	1.151	60.000	13.371	17.391	0.000	23.101	3.931
191	252	825.2729	107.423	437.783	1.149	60.000	13.371	16.986	0.000	23.100	3.931
192	9	954.4603	106.254	434.445	1.202	60.000	14.711	18.435	0.000	22.952	4.325
193	65	954.4603	106.420	435.948	1.147	60.000	14.111	19.351	0.000	23.011	4.149
194	201	954.4603	106.418	435.947	1.146	60.000	14.111	18.947	0.000	23.010	4.149
195	6	1106.2120	105.258	432.612	1.164	60.000	15.475	20.369	0.000	22.870	4.550
196	62	1106.2120	105.361	434.120	1.111	60.000	14.835	21.322	0.000	22.932	4.362
197	198	1106.2120	105.360	434.119	1.110	60.000	14.836	20.907	0.000	22.931	4.362
198	114	1157.0650	104.981	433.566	1.065	60.000	15.043	21.680	0.000	22.930	4.423
199	249	1157.0650	104.980	433.565	1.063	60.000	15.043	21.265	0.000	22.929	4.423

D.4 Lateral Maximum  $P_{cmd}$  Step Input Time Response (45% Triple Failure)

#	srf#	$\bar{q}$	$\phi_{1sec}$	$\phi_{2.8sec}$	$\beta_{max}$	$\delta_{amax}$	$\delta_{amax}$	$\delta_{rmax}$	$\delta_{rmax}$	$\delta_{elevmax}$	$\delta_{elevmax}$
1	119	65.4696	6.348	58.790	2.708	18.260	19.417	17.895	30.000	5.368	5.709
2	253	65.4696	6.346	58.814	2.700	18.260	19.408	17.853	30.000	5.368	5.706
3	118	65.5666	6.356	58.018	2.757	18.288	19.873	17.958	30.000	5.377	5.843
4	122	67.0399	6.614	62.905	2.613	18.724	18.760	17.674	26.581	5.505	5.515
5	256	67.0399	6.612	62.933	2.604	18.724	18.751	17.636	26.506	5.505	5.513
6	121	67.4267	6.703	62.766	2.655	18.837	19.082	17.806	29.346	5.538	5.610
7	255	67.4267	6.701	62.794	2.646	18.837	19.073	17.767	29.263	5.538	5.607
8	124	67.6717	6.697	64.576	2.565	18.912	18.529	17.497	24.050	5.560	5.448
9	116	68.8746	6.977	62.592	2.825	19.259	20.000	18.161	30.000	5.662	5.975
10	251	68.8746	6.974	62.616	2.816	19.259	20.000	18.116	30.000	5.662	5.972
11	115	70.9929	7.366	64.944	3.451	19.880	20.000	18.259	30.000	5.845	6.191
12	10	74.2746	8.003	66.674	3.361	20.839	20.000	19.507	30.000	6.127	6.726
13	66	74.2746	8.054	71.513	2.831	20.845	20.000	18.324	30.000	6.128	5.961
14	202	74.2746	8.051	71.538	2.821	20.844	20.000	18.282	30.000	6.128	5.958
15	113	75.5664	8.254	71.208	3.479	21.222	20.000	18.361	30.000	6.239	6.429
16	250	77.0323	8.580	74.644	2.877	21.653	20.000	18.333	30.000	6.366	6.194
17	258	77.2143	8.522	79.939	2.440	21.715	18.896	17.087	19.620	6.384	5.556
18	125	77.2914	8.515	81.030	2.387	21.739	18.620	16.872	17.838	6.391	5.474
19	259	77.2914	8.512	81.061	2.379	21.739	18.613	16.847	17.772	6.391	5.472
20	37	80.2356	9.221	84.065	2.469	22.597	19.371	17.953	18.964	6.644	5.695
21	93	80.2356	9.363	87.579	2.387	22.600	18.209	17.050	16.524	6.644	5.354
22	229	80.2356	9.360	87.611	2.379	22.600	18.202	17.028	16.462	6.644	5.351
23	15	80.3692	9.225	76.780	2.789	22.628	20.000	18.978	30.000	6.653	6.580
24	71	80.3692	9.251	81.085	2.634	22.633	20.000	17.628	29.526	6.654	5.985
25	207	80.3692	9.248	81.118	2.626	22.633	20.000	17.597	29.444	6.654	5.981
26	33	80.5349	9.284	83.054	2.531	22.683	19.840	18.227	20.601	6.669	5.833
27	89	80.5349	9.400	86.603	2.436	22.687	18.616	17.213	18.583	6.670	5.473
28	225	80.5349	9.398	86.636	2.428	22.686	18.608	17.190	18.533	6.670	5.471
29	28	81.4969	9.533	83.570	2.589	22.963	20.000	18.496	22.750	6.751	5.938
30	84	81.4969	9.623	87.147	2.478	22.967	18.939	17.364	20.851	6.752	5.568
31	220	81.4969	9.620	87.178	2.470	22.967	18.930	17.339	20.794	6.752	5.566
32	1	82.2802	9.538	75.653	3.201	23.184	20.000	19.574	30.000	6.816	7.000
33	57	82.2802	9.538	80.334	2.885	23.191	20.000	18.165	30.000	6.818	6.722
34	193	82.2802	9.535	80.364	2.875	23.191	20.000	18.127	30.000	6.818	6.718
35	7	83.3181	9.801	78.664	2.994	23.489	20.000	19.570	30.000	6.906	7.000
36	63	83.3181	9.807	83.341	2.828	23.496	20.000	18.179	30.000	6.908	6.426
37	199	83.3181	9.804	83.371	2.819	23.496	20.000	18.143	30.000	6.908	6.422
38	19	83.4550	9.942	83.482	2.693	23.533	20.000	18.797	28.034	6.919	6.320
39	75	83.4550	9.990	87.626	2.555	23.538	19.852	17.495	25.674	6.920	5.837
40	211	83.4550	9.987	87.656	2.546	23.538	19.842	17.469	25.599	6.920	5.834
41	25	83.7191	10.052	85.880	2.633	23.611	20.000	18.681	24.865	6.942	6.083

#	srf#	$\bar{q}$	$\phi_{1sec}$	$\phi_{2.8sec}$	$\beta_{max}$	$\delta_{a_{max}}$	$\delta_{a_{max}}$	$\delta_{r_{max}}$	$\delta_{r_{max}}$	$\delta_{elev_{max}}$	$\delta_{elev_{max}}$
42	81	83.7191	10.126	89.726	2.511	23.617	19.314	17.460	22.868	6.943	5.678
43	217	83.7191	10.123	89.756	2.502	23.616	19.305	17.435	22.804	6.943	5.676
44	34	87.3860	11.245	97.290	2.518	24.684	19.098	18.535	18.099	7.257	5.615
45	90	87.3860	11.369	100.719	2.407	24.688	17.978	17.395	16.941	7.258	5.286
46	226	87.3860	11.366	100.753	2.399	24.688	17.971	17.379	16.897	7.258	5.283
47	127	88.7159	11.963	108.774	2.268	25.081	16.599	16.600	13.369	7.374	4.880
48	261	88.7159	11.960	108.806	2.261	25.081	16.596	16.591	13.312	7.374	4.879
49	38	89.3983	12.127	104.577	2.458	25.269	18.058	18.551	15.253	7.429	5.309
50	94	89.3983	12.209	107.658	2.344	25.274	17.119	17.353	14.028	7.431	5.033
51	230	89.3983	12.205	107.691	2.336	25.274	17.114	17.344	13.994	7.431	5.032
52	11	91.6970	11.720	93.552	2.872	25.943	20.000	19.488	30.000	7.627	6.881
53	67	91.6970	11.711	97.710	2.687	25.950	20.000	17.937	29.919	7.629	6.287
54	203	91.6970	11.708	97.743	2.678	25.950	20.000	17.911	29.821	7.629	6.283
55	41	94.3473	13.404	116.605	2.334	26.725	17.282	17.498	13.731	7.857	5.081
56	97	94.3473	13.351	119.619	2.204	26.734	16.476	16.098	12.429	7.860	4.844
57	233	94.3473	13.348	119.648	2.197	26.733	16.474	16.094	12.377	7.860	4.843
58	262	101.0962	14.575	133.644	1.975	28.728	16.374	13.966	10.299	8.446	4.814
59	16	102.4478	14.301	111.231	2.572	29.085	20.000	18.163	25.785	8.551	6.760
60	72	102.4478	14.171	114.442	2.402	29.098	20.000	16.567	23.790	8.555	6.338
61	208	102.4478	14.167	114.476	2.394	29.097	20.000	16.556	23.712	8.555	6.334
62	263	103.7392	15.409	139.149	1.946	29.501	16.229	13.785	9.960	8.673	4.771
63	42	106.1299	16.503	138.765	2.212	30.177	17.074	16.577	12.005	8.872	5.020
64	98	106.1299	16.442	141.391	2.050	30.186	16.439	15.000	10.612	8.875	4.833
65	234	106.1299	16.442	141.422	2.044	30.186	16.438	15.008	10.573	8.875	4.833
66	264	106.4162	16.340	144.893	1.917	30.282	16.024	13.604	9.623	8.903	4.711
67	20	109.0025	16.197	125.746	2.453	31.000	20.000	17.852	21.544	9.114	6.330
68	76	109.0025	16.048	128.730	2.287	31.014	20.000	16.235	20.195	9.118	6.024
69	212	109.0025	16.044	128.763	2.279	31.013	20.000	16.235	20.137	9.118	6.021
70	46	109.1273	17.151	147.726	2.056	31.069	16.469	14.877	10.621	9.134	4.842
71	102	109.1273	17.311	150.567	1.892	31.073	15.834	13.401	9.314	9.136	4.655
72	238	109.1273	17.315	150.602	1.886	31.073	15.831	13.413	9.282	9.135	4.654
73	29	110.1905	17.318	136.358	2.371	31.343	19.153	17.990	16.911	9.215	5.631
74	85	110.1905	17.182	138.434	2.211	31.357	18.486	16.376	15.888	9.219	5.435
75	221	110.1905	17.177	138.457	2.204	31.356	18.482	16.383	15.843	9.219	5.434
76	8	110.9265	15.665	114.165	2.568	31.564	20.000	17.803	25.769	9.280	7.000
77	64	110.9265	15.486	116.837	2.393	31.578	20.000	16.087	24.068	9.284	7.000
78	200	110.9265	15.481	116.869	2.385	31.578	20.000	16.079	24.001	9.284	7.000
79	47	111.8726	18.219	153.546	2.007	31.867	16.208	14.626	10.153	9.369	4.765
80	103	111.8726	18.372	156.026	1.846	31.872	15.652	13.156	8.911	9.370	4.602
81	239	111.8726	18.377	156.061	1.840	31.872	15.650	13.172	8.882	9.370	4.601
82	48	114.6519	19.351	159.327	1.956	32.675	15.950	14.368	9.690	9.606	4.689

#	srf#	$\bar{q}$	$\phi_{1sec}$	$\phi_{2.8sec}$	$\beta_{max}$	$\delta_{a_{max}}$	$\delta_{a_{max}}$	$\delta_{r_{max}}$	$\delta_{r_{max}}$	$\delta_{elev_{max}}$	$\delta_{elev_{max}}$
83	104	114.6519	19.507	161.545	1.799	32.680	15.449	12.906	8.513	9.608	4.542
84	240	114.6519	19.513	161.579	1.793	32.679	15.447	12.926	8.488	9.608	4.541
85	49	117.4653	20.552	165.078	1.903	33.491	15.691	14.105	9.233	9.846	4.613
86	105	117.4653	20.721	167.116	1.751	33.496	15.225	12.649	8.121	9.848	4.476
87	241	117.4653	20.727	167.150	1.745	33.495	15.224	12.674	8.099	9.848	4.476
88	50	120.3129	21.826	170.805	1.849	34.315	15.426	13.836	8.787	10.089	4.535
89	106	120.3129	22.018	172.729	1.702	34.320	14.981	12.385	7.737	10.090	4.404
90	242	120.3129	22.024	172.762	1.697	34.320	14.979	12.414	7.718	10.090	4.404
91	43	121.8328	22.031	170.781	2.041	34.754	15.940	15.352	9.954	10.218	4.686
92	99	121.8328	21.974	172.181	1.866	34.764	15.657	13.689	8.679	10.221	4.603
93	235	121.8328	21.975	172.206	1.861	34.764	15.658	13.717	8.656	10.221	4.603
94	51	123.1945	23.179	176.513	1.793	35.148	15.153	13.561	8.353	10.333	4.455
95	107	123.1945	23.002	177.613	1.660	35.160	15.002	12.044	7.376	10.337	4.411
96	243	123.1945	23.000	177.628	1.655	35.160	15.007	12.076	7.360	10.337	4.412
97	52	126.1103	24.374	181.721	1.745	35.993	15.044	13.263	7.967	10.582	4.423
98	108	126.1103	23.965	182.427	1.616	36.011	15.056	11.643	7.000	10.587	4.426
99	244	126.1103	23.963	182.442	1.611	36.010	15.060	11.678	6.987	10.587	4.428
100	53	129.0601	25.335	186.375	1.693	36.852	15.129	12.826	7.547	10.835	4.448
101	109	129.0601	24.941	187.245	1.569	36.871	15.115	11.187	6.606	10.840	4.444
102	245	129.0601	24.938	187.260	1.564	36.871	15.119	11.223	6.595	10.840	4.445
103	2	129.4213	19.958	133.629	2.339	36.957	20.000	16.540	22.278	10.866	7.000
104	58	129.4213	19.948	137.383	2.215	36.974	20.000	14.992	21.350	10.870	7.000
105	194	129.4213	19.943	137.415	2.208	36.974	20.000	15.002	21.292	10.870	7.000
106	17	129.8252	21.747	155.394	2.307	37.067	20.000	16.799	19.900	10.898	7.000
107	73	129.8252	21.690	158.873	2.161	37.085	20.000	15.173	18.982	10.903	6.411
108	209	129.8252	21.686	158.905	2.154	37.084	20.000	15.194	18.928	10.903	6.407
109	30	129.9582	23.847	172.563	2.217	37.092	18.366	17.266	14.815	10.905	5.400
110	86	129.9582	23.757	174.541	2.048	37.110	17.781	15.499	13.789	10.910	5.227
111	222	129.9582	23.751	174.561	2.042	37.109	17.780	15.530	13.746	10.910	5.227
112	26	130.0074	23.108	168.243	2.247	37.112	19.495	17.114	16.684	10.911	5.732
113	82	130.0074	23.027	170.158	2.084	37.130	18.863	15.392	15.529	10.916	5.546
114	218	130.0074	23.022	170.178	2.078	37.129	18.860	15.421	15.481	10.916	5.545
115	35	130.0653	24.599	177.059	2.170	37.119	17.322	17.141	12.905	10.913	5.093
116	91	130.0653	24.500	179.091	1.998	37.137	16.799	15.357	12.024	10.918	4.939
117	227	130.0653	24.495	179.111	1.993	37.136	16.801	15.392	11.987	10.918	4.939
118	21	130.1006	22.463	163.076	2.276	37.144	20.000	16.938	18.640	10.920	6.132
119	77	130.1006	22.393	165.989	2.119	37.161	19.984	15.258	17.393	10.925	5.875
120	213	130.1006	22.388	166.008	2.113	37.161	19.979	15.284	17.340	10.925	5.874
121	44	131.7744	26.079	190.060	1.915	37.641	15.328	14.472	8.721	11.066	4.506
122	100	131.7744	25.519	189.792	1.756	37.659	15.565	12.824	7.620	11.072	4.576
123	236	131.7744	25.516	189.806	1.751	37.658	15.569	12.863	7.605	11.072	4.577

#	srf#	$\bar{q}$	$\phi_{1sec}$	$\phi_{2.8sec}$	$\beta_{max}$	$\delta_{amax}$	$\delta_{amax}$	$\delta_{rmax}$	$\delta_{rmax}$	$\delta_{elevmax}$	$\delta_{elevmax}$
124	54	132.0441	26.305	191.032	1.639	37.722	15.218	12.327	7.112	11.090	4.474
125	110	132.0441	25.928	192.070	1.518	37.742	15.181	10.670	6.194	11.096	4.463
126	246	132.0441	25.926	192.084	1.514	37.741	15.185	10.711	6.185	11.096	4.464
127	39	134.8266	26.802	190.762	2.006	38.516	16.057	15.480	9.761	11.324	4.721
128	95	134.8266	26.457	191.494	1.842	38.534	16.012	13.780	9.124	11.329	4.708
129	231	134.8266	26.454	191.511	1.837	38.534	16.017	13.824	9.094	11.329	4.709
130	55	135.0621	27.286	195.696	1.581	38.601	15.310	11.770	6.663	11.349	4.501
131	111	135.0621	26.927	196.904	1.465	38.622	15.254	10.098	5.765	11.355	4.485
132	247	135.0621	26.925	196.918	1.461	38.622	15.258	10.139	5.759	11.355	4.486
133	56	138.1142	28.277	200.371	1.522	39.491	15.405	11.153	6.200	11.610	4.529
134	112	138.1142	27.936	201.752	1.410	39.513	15.335	9.465	5.320	11.617	4.509
135	248	138.1142	27.933	201.765	1.406	39.513	15.339	9.509	5.317	11.617	4.510
136	45	167.7286	38.416	240.786	2.155	48.097	16.549	4.749	3.485	14.141	4.865
137	101	167.7286	37.892	242.743	1.992	48.129	16.602	3.654	2.856	14.150	4.881
138	237	167.7286	37.887	242.773	1.986	48.128	16.608	3.699	2.831	14.150	4.883
139	22	170.3164	37.427	229.638	3.108	48.779	20.000	8.400	11.312	14.341	6.049
140	78	170.3164	37.157	232.254	2.831	48.809	19.791	7.114	9.719	14.350	5.818
141	214	170.3164	37.150	232.279	2.821	48.809	19.788	7.160	9.668	14.350	5.818
142	40	208.2658	52.297	300.866	2.051	59.839	18.372	2.911	2.648	17.593	5.401
143	96	208.2658	51.606	302.760	1.896	59.888	18.593	2.170	1.913	17.607	5.466
144	232	208.2658	51.598	302.783	1.888	59.887	18.598	2.157	1.884	17.607	5.468
145	31	215.9733	56.828	312.512	2.609	60.000	18.148	5.574	5.756	18.211	5.335
146	87	215.9733	55.776	312.234	2.349	60.000	18.498	4.162	4.517	18.228	5.438
147	223	215.9733	55.764	312.247	2.341	60.000	18.507	4.233	4.477	18.228	5.441
148	126	222.8766	56.553	325.076	1.747	60.000	19.333	1.884	0.981	18.856	5.684
149	260	222.8766	56.543	325.098	1.740	60.000	19.337	1.870	0.953	18.855	5.685
150	3	228.5562	54.188	265.617	2.627	60.000	20.000	5.057	9.738	19.268	7.000
151	59	228.5562	53.484	264.458	2.465	60.000	20.000	3.800	8.549	19.286	7.000
152	195	228.5562	53.472	264.473	2.460	60.000	20.000	3.845	8.498	19.286	7.000
153	12	254.7139	65.990	323.377	2.538	60.000	20.000	4.061	7.367	21.156	7.000
154	68	254.7139	65.151	323.599	2.351	60.000	20.000	3.371	5.875	21.178	7.000
155	204	254.7139	65.136	323.612	2.346	60.000	20.000	3.368	5.828	21.178	7.000
156	36	264.5698	68.899	366.988	1.882	60.000	20.000	1.530	1.178	21.414	6.100
157	92	264.5698	68.071	369.269	1.745	60.000	20.000	1.537	0.391	21.435	6.003
158	228	264.5698	68.057	369.284	1.738	60.000	20.000	1.534	0.361	21.435	6.004
159	32	333.6127	78.171	388.904	1.623	60.000	20.000	1.429	0.000	22.727	7.000
160	88	333.6127	77.595	393.604	1.541	60.000	20.000	1.354	0.000	22.753	6.598
161	224	333.6127	77.581	393.612	1.537	60.000	20.000	1.352	0.000	22.753	6.597
162	23	333.8201	79.577	388.620	2.057	60.000	20.000	2.194	1.931	22.666	7.000
163	79	333.8201	78.762	388.749	1.909	60.000	20.000	2.203	0.804	22.695	7.000
164	215	333.8201	78.748	388.767	1.904	60.000	20.000	2.201	0.769	22.695	7.000

#	srf#	$\bar{q}$	$\phi_{1sec}$	$\phi_{2.8sec}$	$\beta_{max}$	$\delta_{amax}$	$\delta_{amax}$	$\delta_{rmax}$	$\delta_{rmax}$	$\delta_{elevmax}$	$\delta_{elevmax}$
165	123	357.0172	80.436	402.505	1.450	60.000	20.000	1.248	0.000	23.208	6.689
166	257	357.0172	80.423	402.515	1.447	60.000	20.000	1.246	0.000	23.207	6.687
167	27	416.6143	86.467	407.980	1.454	60.000	20.000	1.348	0.000	23.972	7.000
168	83	416.6143	86.121	414.893	1.428	60.000	20.000	1.391	0.000	24.001	7.000
169	219	416.6143	86.108	414.912	1.425	60.000	20.000	1.390	0.000	24.001	7.000
170	13	499.2391	89.428	409.119	1.756	60.000	20.000	2.034	0.000	23.786	7.000
171	69	499.2391	89.054	409.726	1.685	60.000	20.000	2.032	0.000	23.824	7.000
172	205	499.2391	89.044	409.737	1.682	60.000	20.000	2.029	0.000	23.823	7.000
173	24	503.8640	89.013	409.922	1.378	60.000	20.000	1.326	0.000	23.873	7.000
174	80	503.8640	88.727	415.223	1.352	60.000	20.000	1.631	0.000	23.907	7.000
175	216	503.8640	88.716	415.235	1.349	60.000	20.000	1.458	0.000	23.906	7.000
176	4	514.2514	88.853	401.014	2.007	60.000	20.000	2.700	0.898	23.715	7.000
177	60	514.2514	88.454	400.424	1.897	60.000	20.000	2.661	0.000	23.757	7.000
178	196	514.2514	88.445	400.438	1.894	60.000	20.000	2.658	0.000	23.756	7.000
179	120	551.8250	89.597	416.677	1.243	60.000	20.000	2.315	0.000	23.879	7.000
180	254	551.8250	89.587	416.685	1.240	60.000	20.000	2.139	0.000	23.879	7.000
181	18	618.5337	90.901	410.958	1.309	60.000	20.000	2.667	0.000	23.755	7.000
182	74	618.5337	90.670	415.556	1.269	60.000	20.000	3.133	0.000	23.794	7.000
183	210	618.5337	90.662	415.563	1.267	60.000	20.000	2.946	0.000	23.793	7.000
184	5	699.9532	90.956	407.961	1.608	60.000	20.000	2.727	0.000	23.577	7.000
185	61	699.9532	90.686	407.721	1.543	60.000	20.000	3.349	0.000	23.625	7.000
186	197	699.9532	90.681	407.726	1.540	60.000	20.000	3.148	0.000	23.624	7.000
187	14	771.1717	92.011	410.261	1.224	60.000	20.000	4.120	0.000	23.617	7.000
188	70	771.1717	91.813	415.036	1.185	60.000	20.000	4.729	0.000	23.663	7.000
189	206	771.1717	91.809	415.041	1.183	60.000	20.000	4.527	0.000	23.662	7.000
190	117	825.2729	91.920	415.046	1.108	60.000	20.000	5.312	0.000	23.641	7.000
191	252	825.2729	91.916	415.050	1.106	60.000	20.000	5.108	0.000	23.640	7.000
192	9	954.4603	91.160	401.599	1.113	60.000	20.000	5.294	0.000	23.515	7.000
193	65	954.4603	90.873	407.777	1.084	60.000	20.000	6.059	0.000	23.565	7.000
194	201	954.4603	90.871	407.780	1.083	60.000	20.000	5.852	0.000	23.564	7.000
195	6	1106.2120	90.071	391.574	1.041	60.000	20.000	5.956	0.000	23.452	7.000
196	62	1106.2120	89.704	398.163	1.011	60.000	20.000	6.829	0.000	23.498	7.000
197	198	1106.2120	89.703	398.165	1.009	60.000	20.000	6.622	0.000	23.497	7.000
198	114	1157.0650	89.218	394.819	0.951	60.000	20.000	7.001	0.000	23.497	7.000
199	249	1157.0650	89.217	394.821	0.950	60.000	20.000	6.794	0.000	23.496	7.000

*D.5 Lateral Channel Disturbance Time Response*

#	srf#	$\bar{q}$	$\phi_{1sec}$	$\phi_{2.8sec}$	$\beta_{max}$	$\delta_{amax}$	$\delta_{amax}$	$\delta_{rmax}$	$\delta_{rmax}$	$\delta_{elevmax}$	$\delta_{elevmax}$
1	119	65.4696	2.571	6.946	0.445	0.161	0.000	6.558	3.276	0.047	0.000
2	253	65.4696	2.569	6.951	0.444	0.163	0.000	6.576	3.269	0.048	0.000
3	118	65.5666	2.563	6.820	0.448	0.132	0.000	6.632	3.301	0.039	0.000
4	122	67.0399	2.611	7.198	0.428	0.242	0.000	6.341	3.137	0.071	0.000
5	256	67.0399	2.608	7.203	0.428	0.244	0.000	6.359	3.131	0.072	0.000
6	121	67.4267	2.624	7.099	0.433	0.213	0.000	6.445	3.171	0.063	0.000
7	255	67.4267	2.622	7.104	0.432	0.215	0.000	6.463	3.165	0.063	0.000
8	124	67.6717	2.614	7.297	0.419	0.282	0.000	6.210	3.059	0.083	0.000
9	116	68.8746	2.647	6.764	0.442	0.129	0.000	6.664	3.240	0.038	0.000
10	251	68.8746	2.644	6.768	0.441	0.131	0.000	6.683	3.233	0.038	0.000
11	115	70.9929	2.687	6.663	0.439	0.110	0.000	6.696	3.209	0.032	0.000
12	10	74.2746	2.672	6.570	0.438	0.122	0.000	7.142	3.250	0.036	0.000
13	66	74.2746	2.794	6.842	0.427	0.148	0.000	6.620	3.106	0.043	0.000
14	202	74.2746	2.792	6.845	0.426	0.149	0.000	6.640	3.099	0.044	0.000
15	113	75.5664	2.787	6.603	0.428	0.097	0.000	6.687	3.111	0.029	0.000
16	250	77.0323	2.839	6.727	0.421	0.120	0.000	6.664	3.055	0.035	0.000
17	258	77.2143	2.838	7.400	0.378	0.324	0.000	6.135	2.727	0.095	0.000
18	125	77.2914	2.839	7.541	0.370	0.374	0.000	6.001	2.662	0.110	0.000
19	259	77.2914	2.837	7.543	0.369	0.374	0.000	6.021	2.658	0.110	0.000
20	37	80.2356	2.865	7.446	0.373	0.365	0.000	6.426	2.718	0.107	0.000
21	93	80.2356	2.987	7.619	0.367	0.365	0.000	6.100	2.638	0.107	0.000
22	229	80.2356	2.984	7.621	0.367	0.365	0.000	6.121	2.634	0.107	0.000
23	15	80.3692	2.792	6.699	0.406	0.163	0.000	6.948	2.992	0.048	0.000
24	71	80.3692	2.900	6.892	0.392	0.169	0.000	6.443	2.836	0.050	0.000
25	207	80.3692	2.897	6.894	0.391	0.169	0.000	6.464	2.831	0.050	0.000
26	33	80.5349	2.857	7.276	0.381	0.314	0.000	6.556	2.781	0.092	0.000
27	89	80.5349	2.977	7.453	0.373	0.314	0.000	6.185	2.683	0.092	0.000
28	225	80.5349	2.975	7.454	0.372	0.314	0.000	6.205	2.679	0.092	0.000
29	28	81.4969	2.879	7.148	0.387	0.273	0.000	6.689	2.828	0.080	0.000
30	84	81.4969	2.996	7.321	0.377	0.269	0.000	6.274	2.712	0.079	0.000
31	220	81.4969	2.994	7.323	0.376	0.269	0.000	6.295	2.708	0.079	0.000
32	1	82.2802	2.795	6.386	0.418	0.087	0.000	7.155	3.080	0.026	0.000
33	57	82.2802	2.904	6.598	0.403	0.095	0.000	6.621	2.911	0.028	0.000
34	193	82.2802	2.902	6.599	0.402	0.095	0.000	6.642	2.905	0.028	0.000
35	7	83.3181	2.842	6.512	0.413	0.110	0.000	7.117	3.038	0.032	0.000
36	63	83.3181	2.952	6.713	0.399	0.113	0.000	6.596	2.875	0.033	0.000
37	199	83.3181	2.949	6.714	0.398	0.113	0.000	6.618	2.869	0.033	0.000
38	19	83.4550	2.888	6.864	0.392	0.196	0.000	6.868	2.874	0.058	0.000
39	75	83.4550	3.000	7.030	0.379	0.190	0.000	6.389	2.732	0.056	0.000
40	211	83.4550	2.998	7.031	0.378	0.190	0.000	6.410	2.728	0.056	0.000
41	25	83.7191	2.923	7.016	0.387	0.231	0.000	6.797	2.831	0.068	0.000

#	srf#	$\bar{q}$	$\phi_{1sec}$	$\phi_{2.8sec}$	$\beta_{max}$	$\delta_{amax}$	$\delta_{amax}$	$\delta_{rmax}$	$\delta_{rmax}$	$\delta_{elevmax}$	$\delta_{elevmax}$
42	81	83.7191	3.042	7.181	0.376	0.222	0.000	6.347	2.703	0.065	0.000
43	217	83.7191	3.039	7.183	0.375	0.223	0.000	6.369	2.699	0.065	0.000
44	34	87.3860	3.138	7.373	0.372	0.293	0.000	6.714	2.700	0.086	0.000
45	90	87.3860	3.265	7.498	0.362	0.279	0.000	6.316	2.591	0.082	0.000
46	226	87.3860	3.262	7.499	0.361	0.280	0.000	6.339	2.588	0.082	0.000
47	127	88.7159	3.426	7.829	0.342	0.373	0.000	5.943	2.416	0.110	0.000
48	261	88.7159	3.423	7.829	0.341	0.374	0.000	5.966	2.414	0.110	0.000
49	38	89.3983	3.307	7.585	0.366	0.332	0.000	6.741	2.649	0.098	0.000
50	94	89.3983	3.419	7.670	0.354	0.319	0.000	6.307	2.528	0.094	0.000
51	230	89.3983	3.416	7.670	0.354	0.320	0.000	6.331	2.525	0.094	0.000
52	11	91.6970	3.048	6.691	0.387	0.126	0.000	7.063	2.815	0.037	0.000
53	67	91.6970	3.144	6.806	0.371	0.115	0.000	6.535	2.651	0.034	0.000
54	203	91.6970	3.141	6.806	0.370	0.115	0.000	6.558	2.646	0.034	0.000
55	41	94.3473	3.483	7.659	0.336	0.349	0.000	6.169	2.396	0.103	0.000
56	97	94.3473	3.570	7.709	0.321	0.402	0.000	5.675	2.243	0.118	0.000
57	233	94.3473	3.568	7.709	0.321	0.401	0.000	5.699	2.242	0.118	0.000
58	262	101.0962	3.705	7.722	0.274	0.491	0.000	4.839	1.858	0.144	0.000
59	16	102.4478	3.243	6.655	0.339	0.113	0.000	6.648	2.452	0.033	0.000
60	72	102.4478	3.312	6.708	0.322	0.109	0.000	6.060	2.286	0.032	0.000
61	208	102.4478	3.310	6.707	0.321	0.109	0.000	6.085	2.284	0.032	0.000
62	263	103.7392	3.819	7.682	0.269	0.503	0.000	4.802	1.817	0.148	0.000
63	42	106.1299	3.776	7.431	0.300	0.366	0.000	5.694	2.095	0.108	0.000
64	98	106.1299	3.863	7.435	0.283	0.434	0.000	5.231	1.943	0.128	0.000
65	234	106.1299	3.861	7.434	0.283	0.433	0.000	5.257	1.943	0.127	0.000
66	264	106.4162	3.950	7.634	0.264	0.515	0.000	4.779	1.782	0.152	0.000
67	20	109.0025	3.428	6.718	0.319	0.123	0.000	6.448	2.292	0.036	0.000
68	76	109.0025	3.491	6.741	0.303	0.149	0.000	5.882	2.135	0.044	0.000
69	212	109.0025	3.489	6.739	0.302	0.148	0.000	5.908	2.134	0.043	0.000
70	46	109.1273	3.952	7.579	0.273	0.462	0.000	5.082	1.864	0.136	0.000
71	102	109.1273	4.084	7.578	0.260	0.524	0.000	4.730	1.746	0.154	0.000
72	238	109.1273	4.083	7.577	0.260	0.524	0.000	4.757	1.747	0.154	0.000
73	29	110.1905	3.639	6.935	0.315	0.193	0.000	6.376	2.253	0.057	0.000
74	85	110.1905	3.707	6.938	0.298	0.244	0.000	5.839	2.097	0.072	0.000
75	221	110.1905	3.705	6.936	0.298	0.242	0.000	5.866	2.096	0.071	0.000
76	8	110.9265	3.225	6.361	0.319	0.059	0.000	6.572	2.297	0.017	0.000
77	64	110.9265	3.277	6.391	0.302	0.056	0.000	5.959	2.134	0.016	0.000
78	200	110.9265	3.275	6.390	0.301	0.056	0.000	5.985	2.132	0.016	0.000
79	47	111.8726	4.081	7.496	0.269	0.465	0.000	5.062	1.830	0.137	0.000
80	103	111.8726	4.207	7.484	0.255	0.521	0.000	4.711	1.714	0.153	0.000
81	239	111.8726	4.207	7.482	0.255	0.520	0.000	4.738	1.715	0.153	0.000
82	48	114.6519	4.213	7.410	0.264	0.464	0.000	5.047	1.797	0.137	0.000

#	srf#	$\bar{q}$	$\phi_{1sec}$	$\phi_{2.8sec}$	$\beta_{max}$	$\delta_{amax}$	$\delta_{amax}$	$\delta_{rmax}$	$\delta_{rmax}$	$\delta_{elevmax}$	$\delta_{elevmax}$
83	104	114.6519	4.339	7.389	0.251	0.516	0.000	4.694	1.683	0.152	0.000
84	240	114.6519	4.338	7.387	0.250	0.516	0.000	4.722	1.685	0.152	0.000
85	49	117.4653	4.349	7.321	0.259	0.462	0.000	5.036	1.764	0.136	0.000
86	105	117.4653	4.477	7.291	0.246	0.511	0.000	4.678	1.653	0.150	0.000
87	241	117.4653	4.476	7.289	0.246	0.511	0.000	4.707	1.654	0.150	0.000
88	50	120.3129	4.488	7.231	0.254	0.458	0.000	5.025	1.730	0.135	0.000
89	106	120.3129	4.623	7.193	0.242	0.504	0.000	4.662	1.621	0.148	0.000
90	242	120.3129	4.622	7.190	0.241	0.504	0.000	4.692	1.623	0.148	0.000
91	43	121.8328	4.408	7.114	0.268	0.420	0.000	5.372	1.838	0.124	0.000
92	99	121.8328	4.479	7.080	0.252	0.464	0.000	4.944	1.706	0.136	0.000
93	235	121.8328	4.477	7.078	0.252	0.464	0.000	4.973	1.707	0.136	0.000
94	51	123.1945	4.631	7.140	0.249	0.451	0.000	5.016	1.697	0.133	0.000
95	107	123.1945	4.692	7.102	0.235	0.492	0.000	4.590	1.579	0.145	0.000
96	243	123.1945	4.689	7.099	0.235	0.492	0.000	4.619	1.580	0.145	0.000
97	52	126.1103	4.729	7.055	0.244	0.440	0.000	4.977	1.659	0.129	0.000
98	108	126.1103	4.752	7.013	0.229	0.479	0.000	4.502	1.533	0.141	0.000
99	244	126.1103	4.749	7.010	0.229	0.480	0.000	4.531	1.534	0.141	0.000
100	53	129.0601	4.772	6.974	0.237	0.424	0.000	4.881	1.608	0.125	0.000
101	109	129.0601	4.811	6.927	0.222	0.466	0.000	4.402	1.485	0.137	0.000
102	245	129.0601	4.809	6.924	0.222	0.467	0.000	4.432	1.486	0.137	0.000
103	2	129.4213	3.445	6.179	0.277	0.029	0.000	6.164	1.969	0.009	0.000
104	58	129.4213	3.528	6.214	0.265	0.041	0.000	5.624	1.856	0.012	0.000
105	194	129.4213	3.526	6.213	0.265	0.040	0.000	5.653	1.855	0.012	0.000
106	17	129.8252	3.757	6.414	0.277	0.101	0.000	6.075	1.963	0.030	0.000
107	73	129.8252	3.840	6.428	0.264	0.135	0.000	5.550	1.841	0.040	0.000
108	209	129.8252	3.837	6.426	0.263	0.134	0.000	5.581	1.840	0.039	0.000
109	30	129.9582	4.126	6.610	0.278	0.223	0.000	6.056	1.967	0.066	0.000
110	86	129.9582	4.217	6.590	0.263	0.273	0.000	5.545	1.826	0.080	0.000
111	222	129.9582	4.214	6.588	0.262	0.272	0.000	5.577	1.827	0.080	0.000
112	26	130.0074	3.996	6.556	0.278	0.178	0.000	6.061	1.966	0.052	0.000
113	82	130.0074	4.083	6.549	0.263	0.222	0.000	5.544	1.832	0.065	0.000
114	218	130.0074	4.080	6.547	0.263	0.222	0.000	5.576	1.832	0.065	0.000
115	35	130.0653	4.265	6.651	0.276	0.271	0.000	5.981	1.946	0.080	0.000
116	91	130.0653	4.360	6.616	0.260	0.327	0.000	5.482	1.801	0.096	0.000
117	227	130.0653	4.357	6.614	0.259	0.326	0.000	5.515	1.802	0.096	0.000
118	21	130.1006	3.877	6.488	0.277	0.137	0.000	6.064	1.962	0.040	0.000
119	77	130.1006	3.961	6.491	0.263	0.176	0.000	5.542	1.834	0.052	0.000
120	213	130.1006	3.959	6.489	0.263	0.175	0.000	5.573	1.834	0.052	0.000
121	44	131.7744	4.828	6.866	0.251	0.426	0.000	5.221	1.703	0.125	0.000
122	100	131.7744	4.778	6.853	0.234	0.449	0.000	4.771	1.574	0.132	0.000
123	236	131.7744	4.775	6.850	0.234	0.450	0.000	4.803	1.576	0.132	0.000

#	srf#	$\bar{q}$	$\phi_{1sec}$	$\phi_{2.8sec}$	$\beta_{max}$	$\delta_{amax}$	$\delta_{amax}$	$\delta_{rmax}$	$\delta_{rmax}$	$\delta_{elevmax}$	$\delta_{elevmax}$
124	54	132.0441	4.813	6.895	0.229	0.407	0.000	4.771	1.555	0.120	0.000
125	110	132.0441	4.870	6.843	0.215	0.453	0.000	4.290	1.434	0.133	0.000
126	246	132.0441	4.867	6.840	0.215	0.454	0.000	4.321	1.436	0.133	0.000
127	39	134.8266	4.656	6.690	0.257	0.347	0.000	5.501	1.774	0.102	0.000
128	95	134.8266	4.678	6.660	0.241	0.387	0.000	5.047	1.643	0.114	0.000
129	231	134.8266	4.675	6.658	0.241	0.387	0.000	5.081	1.645	0.114	0.000
130	55	135.0621	4.854	6.818	0.221	0.391	0.000	4.648	1.500	0.115	0.000
131	111	135.0621	4.929	6.761	0.208	0.440	0.000	4.166	1.382	0.129	0.000
132	247	135.0621	4.926	6.759	0.208	0.441	0.000	4.197	1.384	0.130	0.000
133	56	138.1142	4.894	6.744	0.213	0.374	0.000	4.511	1.444	0.110	0.000
134	112	138.1142	4.987	6.683	0.201	0.427	0.000	4.030	1.328	0.126	0.000
135	248	138.1142	4.984	6.680	0.200	0.429	0.000	4.060	1.330	0.126	0.000
136	45	167.7286	5.207	6.327	0.253	0.180	0.000	2.364	0.843	0.053	0.000
137	101	167.7286	5.303	6.288	0.239	0.191	0.000	2.116	0.772	0.056	0.000
138	237	167.7286	5.299	6.286	0.239	0.193	0.000	2.139	0.774	0.057	0.000
139	22	170.3164	4.648	6.084	0.311	0.113	0.000	3.238	1.096	0.033	0.000
140	78	170.3164	4.720	6.092	0.294	0.143	0.000	2.973	1.009	0.042	0.000
141	214	170.3164	4.716	6.090	0.294	0.143	0.000	2.999	1.010	0.042	0.000
142	40	208.2658	5.401	6.049	0.220	0.074	0.000	2.208	0.732	0.022	0.000
143	96	208.2658	5.511	6.027	0.208	0.137	0.000	1.976	0.668	0.040	0.000
144	232	208.2658	5.507	6.024	0.207	0.134	0.000	2.002	0.669	0.039	0.000
145	31	215.9733	5.414	5.970	0.256	0.080	0.000	2.856	0.880	0.023	0.000
146	87	215.9733	5.401	5.943	0.238	0.103	0.000	2.575	0.798	0.030	0.000
147	223	215.9733	5.398	5.940	0.238	0.105	0.000	2.605	0.800	0.031	0.000
148	126	222.8766	5.593	5.964	0.191	0.195	0.000	1.804	0.658	0.057	0.000
149	260	222.8766	5.589	5.961	0.191	0.192	0.000	1.829	0.658	0.056	0.000
150	3	228.5562	4.803	5.916	0.261	0.024	0.000	3.091	1.016	0.007	0.000
151	59	228.5562	4.799	5.896	0.249	0.029	0.000	2.804	1.009	0.009	0.000
152	195	228.5562	4.796	5.894	0.249	0.029	0.000	2.833	1.008	0.009	0.000
153	12	254.7139	5.057	5.807	0.242	0.026	0.000	2.993	0.938	0.008	0.000
154	68	254.7139	5.084	5.798	0.227	0.040	0.000	2.704	0.925	0.012	0.000
155	204	254.7139	5.081	5.797	0.227	0.041	0.000	2.736	0.925	0.012	0.000
156	36	264.5698	5.483	5.892	0.188	0.132	0.000	2.031	0.675	0.039	0.000
157	92	264.5698	5.640	5.902	0.178	0.192	0.000	1.807	0.669	0.056	0.000
158	228	264.5698	5.637	5.899	0.177	0.190	0.000	1.835	0.668	0.056	0.000
159	32	333.6127	5.488	5.823	0.165	0.144	0.000	1.906	0.677	0.042	0.000
160	88	333.6127	5.678	5.864	0.156	0.187	0.000	1.693	0.670	0.055	0.000
161	224	333.6127	5.675	5.863	0.156	0.186	0.000	1.721	0.670	0.055	0.000
162	23	333.8201	5.424	5.794	0.192	0.037	0.000	2.476	0.790	0.011	0.000
163	79	333.8201	5.460	5.787	0.181	0.061	0.000	2.225	0.780	0.018	0.000
164	215	333.8201	5.458	5.785	0.180	0.060	0.000	2.257	0.780	0.018	0.000

### Appendix E. Matlab's "Linmod" Function

Phillips employed *Matlab's* "linmod" macro to generate the  $C^*/\delta_e$  transfer function in the longitudinal design and to close the dutch roll damper loop in the lateral/directional design. In this research some problems were identified with linmod after the  $C^*/\delta_e$  transfer functions used in Phillips' research did not match those generated in this design for the same plant sets. Phillips' functions had spurious feedforward terms and zeros in the extreme left half plane not found when  $C^*$  was generated via matrix manipulation. These discrepancies prompted an investigation of the entire transfer function generation scheme employed in the two designs. The only difference in the algorithms stemmed from the generation of  $C^*$ . Assuming that the linmod function was simply written incorrectly, the longitudinal design proceeded without it. However in the lateral channel Phillips' models matched identically to those generated via matrix manipulation, so the problem was more involved than originally assumed. It appears after analyzing the linmod function that the addition of a nonlinear weighting scheme (Fig 5.2) in the longitudinal design caused linmod to produce the incorrect  $C^*$  transfer functions.

To understand the ramifications of these incorrect transfer functions on Phillips' design, his compensator was loaded into QFTCAD along with the correct longitudinal transfer functions. Fortunately the additional zeros introduced by linmod, only mildly effected Phillips' design. From the stability validation plot found in Fig. E.1, Phillips' compensator maintained the required stability margin for all plant cases except those high  $\bar{q}$  plants (above 700 (lbs/ft<sup>2</sup>)).

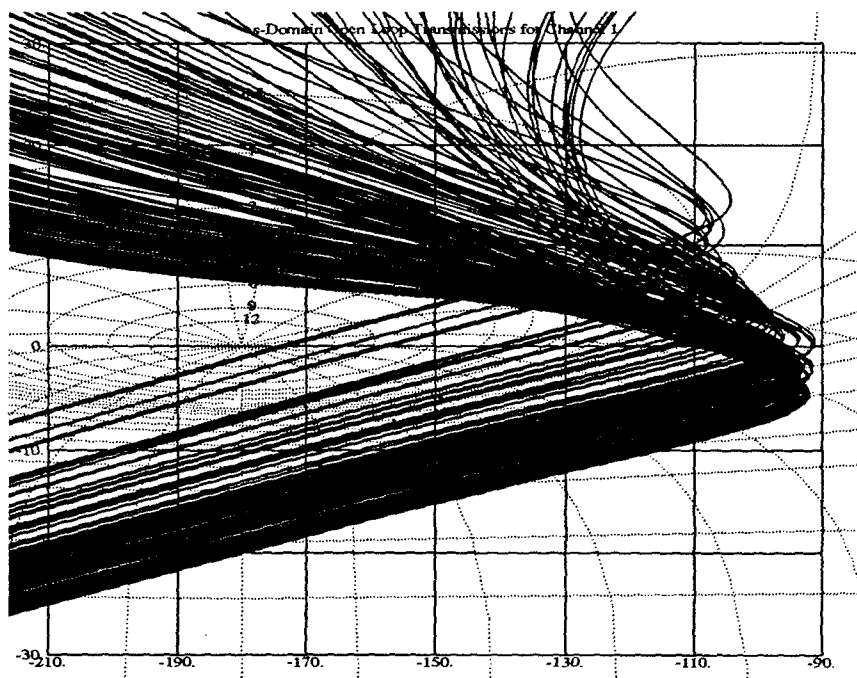


Figure E.1 Phillips' Compensated system Stability Validation

## Bibliography

1. ASA/ENES, Wright-Patterson AFB, OH 45433-6503. *Flying Qualities of Piloted Aircraft (Mil-Std 1797A)*, January 1990.
2. Blakelock, John H. *Automatic Control of Aircraft and Missiles* (Second Edition). New York: John Wiley & Sons, Inc., 1991.
3. Century Computing, Inc., 4141 Colonel Glen Hwy., Dayton, OH 45431-1662. *Simulation/Rapid-Prototyping Facility*, October 1992. Draft Sun/Unix Version.
4. Clough, Bruce T. *Reconfigurable Flight Control System for a STOL Aircraft using Quantitative Feedback Theory*. MS thesis, Air Force Institute of Technology, 1985.
5. D'Azzo, John J. and Constantine H. Houppis. *Linear Control System Analysis and Design, Conventional and Modern* (Fourth Edition). New York: McGraw-Hill, 1995.
6. Eide, Peter Captain. Notes and Comments from Maj Phillips' QFT FCS Aviator Checkout Flight. 25 APR 1995.
7. Horowitz, Isaac. "Application of Quantitative Feedback Theory (QFT) to Flight Control Problems," *IEEE Proceedings on Decision and Control*, 5:2593-2596 (December 1990).
8. Houppis, Constantine H. *Proceedings of the Quantitative Feedback Theory Symposium*. Technical Report WL-TR-92-3068, Wright-Patterson AFB, OH 45433-6553: Flight Dynamics Laboratory WL/FIGS, January 1992.
9. Houppis, Constantine H. *Quantitative Feedback Theory (QFT) For the Engineer*. Technical Report WL-TR-95-3061, Wright-Patterson AFB, OH 45433-6553: Flight Dynamics Directorate, June 1995.
10. Houppis, Dr. Constantine H. Personal Interview. Spring Quarter, 1995.
11. Keating, Mark S. *Design of a Flight Controller for an Unmanned Research Vehicle with Control Surface Failures using Quantitative Feedback Theory*. MS thesis, Air Force Institute of Technology, 1993.
12. Menke, Timothy. *Multiple Model Adaptive Estimation Applied to the Vista F-16 with Actuator and Sensor Failures*. MS thesis, Air Force Institute of Technology, 1992.
13. Neumann, Kurt N. *A Digital Rate Controller for the Control Reconfigurable Combat Aircraft Designed using Quantitative Feedback Theory*. MS thesis, Air Force Institute of Technology, 1988.
14. Pachter, Meir. Class Notes for EE641. Spring Quarter, 1995.
15. Phillips, Scott M. *A Quantitative Feedback Theory FCS Design Including Configuration Variation*. MS thesis, Air Force Institute of Technology, 1994.
16. Reynolds, Odell R. *Design of a Subsonic Envelope Flight Control System for the VISTA F-16 using Quantitative Feedback Theory*. MS thesis, Air Force Institute of Technology, 1993.
17. Roskam, Jan. *Flight Dynamics of Rigid and Elastic Airplanes*. Kansas: Roskam Aviation and Engineering Corporation, 1976.

18. Rubertus, Duane P. "Self-Repairing Flight Control Systems Overview," *Proceedings of the IEEE*, 1:2600-2608 (December 1983).
19. Sating, Richard R. *Development of an Analog MIMO Quantitative Feedback Theory (QFT) CAD Package*. MS thesis, Air Force Institute of Technology, 1992.
20. The MathWorks, Inc., 24 Prime Park Way, Natick, MA 01760. *Simulink*, March 1992. Copyright 1990-92.
21. Trosen, Dennis W. *Development of an Air-to-Air Refueling Automatic Flight Control System using Quantitative Feedback Theory*. MS thesis, Air Force Institute of Technology, 1993.
22. WL/FIGXF, Wright-Patterson AFB, OH 45433-6553. *VISTA/NF-16D Technical Data for Customer Usage*, August 1991.

*Vita*

Vincent Joseph Cacciatore [REDACTED]

[REDACTED]. Though he spent 6 years in Boston's South Shore area, Pennsylvania has always been called home. With astronaut aspirations, he decided to pursue a Bachelors degree in Electrical Engineering Engineering. Vincent matriculated into Lehigh University in 1990 and received a 4 year AFROTC scholarship to finance the experience. Earning a B.S.E.E degree with honors and his commission as a Second Lieutenant in the United States Air Force, he was selected to attend the Air Force Institute of Technology for his first assignment. Upon completion of a Masters of Science degree in Electrical Engineering, Vincent will proceed to Phillips Lab, Kirkland AFB, New Mexico. Vincent is a member of Tau Beta Pi, Omicron Delta Kappa and an Eagle Scout.

Permanent address: 25 Longview Road  
Glen Mills, PA 19342

VITA-1

REPORT DOCUMENTATION PAGE			Form Approved OMB No. 0704-0188	
Public reporting burden for this collection of information is estimated to average 1 hour per response, including the time for reviewing instructions, searching existing data sources, gathering and maintaining the data needed, and completing and reviewing the collection of information. Send comments regarding this burden estimate or any other aspect of this collection of information, including suggestions for reducing this burden, to Washington Headquarters Services, Directorate for Information Operations and Reports, 1215 Jefferson Davis Highway, Suite 1204, Arlington, VA 22202-4302, and to the Office of Management and Budget, Paperwork Reduction Project (0704-0188), Washington, DC 20503.				
1. AGENCY USE ONLY (Leave blank)	2. REPORT DATE December 1995	3. REPORT TYPE AND DATES COVERED Master's Thesis		
4. TITLE AND SUBTITLE A QUANTITATIVE FEEDBACK THEORY FCS DESIGN FOR THE SUBSONIC ENVELOPE OF THE VISTA F-16 INCLUDING CONFIGURATION VARIATION AND AERODYNAMIC CONTROL EFFECTOR FAILURES			5. FUNDING NUMBERS	
6. AUTHOR(S) Vincent J. Cacciatore Second Lieutenant, USAF				
7. PERFORMING ORGANIZATION NAME(S) AND ADDRESS(ES) Air Force Institute of Technology, WPAFB OH 45433-6583			8. PERFORMING ORGANIZATION REPORT NUMBER AFIT/GE/ENG/95D-04	
9. SPONSORING/MONITORING AGENCY NAME(S) AND ADDRESS(ES) Captain Peter Eide WL/FIGS 2210 Eighth St STE 11 Wright-Patterson AFB, OH 45433-7521			10. SPONSORING/MONITORING AGENCY REPORT NUMBER	
11. SUPPLEMENTARY NOTES				
12a. DISTRIBUTION/AVAILABILITY STATEMENT Approved for public release; Distribution Unlimited			12b. DISTRIBUTION CODE	
13. ABSTRACT (Maximum 200 words)  Fault tolerant flight control systems for combat aircraft are an alternative to excessively redundant aircraft designs or reconfigurable control laws. However, due to the range of flight conditions within a combat aircraft's operational flight envelope, the variety of its configurations, and the unavailability of an aerodynamic data base for damaged aircraft, designing fault tolerant systems is a complicated endeavor. Quantitative Feedback Theory is a robust control design technique especially well suited to manage the structured parametric uncertainty inherent in this problem, and consequently is applied as the primary design tool for this research. Furthermore, realistic failure models are developed for the VISTA F-16 and physical saturation constraints are applied to the control effectors. The ensuing fault tolerant design is subjected to realistic control inputs and validated with the applicable MILSTD specifications.				
14. SUBJECT TERMS Quantitative Feedback Theory, QFT, FCS, VISTA, F-16, Subsonic Envelope, Configuration Variation, Failure Modeling			15. NUMBER OF PAGES 224	
			16. PRICE CODE	
17. SECURITY CLASSIFICATION OF REPORT UNCLASSIFIED	18. SECURITY CLASSIFICATION OF THIS PAGE UNCLASSIFIED	19. SECURITY CLASSIFICATION OF ABSTRACT UNCLASSIFIED	20. LIMITATION OF ABSTRACT UL	

## GENERAL INSTRUCTIONS FOR COMPLETING SF 298

The Report Documentation Page (RDP) is used in announcing and cataloging reports. It is important that this information be consistent with the rest of the report, particularly the cover and title page. Instructions for filling in each block of the form follow. It is important to *stay within the lines* to meet *optical scanning requirements*.

**Block 1. Agency Use Only (Leave blank).**

**Block 2. Report Date.** Full publication date including day, month, and year, if available (e.g. 1 Jan 88). Must cite at least the year.

**Block 3. Type of Report and Dates Covered.** State whether report is interim, final, etc. If applicable, enter inclusive report dates (e.g. 10 Jun 87 - 30 Jun 88).

**Block 4. Title and Subtitle.** A title is taken from the part of the report that provides the most meaningful and complete information. When a report is prepared in more than one volume, repeat the primary title, add volume number, and include subtitle for the specific volume. On classified documents enter the title classification in parentheses.

**Block 5. Funding Numbers.** To include contract and grant numbers; may include program element number(s), project number(s), task number(s), and work unit number(s). Use the following labels:

C - Contract	PR - Project
G - Grant	TA - Task
PE - Program Element	WU - Work Unit Accession No.

**Block 6. Author(s).** Name(s) of person(s) responsible for writing the report, performing the research, or credited with the content of the report. If editor or compiler, this should follow the name(s).

**Block 7. Performing Organization Name(s) and Address(es).** Self-explanatory.

**Block 8. Performing Organization Report Number.** Enter the unique alphanumeric report number(s) assigned by the organization performing the report.

**Block 9. Sponsoring/Monitoring Agency Name(s) and Address(es).** Self-explanatory.

**Block 10. Sponsoring/Monitoring Agency Report Number.** (If known)

**Block 11. Supplementary Notes.** Enter information not included elsewhere such as: Prepared in cooperation with...; Trans. of...; To be published in.... When a report is revised, include a statement whether the new report supersedes or supplements the older report.

**Block 12a. Distribution/Availability Statement.** Denotes public availability or limitations. Cite any availability to the public. Enter additional limitations or special markings in all capitals (e.g. NOFORN, REL, ITAR).

**DOD** - See DoDD 5230.24, "Distribution Statements on Technical Documents."

**DOE** - See authorities.

**NASA** - See Handbook NHB 2200.2.

**NTIS** - Leave blank.

**Block 12b. Distribution Code.**

**DOD** - Leave blank.

**DOE** - Enter DOE distribution categories from the Standard Distribution for Unclassified Scientific and Technical Reports.

**NASA** - Leave blank.

**NTIS** - Leave blank.

**Block 13. Abstract.** Include a brief (*Maximum 200 words*) factual summary of the most significant information contained in the report.

**Block 14. Subject Terms.** Keywords or phrases identifying major subjects in the report.

**Block 15. Number of Pages.** Enter the total number of pages.

**Block 16. Price Code.** Enter appropriate price code (*NTIS only*).

**Blocks 17 - 19. Security Classifications.** Self-explanatory. Enter U.S. Security Classification in accordance with U.S. Security Regulations (i.e., UNCLASSIFIED). If form contains classified information, stamp classification on the top and bottom of the page.

**Block 20. Limitation of Abstract.** This block must be completed to assign a limitation to the abstract. Enter either UL (unlimited) or SAR (same as report). An entry in this block is necessary if the abstract is to be limited. If blank, the abstract is assumed to be unlimited.